Mutational and Functional Analyses of Bardet-Biedl Syndrome

Helen Louise May-Simera

Molecular Medicine Unit
Institute of Child Health
London

A thesis submitted for the degree of Doctor of Philosophy
to the University of London

December, 2007

ProQuest LLC
789 East Eisenhower Parkway
P.O. Box 1346
Ann Arbor, MI 48106-1346

Abstract

This thesis investigates some of the underlying causes of Bardet-Biedl syndrome, a leading example of emerging ciliopathies. Bardet-Biedl syndrome (BBS) is a heterogeneous disorder with primary features that include age-related retinal dystrophy, obesity, polydactyly, renal dysplasia, reproductive tract anomalies and cognitive impairment. To date 12 loci have been found to be causative for the disease (BBS1-12) and evidence suggests that aspects of the BBS phenotype may result from defective ciliogenesis/basal body function. The aims of this project were to identify new genes involved with the disease, analyse the phenotype of the Bbs6$^{-/-}$ mouse and further elucidate the mechanism of the disease in a zebrafish model.

Pathogenic sequence mutations identified in candidate genes aided the identifictaion of *BBS3* and *BBS5*. Further candidate genes were identified through the mapping of translocation breakpoints in a BBS patient. A yeast two-hybrid screen, using Bbs6 as bait, revealed several potential protein interactions. Phenotypical analysis of the *Bbs6*$^{-/-}$ mouse showed features comparable to BBS patients and other *Bbs* null mice, confirming its value as a model for further study. Further investigations of BBS proteins in the cochlea suggested a role beyond that of cilia and basal body function, namely that BBS proteins play distinct roles in the processes of microtubule nucleation and growth. Observed disruption of cochlear stereociliary bundles, along with other phenotypes associated with planar cell polarity (PCP) mutants, implied cilia might be involved in PCP signalling. This observation was supported by further analysis in the zebrafish. Disruption of *bbs8* resulted in similar phenotypes to other PCP mutants, and laterality defects, thought to arise from defective cilia function at the Kupffer's Vesicle, were enhanced on a PCP mutant background.

The results presented in this thesis pave the way for further investigation with a view to broadening the knowledge of the developmental processes behind BBS and also the processes behind the development of other signaling pathways, tissues and organ systems.

Table of Contents

Abstract 2
Table of Contents 3
Figure Legend 9
Table Legend 11
Appendices 12
Acknowledgements 15
Abbreviations 16

Chapter 1: Introduction 21
1.1 Bardet-Biedl Syndrome 21
1.1.1 History 21
1.1.2 Prevalence 22
1.1.3 Diagnosis 23
1.1.4 Clinical Features 25
1.1.5 Heterozygous Effects 30
1.1.6 Related Syndromes 31
1.2 The Genetics of BBS 33
1.2.1 BBS1 34
1.2.2 BBS2 34
1.2.3 BBS3 35
1.2.4 BBS4 35
1.2.5 BBS5 37
1.2.6 BBS6 37
1.2.7 BBS7 38
1.2.8 BBS8 40
1.2.9 BBS9 41
1.2.10 BBS10 42
1.2.11 BBS11 42
1.2.12 BBS12 42
1.2.13 Complex Inheritance in BBS 45
1.3 Cilia 46
1.3.1 Structure and Function 46
1.3.2 Intraflagellar Transport 48
1.3.3 Cilia and disease 51
1.3.4 Cilia, signalling and the cell cycle 54
1.3.5 The role of cilia in BBS 55
1.4 Animal models of BBS 57
1.5 BBS protein complexes 57
1.6 Aims of this thesis 59

Chapter 2: Materials and Methods 60
2.1 Materials 60
2.1.1 Reagents 60
2.1.2 Stock Solutions 60
2.1.3 DNA Samples 62
2.2 Methods 63

2.2.1 Fluorescent in situ hybridisation (FISH) 63
2.2.1.1 Mammalian Cell Culture 63
2.2.1.2 Preparation of metaphase spreads 63
2.2.1.3 Slide Preparation for DNA fibres 64
2.2.1.4 Preparation of BAC probes 65
2.2.1.5 Nick Translation of BAC probes 65
2.2.1.6 Probe Precipitation 66
2.2.1.7 Fluorescence *in situ* hybridisation, washes and detection 66
2.2.2 Amplification of DNA by Polymerase Chain Reaction (PCR) 67
2.2.2.1 DNA extraction from blood 67
2.2.2.2 Primer design for direct sequencing 67
2.2.2.3 Polymerase Chain Reaction 68
2.2.2.4 PCR optimisation 69
2.2.2.5 Agarose gel electrophoresis 70
2.2.2.6 Purification of PCR products 70
2.2.3 Sequencing 71
2.2.3.1 Cycle sequencing 71
2.2.3.2 Sephadex desalting 72
2.2.3.3 Sequencing on the MegaBACE 73
2.2.3.4 Sequence Analysis 73
2.2.4 Restriction Digests 73
2.2.5 Reverse transcription and RT-PCR 74
2.2.6 Cloning 74
2.2.6.1 Preparation of insert 74
2.2.6.2 Ligations 75
2.2.6.3 Transformation of ligations 76
2.2.7 Yeast two-hybrid screen 77
2.2.7.1 Small scale transformation 77
2.2.7.2 Autoactivation test 78
2.2.7.3 Large scale transformation 78
2.2.7.4 Transformation efficiency 79
2.2.7.5 First round of selection – Histidine 79
2.2.7.6 Second round of selection – Adenine 79
2.2.7.7 Isolation of prey plasmid 80
2.2.7.8 Amplification and identification of the prey cDNA sequence 80
2.2.7.9 Testing for autoactivation of prey 81
2.2.8 Analysis of $Bbs6^{-/-}$ Mouse 82
2.2.8.1 DNA extraction from tail tips 82
2.2.8.2 Harvesting organs 82
2.2.8.3 Embedding and sectioning 82
2.2.8.4 Hematoxylin and eosin staining 84
2.2.8.5 β-galactosidase assay 84
2.2.8.6 Preyer reflex test 85
2.2.8.7 Distortion product otoacoustic emissions 85
2.2.8.8 Buried food pellet recovery 85
2.2.9 Immunohistochemistry 86
2.2.9.1 Animals 86
2.2.9.2 Preparation of tissue 86

2.2.9.3 Confocal immunofluorescence 87
2.2.9.4 Antibodies 87
2.2.9.5 Electron microscopy 87
2.2.9.6 Expression analysis of Bbs6 transcript 88
2.2.10 Zebrafish analysis 88
2.2.10.1 Zebrafish lines 88
2.2.10.2 Morpholino antisense oligonucleotide Injection 88
2.2.10.3 Whole-mount RNA *in situ* hybridisation 89
2.2.10.4 Immunohistochemistry in zebrafish 91
2.2.10.5 Imaging 92

Chapter 3: Mapping translocation breakpoints in an Iranian BBS patient by fluorescent in situ hybridisation 93
3.1 Introduction 93
3.2 Materials and Methods 96
3.2.1 Preparation of chromosomal probes 96
3.2.2 Preparation of metaphase spreads from patient cells 96
3.2.3 Preparation of genomic DNA from EBV cell lines 96
3.2.3 Fluorescent *in situ* Hybridisation 96
3.2.4 Sequencing 97
3.2.5 Other methods 97
3.2.6 Websites 97
3.3 Results 98
3.3.1 Analysis of known BBS genes in Iranian patient 98
3.3.2 Breakpoint on chromosome 3 98
3.3.3 Breakpoint on chromosome 10 103
3.3.4 Re-analysis of breakpoint on chromosome 3 106
3.4 Discussion 110
3.5 Summary 113

Chapter 4: Mutational analyses 114
4.1 Introduction 114
4.1.1 *BBS5* 114
4.1.2 *BBS3* 116
4.1.3 *MGC1203* 118
4.2 Materials and Methods 120
4.2.1 Amplification of DNA by Polymerase Chain Reaction (PCR) 120
4.2.2 Sequencing of PCR Products 120
4.3 Results 121
4.3.1 *BBS5* 121
4.3.2 *BBS3* 122
4.3.3 *MGC1203* 124
4.4 Discussion 126
4.4.1 *BBS5* 126
4.4.2 *BBS3* 128
4.4.3 *MGC1203* 132
4.4.3 General Discussion 134
4.5 Summary 136

Chapter 5: Yeast two-hybrid screen using murine BBS6 as bait 137
5.1 Introdution 137
5.1.1 The theory behind the yeast two-hybrid system 137
5.1.2 Previous yeast two-hybrid screens involving BBS proteins 141
5.1.3 The BBS6 protein 142
5.2 Materials and Methods 144
5.2.1 Cloning 144
5.2.2 Yeast two-hybrid screen 144
5.2.3 Identification of positive clones 145
5.2.4 Confirmation off positive clones 145
5.3 Results 146
5.3.1 Autoactivation test 146
5.3.2 Transformation efficiency 146
5.3.3 First round of selection 146
5.3.4 Second round of selection 147
5.3.5 Identification of positive clones 147
5.3.6 Further analysis of positive clones 150
5.4 Discussion 155
5.5 Summary 163

Chapter 6: Phenotypic analysis of the *Bbs6*$^{-/-}$ mouse 164
6.1 Introduction 164
6.2 Materials and Methods 167
6.2.1 Generation of *Bbs6*$^{-/-}$ mice 167
6.2.2 Genotyping of pups 167
6.2.3 RT-PCR 168
6.2.4 Analysis of weight gain 168
6.2.5 Histology and immunofluorescence 168
6.2.6 Hearing and olfaction analysis 169
6.2.7 Analysis of fertility 169
6.3 Results 171
6.3.1 Generation of mice with disruption of *Bbs6* 171
6.3.2 Analysis of primary features of BBS 172
6.3.3 Analysis of secondary features of BBS 175
6.4 Discussion 180
6.5 Summary 187

Chapter 7: Evaluation of Bbs6 in the organ of Corti 188
7.1 Introduction 188
7.1.1 The cochlea 189
7.1.2 Stereocilia 191
7.1.3 The kinocilium and orientation of hair cells 193
7.1.4 Expression analysis of Bbs6 195
7.1.5 Auditory deficiencies in BBS patients 196
7.2 Materials and Methods 198
7.2.1 Further analysis of hearing deficit in *Bbs6* mutant animals 198
7.2.2 Analysis of the organ of Corti in Bbs6 mutant animals 198

7.2.3 Analysis of Bbs6 expression in the developing cochlea 198
7.3 Results 199
7.3.1 *Bbs6*$^{-/-}$ mice show progressive hearing loss 199
7.3.2 Stereociliary bundle abnormalities are observed in the cochlear outer hair cells of *Bbs6*$^{-/-}$ mice 200
7.3.3 Abnormal stereociliary bundles still have a kinocilium, but its association is perturbed 203
7.3.4 X-gal assays reveal differential expression pattern of *Bbs6* in the adult compared to the developing organ of Corti 205
7.3.5 Bbs6 is a ubiquitous basal body protein in vivo and has a unique pattern of expression during development of the organ of Corti 207
7.4 Discussion 215
7.5 Summary 221

Chapter 8: Expression of BBS6 interacting proteins in the cochlea 222
8.1 Introduction 222
8.1.1 The BBS6:BBS2 interaction 223
8.1.2 Additional interactors of BBS6 223
8.2 Materials and Methods 226
8.2.1 Confocal immunoflurosecence 226
8.3 Results 227
8.3.1 Expression of BBS2 in the developing murine cochlea 227
8.3.1.1 BBS2 associates with the actin cytoskeleton and microtubules in postnatal pillar cells 227
8.3.1.2 Bbs2 associates with actin cytoskeleton in non-sensory supporting cells, stereocilia and basal bodies in sensory hair cells prior to the onset of hearing 229
8.3.1.3 Basal body mislocalistion of Bbs2 in Bbs6 mutant OHC 234
8.3.3 Expression of MACF1, CCT6A and KIF1A in the developing murine cochlea 235
8.4 Discussion 241
8.5 Summary 245

Chapter 9: Evaluation of Bbs4 in the organ of Corti 246
9.1 Introduction 246
9.1.1 The BBS4 Protein 246
9.1.2 BBS4 in the mouse 250
9.1.3 The microtubule aspects of BBS 251
9.1.4 Microtubules in the cochlea. 252
9.2 Materials and Methods 255
9.2.1 Confocal immunofluorescence 255
9.2.1 Animals 255
9.3 Results 256
9.3.1 Bbs4 localises to microtubules of the epithelial cell cytoskeleton, basal bodies and primary cilia 256

9.3.2 Bbs4 localises along pillar cell microtubules as they develop, but expression is reduced in the mature organ of Corti 258
9.3.3 BBS4 localises to apical ends of Kolikers cells 260
9.3.4 Expression analysis of PCM-1 in the organ of Corti 262
9.3.5 Expression analysis of p150glued in the organ of Corti 263
9.3.6 Analysis of the *Bbs4*$^{-/-}$ cochlea 264
9.4 Discussion 268
9.4.1 Bbs4 268
9.4.2 BBS protein localisation in the organ of Corti 271
9.5 Summary 275

Chapter 10: BBS and Zebrafish 276
10.1 Introduction 276
10.1.1 Use of zebrafish as a model organism 276
10.1.2 Using morpholinos to model disease 277
10.1.3 Zebrafish models of BBS 278
10.2 Materials and Methods 280
10.2.1 Embryo culture and zebrafish stocks 280
10.2.2.Morpholino antisense oligonucleotide injection 280
10.2.3 RNA *in situ* localisation and immunohistochemistry 280
10.2.4 Imaging 281
10.3 Results 282
10.3.1 *bbs8* expression in wild-type embryos 282
10.3.2 *bbs8* Morpholino injections in wild-type zebrafish 284
10.3.3 Further analysis of *bbs8* in the zebrafish 287
10.3.3.1 *In situ* hybridization of *eng2a*, *shh* and *emx1* in wild-type vs *bbs8* morpholino injected embryos 287
10.3.3.2 Injection of *bbs8* morpholino into *smo* zebrafish 289
10.3.3.3 Injection of *bbs8* morpholino into *tri* Zebrafish 291
10.3.3.4 Laterality defects in *bbs8* morphant *tri* zebrafish 293
10.3.3.5 Laterality is caused by Kupffer's vesicle defects 296
10.4 Discussion 299
10.5 Summary 307

Chapter 11: Conclusion 308
11.1 Further BBS loci 309
11.2 BBS protein interactors 311
11.3 Microtubule function of BBS proteins 312
11.4 Animal models of BBS 314
1.5 Cilia and signaling pathways 315
References 321
Appendices 345

Figure Legend

Figure 1.1: Primary features of BBS. 29
Figure 1.2: A potential domain shared between multiple BBS proteins. 40
Figure 1.3: The arrangement of microtubules in a cilium or flagellum. 47
Figure 1.4: The IFT transport machinery. 49
Figure 1.5: Schematic representation of the localisation of the BBS proteins to the cilium and body. 51
Figure 1.6: Cilia found in sensory organs. 53

Figure 3.1: Iranian BBS pedigree. 94
Figure 3.2: Karyotype of BBS patient showing break point and predicted position of *BBS3*. 94
Figure 3.3: Metaphase spread showing BAC located below the breakpoint. 98
Figure 3.4: Metaphase spread showing BAC located above the breakpoint. 99
Figure 3.5: The position of BAC probes in relation to the breakpoint on chr 3. 100
Figure 3.6: DNA fibre from Iranian patient II-1. 101
Figure 3.7: Region of human genome sequence showing conservation of comparative genomics. 101
Figure 3.8: The position of BAC probes in relation to the breakpoint on chr 10. 103
Figure 3.9: Metaphase spread showing BAC spanning the breakpoint. 104
Figure 3.10: Location of genes potentially disrupted by breakpoint on chromosome 10. 104
Figure 3.11: Gel showing the RT-PCR product for TUBB4Q 105
Figure 3.12: Chromatogram showing the sequence change in BAIAP1. 106
Figure 3.13: BAIAP1 exon 16 cut with Hpy188III. 107
Figure 3.14: Predicted structure of BAIAP1. 108

Figure 4.1: Diagram of the comparative approach to identify flagellar and basal body proteins. 115
Figure 4.2: Alignment of X boxes. 117
Figure 4.3: Pedigree PB127. 121
Figure 4.4: Pedigree PB140. 122
Figure 4.5: Sequence analysis of *MGC1203*. 125
Figure 4.6: Diagram showing residues mutated in ARL6 in BBS patients. 130

Figure 5.1: The Yeast two-hybrid system. 139
Figure 5.2: Peptide information for Bbs6 interactors. 154
Figure 5.3: Schematic representation of the CHD7, 8 and 9 proteins 155

Figure 6.1: Schematic representation of the site of gene disruption by insertion of a trapping cassette into the Bbs6 genomic region. 167
Figure 6.2: Generation of the $Bbs6^{-/-}$ mouse. 171
Figure 6.3: Mouse weights over a period of six months from birth. 172
Figure 6.4: Analysis of young kidneys. 173
Figure 6.5: Analysis of mature kidneys. 174
Figure 6.6: Graph showing the results of the Mann-Whitney U test carried out on latencies of mice to retrieve buried food treat. 175
Figure 6.7: Immunostaining of the olfactory and respiratory epithelium in eight-week old mice with α-tubulin and dapi. 176
Figure 6.8: Graph to show the average Preyer reflex score of *Bbs6* null mice versus wild-type controls. 177
Figure 6.9: Distortion product otoacoustic emissions in $Bbs6^{-/-}$ mice. 178
Figure 6.10: Analysis of testes from $Bbs6^{-/-}$ mice and wild-type controls. 179

Figure 7.1: A schematic representation of the organ of Corti . 189
Figure 7.2: Scanning electron microscopy (SEM) images of mammalian auditory sensory cells. 192
Figure 7.3: Phalloidin staining on organ of Corti of p2 $Bbs6^{+/+}$ and $Bbs6^{-/-}$ mice. 200
Figure 7.4: Scanning electron microscopy of organ of Corti of adult $Bbs6^{+/+}$mice. 202
Figure: 7.5 Cochlear stereociliary bundle examination in $Bbs6^{-/-}$ mice. 204

Figure 7.6: Staining for β-galactosidase activity in *Bbs6*$^{+/-}$ cochlea counterstained with eosin. 206
Figure 7.7: Bbs6 localises to a dense body at the base of primary cilia. 208
Figure 7.8: Bbs6 is a ubiquitous basal body protein in vivo. 209
Figure 7.9: BBS6 Immunohistochemistry analysis is 'specific'. 210
Figure 7.10: Expression pattern of Bbs6 in the developing organ of Corti. 211
Figure 7.11: Bbs6 expression in the adult organ of Corti. 213
Figure 7.12: Neuronal expression of Bbs6. 214

Figure 8.1: Bbs2 assosiates with actin rich regions in early posnatal pillar cells. 228
Figure 8.2: Bbs2 expression increases with age and associates with actin cytoskeleton and migrating microtubules in postnatal pillar cells. 229
Figure 8.3: Bbs2 expression in p9 organ of Corti. 230
Figure 8.4: Bbs2 expression in p9 outer hair cells. 231
Figure 8.5: Progressive accumulation of Bbs2 expression in p9 outer hair cells. 232
Figure 8.6: Bbs2 expression in adult organ of Corti. 233
Figure 8.7: Bbs2 expression in Bbs6$^{-/-}$ outer hair cells. 234
Figure 8.8: MACF1 expression in p4 cochlea. 236
Figure 8.9: CCT6A expression in adult cochlea. 237
Figure 8.10: KIF1A localizes specifically to the apex of hair cells. 239
Figure 8.11: KIF1A in Bbs6$^{-/-}$ hair cells. 240

Figure 9.1: Model of BBS4 (dys)function. 249
Figure 9.2: Schematic diagrams of microtubule organisation in pillar cells. 254
Figure 9.3: Bbs4 localisation in a P2 organ of Corti. 256
Figure 9.4: Localisation of Bbs4 to primary cilia. 257
Figure 9.5: Bbs4 localisation in the developing organ of Corti. 259
Figure 9.6: Bbs4 localises to the apical ends of Kolikers' cells. 261
Figure 9.7: PCM-1 localisation in the organ of Corti. 262
Figure 9.8: p150^{glued} localisation in the organ of Corti. 263
Figure 9.9: Electron microscopy of a *Bbs4*$^{-/-}$ cochlea. 266
Figure 9.10: PCM-1 staining in *Bbs4*$^{-/-}$ mice. 267

Figure 10.1: In situ hybridisation of bbs8 in developing wild-type zebrafish. 283
Figure 10.2: In situ hybridisation of bbs8 in 24 hpf wild-type zebrafish. 283
Figure 10.3: Injection of 6 ng bbs8 morpholino at 30 hpf. 284
Figure 10.4: Injection of 6 ng bbs8 morpholino at 54 hpf. 285
Figure 10.5: Injection of 6 ng bbs8 morpholino at 78 hpf. 285
Figure 10.6: In situ hybridisation of eng2a in bbs8 mo injected 24hpf zebrafish. 287
Figure 10.7: In situ hybridisation of shh in bbs8 mo injected 24hpf zebrafish. 288
Figure 10.8: In situ hybridisation of emx1 in bbs8 mo injected 24hpf zebrafish. 289
Figure 10.9: Injection of smo zebrafish with bbs8 morpholino. 290
Figure 10.10: Injection of tri zebrafish with bbs8 morpholino. 292
Figure 10.11: Expression of myoD and krox20 in zebrafish with bbs8 morpholino injection. 293
Figure 10.12: Heart looping in 30hpf embryos. 294
Figure 10.13: spaw expression in 15-16 somite embryos. 296
Figure 10.14: Kupffer's vesicle injection vs 1 cell injection. 297
Figure 10.15: Visualisation of Kupffer's vesicle cilia in 16 somite embryos. 298
Figure 10.16: The Shh signaling pathway. 300

Figure 11.1: Ciliary involvement in Wnt signalling. 317
Figure 11.2: Involvement of MACF1 in the Wnt/β-catenin signaling pathway. 319

Table Legend

Table 1.1: Summary of primary and secondary features observed in BBS patients. 25
Table 1.2: Summary of known BBS genes. 44
Table 3.1: Alignment of stretch of protein containing P835 among various species. 109
Table 5.1: Calculations for transformation efficiency for the yeast two-hybrid transformation. 146
Table 5.2: Number of clones remaining at various stages of the yeast two-hybrid screen. 147
Table 5.3: Summary of the 44 proteins predicted to interact with Bbs6. 149
Table 5.4: Bbs6 interactors remaining after further analysis. 153
Table 5.5: Summary of confirmed Bbs6 interactors and their predicted cellular functions. 161
Table 6.1: Overview of the phenotypes observed in mice null for *Bbs* genes. 165
Table 6.2: Summary of phenotype displayed by the *Bbs6* null mice. 181
Table 7.1: Summary of results for progressive hearing study. 199
Table 8.1: Summary of confirmed Bbs6 interactors and their predicted cellular functions. 222
Table 9.1: Summary of results for progressive hearing study on one litter of *Bbs4* mutant mice. 264
Table 11.1: Summary of confirmed Bbs6 interactors and their predicted cellular functions. 311

Appendices

Appendix A: Primer Lists 345
Appendix 1: *BBS1* primer sequences including amplicon size and PCR conditions. 345
Appendix 2: *BBS2* primer sequences including amplicon size and PCR conditions. 346
Appendix 3: *BBS3* primer sequences including amplicon size and PCR conditions. 347
Appendix 4: *BBS4* primer sequences including amplicon size and PCR conditions. 348
Appendix 5: *BBS5* primer sequences including amplicon size and PCR conditions. 349
Appendix 6: *BBS6* primer sequences including amplicon size and PCR conditions. 349
Appendix 7: *BBS7* primer sequences and PCR conditions. 350
Appendix 8: *MGC1203* primer sequences and PCR conditions. 351
Appendix 9:*TUBB4Q* primer sequences including amplicon size and PCR conditions. 352
Appendix 10: *BAIAP1* primer sequences including amplicon size and PCR conditions. 353
Apendix B: Additional yeast information 354
Appendix 1: Genotype of S.cerevisiae yeast used for the yeast two-hybrid screen. 354
Appendix 2: Vector maps for pVP16 and pGBDU plasmids. 354
Apendix 3: Primers used for Cloning and Yeast two-hybrid analysis of Bbs6 355
Apendix 4: Primers used for amplification of the prey cDNA sequence 355
Apendix C: Additional mouse information 356
Appendix 1: Primer sequences for genotyping of the Bbs6-/- mouse. 356
Appendix 2: Primer sequences for genotyping of the Bbs4-/- mouse. 356
Appendix 3: Raw data from the olfactory behavioural tests. 356
Appendix 4: Mouse weights over a period of six months. 357
Apendix D: Antibody Information 358
Appendix 1: Primary antibodies used. 358
Appendix 2: Secondary antibodies used. 358

Für Mami, Lotti, Dida and Daddy.

'If we knew what it was we were doing, it would not be called research, would it.'

Albert Einstein 1879-1955

Acknowlegements

There are so many people I would like to thank that I just don't know where to begin. So I will start at the very beginning, that's a very good place to start……

Firstly I would like to thank my supervisor Phil. For all his time, patience and most importantly encouragement that has supported me over the past few years. A massive thank you and huge hug goes to my 'post doc', Alison Ross. I am still in awe of her fast pipetting abilities and hope to emulate her scientific skills in the future. I also want to thank Beth, who showed me how to 'do a PhD', and has been a great source of scientific and emotional support all the way through.

MMU has virtually become my second home and as such I want to thank Pete Scambler and all the members of the unit, past and present for making my PhD such a great experience. A special mention goes to Jo, Scary, Pazzer, Sarah, Kelly, Vicky and Kerra.

I also want to thank Dan Dan the ear man. 'If he can't scan it no one can.' For the hours of sitting behind the confocal, trying and work out what these damn proteins were up to. Thanks goes to the 'Masas' for allowing me to use their fish facilities. Especially Masa Kai who showed me the ropes when it comes to fish and bestowed upon me much time and patience.

During my PhD I spent six months in Dr Kelley's lab at NIH, in Washington, whom I greatly thank for hosting me. I would like to thank all the members of his lab for their help whilst I was out there, especially Alain Dabdoub, from whom I learnt so much about the ear (especially removing the dreaded tectorial membrane).

I would also like to thank Mark, who was with me through so much of my PhD life and whose friendship and love has supported me throughout.

I could not have got through this final year if it hadn't been for the support of my friends. In particular Ginger Jo (who will kill me for eternalising her name like that), Andrea, Zoe, Niki, Tamara, Joanna and Ruth. But my biggest thanks go to my housemates Suz and Shal, who have been my tower of strength and who have helped me stay sane during the craziness that is writing up.

And Finally I want to thank the BBS patients and their families whom I have gotten to know over the past few years through the LMBBS society. Their energy and enthusiasm has kept me motivated and has been an inspiration throughout.

Abbreviations

3AT	3-aminotriazole
aa	amino acid
ABR	auditory brainstem response
AER	apical ectodermal ridge
AD	activation Domain
ADPKD	autosomal dominant polycystic kidney disease
ANC	anterior neurocranial cartilage
ARF	ADP-ribosylation factor
ARL	ARF-like
ARPKD	autosomal recessive polycystic kidney disease
β-gal	β-galactosidase
BAC	bacterial artificial chromosome
BBS	Bardet-Biedl syndrome
BLAST	basic local alignment search tool
BM	basement membrane
BMI	body mass index
bp	base pair
BSA	bovine serum albumin
CC	connecting cilium
CC-RCC	clear cell renal cell carcinoma
CCT	chaperonin containing TCP1
cDNA	complementary DNA
cfu	colony forming units
CGH	comparative genomic hybridisation
CHD	chromodomain helicase DNA binding protein
cM	centiMorgan
CN	cochlea nerve fibre
CRF	chronic renal failure
DAB	3,3-diaminobenzidine tetrahydrochloride
DAPI	4',6-diamidino-2-phenylindole
DBD	DNA binding domain
der	derivative

DHPLC	denaturing high-pressure liquid chromatography
DMEM	dulbecco's modified eagle medium
DMSO	dimethyl sulfoxide
DNA	deoxyribonucleic acid
DNMT	DNA (cytosine-5-)-methyltransferase
dNTP	deoxynucleotide triphosphates
dpf	days post fertilisation
DPOAE	distortion product otoacoustic emissions
dsDNA	double-stranded DNA
E	embryonic stage (mouse)
EBV	epstein barr virus
EDTA	ethylene diamine tetra-acetic acid
EMBL	European molecular biology laboratory
emx1	*empty spiracles homeobox 1*
eng2a	*engrailed 2a*
EHD	EH-domain containing
ERG	electroretinogram
ESRD	end-stage renal disease
EST	expressed sequence tags
ExoSAP	exonuclease I/shrimp alkaline phosphatase
FA	formaldehyde
FABB	flagellar apparatus-basal body
FCS	fetal calf serum
FGF	fibroblast growth factor
FISH	fluorescent *in situ* hybridisation
fp	floor plate
HA	heteroduplex analysis
HGMP	human genome mapping project
hpf	hours post fertilisation
hr	hour
hy	hypothalamus
IFT	intraflagellar transport
IHC	inner hair cell
IPC	inner pillar cell

IS	inner segment (retina)
IQ	Intelligence quotient
kb	kilo base
KIF	kinesin family member
KV	Kupffer's Vesicle
l	litre
LB	Luria Bertani
LMS	Laurence Moon syndrome
LPA	linear polyacrylamide
LR	left-right
Ltap	looptail
m	milli
M	molar
µ	micro
MACF	microtubulin-actin crosslinking factor
Mb	mega base
MCHA	multiplex capillary heteroduplex analysis
MCS	multiple cloning site
min	minute
MKKS	McKusick-Kaufman syndrome
MKS	Meckel syndrome
MO	morpholino
mRNA	messenger RNA
MT	mictrotubules
MTOC	microtubule organising centre
n	nano
NB	nico buffer
NF	neurofilament
NIDDM	non-insulin dependent diabetes mellitus
NPHP	nephronophthisis
NTD	neural tube defects
OAE	otoacoustic emissions
OCT	optimal cutting temperature compound
OD	optical density

OE	olfactory epithelium
O-Glc NAC	O-linked N-acetylglucosamine
OGT	O-linked N-acetylglucosamine transferase
OHC	outer hair cell
ONL	outer nuclear layer (retina)
OPC	outer pillar cell
ORF	open reading frame
OS	outer segments (retina)
OSN	olfactory sensory neurons
p	postnatal
PBL	peripheral blood lymphocytes
PBS	phosphate buffered saline
PC	personal computer
PCM-1	pericentriolar material 1
PCP	planar cell polarity
PCR	polymerase chain reaction
PDZ	postsynaptic density-95/discs large/zona occludens-1
PEG	polyethylene glycol-400
PFA	paraformaldehyde
PilF	pilus formation
PKD	polycystc kidney disease
PTC	premature termination codon
Ptc	*Patched*
PWS	Prader-Wili syndrome
RM	Reissner's membrane
RNA	ribonucleic acid
RNAi	RNA interference
RP	retinitis pigmentosa
RPM	revolutions per minute
RT-PCR	reverse transcriptase PCR
s.d	standard deviation
SD	synthetic dropout
SDS	sodium dodecyl sulphate
SEM	scanning electron microscopy

SG	spiral ganglion
shh	sonic hedgehog
SIFT	sorting intolerant from tolerant
SLS	Senior-Löken syndrome
SMART	simple modular architecture research tool
smo	*smoothened*
SNP	single nucleotide polymorphism
spaw	*south paw*
SR	serine/arginine rich
SV	stria vascularis
TAE	tris-acetate-EDTA
TCP	tail-less complex polypeptide
TD	touchdown PCR program
TEM	transmission electron microscope
TESPA	3-aminopropyltriethoxysilane
TM	tectorial membrane
Tm	melting temperature
TOMM	translocase of outer mitochondrial membrane
TPR	tetratricopeptide repeat
tri	*trilobite*
TRiC	tail-less complex polypeptide ring complex
TRIM	tripartite motif
UASs	upstream activation sequences
UCSC	university of California, santa cruz
UTR	untranslated region
UV	ultra violet
wt	wild type
x-gal	5-bromo-4-chloro-3-indoyl-β-d-galactopyranoside
zl	zona limitans intrathalamica

Chapter 1: Introduction

Bardet-Biedl syndrome (BBS) is a rare genetic disease exhibiting complex patterns of inheritance with a prevalence of 1 in 100,000-160,000 live births in the USA and Northern Europe. It is a clinically heterogeneous disorder with primary features that include: age-related retinal dystrophy, obesity, polydactyly, renal dysplasia, reproductive tract anomalies and cognitive impairment. Classically BBS is inherited in an autosomal recessive manner, however several cases have indicated that BBS can be transmitted in a complex, non-Mendelian fashion, requiring mutations at more than one locus. BBS has recently been classified as a ciliopathy, thought to be caused by cilia and/or basalbody/centrosome dysfunction.

1.1 Bardet-Biedl Syndrome

1.1.1 History

The earliest official report of the disease was in 1865, when John Zachariah Laurence, an opthalmic surgeon, and Robert Moon, his then house-surgeon, published a report describing four out of eight siblings with retinitis pigmentosa (RP), lack of intelligence, short stature for their age and hypogenitalism in the males (Laurence and Moon, 1866). Significantly these patients were later re-examined and found to suffer from spastic paraparesis.

In 1920 George Bardet submitted his MD thesis on hypothalamic obesity, in which he noted that a number of patients also had unusual features such as hexadactyly and RP (Bardet, 1920). Two years later, an Austrian professor of pathology and endocrinology, Artur Biedl, published an account of siblings with congenital deformations (RP and polydactyly) and an 'intellectual torpidity' (Biedl, 1922). Neither Bardet nor Biedl cited the previous paper by Laurence and Moon. In 1925 Solis-Cohen and Weiss (Solis-Cohen and Weiss, 1925) rediscovered this paper and believed the two conditions to be the same, giving it the name Laurence-Moon-Bardet-Biedl or Laurence-Moon-Biedl Syndrome.

In 1969 Klein and Ammann (Klein and Ammann, 1969) published the first clinical and genetic population-based survey of BBS patients. Following a review of the literature, Ammann (Ammann, 1970) noted the differences between the syndromes reported by Laurence and Moon and Bardet and Biedl, thus prompting a split in the nomenclature. Laurence-Moon Syndrome (LMS) is characterised by RP, mental retardation, hypogenitalism and crucially spastic paraparesis, whilst Bardet-Biedl Syndrome (BBS) is characterised by similar features but with the addition of obesity and polydactyly, but notable absence of spastic paraparesis. The renal component of the disease was rarely noted before 1980 and so played no role in the initial accounts of the disease.

There is currently debate within the scientific community as to whether these two syndromes are in actual fact the same, with one perhaps a variant of the other. Interestingly, in a recent study looking at the clinical and genetic epidemiology of BBS in Newfoundland over a 22-year period, out of 46 patients only two were diagnosed clinically as LMS but both had mutations in a BBS gene (Moore *et al.*, 2005).

For the purpose of this study Bardet-Biedl syndrome will be referred to as BBS.

1.1.2 Prevalence

The hereditary nature of this disease had already been commented upon in the first known description by Laurence and Moon (Laurence and Moon, 1866), but only recently has its prevalence been estimated. BBS is estimated to occur in between 1 in 100,000 and 1 in 160,000 live births in the USA and Northern Europe (Klein and Ammann, 1969; Croft *et al.*, 1995; Beales *et al.*, 1997), classifying it as a rare genetic disease. However, there are certain

regions of the world in which BBS is more common. In mixed Arabic populations, the prevalence of BBS is 1 in 36,000, yet among the Bedouins of Kuwait it is as high as 1 in 13,500 (Farag and Teebi, 1989). The explanation for this lies in the high rates of consanguinity within this population, where first cousin marriages are particularly common (Al-Awadi *et al.*, 1985).

The prevalence in Newfoundland, a large island off the East coast of Canada, is 1 in 17,500 (Parfrey *et al.*, 2002). As well as consanguinity, this could be explained by a 'founder effect' of the original settlers, who can be traced back to a handful of families who emigrated from England in the early 1800s.

Due to the lack of medical awareness of this condition, and the difficulty of accurate diagnosis, it is thought that the prevalence of the disease might actually be higher than previously predicted.

In recent years research interest has shifted away from monogenic, Mendelian diseases, which collectively affect only a small fraction of the world's population, towards the more common multifactorial diseases. With BBS being one such rare disease, its study might be seen as improvident. However, whilst the occurrence of the disease itself is rare, the individual symptoms of the phenotype are common (i.e obesity, retinal degeneration, neurological symptoms). Additionally studies of such 'monogenic' diseases greatly improve our understanding of gene function, enable elucidation of both normal and pathological pathways, and ultimately contribute to our understanding of the molecular genetic basis of common complex diseases (Antonarakis, 2006).

1.1.3 Diagnosis

BBS can often be difficult to diagnose due to variation in the clinical phenotype present both between (interfamilial) and within (intrafamilial) families, and because many of the primary features are not present in the young or at birth. Clinicians can often be reluctant to diagnose BBS without

the development of a retinal phenotype. There have been several studies involving BBS patients to investigate the clinical phenotype (Klein and Ammann, 1969; Green *et al.*, 1989; Beales *et al.*, 1999; Moore *et al.*, 2005), the most extensive to date being carried out by Beales *et al.* (1999). In this review the authors propose a new scheme for diagnosis, modifying that proposed by Schachat and Maumenee (Schachat and Maumenee, 1982). Schachat and Maumenee's diagnostic criteria required only the presence of four out of five principal features (retinal degeneration, mental retardation, obesity, polydactyly, hypogonadism). The new diagnostic criteria from Beales *et al.* are the first to take into account the many secondary features often seen in BBS patients. They propose that a diagnosis should be made in the presence of either four primary features or three primary features and two secondary features. A list of primary and secondary features is shown in Table 1.1. The most recent study involving a large collection of patients was a 22-year prospective, population-based, cohort study on the clinical and genetic epidemiology of BBS (Moore *et al.*, 2005).

In the study by Beales *et al.* (1999) the average age of diagnosis was 9 years however the average age at which parents first noted abnormalities in their children was 3 years.

Diagnostic criteria as proposed by Beales *et al.*

Primary Features	
Rod-cone dystrophy	(93%)
Polydactyly	(69%)
Obesity	(72%)
Learning Disabilities	(62%)
Hypogonadism in males	(89%)
Renal anomalies	(52%)
Secondary Features	
Speech disorder/delay	(54%)
Strabismus/cataracts/astigmatism	(7%)
Brachydactyly/syndactyly	(46%/8%)
Developmental delay	(50%)
Polyuria/polydipsia (nephrogenic diabetes insipidus)	(6%)
Ataxia/poor coordination/ imbalance	(40%)
Mild spasticity (especially lower limbs)	(35%)
Diabetes mellitus	(6%)
Dental crowding/hypodontia/small roots/high arched palate	(27%)
Left ventricular hypertrophy/congenital heart disease	(7%)
Hepatic fibrosis	

Table 1.1: Summary of primary and secondary features observed in BBS patients. The disease is diagnosed upon the presence of either four primary features or three primary and two secondary features. In brackets, occurrence of individual phenotype amongst population of BBS patients (Beales *et al.*, 1999).

1.1.4 Clinical features

Presentation of the disease can vary greatly both between and within different families. No significant genotype-phenotype correlation between the various BBS loci has been observed. Previously Beales et al. observed possible minor effects on growth (1997), and Carmi et al. observed differences associated with limb distribution of postaxial polydactyly (1995a). Recently a study has proposed there to be slight phenotype-genotype correlation for the ocular phenotype (Heon *et al.*, 2005). The general lack of a genotype-phenotype relationship could be explained by the various BBS proteins either coming together to form a functional unit, or in their separate involvement of identical cellular processes.

Visual Disorders:

Rod-cone dystrophy (atypical retinitis pigmentosa) is the most consistent finding in patients, making accurate diagnosis difficult in its absence (Fig 1.1a). Retinal degeneration normally begins with night blindness at a mean age of 8.5 years and results in patients being registered blind by a mean age of 15.5 years (Beales *et al.*, 1999). Onset tends to be earlier and progression more rapid than in isolated cases of retinitis pigmentosa, with almost all patients suffering visual loss before their third decade (Klein and Ammann, 1969; Green *et al.*, 1989; Beales *et al.*, 1999). Other ocular abnormalities include astigmatism, strabismus, cataracts, colour blindness, myopia, macular oedema and degeneration, and optic atrophy. These other abnormalities often develop before retinal changes become apparent and can therefore assist in the diagnosis of the disease.

Limb Defects:

Polydactyly is observed in 58-69.1% of patients (Klein and Ammann, 1969; Green *et al.*, 1989; Beales *et al.*, 1999), and is almost exclusively postaxial (Fig 1.1b). The extra digit can vary from a skin tag to a fully formed digit. Polydactylous toes are three times more common than polydactylous fingers. Interestingly monozygous male twins with BBS have been observed, where one twin was born with postaxial polydactyly of three limbs, while the other had no polydactyly (Beales, P., personal communication). This suggests that despite identical genotype and similar intrauterine environment, complex influences affect limb differentiation. Brachydactyly is also present in approximately 50% of BBS patients and is more frequent in the feet than in the hands. A small number of patients also show syndactyly, which is usually partial, involving the second and third toe.

Height and Weight:

The extent of obesity among BBS patients varies between studies due to differences in measurement criteria. Klein and Amman (1969) reported obesity in 96% of their patients and Green *et al.* (1989) reported it in 88%; in

both of these studies patient weights were plotted on distribution charts. In the study by Beales *et al.* (1999), obesity was calculated according to the WHO body mass index classification (BMI=weight ÷ height^2), using this system 72% of patients were classified as overweight (BMI>25kg/m^2), and 52% obese (BMI>30kg/m^2). Excess weight gain does not usually begin until 1-2 years of age and occasionally may not present until puberty. The cause is as yet unknown but it appears to be due to a combination of hyperphagia and altered disposal of calories.

The study by Beales *et al.* (1999) also showed that whilst male BBS patients were significantly shorter than the average population, females were generally shorter but not significantly so (Fig 1.1c). An earlier study had suggested a gene locus effect on height, in which affected offspring were taller compared with their parents in the BBS1 category. However affected subjects in the BBS2 and BBS4 groups were significantly shorter than their parents (Beales *et al.*, 1997).

Learning Difficulties:

The degree of mental retardation observed in patients is difficult to assess, as IQ tests will be greatly affected by the visual impairments in patients. Klein and Ammann (1969) classified their patients as either mildly, moderately or severely mentally retarded and reported observing 'mild feeble-mindedness' in just over half of patients. Green *et al.* (1989) used appropriate verbal and performance tests to assess the IQ of their patients, and found 41% to be mentally retarded (IQ<70). Beales *et al.* (1999) reported 62% of patients having learning difficulties and half of these had received special education of some form. As with all symptoms of the disease, the degree of mental retardation is very varied and many patients have gone on to higher education.

Often patients report a deficit in short term memory, which is counterbalanced by excellent long term memory. A few patients have extraordinary mathematical abilities (Beales, P., personal communication).

Renal Anomalies:

Renal failure is the major cause of morbidity and early mortality in BBS patients. The abnormalities can be divided into structural and functional anomalies. Structural abnormalities include renal cysts, calyceal clubbing and blunting and fetal lobulation (Fig 1.1.d). Functional abnormalities include polydipsia and polyuria, which reflect the underlying inability to concentrate the urine (nephrogenic diabetes insipidus). In the study by Beales *et al.* (1999) 46% of patients that had undergone any radiological investigation of the renal tract were found to have renal abnormalities. Reports of the percentage of patients who develop end-stage renal disease (ESRD) varies. Beales *et al.* (1999) report 5%, whereas O'Dea *et al.* (O'Dea *et al.*, 1996) estimate that 25% of patients will have developed ESRD by the age of 48.

Genital Abnormalities:

In males, hypogonadism is almost universal, a small buried penis with reduced testes volume is usual and 10% have undescended testes at birth (Beales *et al.*, 1999). Males are usually infertile owing to primary gonadal failure. Fertility is more difficult to determine in females; irregular cycles are reported in the majority of women after menstruation (Beales *et al.*, 1999). Female genital abnormalities including vaginal atresia, persistent urogenital sinus and imperforate hymen have been reported (Cramer *et al.*, 1988; Schaap *et al.*, 1998; David *et al.*, 1999). Although initially assumed to be infertile, there have been reports of both male and female BBS patients giving birth to healthy offspring (Green *et al.*, 1989; Beales *et al.*, 1999).

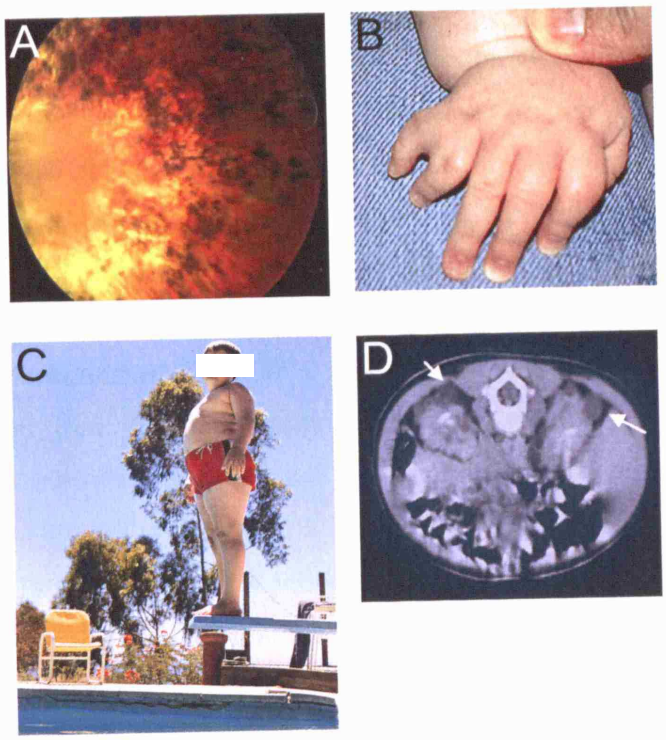

Figure 1.1: Primary features of BBS. A) Fundoscopy from a 32 year old patient showing rod-cone dystrophy. B) Postaxial polydactyly of the hand. C) Truncal obesity. D) Abdominal CT scan of an 11 year old patient, showing irregular shaped kidneys with multiple cysts (arrows).

Secondary Features:

In addition to the primary features of BBS, there are many other features that occur at varying frequency. The 1999 study by Beales *et al.* (1999) was the first to report the presence and frequency of many of the secondary features in a large patient cohort. Developmental delay is seen in about 50% of patients, neurological and motor defects are also common, in particular ataxia and poor co-ordination. Parents often comment on behavioral problems in young BBS patients, with certain traits continuing into adulthood. These include increased levels of emotional immaturity, frequent volatile outbursts, and poor reasoning. Hearing loss is also common; in Beales' study 21% of patients suffered hearing loss as a result of glue ear, but in most cases this was resolved by puberty. An additional three patients (~3%) had unexplained sensorineural hearing loss. Dental anomalies appear to be a common problem. Almost 90% of examined patients had a high arched palate and

malocclusion, crowding of the teeth was also common. Speech delay/deficit, requiring therapy was reported in 54% of patients. A number of patients also had a higher susceptibility to developing asthma. As with many other genetic syndromes, there appears to be a characteristic, albeit subtle, face associated with this syndrome; comprising deep set eyes, hypertelorism with downward-slanting palpebral fissures, a flat nasal bridge with anteverted nares and prominent nasolabial folds, a long philtrum, and a thin upper lip (Beales *et al.*, 1999; Lorda-Sanchez *et al.*, 2001). A study by Kulaga *et al.* (Kulaga *et al.*, 2004) showed that 47% of patients tested were completely or partially anosmic. Diabetes mellitus, congenital heart defects, hypertension and liver complications, are other symptoms that are seen in BBS patients in higher frequencies than in the general population (Klein and Ammann, 1969; Green *et al.*, 1989; Beales *et al.*, 1999).

1.1.5 Heterozygous effects

BBS is predominantly an autosomal recessive disease, the genetics of which is discussed in the following section. Heterozygous carriers of the disease have been shown to have an increased risk of developing features of BBS. The study by Beales et al. (2000) showed that there was an increased risk to parents of BBS patients of developing clear cell renal cell carcinoma (CC-RCC). 1.67% (3 out of 180) of parents developed CC-RCC. This is a 17 times higher incidence over the general population of developing CC-RCC. It was also noted that 4.1% (5 out of 123 siblings) of otherwise unaffected siblings developed renal malformations, a 20 times greater risk than in the general population.

A study by Croft and Swift (Croft and Swift, 1990) looked at a single extended family and found an increased incidence of obesity, renal disease, hypertension and NIDDM (type 2) in relatives of BBS patients. The authors suggested that this was due to partial disease manifestations in the heterozygous state, but also acknowledged that hypertension and diabetes in these individuals may be present as a result of their obesity. The same group

later published findings that 26.7% of fathers of BBS patients in America were obese, as compared to 8.9% of average American males (Croft *et al.*, 1995). In 1999, a study by Beales et al. (1999) found no evidence to support an increased incidence of obesity in relatives. The study was carried out on a large cohort of families and included 109 BBS patients, whereas Croft and Swift looked at just one family.

It has also been suggested that the high prevalence of BBS on the island of Newfoundland could be due to past selection for heterozygous individuals being able to store fat under the adverse conditions often experienced in the harsh winters (See section 1.1.2). To investigate this theory, the most common *BBS1* mutation, M390R (See 1.2.1), was screened in 200 obese and 200 non-obese Newfoundlanders. They found equal numbers of heterozygous mutations in the two groups, indicating that this mutation is not linked to obesity in the general population of Newfoundland (Fan *et al.*, 2004b). In the same study the BMI of obligate heterozygous carriers of *BBS1* mutations, were compared to the BMI of non carriers, no significant differences were found.

1.1.6 Related syndromes

There are many syndromes that share features common to BBS, which can lead to confusion amongst clinicians and possibility of misdiagnosis.

Laurence-Moon syndrome:
As described earlier, (see section 1.1.1) there is currently debate within the scientific community as to whether Laurence-Moon syndrome and Bardet-Biedl syndrome are the same or separate, distinct syndromes. Laurence-Moon patients are unlike BBS patients in that they develop spastic paraparesis and have no polydactyly.

McKusick-Kaufman syndrome (MKKS):

MKKS is more commonly seen in females than males and is predominantly observed in the Amish community. It is characterised by the presence of postaxial polydactyly, hydrometrocolpos (fluid filled uterus at birth) and congenital heart defects in 10-20% of patients (David *et al.*, 1999). In affected males the features are limited to polydactyly and occasionally genital anomalies such as micropenis or hypospadias. To avoid misdiagnosis, infants presenting with polydactyly and hydrometrocolpos should be monitored to see whether additional features of BBS develop. For more information see section 1.2.6.

Alström syndrome:

Truncal obesity, atypical retinitis pigmentosa and renal dysplasia are features common to both BBS and Alström syndrome. However Alström patients are also affected by sensorineural hearing loss, NIDDM, acanthosis nigricans, hypertriglyceridaemia and skeletal abnormalities (Marshall *et al.*, 2007).

Biemond II syndrome:

Features include obesity, polydactyly, hypogenitalism and mental retardation. But instead of retinitis pigmentosa, patients suffer from iris coloboma. Dwarfism is an additional feature of this disease which sets it apart from BBS (Schachat and Maumenee, 1982).

As I will go on to discuss, BBS has been shown to belong to a growing list of human ciliopathies caused by dysfunction of primary cilia and/or centrosomes or basal bodies. Defects in cilia function underlie polycystic kidney disease, retinitis pigmentosa and organ laterality disorders such as *situs inversus* (Rosenbaum and Witman, 2002). Over the past few years, a number of developmental diseases have been shown to be linked to cilial dysfunction. These include nephronophthisis, Joubert syndrome, Alström syndrome and Senior-Loken syndrome (Blacque and Leroux, 2006). Whilst these syndromes are phenotypically related, it remains to be seen whether they share common genetic loci. In support of this is the recently mapped Meckel-Grüber

syndrome, in which affected infants exhibit large occipital encephalocoele associated with renal cysts and sometimes polydactyly (Kyttala *et al.*, 2006; Smith *et al.*, 2006). The affected infants are usually stillborn. It has been proposed that Meckel-Grüber syndrome could be an antenatal presentation of BBS and the identification of BBS mutations in Meckel cases supports this theory (Karmous-Benailly *et al.*, 2005).

1.2 The genetics of BBS

BBS is an autosomal recessive disease displaying complex inheritance patterns. It was initially assumed that mutations in a single locus would account for all BBS cases, but early linkage studies showed that the disorder is in fact genetically heterogeneous. So far twelve loci for the disease have been identified, all of which have been cloned (*BBS1-BBS12*). Despite the mapping of twelve loci for the disease, a large proportion (~25%) of patients remain unlinked to any of these loci (mostly patients of Middle-Eastern or Asian origin), indicating the existence of additional BBS loci within the human genome (Stoetzel *et al.*, 2007).The first three *BBS* genes, (*BBS6*, *BBS2* and *BBS4*) were identified using standard positional cloning techniques. More recently a similar approach identified *BBS10*. High-density single-nucleotide polymorphism (SNP) microarray genotyping was used to identify the two most recently discovered *BBS* genes, *BBS11* and *BBS12*. The remaining six genes were identified with the help of bioinformatics- and genomics-based approaches, by applying these to probe uncloned genetic loci for candidate *BBS* genes. *BBS1* and *BBS7* were identified based on limited protein sequence similarity to *BBS2*, and *BBS8* on account of its protein similarity to *BBS4*. The remainder, *BBS3*, *BBS5* and *BBS9* were identified by the use of comparative genomic analyses.

1.2.1 BBS1

The interval for the most common gene found to be responsible for BBS was mapped in 1994 (Leppert *et al.*, 1994). This gene, *BBS1* (11q13), was finally cloned in 2002 and is comprised of 17 exons (Mykytyn *et al.*, 2002). Mutations in *BBS1* account for 23-56% of BBS cases (Blacque and Leroux, 2006). Within the gene, the M390R mutation is the most commonly reported, accounting for ~80% of cases of *BBS1* (Mykytyn *et al.*, 2003). The function of BBS1 is unknown but it shows 23% identity and 40% similarity over 192 amino acids with BBS2 (Badano *et al.*, 2003a). The predicted protein structure contains a hypothetical domain, predicted to encode a six-bladed β-propeller (see Fig 1.2). A β-propeller is a type of all-β protein architecture characterized by 4-8 blade-shaped beta sheets arranged toroidally around a central axis. Each sheet typically has four antiparallel β-strands twisted so that the first and fourth sheets are almost perpendicular to each other. Such protein domains are found in all organisms, but there is a strong prevalence of such domains in eukaryotes (Chaudhuri *et al.*, 2007).

1.2.2 BBS2

The locus for *BBS2* was the first BBS locus to be found. It was initially mapped to an 18cM interval on chromosome 16q21 by Kwitek-Black *et al.* (1993), which was then reduced to 2cM by haplotype analysis of eight linked pedigrees by Nishimura *et al.* (2001). Physical mapping and sequence analysis led to the identification of *BBS2* at 16q21 (Nishimura *et al.*, 2001). This gene contains 17 coding exons and has a predicted protein product of 721 amino acids. The gene is widely expressed, with strongest expression in the fetal and adult kidney, adult heart, skeletal muscle, thyroid, spinal cord and adrenal gland. Homology screening of the predicted BBS2 protein against the public sequence databases demonstrated that BBS2 has high similarity within a number of other organisms, the mouse protein being 90% identical and 95% similar to the human protein (Nishimura *et al.*, 2001). The function of the gene is as yet unknown, but it shares structural features with *BBS1* and *BBS7*. Within the protein structure, a hypothetical domain predicted to encode

a six-bladed β-propeller structure has been identified (see Fig 1.2). Mutations in *BBS2* account for 8-16% of BBS cases (Blacque and Leroux, 2006).

1.2.3 BBS3

BBS3 was mapped to chromosome 3p12-13 by Sheffield *et al.* (1994) using conventional linkage analysis. In 1998 Young et al. confirmed this locus and reduced the critical region to a 6-cM interval by haplotype analysis on a Newfoundland kindred (Young *et al.*, 1998). The same location for *BBS3* was identified by Ghadami et al. in 2000 through linkage analysis on an Iranian family (Ghadami *et al.*, 2000). The gene was finally cloned in 2004 (Fan et al.), using a bioinformatics screen for ciliary genes in combination with mutational analyses. This bioinfomatic screen is discussed in detail in chapter 4, but it is based upon the identification of a consensus RFX transcription factor binding site (termed an X-box) observed in a subset of genes expressed exclusively in ciliated cells in *C.elegans.* All known *bbs* orthologues were shown to contain such an X-box, and as such genes containing an X-box made good candidates for identification of further disease genes. *BBS3* was identified as *ARL6*, a member of the Ras superfamily of small GTP-binding proteins. ARL6 is the first BBS-associated protein to be identified whose evolutionarily conserved sequence immediately suggests a cellular function, namely that of a small GTP-binding protein involved in membrane-associated intracellular trafficking processes (Takai *et al.*, 2001). Mutations in *BBS3* are thought to only contribute to 2-4 % of BBS cases (Blacque and Leroux, 2006). The identification of *BBS3* is discussed in chapter four.

1.2.4 BBS4

Using DNA pooling in a large Bedouin kindred, *BBS4* was mapped to chromosome 15q23 by Carmi et al (1995b). The gene was cloned in 2001 by Mykytyn *et al.* (2001) and is comprised of 16 exons encoding a 519 amino acid protein. The gene is ubiquitously expressed, including expression in fetal tissue, retina and adipose tissue, with the highest level of expression seen in

the kidney. The genomic sequence for *BBS4* contains 40 Alu repeats, 12 of which are found in intron 2. The high frequency of these repeats may predispose this gene to mutations through unequal homologous recombination events. Mutations in *BBS4* contribute to only 3% of BBS cases (Blacque and Leroux, 2006).

The predicted protein sequence shows strong homology to O-linked N-acetylglucosamine (O-GlcNAc) transferase (OGT)- which has been implicated in insulin resistance and may play a role in diabetes (Mykytyn *et al.*, 2001). The protein also contains 13 tetratricopeptide repeat (TPR) motifs, which are commonly involved in protein-protein interactions (Mykytyn *et al.*, 2001; Kim *et al.*, 2004). More recently BBS4 has been shown to localise to the centriolar satellites of centrosomes and basal bodies of primary cilia. Here it recruits the pericentriolar material 1 protein (PCM-1) and its associated cargo to the satellites by functioning as an adaptor of the $p150^{glued}$ subunit of the dynein transport machinery (Kim *et al.*, 2004). PCM-1 is necessary for microtubule anchoring, cell cycle progression and recruiting several proteins to the centrosome (Kubo *et al.*, 1999; Young *et al.*, 2000; Dammermann and Merdes, 2002).

Silencing of BBS4 in cultured cells leads to PCM-1 mislocalisation and deanchoring of microtubules, arrest of cell division and apoptotic death. It is believed that cellular defects due to *BBS4* mutations arise from its interactions with PCM1 (Kim *et al.*, 2004). BBS4 also interacts with $p150^{glued}$, a subunit of dynactin. In turn dynactin interacts with dynein and is required for dynein-associated movement along microtubules. This suggests that BBS4 is involved in intraflagellar transport (Kim *et al.*, 2004). The BBS4 protein shows partial sequence homology to BBS8 (Ansley *et al.*, 2003). Further analysis of the BBS4 protein is discussed in chapter nine.

1.2.5 BBS5

BBS5 was the fifth locus to be mapped and the first to be found in a large inbred family of European ancestry. Young *et al.* (1999) mapped the gene to chromosome 2q31. A comparative genomics approach that subtracted the nonflagellated proteome of *Arabadopsis* from the shared proteome of the ciliated/flagellated organisms *Chlamydomonas* and human, helped to identify *BBS5* (Li *et al.*, 2004). Mutations in *BBS5* are thought to contribute to only 3% of BBS cases (Blacque and Leroux, 2006). The identification of *BBS5* is discussed in chapter four.

1.2.6 BBS6

BBS6 was the last BBS gene to be mapped by conventional linkage analysis, yet it was the first to be cloned and the first to shed light on the possible function of BBS genes. Following the identification of several Newfoundland samples that were unlinked to BBS1-5 (Woods *et al.*, 1999) it was evident that other loci existed. Katsanis *et al.* (2000) was able to identify a critical interval of 1.9cM on chromosome 20p12.

The gene for McKusick-Kaufman syndrome (MKKS) had recently been identified in the same region (Stone *et al.*, 2000). MKKS comprises hydrometrocolpos (fluid filled uterus at birth), polydactyly, and congenital heart defects. Given the clinical overlap between these two syndromes, and the concordant mapping position of the two genes, it was hypothesised that MKKS was a good candidate gene for BBS6. Two studies confirmed that this was the case by the identification of a number of mutations in the *MKKS* gene in BBS patients (Katsanis *et al.*, 2000; Slavotinek *et al.*, 2000). It was suggested that most mutations in MKKS cause BBS whereas milder, less severe mutations cause MKKS. The MKKS protein shows similarity to type II chaperonins, which aid the folding and structural modification of other proteins (Stone *et al.*, 2000). The protein has been shown to be expressed in a wide range of tissues including heart, brain, liver, skeletal muscle, kidney and retina (Slavotinek *et al.*, 2000). It is thought that the complete loss of function of the

MKKS product, and thus an inability to fold a range of target proteins, is responsible for causing some of the clinical features of BBS. Mutations in this gene are seen in ~6% of cases (Blacque and Leroux, 2006).

Recent studies show that MKKS/BBS6 is a Group II chaperonin-like protein that has recently evolved in animals from a subunit of the eukaryotic chaperonin CCT/TRiC, and diverged rapidly to acquire distinct functions. Cytosolic BBS6 does not oligomerise, unlike other chaperonins, and the majority of BBS6 resides within the pericentriolar material (PCM), a proteinaceous tube surrounding centrioles. During interphase BBS6 is confined to the lateral surfaces of the PCM but during mitosis it relocalises throughout the PCM and is found at the intercellular bridge. Its predicted substrate-binding apical domain is sufficient for centrosomal association and consistent with centrosomal function, silencing of the *BBS6* transcript by RNA interference in different cell types leads to multinucleate and multicentrosomal cells with cytokinesis defects. Restricted tissue distribution of BBS6 suggests it may play a role in ciliated epithelial tissues (Kim *et al.*, 2005).

Phylogenetic analysis of BBS6 shows that it is widely spread in animals. The absence of orthologue *BBS6* genes from *C. elegans* or *Drosophila melanogaster* further suggests that BBS6 emerged before the appearance of vertebrates but after the protosome/deuterostome split (Kim *et al.*, 2005).

Further analysis of the BBS6 protein is discussed in chapter five, six and seven.

1.2.7 BBS7

Unlike the previously cloned BBS genes, BBS7 was not identified using a conventional approach of linkage mapping and positional cloning, rather it was identified though its similarity to *BBS2*. Fragments of the BBS2 peptide sequence were screened against the human EST database (dbEST). Two genes with modest similarity were found. One was shown to be the previously

identified *BBS1* gene, and the other a novel gene known as *BBS7,* in which disease-causing mutations were identified in patients (Badano *et al.*, 2003a). Mutations in BBS7 are found in 3.5% of BBS patients (Blacque and Leroux, 2006).

BBS7 was shown to map to 4q27, a region of the genome not previously associated with BBS genes, and is comprised of 19 exons. The gene is expressed in a wide range of tissues, including testis, ovary, retina, brain and kidney. The BBS7 protein exhibits similarity with a 252-amino acid region of BBS2. SMART analyses of this region of BBS2 detected a hypothetical domain predicted to encode a six-bladed β-propeller structure (Schultz *et al.*, 2000), a prevalent supersecondary structure with mulitple functions (Jawad and Paoli, 2002). Local alignment of BBS1, BBS2 and BBS7 indicate that both BBS1 and BBS7 include partially overlapping portions of this domain (Fig 1.2). Dysfunction of this domain could explain how mutations at different BBS loci result in an identical phenotype (Badano *et al.*, 2003a).

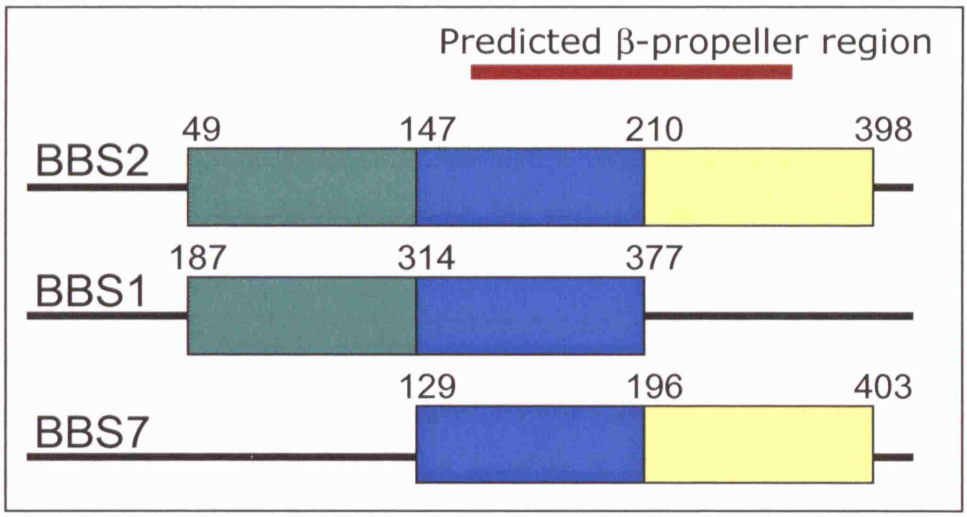

Figure 1.2: A potential domain shared between multiple BBS proteins. Schematic representation of the region of overlap between the three proteins BBS1, BBS2 and BBS7. Regions of homology are depicted in like coloured boxes. Numbers correspond to amino acid residues.

In *Caenorhabditis elegans*, loss of function mutations in *BBS7* result in structural and functional ciliary defects, including shortened/abnormal cilia and chemosensory abnormalities. More specifically BBS7, has been shown to be required for the normal localisation/motility of IFT proteins (Blacque *et al.*, 2004).

1.2.8 BBS8

Identification of the *BBS8* locus has provided us with the most clues as to a possible disease mechanism, namely that BBS proteins play a role in ciliary function. The majority of what is known about *BBS8* is the result of an initial study by Ansley *et al.* (2003).

In the same way that *BBS7* was cloned, *BBS8* was identified by its similarity to another BBS protein, *BBS4*. Fragments of the BBS4 protein were used to screen the conceptual translation of the human genome and dbEST. BBS4 contains at least ten tetratricopeptide repeats (TPRs), which lead to the identification of numerous TPR-containing transcripts. One such transcript

which maps to chromosome 14q32.11, was of particular interest as it contained three tandem TPR domains. Screening of this hypothetical gene, *TTC8,* in BBS patients led to the identification of disease-causing mutations in three pedigrees, confirming that this was a novel BBS gene, thus defining an eighth locus for this disorder, *BBS8.* Mutations in BBS8 contribute to 1-2% of BBS cases (Blacque and Leroux, 2006).

BBS8 generates two alternatively spliced isoforms, and is specifically expressed in ciliated structures such as the connecting cilium of the retina. In cells, BBS8 has been shown to localise to the centrosome. The protein contains eight TPR domains situated towards the carboxyl terminus and exhibits significant similarity to the prokaryotic pilF domain, which is involved in twitching mobility and type-IV pilus assembly (Maurer and Orndorff, 1987; Merz *et al.*, 2000). These data indicate that BBS8 may be involved in the function of cilia, flagella or pseudopodia. Interestingly, one of the patients with mutations in *BBS8* was also shown to have *situs inversus*, a known defect of left-right axis determination caused by dysfunction of the nodal cilium (Nonaka, 1998). Co-localisation studies have shown that the intracellular pattern of BBS8 is similar to BBS4 near the centrosome (Ansley *et al.*, 2003). Importantly it was observed that BBS8 also interacts with the C terminus of the BBS4-interacting protein PCM1. Studies on *C. elegans* show that BBS8 expression is strictly limited to ciliated cells (Ansley *et al.*, 2003) and loss of BBS8 protein function, as with BBS7, results in cilia defects and compromised intraflagellar transport (Blacque *et al.*, 2004).

1.2.9 BBS9

The identification of *BBS9* in 2005 utilised a three pronged approach. Homozygosity mapping in small consanguineous BBS pedigrees, comparative genomics and comparative expression data generated by microarray analysis of $Bbs4^{-/-}$ animals, identified high-priority genes for mutation screening in selected BBS patients. Mutations of the *B1* gene on chromosome 7p in BBS patients concluded this gene to be BBS9 (Nishimura *et al.*, 2005). The B1

protein has no similarity to the other known BBS proteins and its specific function is unknown.

1.2.10 BBS10

Identification of the *BBS10* gene proved it to be a major locus for BBS. In 2006 traditional linkage analysis identified mutations in this gene in about 20% of BBS patients of various ethnic origins. A single-nucleotide insertion at residue 91, leading to premature termination four codons later (C91fsX95) was shown to account for roughly half of mutant alleles (Stoetzel *et al.*, 2006). This gene encodes a previously unknown, vertebrate-specific chaperonin-like 723 residue protein. The sequence homology of BBS10 to archaeal chaperonins and the eukaryotic CCT proteins (chaperonin containing TCP-1; proteins involved in the folding of actins and tubulins (Valpuesta *et al.*, 2002)) is reminiscent of BBS6 and suggests possible roles in protein folding or assembly (Stoetzel *et al.*, 2006).

1.2.11 BBS11

Homozygosity mapping using SNP microarrays identified *TRIM32*, an E3 ubiquitin ligase as *BBS11*. Whilst the authors state that *TRIM32* expression is strongly correlated with expression of other BBS genes (in the mammalian eye and hypothalamus) and knockdown of TRIM32 in zebrafish reveals similar BBS phenotypes (see chapter ten), the identification of only a single BBS patient with a mutation in this gene casts doubt over its role as a BBS gene (Chiang *et al.*, 2006). Loss of function mutations in this gene causes limb-girdle muscular dystrophy, a disease with no phenotypic overlap with BBS (Saccone *et al.*, 2007).

1.2.12 BBS12

The most recent BBS gene identified to date is *BBS12*. As with *BBS11*, homozygosity mapping using SNP microarrays combined with *in silico*

analysis (database searches/protein sequence alignment) identified a candidate gene predicted to encode a protein with similarity to members of the type II chaperonin superfamily, which includes BBS6 and BBS10. Pathogenic mutations identified in ~5% BBS patients confirmed the identification of *BBS12*. Like *BBS10* and *BBS6*, *BBS12* is only present in vertebrates, from fish to human (a distant BBS6 homologue, however, has been reported in the urochordate C. intestinalis), and together they define a novel branch of the type II chaperonin superfamily (Stoetzel *et al.*, 2007).

These three genes, *BBS6*, *BBS10* and *BBS12*, are characterised by unusually rapid evolution and are likely to perform ciliary functions specific to vertebrates that are important in the pathophysiology of the syndrome. Taken together they account for about one-third of the total BBS mutational load.

The table on the following page summarises all the BBS loci identified to date. So far 12 genes have been cloned. It is likely that yet more BBS genes remain undiscovered as there are still BBS patients with no mutations in the known genes.

Locus	Position	Identification	Protein	Domains	Function	Contribution	Reference
BBS1	11q13	Positional cloning/homology to BBS2	Novel *	β-propeller	Cilia function	23-56%	Mykytyn *et al.*, 2002
BBS2	16q21	Positional cloning	Novel *	β-propeller	Cilia function	8-16%	Nishimura *et al.*, 2001
BBS3	3p13	Positional cloning/ comparative genomics	ARL6	GTP-binding	Vesicle trafficking	2-4%	Fan *et al.*, 2000
BBS4	15q23	Positional cloning	TPRs/OGT	TPR/PilF	Microtublue transport	3%	Mykytyn *et al.*, 2004
BBS5	2q31	Positional cloning/ comparative genomics	Novel		Cilia function	3%	Li *et al.*, 2004
BBS6	20p12	Positional cloning	MKKS	TCP I Chaperonin	Cilia function/putative chaperone	6%	Katsanis *et al.*, 2000
BBS7	4q32	Homology to BBS1/2	Novel*	β-propeller	Cilia function	3.5%	Badano *et al.*, 2003a
BBS8	14q31	Homology to BBS4	TPR	TPR/PilF	Cilia function	1-2%	Ansley *et al.*, 2003
BBS9	7p14	Positional cloning/comparative genomics/comparative expression	B1		Unknown		Nishimura *et al.*, 2005
BBS10	12q21.2	Positional cloning	Novel	TCP I Chaperonin	Putative chaperone	20%	Stoetzel *et al.*, 2006
BBS11	9q33.1	SNP array	TRIM32	Ring WD40 NHL	E3 ubiquitin ligase		Chiang *et al.*, 2006
BBS12	4q27	SNP array/ comparative genomics	Novel		Type II chaperone	5%	Stoetzel *et al.*, 2007

Table 1.2: Summary of known BBS genes. SNP, single nucleotide polymorphism; ARF, ADP-ribosylation factor; ARL, ARL-like; TPR, tetratricopeptide; OGT, O-linked N-acetylglucosamine transferase; MKKS, McKusick-Kaufman syndrome, TRIM, tripartite motif; PilF, pilus formation; TCP tail-less complex polypeptide

1.2.13 Complex inheritance in BBS

Genetic disorders have historically been divided into Mendelian (involving mutational events at one locus) and complex (requiring mutations in more than one gene and/or environmental factors) disorders. Recent studies have suggested that some disorders bridge these two categories whereby the combinatorial effect of mutations at distinct loci is necessary and sufficient for pathogenicity. BBS appears to be an important example of this model of disease transmission as it has been proposed to be inherited either as an autosomal recessive or as an oligogenic trait (Katsanis *et al.*, 2002).

Based on segregation patterns observed within pedigrees and populations, BBS was traditionally considered to be an autosomal recessive disorder. However, in 2001, after screening a cohort of 163 BBS families for mutations in *BBS2* and *BBS6*, a proposed model of triallelic inheritance was put forward, in which three mutant alleles at two loci segregate with the disease (Katsanis *et al.*, 2001). Since then triallelism has been reported to varying degrees in the majority of cloned BBS genes. Oligogenic inheritance has been reported for *BBS1*, *BBS2*, *BBS3*, *BBS4*, *BBS6*, *BBS7* and *BBS10* (Katsanis *et al.*, 2002; Badano *et al.*, 2003b; Beales *et al.*, 2003; Fan *et al.*, 2004a; Stoetzel *et al.*, 2006). This observation suggests that genetic interactions between the different BBS loci may modulate the phenotype, thus contributing to the clinical variability of the disease. Complex inheritance is also suggested by the identification of an excess of heterozygous BBS individuals where only one mutant allele has been discovered, demonstrating that additional BBS gene mutations are necessary for disease manifestation (Beales *et al.*, 2003; Fauser *et al.*, 2003; Hichri *et al.*, 2005).

All BBS loci might interact genetically with each other, but some genes, especially *BBS2* and *BBS6*, are more likely to participate in triallelic inheritance, suggesting a variable ability of BBS proteins to interact genetically with each other (Beales *et al.*, 2003). Triallelic mutations are not always necessary for manifestation of the disease, but might potentiate a

phenotype that is caused by two recessive mutations at an independent locus, thus introducing an additional layer of complexity on the genetic modeling of oliogogenicity (Badano *et al.*, 2003b).

Evidence for non-Mendelian inheritance has been reported in two other related disorders, Senior Löken syndrome (SLS) and Nephronophthisis (Mollet *et al.*, 2002; Olbrich *et al.*, 2003; Otto *et al.*, 2003) (Hoskins B, Thesis). Furthermore in addition to contributing to non-Mendelian inheritance in BBS patients, *BBS4* and *BBS6* have also be found to be associated with complex inheritance in these two disorders (Hoskins B, Thesis), adding a degree of complexity to the genetic/phenotypic overlap between these syndromes.

1.3 Cilia

As described above, the first breakthrough in the understanding of the aetiology of BBS was the identification of *BBS8*, which showed that BBS was probably caused by a defect at the basal body of ciliated cells (Ansley *et al.*, 2003). Since then this link has been corroborated, and as such BBS has been classified as one of the many emerging ciliopathies. Many of the symptoms associated with the disease are related to primary cilia dysfunction and so understanding this organelle is key to further unraveling the pathological mechanisms underlying the disorder.

1.3.1 Cilia structure and function

Cilia and flagella are long appendages that extend from the cell body. These structures are usually referred to as 'cilia' when they occur together in large numbers, or as 'flagella' when they occur singly. In either case they have a similar internal structure (9+0 vs 9+2; see Fig. 1.3) and are composed of many of the same proteins so the terms are often used interchangeably.

Cilia and flagella contain a long microtubular axoneme surrounded by an external membrane that is continuous with the plasma membrane of the cell

(Fig 1.3). There are two types of cilia, which differ slightly in their structure and function. In nearly all motile cilia, the internal structure consists of a '9+2' axoneme that contains nine outer doublet microtubules and two central microtubules. The axoneme also contains inner and outer dynein arms that generate the force for motility, and radial spokes which regulate the motile machinery along with central pair projections. Many vertebrate cells have a single cilium called a 'primary' cillium. These are generally non-motile and have a '9+0' axoneme, lacking the central pair of microtubles present in motile cilia.

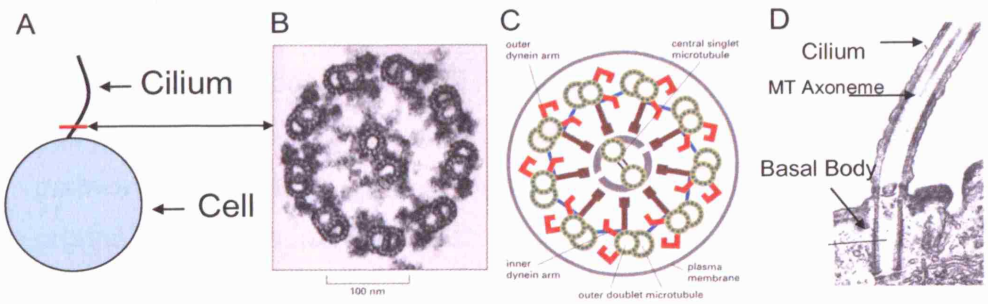

Figure 1.3: The arrangement of microtubules in a cilium or flagellum. A) Schematic representation of a cilium. Red bar and arrow show plane of cross section for electron micrograph in B. B) Electron micrograph of the flagellum of *Chlamydomonas* shown in cross-section, illustrating the distinctive '9+2' arrangement of microtubules in motile cilia. C) Diagram of the parts the various projections from the microtubules link them together and occur at regular intervals along the length of the axoneme. D) Electron micrograph of a cilium shown as a length wise cross section. A,B,C taken from Molecular Biology of the Cell, Third Edition. D, adapted from http://www.cytochemistry.net/microanatomy/epithelia/cilia1.jpg MT Microtubular

At its proximal end, the cilial axoneme is continuous with a basal body, consisting of a ring of three triplet microtubles, which anchors it in the cell (Rosenbaum and Witman, 2002). The basal body is a modified centriole that serves as the foundation upon which the cilium is constructed. Cilia grow from the distal end of the basal body, and the doublet microtubules are directly nucleated by the microtubules found in the basal body (Deane *et al.*, 2001). Moreover the basal body appears to act as a docking site for proteins involved

in ciliary transport (Deane *et al.*, 2001). The majority of the BBS proteins have been localised to the basal body and/or ciliary axoneme (see figure 1.5) (Beales, 2005).

Motile cilia serve to move fluid across membrane surfaces, for example mucus in the airway. Non-motile primary cilia transduce a multitude of sensory stimuli, including chemical concentrations of growth factors, hormones, odorants, and developmental morphogens, as well as osmolarity, light intensity and fluid flow. Several properties of cilia facilitate their role as sensory transducers. They project away from the cell body, and so serve as good probes of the external milieu; their overlying membrane and cytoplasmic contents are relatively well isolated from the cell body; the machinery for their assembly makes possible rapid, regulated transport to and from the cell body; and the assembly machinery seems exploitable for use directly in signaling pathways (Snell *et al.*, 2004). Indeed cilia play key roles in many sensory organs. For example, the outer segments of retinal rod cells are modified, non-motile cilia (Tsujikawa and Malicki, 2004), odorant receptors in the olfactory epithelium contain cilia of olfactory neurons (Kulaga *et al.*, 2004), even many neurons in the brain contain primary cilia (Fuchs and Schwark, 2003).

Cilia have evolved a complex ultrastructure to accommodate their diverse functions, and extensive molecular machinery has developed to support the assembly of these organelles. The cilium itself does not contain any machinery for protein synthesis and so all proteins needed for its maintenance and function must be transported along its microtubular axoneme. This process has been termed intraflagellar transport and is integral to the cilium's structure and function (Cole, 2003).

1.3.2 Intraflagellar transport

During ciliary growth, the axoneme is assembled by the addition of new subunits to its distal tip. As cilia lack the machinery for new protein synthesis,

all materials needed are transported along the axoneme by a process called intraflagellar transport (IFT). During IFT, non-membrane-bound particles are moved continuously along the axonemal doublet microtubules, just beneath the base of the membrane (Fig 1.4). Much of our knowledge of the protein machinery and basic biology has come from studies of the biflagellate alga *Chlamydomonas reinhardtii*. In 1993 Kozminski et al. (Kozminski *et al.*, 1993) observed particles of varying sizes moving in both the anterograde (base to tip) and retrograde (tip to base) direction along the *Chlamydomonas* flagellum. Upon observing varying rates of anterograde and retrograde transport they hypothesised that different motor molecules were involved. Additionally, all flagellar microtubles are orientated with their plus ends at the distal tip (Allen and Borisy, 1974), therefore there must be separate motors for anterograde and retrograde IFT. The specific motors that move IFT particles were defined using mutants that were defective for the genes encoding motor subunits. The anterograde motor was shown to be kinesin-II, a heterotrimeric kinesin (Kozminski *et al.*, 1993), and the retrograde transport motor was identified as cytoplasmic dynein 1b (Pazour *et al.*, 1998; Pazour *et al.*, 1999).

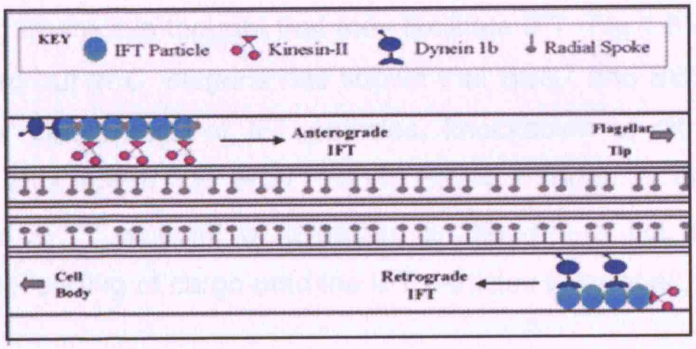

Figure 1.4: The IFT transport machinery. During IFT linear arrays of IFT particles are transported towards the tip of the flagellum by Kinesin-II and back towards the cell body by dynein 1b. The IFT particles, which are composed of at least 17 different proteins, are believed to be carrying precursors that are necessary for the assembly of the axoneme. The IFT particles are linked to the flagellar membrane, which indicates that their cargo might also include membrane proteins. Figure taken from http://www.proweb.org/kinesin/IFT.html

During IFT these motors transport linear arrays of IFT particles, also known as IFT rafts along the axoneme (Brown and London, 1998). IFT rafts are divided

into two complexes: Complex A which is composed of at least five distinct polypeptides, and Complex B comprising at least 12 polypeptides (Cole *et al.*, 1998; Piperno *et al.*, 1998). Experiments have shown that IFT particle proteins are recycled after they have returned to the cell body. The mechanisms by which IFT-particle turn-around, cargo loading and release, and motor exchange occurs at the base and tip of the flagellum are unknown, but it might involve phosphorylation and dephosphorylation of motors and/or their associated proteins.

The amino acid sequences of many of the *Chlamydomonas* IFT particle proteins have been predicted, and database searches show that virtually all have homologues in many other ciliated organisms including *C.elegans*, *Drosophila melanogaster*, mouse and human, but not in organisms that lack cilia such as yeast and *Arabidopsis thaliana*. It is therefore probable that IFT is an ancient process that is necessary for assembly and maintenance of all eukaryotic cilia and flagella.

Many of the BBS proteins have been shown to localise to the cilium and/or the basal body, where it is thought that they facilitate IFT (Fig 1.5)(Beales, 2005). Work carried out in *C. elegans* has shown that BBS7 and BBS8 proteins are required for stabilisation of IFT particles, knockdown of either resulting in diminished cilia length (Ou *et al.*, 2005). BBS4, through its direct interaction with the $p150^{Glued}$ subunit of dynactin, is thought to act as an adaptor, assisting the loading of cargo onto the IFT particles (Kim *et al.*, 2004).

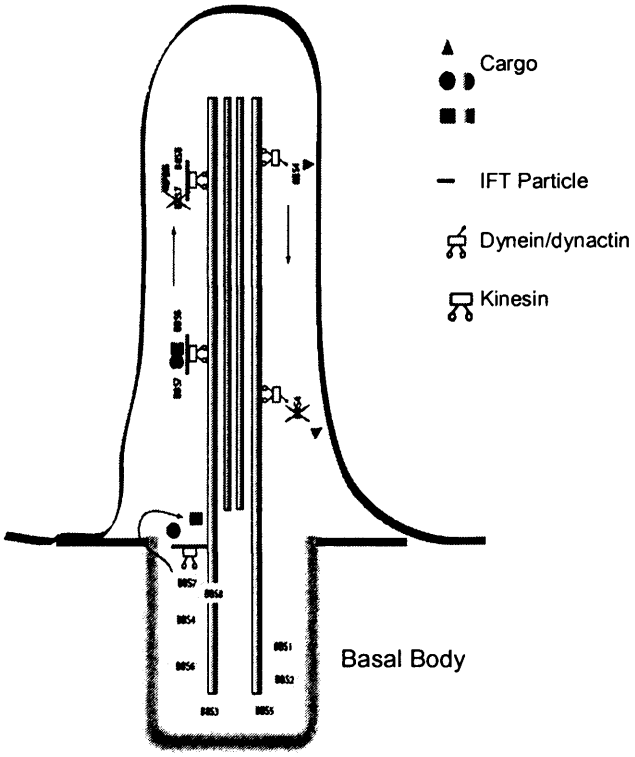

Figure 1.5: Schematic representation of the localisation of the BBS proteins to the cilium and basal body. BBS4, BBS7 and BBS8 have been shown to facilitate the assembly of IFT proteins onto IFT particles. Figure adapted from (Beales, 2005).

1.3.3 Cilia and disease

Discovery of the IFT process has led to a better understanding of the role cilia play in normal physiology and disease. As the cilium is a ubiquitous organelle, mutations that affect its structure or function have a wide range of effects.

The first correlation between IFT and disease came as a result of the characterisation of several IFT particle proteins, and recently Jeune asphyxiating thoracic dystrophy was identified as the first human disease directly caused by defects in an IFT protein, IFT80 (Beales *et al.*, 2007). However initial findings were based on the *Chlamydomonas* Complex B subunit, IFT88, which has an ortholog in the mouse encoded by the *Tg737* gene. *Chlamydomonas* with defects in IFT88 lack flagella, whilst mice with a mutation in *Tg737* develop autosomal recessive polycystic kidney disease (ARPKD)(Pazour *et al.*, 2000). ARPKD is characterised by epithelial cell

proliferation, cysts in the kidney and various cardiovascular problems. The mouse *Tg737* product (polaris) is localised to the basal bodies and along the ciliary axoneme and has been implicated in left-right patterning. In both mice and humans, ARPKD involves the altered differentiation and proliferation of the epithelial cells in the collecting ducts and tubules of the kidney. The primary cilium on each renal tubule cell functions as a flow sensor and it is presumed that this process is in some way altered in the disease state.

Autosomal-dominant polycystic kidney disease (ADPKD) has a similar phenotype to ARPKD, although the symptoms may not become apparent until the patient reaches middle age (Grantham *et al.*, 1996). Primary defects are in the genes *PKD1* and *PKD2,* encoding the protein polycystin 1 and 2, both of which are located primarily on the ciliary membrane (Pazour *et al.*, 2002b; Yoder *et al.*, 2002). Localisation of the polycystins strongly indicates that the kidney primary cilium is a sensory organelle that initiates a signal transduction pathway that controls cell differentiation and proliferation. Additionally it has been shown that when bent, kidney primary cilia initiate a Ca^{2+} signal that spreads throughout the cell (Praetorius and Spring, 2001). This supports the hypothesis that these cilia are mechanoreceptors that monitor the rate of fluid flow through the collecting ducts and tubules (Schwartz *et al.*, 1997).

Cilia, or structures derived from cilia are also involved in the development and function of several sensory organs, including the retina, inner ear and nasal epithelium (Fig 1.6). IFT plays an important part in maintaining the outer segments of retinal rod and cone cells. The inner segments (IS) and outer segments (OS) of vertebrate photoreceptor cells are joined by a narrow cytoplasmic bridge containing a modified cilium, the connecting cilium (9+0 and non-motile) (Fig 1.6 A). Protein synthesis occurs in the IS and proteins are then transported to the OS via IFT (De Robertis, 1958; Young, 1976). The degeneration of rod cells that results from defects in IFT-motor and IFT-particle proteins is very similar to that observed in retinitis pigmentosa. Mice with a mutation in *Tg737* display progressive retinal degradation which leads to a complete degeneration of rod cells (Pazour *et al.*, 2002a).

Cilia are also found on the hair cells within the inner ear (Fig 1.6 B). The hair bundles on these cells are formed from rows of stereocilia, microvillar-like projections that contain actin and are sometimes known as stereovilli. These are not true cilia, a single true cilium, the kinocilium, lies behind the row of the tallest stereocilia. In mammals the kinocilium disappears soon after birth, but it has an important role in positioning the stereocilia, which are responsible for producing an electrical signal, or receptor potential, in response to mechanical stimulation. Disruption of the stereocilia can cause hearing defects such as in Usher Syndrome (Self *et al.*, 1998; Alagramam *et al.*, 2001; Di Palma *et al.*, 2001; Johnson *et al.*, 2003)

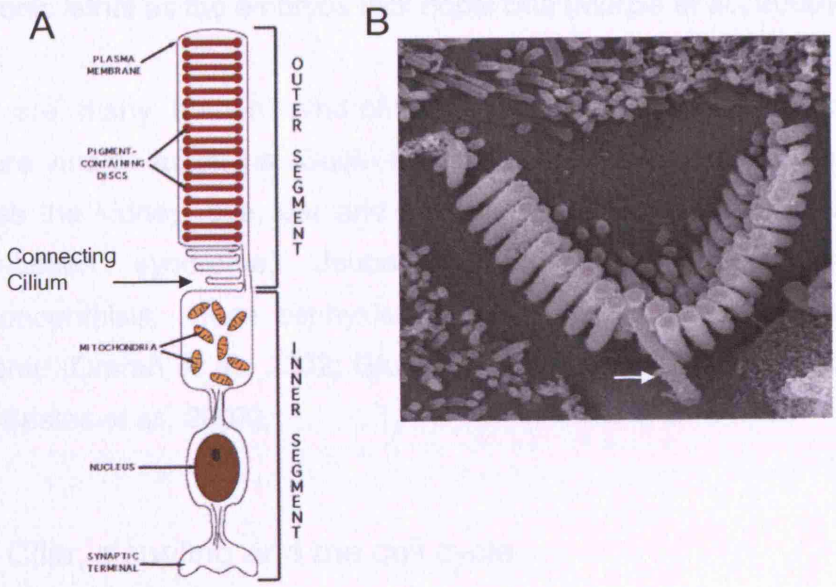

Figure 1.6: Cilia found in sensory organs. A) The vertebrate photoreceptor cell. Inner and Outer segments are connected via a narrow cytoplasmic bridge containing a modified cilium, across which particles are transported. http://www.chemistry.wustl.edu/~edudev/LabTutorials/Vision/Vision.html.B) Scanning electron microscopy image of an almost mature hair bundle of a mammalian auditory sensory cell. The 'v' shaped bundle consists of three rows of stereocilia (actin filaments, not true cilia). A true cilium, the kinocilium (white arrow) is involved in the establishment of the bundle. Picture from (Frolenkov *et al.*, 2004).

Cilia also play an important role in the olfactory epithelium of mammals (Nakamura, 2000). The olfactory receptor neuron is a highly specialised example of a ciliated cell in which the apical process terminates in a complex

structure, the dendritic knob, containing multiple basal bodies. Eight or more immotile cilia emanate from this dendritic knob and extend into the mucus (Menco, 1994). Studies in *C. elegans* have shown a role for cilia in osmotic sensing, chemoreception and mating behaviour (Sloboda, 2002).

It has recently been suggested that failure to develop correct left-right (LR) asymmetry (known as *situs inversus*) is established entirely by a ciliary mechanism. Motile Ird-(axonemal left-right dynein)-containing monocilia generate nodal flow, and non-motile polycystin-2 containing cilia sense nodal flow initiating an asymmetric calcium signal at the left border of the node (McGarth *et al.*, 2003). A complete knockout of the mouse *Tg737* gene is embryonic lethal as the embryos lack nodal cilia (Murcia *et al.*, 2000).

There are many human syndromes/diseases caused by defects in cilia structure and/or functions. Such syndromes affect several organ systems such as the kidney, eye, ear and formation of LR symmetry. They include Senior-Loken syndrome, Joubert syndrome, Kartagener syndrome, Nephronophthisis, Jeune asphyxiating thoracic dystrophy and Bardet-Biedl syndrome (Omran *et al.*, 2002; Giusto and Sciubba, 2004; Kumandas *et al.*, 2004; Beales *et al.*, 2007).

1.3.4 Cilia, signaling and the cell cycle

The unique properties of cilia (projection from cell body, IFT machinery) could account for their use in cellular signalling. Several receptors with known extracellular ligands are present on cilia, such as integrins on MDCK cilia and somatostatin receptors on neuronal cilia (Brailov *et al.*, 2000; Praetorius *et al.*, 2004). Recently cilia have been implicated in the Wnt and Shh developmental signalling pathways. Receptors for both of these pathways have been localised to the cilium (Corbit *et al.*, 2005; Ross *et al.*, 2005) and various animal knockouts are providing further evidence to support this connection (Bisgrove and Yost, 2006; Singla and Reiter, 2006). More recently its been shown that the cilium and basal body are involved in the regulation of Wnt

signaling by a combination of selective proteolysis and regulation of phosphorylation and that defective Wnt signalling may be causally related to a number of phenotypes associated with ciliopathies (Gerdes *et al.*, 2007).

Of further interest is the association of the basal body with cell cycle progression. Centrioles are the defining unit of both basal bodies and centrosomes, and malfunction of proteins associated with centrioles could interfere with their centrosomal function, cell cycle progression and cell proliferation (Beisson and Wright, 2003). Centriole duplication is co-ordinated with the cell cycle. Entry into the cell cycle is preceded by cilium resoportion, whilst exit from mitosis and cellular differentiation is accompanied by cilium assembly. It is plausible that signalling via cilia could regulate this process, defects resulting in disrupted proliferation and cellular differentiation. Knock down of *BBS4* and *BBS6* in cultured cells has shown cell cycle related defects such as arrest of cell division and apoptotic cell death (Kim *et al.*, 2004; Kim *et al.*, 2005).

1.3.5 The role of cilia in BBS

As already alluded to in some of the previous sections, BBS has been shown to be caused by defective basal body/cilia function. Since this initial hypothesis was proposed, there have been further lines of evidence supporting this association.

The first link between BBS and cilia arose from the cloning of *BBS8.* In one family a homozygous null *BBS8* mutation leads to BBS with randomisation of left-right symmetry, a known defect of nodal cilia. *BBS8* encodes a protein with a prokaryotic pilF domain, involved in pilus formation and twitching mobility, which localises specifically to centrosomes and basal bodies within ciliated structures. Double staining experiments showed that BBS4 also localised to the centrosome as well as BBS8. Interestingly BBS8 was shown to interact with PCM1, a protein thought to be involved in ciliogenesis which is known to interact with BBS4 (Ansley *et al.*, 2003). Since these initial findings,

the majority of the BBS proteins have been localised to the basal body and/or ciliary axoneme (see figure 1.5)(Beales, 2005).

Following the initial observations, other studies, mainly done in *C.elegans,* went on to confirm the link between BBS and cilia. Four known *C.elegans* homologues of human *BBS* genes (*bbs-1, bbs-2, bbs-7 and bbs-8)* were shown to be expressed exclusively in a small subset of cells (sensory neurons) harbouring cilia (Ansley *et al.*, 2003). Interestingly computational analyses of the 5' untranslated regions of *C.elegans bbs-1, bbs-2, bbs-7* and *bbs-8* genes revealed a 14bp imperfect repeat termed the X-box lying about 100bp upstream of the start codon. The transcripton factor regulating the expression of X-boxes in *C.elegans,* DAF-19, is a member of the RFX protein family and is required for cilia formation (Swoboda *et al.*, 2000; Blacque *et al.*, 2004). Cellular localisation of *C.elegans* bbs-1, bbs-2, bbs-7 and bbs-8 identified these proteins at the ciliary transition zones and along the ciliary axonemes. Transition zones in *C.elegans* are analogous to basal bodies and consist of microtubule-rich constrictions at the base of cilia (Perkins *et al.*, 1986; Blacque *et al.*, 2004). Localisation of the bbs proteins in *C.elegans* overlapped with that of IFT proteins such as osm-5, osm-6, xbx-1 and che-13 and both anterograde and retrograde movement of the bbs proteins were observed in wild-type animals (Blacque *et al.*, 2004). Loss of *C. elegans* bbs-7 and bbs-8 protein function was shown to result in structural and functional ciliary defects, including shortened/abnormal cilia and chemosensory abnormalities. Finally it was demonstrated that bbs-7 and bbs-8 are required for normal localisation/motility of IFT proteins osm-5/Polaris and che-11 and to some extent che-2, in *C. elegans* (Blacque *et al.*, 2004).

Mouse models of the disease have also supported the cilia hypothesis. Four BBS mouse mutants have been reported (*Bbs1*, *Bbs2*, *Bbs4* and *Bbs6*) (Kulaga *et al.*, 2004; Mykytyn *et al.*, 2004; Nishimura *et al.*, 2004; Ross *et al.*, 2005). All of these mouse models partially recapitulate the human phenotype and have defects associated with cilia function including retinal degeneration, anosmia and infertility. These mouse models of the disease are discussed in more detail in chapter six.

Many clinical aspects of the BBS phenotype can be explained by a ciliary defect, such as retinal degeneration due to compromised transport across the photoreceptor-connecting cilium, and the incidence of polycystic kidneys due to disrupted mechanosensation at the primary cilium of renal tubular cells. Anosmia and sensorineural hearing loss, secondary features of the disease, can also be attributed to ciliary defects. With cilia being involved in the process of developing left-right (LR) symmetry, it is highly probable that they are also involved in the development of the body plan and thus potentially the occurence of polydactyly. Recent implications of cilia involved in signalling processes could go towards explaining some of the more complex symptoms of the disease such as obesity, hypertension and behavioural anomalies.

1.4 Animal models of BBS

Animal models of the disease are playing a vital role in the elucidation of the BBS proteins' function. BBS knock down in the ciliated *C. elegans* worm confirmed the ciliary component of the disease (see above). Mouse models have been shown to recapitulate many of the phenotypes observed in BBS patients, and enable more detailed investigation of BBS gene function in a mammalian system (see chapter six). Recently the zebrafish model system has been employed, in order to further model disease pathogenesis. This is discussed in chapter ten.

1.5 BBS proteins complexes

All the evidence so far has suggested that BBS proteins may share a common function as adaptor proteins mediating trafficking of a number of cellular components. A common pathway is one explanation as to how mutations in a number of different genes can give the indistinguishable phenotype seen in BBS patients. A further argument could be that the BBS proteins associate with one another in a functionally dependent manner. Indeed interactions between various BBS proteins have been identified and are discussed in

chapter five. In support of this, recent findings in vertebrate cells have identified a complex composed of seven of the BBS proteins which also associates with PCM-1 and α/β tubulin. This newly identified complex, termed the BBSome, localises to non-membranous centriolar satellites in the cytoplasm and also to the cilia membrane (Nachury *et al.*, 2007). This BBSome has been shown to be required for ciliogenesis but is dispensible for centriolar satellite function. The ciliogenic function of the BBSome complex is linked to the Rab8 nucleotide exhange factor. Rab8 localises to the basal body and is in contact with BBS1. It targets vesicles to the cilium, promoting ciliary membrane elongation, following GTP loading (Nachury *et al.*, 2007). The association of BBS proteins with one another could also explain the oligogenic properties of the disease in regard to inheritance, penetrance and phenotypic variation amongst patients.

1.6 Aims of this thesis

The last few years have seen a rapid expansion in our understanding of the aetiology underlying Bardet-Biedl syndrome. Upon identification of the mapped genes, research has focused on elucidating the function of BBS proteins. The studies carried out in this thesis have contributed to this work. Initial mapping and mutational analyses aided the identification of novel BBS genes. Subsequently a yeast two-hybrid screen using Bbs6 as bait was performed to identify potential protein interactors. Concurrently phenotypic analysis was carried out on a Bbs6 knock out mouse model. Additionally BBS protein expression in an *in vivo* model system (the developing cochlea) further implicated the BBS proteins in cellular processes. Finally a further model organism (the zebrafish) was employed for investigating the function of the BBS8 protein.

Chapter 2: Materials and Methods

2.1 Materials

2.1.1 Reagents

All reagents were of AnalaR grade and supplied by Sigma Aldrich or BDH unless otherwise stated. Solutions were made using Milli-Q purified water and autoclaved where appropriate.

2.1.2 Stock Solutions

20x SSC	3 M NaCl, 0.3 M NaCitrate (pH 7.0)
Hybridisation Buffer	50% FA, 10% Dextran Sulfate, 2 x SSC, 1 x PBS
ST Buffer	0.05% Tween 20, 2 x SSC
TE Buffer	10 mM Tris-HCl, 1 mM EDTA (pH 8.0)
LB Broth	1% Bactotryptone, 0.5% Bactoyeast, 1% NaCl
LB Agar	2% Bactoagar, LB Broth
NB Buffer (10x)	100 mM Tris-HCl, 400 mM NaCl, 15 mM $MgCl_2$, 2.5 mM Spermidine.
dNTP Mix (10x)	2 mM dATP, 2 mM dCTP, 2 mM dGTP, 2 mM dTTP.
TAE Buffer (10x)	0.4 M Tris-acetate, 10 mM EDTA
DNA Ladder	0.1 μg/μl DNA Ladder, 20% loading buffer in 1x TE (pH 8.0)
Loading buffer	20% glycerol, 0.25% Bromophenol blue
Tail Lysis Buffer	100 mM Tris (pH8.5), 5 mM EDTA, 0.2% SDS, 200 mM NaCl, 100μg/ml Proteinase K (added immediately prior to use).
X-Gal Staining Solution	20 mM $K_3Fe(CN)_6$, 20 mM $K_4Fe(CN)_6$-$3H_20$, 2 mM $MgCl_2$, 0.01% DOC, 0.02% NP-40, made up in PBS, 1 mg/ml X-gal (added immediately prior to use).

Buffer T	0.1 M Tris (pH7.5), 0.15 M NaCl, 0.1% Triton X-100
Block T	10% FCS in Buffer T
EM Fix	2.5% glutaraldehyde in 0.1 M cacodylate buffer with 3 mM $CaCl_2$ (pH7.3)
Bouins Solution	0.9% w/v picric acid, 9% v/v formaldehyde, 5% v/v acetic acid. (Sigma)
YPAD Broth	10 g/l Bacto-Yeast Extract, 20 g/l Bacto-Peptone (autoclaved), to which was added 2% filter sterilised glucose, 0.002% filter sterilised Adenine .
YPAD Agar	20g/l Bacto-Agar in YPAD Broth
SD Broth	0.67% Bacto-Yeast nitrogen base without amino acids autoclaved. To which was added 2% filter sterilized glucose and filter sterilized supplements, depending on selection criteria
SD Agar	20g/l Bacto-Agar in SD Broth
Supplements	Adenine sulphate 0.2%, Uracil 0.2%, L-Tryptophan 1%, L-Histidine HCl 1%, L-Methionine 1%, L-Leucine 1%, 1M 3-Aminotriazole must be added in the absence of L-Histidine HCl. 180mg/l α-X-gal.
10x TE	0.1M tris (pH 7.5), 0.10M EDTA
10X LiOAc	1M lithium acetate (autoclaved)
50% PEG-4000	500g/l polyethylene glycol-4000 (autoclaved)
1XTE/LiOAc	Immediately before use: 1 part 10x TE, 1 part 10x LiOAc, 8 parts sterile distilled H_20
1XTE/LiOAc/PEG	Immediately before use: 1 part 10x TE, 1 part 10x LiOAc, 8 parts 50% PEG-4000
PBST	PBS/0.5% Triton X-100
Fish Block	10% goat serum(heat inactivated)/1% DMSO/ PBST
10x DIG-nucleotide mix	10 µl 10mM dA,G and CTP/ 6.5 µl 10mM UTP/ 3.5µl 10mM Dig-11-UTP
PBTw	PBS/0.1% Tween-20
PK	1000x Proteinase K 10mg/ml

Maleic Acid Buffer	150 mM NaCl, 100 mM Maleic Acid (pH 7.5, higher pH required to dissolve MA)
Prehyb Solution (Hyb -)	50% formamide, 5x SSC, 0.1% Tween 20 (pH 6.0, stored at -20°C)
Hyb Solution (Hyb +)	50% formamide, 5x SSC, 0.1% Tween 20, 5 mg/ml T-RNA, 50mg/ml Heparin (pH 6.0, stored at -20°C)
Fish H_2O	UV illuminated, filtered through activated charcoal, 60 ug/ml Instant Ocean salt mix.
DAPI Solution (Fish)	Bis-Benzimide H33342 trihydrochloride 0.1% stock (1 mg/mL), Bis-Benzimide H33258 0.1% stock (1 mg/mL). Working solution: 1 ml of each into 50 ml PBS.

2.1.3 DNA samples

Patients were diagnosed with BBS by a clinician, based on published diagnostic criteria (Beales *et al.*, 1999). Where possible, samples from unaffected siblings and parents were also taken. For all samples, informed consent was obtained from either the individual, or in the case of a child, from a parent. DNA extraction from blood was performed using the PUREGENE DNA Purification kit (Gentra) or was carried out by the North East Thames Regional Genetics Laboratory. DNA samples from affected individuals were aliquoted at 30ng/µl in a 96-well plate format for PCR amplification.

2.2 Methods

2.2.1 Fluorescent *in situ* hybridisation (FISH)

2.2.1.1 Mammalian Cell Culture

EBV-transformed patient B-cell lymphoblastoid cell lines were cultured in suspension of RPMI 1640 Medium with Glutamax –1 (Gibco) supplemented with 1% penicillin-streptomycin (10,000 units/ml; Gibco) and 10% fetal calf serum. Cells were maintained at 37°C in a humidified atmosphere containing 95% O_2 and 5% CO_2. For long term storage, cells were harvested by centrifugation at 500 x *g* for 5 minutes and the pellet resuspended at $2.0x10^6$ cells/ml in fetal calf serum containing 10% DMSO. 1 ml aliquots were placed in cryotubes, allowed to freeze slowly at –80°C overnight and then transferred to liquid nitrogen the following day.

When required again, cells where taken out of liquid nitrogen, thawed at room temperature for one minute and 37°C for 5 minutes, before being added to 5ml medium. Cells were spun down at 250 x *g* for 5 minutes, and the pellet re-suspended in fresh pre-warmed media, in order to remove traces of DMSO.

2.2.1.2 Preparation of metaphase spreads

Metaphase spreads were prepared from healthy 50 ml cell cultures. Cells were spun down and resuspended in fresh culture medium 24 hours before harvesting. Mitotic arrest was induced by incubating a uniform cell suspension with colcemid (10 μg/ml) to a final concentration of 10 μl/ml for 1 hour at 37°C, 95% O_2 and 5% CO_2. Cells were subsequently spun down at 500 x *g* for 8 minutes and the supernatant removed carefully. The cell pellet was resuspended in 25-30 ml 75 mM KCl and returned to the incubator for 10 minutes. As this solution is hypotonic, it forces water to enter the cells and spread out the chromosomes.

Cells were again spun down at 500 x *g* for eight minutes, supernatant discarded and resuspended in 25-30 ml fresh fixative solution (3:1 methanol:glacial acetic acid). Fix solution dehydrates the cells and removes histone proteins. This fixative wash step was repeated for a total of three times. Finally the cell pellet was resuspended in 3-5 ml of fixative solution and stored at -20°C.

The cell suspension was further diluted 1 in 3 with fresh fixative and dropped from 20-30 cm onto glass slides that had been kept at –20°C and subsequently humidified. This enabled the chromosomes to spread out when the cells burst as they were dropped from above. Slides were dried and a diamond marker used to locate the drop. Finally the slides were flooded with fresh fix solution and left to dry, after which they were further flooded with 70% glacial acetic acid. Metaphase spreads were stored at 4°C until needed.

2.2.1.3 Slide Preparation for DNA fibres

DNA fibres were prepared from 3 mls of cell suspension. Cells were centrifuged for 5 minutes at 500 x *g*, resuspended in 3mls of PBS and recentrifuged. This wash step was repeated twice. After the final wash the cells were resuspended in 1 ml PBS. 10 μl of this cell suspension was spread over a 1 cm area on the upper part of a clean microscope slide and allowed to air dry. The slides used had been previously soaked in 96 % ethanol and allowed to air dry. Slides were then fitted onto a plastic Shandon coverplate (Thermo Electron) and held together vertically with the dried cell suspension at the top of the slide facing the chamber. 150 μl lysis solution (5 parts 70mM NaOH, 2 parts absolute ethanol) was loaded into the top chamber of the coverplate and allowed to slowly flow down between the slide and coverplate. Once the meniscus had reached the top of the cell spot, 150 μl 96 % ethanol was loaded into the chamber and allowed to run down the slide slowly. Slides where slowly pulled away from the coverplate and allowed to air dry before being fixed in acetone for 10 minutes. Slides were stored at room temperature for a minimum of 24 hours before hybridisation.

2.2.1.4 Preparation of BAC probes

Appropriate Bacterial artificial chromosomes (BACs) were received as stab cultures supplied by BAC PAC. On arrival, bacteria were streaked out onto LB plates containing 20 μg/ml chloramphenicol and left to grow overnight at 37°C. A starter culture of 5ml LB broth with 20 μg/ml chloramphenicol was inoculated with one colony and placed at 37°C under vigorous shaking overnight. 1 ml of the starter colony was transferred into a 1 L culture flask containing 500 ml LB with 20 μg/ml chloramphenicol and left to grow overnight. 15% glycerol stocks were prepared from the starter culture and stored at -80°C.

Cells were harvested and the DNA was isolated using a Qiagen plasmid purification protocol for low copy number plasmids (MAXIPREP), following manufacturers instructions. The final DNA pellet was dissolved in 100-200μl TE buffer. Quality and quantity was determined by measurement of OD_{260}/OD_{280} values.

2.2.1.5 Nick Translation of BAC probes

To obtain 300-500 bp labelled DNA fragments suitable for FISH, purified BAC DNA was nick translated using a Nick Translation Kit (Vysis). This reaction employs two enzymes, deoxyribonuclease I (DNase I), which nicks the DNA, and *E. Coli* DNA polymerase I, which generates the nick translation fragments by incorporating a fluorescent nucleotide in the DNA strand as it repairs the nicks. Together these enzymes incorporate a fluorescent label into the DNA probes. Reactions were carried out in a total volume of 50 μl containing:

1 μg BAC DNA, 0.5 nM SpectrumGreen or SpectrumOrange dUTP, 0.5 nM dTTP, 1 nM of each dATP, dCTP, dGTP, 1 x nick translation buffer, 5 Units nick translation enzyme and sufficient nuclease-free water to bring the reaction volume up to 50μl.

All the components were added to the nuclease-free water in the above order, briefly vortexed and centrifuged. Reaction mixtures were incubated at 15°C for 8-16 hours, after which the reaction was stopped by heating to 70°C for 10 minutes. Probe size was determined by running an aliquot of the sample on a 1% agarose gel. The desired probe size was between 50-500 bp with an average size of 300 bp. If this had not been achieved, nick translation was repeated, varying the incubation time accordingly. For long-term storage, nick translated samples were stored at -20°C.

2.2.1.6 Probe Precipitation

Probes were precipitated with human Cot-1 DNA and herring testes DNA, in order to suppress cross-hybridisation to human repetitive DNA during hybridisation, as well as to remove unincorporated nucleotides. 20 μl of nick translated sample was added to 6 μg Cot-1 (Invitrogen), 12 μg herring testes DNA (Promega) and made up to 50 μl with sterile water. These components were vortexed and briefly spun down, after which 4 μl 3 M sodium acetate and 112 μl 100% ethanol were added. The precipitation mixture was kept at -80°C for 40 minutes then centrifuged at 100 x *g* at 4°C for 30 minutes. The supernatant was removed and the pellet resuspended in 40 μl hybridisation buffer at 37°C overnight. For long-term storage precipitated samples were stored at -20°C.

2.2.1.7 Fluorescence *in situ* hybridisation, washes and detection

Metaphase spreads were left in 2 x SSC at 4°C for 1 hour, then dehydrated through 70% ethanol, 90% ethanol and finally 100% ethanol for 5 minutes each and then left to air dry. For the hybridisation step 15 μl of the precipitated nick translation mixture and 2 μl diluted control probe (diluted to manufacturers instructions) were mixed together and pipetted onto the centre of the slide. Control probes were hybridised simultaneously, diluted according to manufactures specifications. A 22 x 22mm coverslip was applied to the

slide and sealed with a thick layer of glue around the edge (weldtite vulcronising rubber solution from a bicycle shop). Slides were placed in a hybridisation chamber, denatured at 73°C for 1 minute and incubated at 37°C overnight. The glue and coverslip were then removed and slides washed to remove any unbound probe. Slides were washed in ST buffer for 3 minutes at room temperature, 0.4 x SSC/0.3% NP-40 at 72°C for 2 minutes and finally in ST again for 5 minutes. Slides were left to dry before applying mounting medium containing DAPI (4',6-diamidino-2-phenylindole) (Vector Labs) in order to stain chromosomal DNA. The slides were then covered with fresh coverslips, excess mounting medium was blotted away with tissue and the coverslips sealed. Throughout this process slides were kept in the dark.

Slides were viewed under a Zeiss Axioskop fluorescent microscope and images were taken using a Photometrics camera with SmartCapture software.

2.2.2 Amplification of DNA by Polymerase Chain Reaction (PCR)

2.2.2.1 DNA extraction from blood

DNA was extracted from blood using the PUREGENE DNA Purification kit (Gentra) following manufacturers instructions. Informed consent was obtained from either the individual or a parent.

2.2.2.2 Primer design for direct sequencing

The Primer3 programme (available on the internet http://frodo.wi.mit.edu) was used for primer design and the primers were ordered through either MWG or Sigma. PCR primers for amplifying exons were designed from the genomic sequence and were selected on the following criteria; GC content approximately 50-60%, length between 20-30bp, absence of repeat sequences, distance from beginning/end of exon approximately 50bp. Forward and reverse primers were chosen that had similar melting

temperatures (Tm) and would not anneal to one another. Primers were checked on Amplify, a virtual PCR program before ordering. The primer sequences used are given in the Appendix along with their optimal conditions.

2.2.2.3 Polymerase Chain Reaction

Reactions were carried out in a final volume of 25 μl and done in either multi-well plates or PCR tubes. The following PCR mix and conditions were used for the majority of the PCRs:
20-50 ng of genomic DNA
1x NB buffer
200 μM of each dNTP
5 pmol forward primer
5 pmol reverse primer
1 U Taq Polymerase (Bioline)
In sterile distilled water

PCR programs used were either:

1. A two-step touchdown program (TD55). The samples were denatured at 95°C for 5 minutes. This was followed by ten cycles of amplification, consisting of a denaturation step at 95°C for 30 seconds, an annealing step, starting at 65°C and decreasing by 1°C each cycle, for 30 seconds, and finally an elongation step at 72°C for 1 minute. These cycles were followed by 25 further cycles with the annealing temperature at 55°C. The reaction was ended with a final elongation step at 72°C for 10 minutes.
2. A standard PCR program of 95°C for 2 minutes, followed by 30 cycles of 95°C for 30 seconds, an annealing temperature dependent on the specific fragment (typically between 55-71) for 30 seconds and an elongation step at 72°C for 45 seconds; followed by a final extension step of 72°C for 10 minutes.

3. The Failsafe PCR program ran as follows. 94°C for 1 minute followed by 30 cycles of 94°C for 30 seconds and 72°C for 1 minute.
4. PCR reactions carried out with Amplitaq gold required an initial incubation at 95°C for 10 minutes, in order to activate the polymerase.

An aliquot of each sample was checked by agarose gel electrophoresis.

2.2.2.4 PCR optimisation

Temperature: The optimum annealing temperature for each primer pair was established by carrying out a gradient PCR in which the annealing temperature varies along the plate. The temperature typically ranged from 52°C -68°C.

$MgCl_2$: The standard PCR buffer contained 1.5mM $MgCl_2$. This could be adjusted to find the optimal concentration, usually between 1 mM and 6 mM $MgCl_2$.

DMSO and Betaine: Addition of Betaine (0.5-2.0 mol) or DMSO (10%) to the PCR mix was also sometimes used to improve difficult PCR reactions.

Failsafe: For difficult reactions, the FAILSAFE PCR PreMix Selection Kit (Epicentre) was used. Primers were tested in a PCR reaction using the FAILSAFE Enzyme Mix with one of the 12 different buffers (2 x FAILSAFE PCR PreMix A-L). The reaction mix comprised of 1 x PreMix (A-L), 5 pmol of each primer (forward and reverse), 30 ng DNA and 1.25 U FAILSAFE enzyme mix. The FAILSAFE PCR program was used (see 2.2.2.2)

Amplitaq Gold: Some PCR reactions were improved by using a 'Hot Start' enzyme such as Amplitaq Gold

M13 tag: Addition of an M13 tag (Forward - TGTAAAACGACGGCCAGT, Reverse – CAGGAAACAGCTATGACC), appeared to improve the stability of certain primers.

2.2.2.5 Agarose gel electrophoresis

A 1% agarose gel was used to check the products of a PCR reaction. The agarose was weighed and added to the appropriate volume of 1 x TAE buffer. This was heated in a microwave until the agarose had dissolved and cooled to approximately 50-60°C. Ethidium bromide at a final concentration of 0.5µg/ml was added to the agarose gel. The gel was then poured into a gel tray of appropriate size, containing combs, and left to set. Once the gel had set the combs were removed and the gel placed in its gel tank containing enough 1 x TAE buffer to cover the gel. The samples were prepared by mixing approximately 5 µl sample with 1 µl loading buffer containing glycerol and bromophenol blue, and loaded onto the gel. An appropriate DNA ladder (100 bp or 1 Kb ladder) was also loaded onto the gel. Electrophoresis was carried out at 50-150 V until the fragments had separated sufficiently. DNA fragments contained within the gel were visualised under UV light on a transilluminator, and then photographed.

2.2.2.6 Purification of PCR products

Following PCR amplification samples were checked by agarose gel electrophoresis. Samples containing just one band were purified by ExoSap, which removed excess primers, nucleotides and single stranded DNA. For samples containing more than one band, gel extraction was carried out to isolate and purify the fragment of correct size.

ExoSap

For a PCR reaction volume of up to 25 µl, 5 µl of the ExoSap mixture was added, which comprised of:

20 U Exonuclease I (E.coli)

2 U Shrimp alkaline phosphatase

1 x dilution buffer (50mM Tris-HCl, pH 8.0)

In sterile distilled water.

The ExoSap mix was added to the PCR products, mixed, and incubated for 15-30 minutes at 37°C. Enzymes were inactivated by further incubation for 15 minutes at 80°C. The exonuclease degrades any single stranded DNA, whilst the shrimp alkaline phosphatase removes the 5'-phosphate groups from DNA and dNTPs, which prevents digested fragments from reannealing.

Gel extraction

Gel extraction was carried out using the Qiagen QIAquick gel extraction kit following the manufactures instructions and eluted from the column in 30 μl EB buffer.

2.2.3 Sequencing

2.2.3.1 Cycle sequencing

Cycle sequence reactions were set up using BigDye Terminator v3.1 (Applied Biosystems) for running on the MegaBACE (Amersham Biosciences), which uses the dideoxynucleotide chain termination method for sequencing. During the annealing step dideoxynucleotides are incorporated into the DNA sequence and act as chain terminators by preventing further deoxynucleotides from being incorporated into the product. This happens at different positions along the stretch of DNA to be sequenced, resulting in different length sequences of the DNA strand all ending with a dideoxynucleotide. Each of the dideoxynucleotides is labelled with fluorescein and a differently coloured rhodamine dye. When run on the MegaBACE, fluorescien absorbs energy from the laser and transfers it to the rhodamine dye, which then emits light at a certain wavelength characteristic for that dye. In this manner the content and order of nucleotides along the sequence can be identified.

Sequencing reactions were carried out in either 10 μl or 15 μl reaction volumes, depending on the quality of the PCR product.

10μl reaction volumes contained the following:

3μl purifed PCR product

5pmol forward OR reverse primer
1μl BigDye premix
2μl dilution buffer
Made up to 10 μl with sterile distilled water

15μl reaction volumes contained the following:
6μl purifed PCR product
5pmol forward OR reverse primer
2μl BigDye premix
2μl dilution buffer
Made up to 15 μl with sterile distilled water

The tubes/plates were sealed and placed in a thermocycler (Eppendorf, Perkin Elmer, GRI) for 35 cycles of the sequencing program consisting of an initial denaturing step at 95°C for 2 minutes; then cycling through denaturing at 95°C for 20 seconds, annealing at 50°C for 10 seconds and an extension step at 60°C for 3 minutes. The reaction volume was topped up to 20 μl with sterile water before desalting.

2.2.3.2 Sephadex desalting

Sephadex plates were prepared by addition of 300 μl sterile water to each well of specialised 96 well plates containing dry sephadex powder. Plates were left in an airtight container at 4°C for a minimum of 3 hours to allow the resin to hydrate. Prior to use, plates were centrifuged at 910 x *g* for 5 minutes at 4°C. After addition of a further 200 μl of sterile water, this process was done a second time to wash the resin to removing any salts or ions present. The sequencing products were then added to the centre of each well and eluted into a clean plate by centifugation at 910 x *g* for 5 minutes at 4°C.

2.2.3.3 Sequencing on the MegaBACE

Denaturing matrix tubes were taken from storage at 4°C, left to reach room temperature and centrifuged at 4000rpm for 4 minutes. Buffer tubes and a skirted 96 well plate were filled with 1 x linear polyacrylamide (LPA) buffer (Amersham Biosciences). The laser filters, instrument template, instrument configuration and file storage were changed as necessary for a sequencing run. The capillary tips in the MegaBACE were rinsed with distilled water and filled with 3% Long Range linear polyacrylamide (LPA) matrix. Following matrix equilibration and a short pre-run, the capillary tips were rinsed again and samples injected at 3 kV for 60 seconds and run at 9 kV for 100 minutes.

2.2.3.4 Sequence Analysis

Sequence analysis was carried out using Sequencher version 4.2. Sequencing files from the MegaBACE were downloaded in ABD format and opened in sequencher. Sequences were aligned with one another and with the known sequence for the given region. Discrepancies between the sequences were checked to identify possible changes.

2.2.4 Restriction Digests

In the event that an observed sequence alteration in a patient sample affected a restriction site (either creating or abolishing a cut site), a restriction digest using the corresponding enzyme was carried out to confirm the sequence change. Possible enzymes were identified using the NEB webcutter website. Restriction digests were performed on the PCR product of the amplified exon in question in the patient, a control sample and also any available relatives of the patient. Digests were carried out in a 20 µl volume containing 10 µl PCR product, 20 Units enzyme (New England Biolabs), 1X enzyme reaction buffer and 1x BSA made up to 20 µl with sterile distilled water. After gentle mixing, the reactions were incubated at the required temperature for the enzyme

(typically 37°C or 55°C) overnight. An aliquot of the digest was then run out on an agarose gel and samples from the patient and any relatives were compared to the pattern of bands seen in the control sample to confirm the presence of the sequence change.

2.2.5 Reverse transcription and RT-PCR

Extracted RNA was initially reverse transcribed with SuperScript™II Reverse transcriptase (Invitrogen) to synthesise first-strand cDNA. Reactions were carried out in a 20 µl reaction volume in nuclease-free microcentrifuge tubes. Mixtures consisted of 1-5 µg of total RNA, 50 ng of random primers, and 10mM of each dATP, dGTP, dCTP, dTTP, in a total volume of 12 µl sterile distilled water. The mixture was heated at 65°C for 5 minutes and then quickly chilled on ice. The contents of the tube was collected by brief centrifugation after which First-Strand buffer (to a final concentration of 1X), 0.1 M DTT and 40 Units RNase OUT™ Recombinant Ribonuclease Inhibitor were added. The contents of the tube were gently mixed and incubated at 25°C for 10 minutes. 200 units of the SuperScript enzyme was subsequently added and mixed by pipetting up and down. A 50 minute incubation at 42°C followed. The reaction was inactivated by heating at 70°C for 15 minutes. The resulting cDNA was then used as a template for amplification by RT-PCR.

RT-PCR was performed as standard PCRs. The only differences being the template, instead of using genomic DNA, cDNA resulting from reverse transcription was used, and that primers were designed to be specifically intron-crossing.

2.2.6 Cloning

2.2.6.1 Preparation of insert

Primers were designed to amplify the entire coding region of mouse Bbs6. A restriction site for *Eco*R1 was added to the forward primer and one for *Sal*1 to the reverse primer, in order for the amplified insert to be cloned into the

*Eco*R1 and *Sal*1 sites of the multiple cloning site (MCS) of the pGBDU plasmid (Gift from P. Ataliotis) (primer sequences and vector maps are given in appendix B).

PCR amplification of the insert was carried out using a Poly U enzyme (Stratagene) as described in section 2.2.2 under the following conditions; 1ng mouse 7-day embryo cDNA was used as template, annealing temperature was decreased to 48°C, extension period was increased to two minutes, number of cycles was increased to 35, 10% DMSO was added to the reaction.

The resulting PCR product was gel extracted using the Qiagen QIAquick gel extraction kit (Qiagen) following the manufacturer's instructions and eluted from the column in 30µl EB buffer.

The amplified Bbs6 cDNA, as well as 5ng pGBDU-c3 plasmid vector was digested with 50 U *Eco*R1 and 10 U *Sal*1 at 37°C overnight. After which the plasmid vector was dephosphorylated by a further 1 hour incubation at 37°C with addition of two units (2µl) shrimp alkaline phosphatase. The reaction was terminated with a 15 minute incubation at 65°C.

The resulting vector plasmid was gel excised, and the Bbs6 insert column purified. Quantity of DNA was calculated by electrophoresis of samples alongside a Low DNA Mass™ Ladder and High DNA Mass™ Ladder (Invitrogen).

2.2.6.2 Ligations

Ligations were carried out at 16°C overnight using 50 ng vector DNA. The amount of insert DNA was varied to be in 3:1 and 1:1 molar ratios with the vector. One unit of T4 DNA ligase enzyme (Invitrogen) was used per reaction, ligase buffer was added to a final concentration of 1x and sterile distilled water was added to bring the final volume up to 10 µl. A vector-only ligation was also set up. For long term storage ligation products were kept at -20°C.

2.2.6.3 Transformation of ligations

Ligations were transformed into JM109 *E-coli* competent cells. 2 µl of the ligations were added to an aliquot of cells and left on ice for 20 minutes before being heat-shocked at 42ºC for 45 seconds. Transformations were then placed back on ice for 2 minutes before addition of 1 ml LB broth. After 1 hour of vigorous shaking at 37ºC, 50 µl of the transformation was spread on LB agar plates containing ampicillin. The remainder of the cells were spun at 250 x g for 3 minutes, resuspended in 50 µl LB, and spread on a second ampicilin plate. Plates were incubated at 37ºC overnight.

Colonies grew on plates streaked with vector-insert transformations but virtually no colonies grew on plates streaked with vector only transformations, implicating that the dephosphorylation was successful and that the vector had not religated.

Ten colonies were chosen at random and used to inoculate 5 ml cultures of LB broth containing ampicilin. Simultaneously each colony was streaked onto an LB agar plate containing ampicilin. After vigorous shaking at 37ºC overnight, DNA was extracted using a Qiagen Miniprep kit, following the manufacturers instructions. Resulting DNA was digested and sequenced to check for the presence of the correct insert. Direct sequencing of the plasmid was carried out as previously described in section 2.2.3 with the addition of a denaturing step involving the miniprep DNA, primers and sterile distilled water at 95ºC for 1 minute before being snap cooled on ice, followed by addition of the BigDye premix and sequencing buffer. The sequencing program consisted of an initial denaturing step at 95ºC for 2 minutes; then 35 cycles of denaturing at 95ºC for 50 seconds, annealing at 50ºC for 10 seconds and an extension step at 60ºC for 3 minutes (sequencing primers are given in the appendix).

On identification of a plasmid with the correct insert, a 100 ml culture was set up and DNA extracted using a Qiagen Maxi prep kit to obtain sufficient DNA

for the subsequent yeast two-hybrid screen. Additionally an 80% glycerol stock was made from the culture and stored at -80°C.

2.2.7 Yeast two-hybrid screen

2.2.7.1 Small scale transformation

A single colony of PJ69-4A (see appendix B) was used to inoculate a 5 ml culture of YPAD broth and grown overnight at 30°C with shaking. The following day the optical density (OD_{600}) of the starter culture was measured and an appropriate volume was used to inoculate a 60 ml YPAD culture at OD_{600}=0.1. The culture was incubated at 30°C with shaking until an OD_{600} of between 0.5 and 0.7 was reached. Following the incubation, the culture was spun at 1500 x g for 5 minutes. Pelleted cells were washed in 20 ml sterile distilled water before being centrifuged a second time and subsequently resuspended in 300 µl of 1 x TE/LiOAc. Carrier DNA (Herring testes DNA, Clontech) was incubated at 95°C for 5 minutes before being snap cooled on ice. 100 ng pGBDU-Bbs6 and 50 µg carrier DNA was added to 100 µl cell suspension in a sterile 1.5 ml eppendorf tube. The contents of the tube were mixed by inversion before addition of 300 µl of 1 x TE/LiOAc/PEG and consequent incubation at 30°C with shaking for 30 minutes. Following the addition of 70 µl dimethyl sulfoxide (DMSO), cells were incubated for a further 15 minutes at 42-45°C without shaking. Cells were then spun down by brief centrifugation for 10 seconds at 1500 x g and resuspended in 0.5 ml sterile distilled water. The cell suspension was plated onto a fresh SD-Ura agar plate and incubated at 30°C for two days. Resulting colonies were streaked out on a fresh SD-Ura agar plate in order to generate fresh colonies to test for autoactivation.

2.2.7.2 Autoactivation test

Colonies resulting from the small scale transformation were streaked onto SD-Ura, SD-Ura-Ade, and SD-Ura-His+3AT (3-aminotriazole) plates and incubated for a further four to five days. The absence of growth on either SD-Ura-Ade or SD-Ura-His+3AT plates indicated that there was no autoactivation of the system by the GAL4 binding domain-Bbs6 fusion protein (pGBDU-Bbs6 protein). 3AT is an inhibitor of the histidine pathway and is added to the media to suppress leaky expression of *HIS3*.

2.2.7.3 Large scale transformation

Following the small scale transformation of PJ69-4A with the pGBDU-Bbs6 bait plasmid, a library screen was carried out using a large-scale transformation procedure to introduce the library plasmids into the pGBDU-Bbs6 transformed yeast. A whole scraping of a streak from the SD-Ura plates used in the autoactivation test was used to inoculate a 200 ml SD-Ura culture. The culture was incubated at 30°C with shaking for 24 hours. The optical density (OD_{600}) of this starter culture was measured and a sufficient volume was used to inoculate 1 litre YPAD (prewarmed for 30 minutes at 30°C) at OD_{600}=0.1-0.2. This culture was incubated at 30°C with shaking until the OD_{600} reached between 0.5 and 0.7. Once the required OD had been reached the culture was spun at 960 x g for 5 minutes. Pelleted cells were washed in 500 ml TE before being centrifuged a second time and subsequently resuspended in 20 ml 1 x TE/LiOAc in a 1 litre conical flask. 10 mg carrier DNA (Herring testes DNA, Clontech) was incubated at 95°C for 5 minutes before being snap cooled on ice. Denatured carrier DNA and 250 µg library plasmid DNA (125 µg E9.5 whole embryo cDNA library and 125 µg E10.5 whole embryo cDNA library made by Paris Ataliotis) were added to the 20 ml cell suspension. The contents of the conical flask were mixed by swirling. Following addition of 140 ml 1 x TE/LiOAc/PEG, the culture was incubated at 30°C with shaking for 30 minutes. Following the addition of 17.6 ml DMSO, the contents of the conical flask was mixed gently and aliquoted equally into

ten 50 ml falcon tubes. Cells were heat shocked at 42°C for six minutes and immediately added to 400 ml room temperature YPAD broth containing no glucose. Cells were pelleted at 950 x g for five minutes and washed in 500 ml YPAD broth containing no glucose. Following another round of centrifugation, cells were resuspended in 1 litre YPAD (containing glucose) pre-warmed to 30°C, and incubated for a further hour at 30°C with shaking. Cells were then pelleted, washed in 500 ml SD-Ura-Leu prewarmed to 30°C, pelleted a second time and finally resuspended in 1 litre SD-Ura-Leu prewarmed to 30°C. The culture was incubated at 30°C with shaking for 9-10 hours.

Following incubation, cells were pelleted and washed twice in SD without glucose. They were finally resuspended in 10 ml SD-Ura-Leu-His+3AT.

2.2.7.4 Transformation efficiency

10 µl of the cell suspension resulting from the large scale transformation was taken and serially diluted (1:10, 1:100, 1:1000, 1:10,000, 1:100,000 and 1:1,000,000) to calculate the transformation efficiency. Each dilution was plated out onto a SD-Ura-Leu plate and incubated at 30°C for three days before the number of colonies on each plate was counted.

2.2.7.5 First round of selection - Histidine

The remainder of the 10 ml cell suspension resulting from the large scale transformation was plated out onto large (25cm) SD-Ura-Leu-His+3AT plates in 550 µl aliquots. These were then incubated at 30°C. Colonies emerging after day four to seven days growth, were picked and more stringently assessed for colony growth.

2.2.7.6 Second round of selection – Adenine

Colonies emerging from the first round of selection, were subsequently streaked onto individual grids of large gridded SD-Ura-Leu-Ade+X-α-gal

plates. The addition of the X-α-gal allows for a more stringent assessment of colony growth, as resulting blue colonies demonstrate the ability to transactivate the *lac*Z reporter gene. After 2-3 days, colonies streaked onto these plates were assessed for growth and colour change.

2.2.7.7 Isolation of prey plasmid

Following the second round of selection, the prey plasmid was isolated to enable identification of the positive clone. Colonies identified as positive after the second round of selection were picked and used to inoculate 2 ml SD-Leu (enriching for only the prey and not the bait plasmid). Cultures were allowed to grow for 24 hours at 30°C with shaking. 200 µl of these cultures were used to make 80% glycerol stocks and kept at -80°C for long-term storage. Remaining cells were pelleted at 500 x *g* for 5 minutes and resuspended in 50 µl 50mM Tris-HCl (pH7.5), 1.2M sorbitol, 10mM EDTA and 10mM betamercaptoethanol (added just before use). After addition of 200 U lyticase enzyme, cells were incubated overnight at 37°C without shaking. Resulting spheroplasts were collected by centrifugation at 250 x *g* for 5 minutes. Subsequently DNA extraction was performed using a Qiagen mini prep kit, following manufacturers instructions. The resulting DNA pellet was dissolved in 25 µl TE.

2.2.7.8 Amplification and identification of the prey cDNA sequence

Isolated and extracted prey plasmid DNA was amplified by PCR and sequenced. PCR reactions were carried out as standard (see section 2.2.2) using 1 µl of DNA from the above mentioned step. Annealing temperature was 60°C and the number of cycles was increased to 35. The sequence for the 509 VP16 forward and 510 VP16 reverse primers used to amplify the prey insert are given in the appendix. Purification and sequencing of resulting PCR products were carried out as described in section 2.2.2. The resulting sequences were used to search the blastn database (http://www.ncbi.nlm.nih.gov/BLAST/) to identify the cDNA insert.

2.2.7.9 Testing for autoactivation of prey

For further analysis of protein interactions identified from potentially interesting clones, prey clones had to be isolated and tested for autoactivation in the yeast two-hybrid system. Prey DNA that had been isolated as described in 2.2.8.7 Isolation of prey plasmid, was used for electroporation of E-Shot™ DH10B™-T1^{R} Electrocompetent Cells (Invitrogen) following manufacturers instructions. Colony PCR was carried out on resulting colonies to identify those containing the prey plasmid. Colony PCR involved picking a single colony with a sterile toothpick and 'dabbing' it into the PCR mixture before re-streaking the colony onto a fresh plate. On identification of colonies that harboured an insert, this fresh 'streak' was used to inoculate a culture from which the prey plasmid was isolated using a Qiagen Mini prep kit following manufactures instructions. Direct sequencing of the resulting prey plasmid was carried out as described 2.2.7.3, to verify that the desired plasmid had been isolated.

The resulting prey plasmid was transformed back into yeast as described in the small scale transformation protocol 2.2.7.1. This transformation was done in duplicate, once in addition of the bait plasmid, pGBDU-Bbs6, and once with the addition of an empty pGBDU plasmid. Following the transformation, cells were plated onto SD-Ura-Leu plates, to select for colonies containing both plasmids. To test for interaction of the two plasmids or autoactivation of the prey plasmid, the co-transformed colonies were streaked onto SD-Ura-Leu-Ade+X-α-gal plates. This was done in triplicate for each condition. An interaction between the bait and prey was confirmed if the colonies transformed with the prey plasmid and pGBDU-Bbs6 grew on these plates and turned blue, in the absence of growth from colonies transformed with the prey plasmid and empty pGBDU. If colonies transformed with prey plasmid and empty pGBDU were able to grow on the SD-Ura-Leu-Ade+x-α-gal plates, it indicated that the prey colonies autoactivate, rendering the interaction invalid.

2.2.8 Analysis of *Bbs6*$^{-/-}$ Mouse

2.2.8.1 DNA extraction from tail tips

DNA was extracted from tail tips taken from pups aged 9-13 days for genotyping. Approx 5 mm tail tips were digested in 500 µl tail lysis buffer (see stock solutions) at 55°C overnight. For DNA precipitation 500 µl isopropanol was added and samples were spun down at 100 x *g* for 30 minutes at 4°C. The DNA pellet was resuspended in 250-400 µl depending on pellet size. 1 µl was used for PCR.

2.2.8.2 Harvesting organs

Mice were killed by cervical dislocation. Organs of interest were dissected, washed briefly in PBS and fixed in either 4% formaldehyde (FA) or 4% paraformaldehyde (PFA) for at least 24 hr at 4°C. Larger organs such as the brain and the kidneys were fixed for longer. To aid the fixation process in the cochlea, a small hole was made in the apex and at the bottom, with the smallest needle available. Adult snouts were fixed in Bouins solution (see 2.1.2 Stock Solutions) for a minimum of 3-4 days. Adult cochlea were stored in 4.13% EDTA, pH 7.3 at 4°C for 3-4 days for de-calcification post fixation.

2.2.8.3 Embedding and sectioning

Wax Embedding

Smaller organs were dehydrated through a series of ethanol concentrations (70%, 90% and 100%) in PBS for 60 minutes each. They were placed in a 1:1 mixture of 100% ethanol:Histoclear for 30 minutes, before being placed in 100% Histoclear for 30 minutes. These washes were carried at room temperature under gentle shaking. For embedding, organs were taken out of Histoclear and placed in a 1:1 mixture of Histoclear:molten mounting wax for 30 minutes at 55°C. The Histoclear:wax solution was replaced with fresh wax

three times for 30 minutes each, before the organs were placed in the bottom of a plastic well and covered with more fresh wax. Orientation of organs in the wells was important as this determined the cutting angle on the microtome.

Kidneys were initially dehydrated in 70% ethanol overnight. Each subsequent step was carried out as above, however the length of time for each step was doubled to allow complete penetration of the various solutions, due to the larger size of this organ.

For adult cochlea, dehydration and wax embedding was carried out under vacuum in a wax embedding machine to allow the solutions to fully infiltrate the organ. Cochlea were orientated in such a way, that upon sectioning, slices would be cut through all three cochlear turns simultaneously.

Wax embedded organs were left to set at room temperature for a period of 24 hours before sectioning began. Immediately prior to sectioning, wax blocks containing organs were chilled to 4°C and kept on ice. Wax sections were cut at 4-6 μM thickness, allowed to smooth out by floating on the surface of a water bath heated to 55°C, and were then dried on glass slides. To enable the sections to adhere to the glass slides better, they were 'baked' in an oven at 65°C for 10 minutes. Wax sections could be stored indefinitely at room temperature.

OCT Embedding

After fixation, organs were left to equilibrate in 20% sucrose in PBS at 4°C overnight. Organs were frozen in Optimal Cutting Temperature compound (OCT) on dry ice. OCT was poured into an appropriately sized mould and the organ inserted in the required orientation. The mould was placed on to dry ice, to quickly freeze the OCT, thus embedding the organ. OCT embedded organs were stored at -80°C.

OCT embedded organs were sectioned on a cryostat set at approximately -22°C. Embedded organs were removed from the moulds and fixed onto a specialised platform with fresh OCT. Sections were cut at 4-6 μM thickness,

collected onto glass slides and allowed to dry on a hot plate. For long term storage OCT sections were kept at -80°C.

For wax embedded and OCT embedded organs, sections were mounted onto either TESPA coated glass slides or positively charged SuperFrost + glass slides (BDH).

2.2.8.4 Hematoxylin and eosin staining

Wax embedded sections were stained with hematoxylin and eosin to enable visualisation of nuclei and cytoplasm. To remove the wax, sections were placed twice in 100% Histoclear for 5 minutes. Subsequently sections were re-hydrated through a series of ethanol solutions 100%, 90%, 80%, 70%, 50% for a minute each. Before being stained sections were washed for 2 minutes under running tap water. Sections were stained in 100% hematoxylin solution for up to 2 minutes. Subsequently sections were again washed for 2 minutes under running tap water and slowly dehydrated through a series of ethanol solutions 50%, 70%, 80%, 90% and 100% for a minute each. Following dehydration, sections were stained with 25% alcohol based eosin for 3 minutes and then washed twice for 1 minute in 100% ethanol. Finally slides were placed in histoclear for 10 minutes before being left to dry.

Coverslips were glued onto the slides with DPX, allowing the sections to be viewed under a microscope. Once dry, slides could be stored at room temperature indefinitely.

2.2.8.5 β-galactosidase assay

Dissected organs were lightly fixed for 10-30 minutes, depending on organ size, in 4% formaldehyde/ 2 mM $MgCl_2$/ PBS. After subsequent washing in PBS/ 2 mM $MgCl_2$, they were incubated with gentle shaking in X-gal staining solution (see stock solutions) at 37°C for 5 to 16 hours. Stained organs were

then washed once with PBS and twice with methanol, after which they were fixed properly to allow wax embedding.

Following a light fix for 10 minutes, adult cochlea were stored in 4.13% EDTA/ 2 mM $MgCl_2$ for 2-3 days prior to incubation in the staining solution. This enabled the solution to fully penetrate the organ.

2.2.8.6 Preyer reflex test

To test the Preyer reflex a custom made click-box (MRC Institute of Hearing Research, Nottingham) was held 30 cm above the mouse and a calibrated 19.5 Hz toneburst at an intensity of 90 dB SPL was administered. The mouse was given a score of 1.0 if it was judged to respond well by flicking its ears flat against the head (Preyer reflex), a score of 0.5 if there was a mild response, and a score of 0.0 if there was no response whatsoever. The investigator was blind to the genotype of the animal tested.

2.2.8.7 Distortion product otoacoustic emissions

Distortion product otoacoustic emissions (DPOAEs) were measured in each ear utilising the IL0292 DP instrument (Otodynamics Ltd, Hatfield). A clinical infant ear probe was adapted with a tapered tube to fit the mouse ear. A power averaged mean level of emission obtained with equal 70 dB SPL stimuli (f_2/f_1=1.2) was calculated from each recording from mutant mice and subsequently compared with similar values from wild-type controls. The corresponding mean dB SPL power scores for noise were also calculated and only values above noise regarded as positive emissions. Data was only obtained at frequencies from 3.5-kHz up to 7-kHz from the mice.

2.2.8.8 Buried food pellet recovery

Mice were given Cheerios® (a sugar coated cereal) as part of their diet for a two-week period prior to testing, to acquaint them with the treat. They were

subsequently deprived of food overnight for 16 hours before testing. In each trial a single mouse was placed into a clean test cage and the latency was measured to retrieve the buried treat. This was defined as the time taken for the mouse to uncover the food and grasp it in its forepaws and/or teeth. The food pellet was placed approximately 0.5 cm below the surface of the bedding material, and its location changed randomly on each test day. Mice were tested on three separate occasions, each trial being separated by one week. The experimenter was always blind to the genotype of the animal being tested.

2.2.9 Immunohistochemistry

2.2.9.1 Animals

Expression analysis was performed on mouse cochlea (CD1 or 50:50 129Sv/Ev:C57BL/6J background) over a period of ages E13.5-P12 (embryonic day 13.5/postnatal day 12). *Bbs6*$^{-/-}$ mice were generated and identified as described in section 6.2.1. The period 0-24 hrs after birth was assigned to day 0 (P0).

2.2.9.2 Preparation of tissue

Animals were culled by cervical dislocation, cochleae dissected and fixed in 4% paraformaldehyde for a minimum of two hours at room temperature or overnight at 4°C. For whole-mount preparations, organ of Corti were dissected prior to staining. For transverse cryo-sections, cochleae were embedded in OCT Embedding Medium (R A Lamb) under vacuum and frozen at -80°C, before cutting on a cryostat at 8 µm thickness. Sections were mounted onto Superfrost Plus (VWR International) glass slides and dried at 45°C for five minutes before storage at -80°C.

2.2.9.3 Confocal immunofluorescence

Frozen sections were allowed to reach room temperature before being washed once with PBS for five minutes to remove OCT. The following protocol was carried out on both whole mount tissue and sections. Tissue was permeabilised by washing three times for five minutes with buffer T (0.1M Tris, pH 7.5, 0.15M NaCl, 0.1% Triton X-100), then incubated in Mouse-on-Mouse (MOM) IgG reagent (made up to suppliers specifications) in buffer T for one hour at room temperature. This was followed by a second blocking step with block T (10% FCS in buffer T) for one hour at room temperature. Tissue was incubated with primary antibodies diluted in block T for two hours at room temperature or overnight at 4°C. Following washes in buffer T, tissue was incubated with secondary antibodies diluted in block T in the dark for two hours at room temperature. Following washes in buffer T, tissue was mounted with Vectashield containing DAPI (Vector Laboratories). Tissue was stored at 4°C in the dark. Imaging was carried out with Dr. D. Jagger, using a Zeiss LSM500 confocal laser-scanning microscope equipped with a 63X oil immersion objective (N.A. 1.4), in multi-track mode to prevent cross-talk between channels. Data was analysed using LSM 5 Image Browser.

2.2.9.4 Antibodies

Primary antibodies were either bought from given suppliers or obtained from collaborators. See appendix D for a table of all antibodies used, origins and final concentrations. Primary antibodies were detected using tagged secondary antibodies, either anti-rabbit or anti-mouse conjugated with Alexa Fluor 488 and 594 (Molecular Probes; 1:200). In some experiments actin was labelled with FITC-tagged phalloidin (Sigma; 1:1000), this was done in conjunction with the secondary antibody incubation.

2.2.9.5 Electron microscopy

Cochlea were dissected from sacrificed animals and a small hole was made in the apex to allow entry of the fixative. They were then placed in EM fix (2.5%

glutaraldehyde in 0.1 M cacodylate buffer with 3 mM CaCl2, pH 7.3). Cochleas were then dissected in cacodylate buffer to isolate the organ of Corti and prepared for SEM (Scanning electron microscopy). SEM was carried out by Prof. Andy Forge at the Centre for Auditory Research, UCL Ear Institute, London.

2.2.9.6 Expression analysis of Bbs6 transcript

β-galactosidase assays were performed on P0 and adult cochlea from heterozygous animals, no *β-galactosidase* activity was detected in wild-type animals. Assays were carried out as described in section 2.2.8.5.

2.2.10 Zebrafish analysis

2.2.10.1 Zebrafish lines

Zebrafish, *Danio rerio*, were maintained at 28.5 °C on a 14h/10h light/dark cycle. TL wild-type embryos were collected in Fish water from natural matings, cultured and staged by developmental time and morphological criteria. We used the trilobite (*tri*) allele tri^{m209} and the sonic hedgehog mutant smoothened (smo b577 or smo b641). Mutant embryos were obtained by incrossing heterozygous carriers. To allow embryos to develop normally they were incubated at 28.5°C. Incubation temperature was adjusted to 25 °C or 31 °C to decrease/increase speed of development accordingly.

2.2.10.2 Morpholino antisense oligonucleotide injection

Translational morpholinos against the start ATG of *bbs5* (NM_200299) and *bbs8* (ttc8:BC062872) were designed by and obtained from Gene Tools (Oregon). Morpholino antisense oligo sequence for *bbs5:* TCTCACCGGAGAAACACCACACACA. Morpholino antisense oligo sequence for *bbs8:* GATCACTGTCTGCGTATATTGTCGA. Diluted morpholino was

injected into zebrafish embryos at the 1-2 cell stage. Injected embryos were observed for up to 72 hours and then imaged.

2.2.10.3 Whole-mount RNA *in situ* hybridisation

Riboprobe Preparation

Riboprobes were synthesised from linearised DNA templates using T3,T7 or SP6 polymerases. See appendix for a list of probes used with relevant enzyme information.

Plasmid DNA was linearised by restriction digest as described in section 2.2.4. Typically 25 µl reactions were set up and digests were incubated for a maximum of two hours. An aliquot of the digest was run out on a 1% agarose gel to confirm linearisation. Following treatment with 1 µl Proteinase K (10mg/ml) at 37°C for 30 minutes, phenol chloroform extraction of the plasmid DNA was performed twice. An equal volume of phenol chloroform was added to the digest and spun at 100 x g for 5 minutes. The top phase was transferred into a new eppendorf tube and the process was repeated. The DNA template was then precipitated with sodium acetate by adding 2.5 x volume 100% ethanol and 0.1 x volume 3M sodium acetate, pH 5.2. Reagents were mixed by vortexing and left at -20°C for a minimum of 1 hour. Precipitated DNA was spun at 100 x g for 30 minutes and washed in 70% ethanol. Prior to transcription, an aliquot of the DNA template was run on an agarose gel.

Transcription reactions were carried out in a final volume of 20 µl made up in sterile distilled water. Reagents for transcription were supplied by Roche. The following transcription mix was incubated for a minimum of 2 hours at 37°C:

1 µg DNA (from precipitated linearisation)
1x transcription buffer
1x DIG-nucleotide mix
0.1M DTT
1µl Rnasin
1U T3/T7/SP6 polymerase enzyme

In sterile distilled water

1U of DNase was added to the transcription and incubated for a further 15 minutes at 37°C. Addition of 1µl of 0.5M EDTA, pH 8.0 stopped the reaction. Post transcription, an aliquot of the RNA template was run on an agarose gel. For precipitation the reaction volume was made up to 50 µl with sterile distilled water. Removal of unincorporated nucleotides was carried out using a ProbeQuant™ G-50 Micro Column (Amersham Biosciences). The 50 µl sample was spun through the column following the manufactures instructions. The eluted sample was precipitated for a minimum of 1 hour at -20°C with 0.25 x volume 10M NH_4OAc and 3 x volume 100% prechilled (-20°C) ethanol. The precipitated probe was spun at 100 x g for 15 minutes, washed in 70% prechilled ethanol and the final pellet was resuspended in 20 µl prehybridisation solution (Hyb -). The probe was stored at -20°C.

In Situ Hybridisation

Embryos were dechorionated in Fish water and fixed overnight at 4°C in 4% paraformaldehyde/PBS. Embryos were then washed in PBS and subsequently in 100% methanol. Embryos were then placed in 100% methanol at -20°C for a minimum of 2 hours. Embryos were rehydrated by rinsing in 75% methanol/PBTw (PBS/0.1% Tween-20), 50% methanol/PBTw, 25% methanol/PBTw and followed by two final washes in PBTw for 5 minutes each. Proteinase K (PK) digestion was carried out in 1 x PK in PBTw. Length of time required was dependent on the age of the embryo.

Up to tailbud: No PK

2-10 somites: In and out of PK

10-15 somites: 4 minutes PK

16-26 somites: 5 minutes PK

24 hrs: 20 minutes PK

30 hrs: 30 minutes PK

Following PK digestion, embryos were rinsed twice in PBTw and refixed in 4% paraformaldehyde/PBS for 20 minutes at room temperature. Embryos were subsequently rinsed three times in PBS and washed twice for 5 minutes with PBTw. To prehybridise, PBTw was removed and replaced with prehyb

solution (Hyb-). Embryos were incubated in Hyb- for at least 2 hours at 65°C. The *in situ* probe was diluted in hybridisation solution (Hyb +) as required. Diluted probe was stored at -20°C and could be reused. Prior to hybridisation, the probe mix was heated to 95°C for 5 minutes. Embryos were incubated in preheated probe mix overnight at 65°C. Following this hybridisation, the following washed were carried out at 65°C:

1x 5 minutes in Hyb-

1x 5 minutes in 25% Hyb-/75% 2x SSC

1x 10 minutes in 2x SSC

3x 30 minutes in 0.2x SSC

Embryos were subsequently rinsed twice in maleic acid buffer (MAB) at room temperature. Embryos were blocked by incubation for 2-3 hours in 2% Blocking Agent (Boehringer) made up in MAB (MABI) at room temperature. MABI was replaced with an anti-DIG-AP antibody made up in MABI (1 in 6000) and left overnight at 4°C. Following a minimum of 6 washes of 15 minutes each, the embryos were rinsed twice in 0.1M Tris pH 9.5/0.1% Tween-20. Embryos were then transferred into a tube containing NBT/BCIP solution (NBT/BCIP Ready-To-Use Tablets, Roche), and incubated in the dark until the colour reaction was complete. Incubation was carried out at room temperature, but for the first 30 minutes of incubation, embryos were kept at 4°C to avoid too rapid a response. Once the reaction was complete, embryos were rinsed three times in PBS and refixed in 4% paraformaldehyde/PBS for 20 minutes at room temperature. Two final washes in PBS were carried out before equilibrating in 70% glycerol/PBS prior to examination.

2.2.10.4 Immunohistochemistry in zebrafish

For immunolocalisation of the Kupfer's vesicle, immunohistochemistry was performed on whole-mount eight somite stage embryos. Post dechorionation, embryos were fixed in 80% methanol/ 20% DMSO overnight at 4 °C. They were then rehydrated through 75%, 50% and 25% methanol/PBS before being washed several times in PBST (0.5% triton/PBS). Embryos were blocked over night in Fish block (10% goat serum (heat inactivated)/1%

DMSO/ PBST) at 4°C. Embryos were incubated with primary antibody, diluted in Fish block overnight at 4°C. Following several vigorous washes with PBST at room temperature and under shaking, embryos were further blocked for two hours at room temperature in Fish block. Incubation with secondary antibody made up in Fish block was done overnight at 4°C. Following a further round of vigorous washing several times with PBST, embryos were stained with DAPI solution for two hours at 4°C. Embryos were stored in PBS at 4°C for a maximum of one week before being dissected and mounted. Dissections were done in Fish water under a dissection microscope to remove the yolksac and orientate the Kupfer's vesicle upright before mounting in 1% agarose.

A monoclonal anti-acetylated tubulin antibody (1 in 400, Sigma) was used to stain the cilia. Primary antibodies were detected using a tagged anti-mouse secondary antibody conjugated with Alexa Fluor 488 (1:200, Molecular Probes).

2.2.10.5 Imaging

For obtaining images of the embryos after morpholino injection, live embryos were anaesthetised with tricaine methanesulphonate and transferred into 3% methyl cellulose. *In situ* hybridisation specimens were equilibrated in 70% glycerol/PBS. Embryos were photographed with a Nikon dissecting microscope. Images were captured with a digital camera (Zeiss Axio Cam MRm) and processed using Adobe Photoshop. A Lecia Confocal microscope was used for confocal microscopy imaging of the Kupfer's vesicle. Images were processed using Volocity (Improvision) software.

Chapter 3: Mapping translocation breakpoints in an Iranian BBS patient by fluorescent *in situ* hybridisation

Aim: To map the translocation breakpoints of a patient with BBS on chromosome 3p and 10p and to identify candidate genes.

3.1 Introduction

In 1994 a third locus, following *BBS1* and *BBS2* (see chapter 1.2.), was mapped to chromosome 3 (3p12-13). The initial linkage analysis was performed on an Arab-Bedouin kindred and localised the putative BBS3 gene to a 11-cM region between D3S1254 and D3S1302 (Sheffield *et al.*, 1994). Haplotype analysis on inbred families on the island of Newfoundland refined this interval, narrowing the critical region to 6-cM between D3S1595 and D3S1753 (Young *et al.*, 1998). In 2000 a family from Iran, not related to either of the two other reported families (the Arab-Bedouin and the Newfoundland families), showed linkage to this region (maximum LOD score = 4.15 and recombination fraction $\theta = 0$, at D3S1603)(Ghadami *et al.*, 2000). Whilst this result did not contribute to narrowing the critical region, it did confirm previous assignment for BBS3.

An Iranian BBS patient was identified with a paternally inherited balanced reciprocal translocation t(3;10)(p13;p15.3) (Fig 3.1). Mutational analysis of all other BBS loci at that time had not revealed any pathogenic mutations. The patient was diagnosed with BBS upon displaying all the classical signs; retinitis pigmentosa, polydactyly, obesity, renal dysplasia, mild learning difficulties and self-limiting hepatic failure. G-banding karyotype analysis indicated that the breakpoint was at 3p13 and 10p15. Therefore, given that the published linkage interval for *BBS3* was 3p13-12, it was hypothesised that the 3p breakpoint of the translocation might disrupt the, as yet unidentified, BBS3 gene (Fig 3.2).

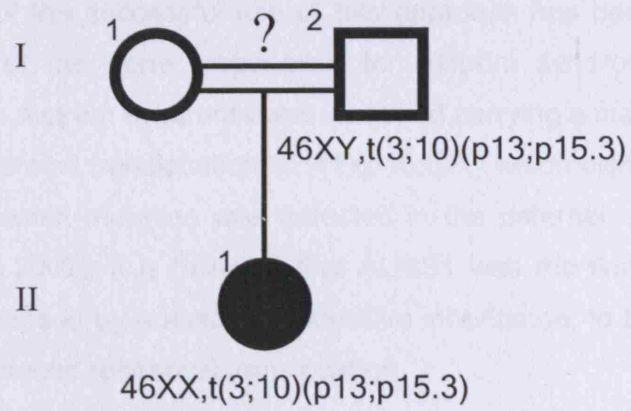

Figure 3.1: Iranian BBS pedigree. The affected daughter (II-1) has inherited the translocation from her unaffected father (I-2). The patient has no siblings and neither of her parents are affected. Consanguinity cannot be ruled out.

The hypothesis for this study was that the paternal copy of *BBS3* was disrupted by the translocation, and the maternal copy of the gene contains a pathogenic mutation such as a coding sequence change. In order to test this hypothesis it was decided that fluorescence *in situ* hybridisation (FISH) analysis should be performed on EBV cell lines from II-1 in order to refine the translocation breakpoint and to identify potential candidate BBS genes.

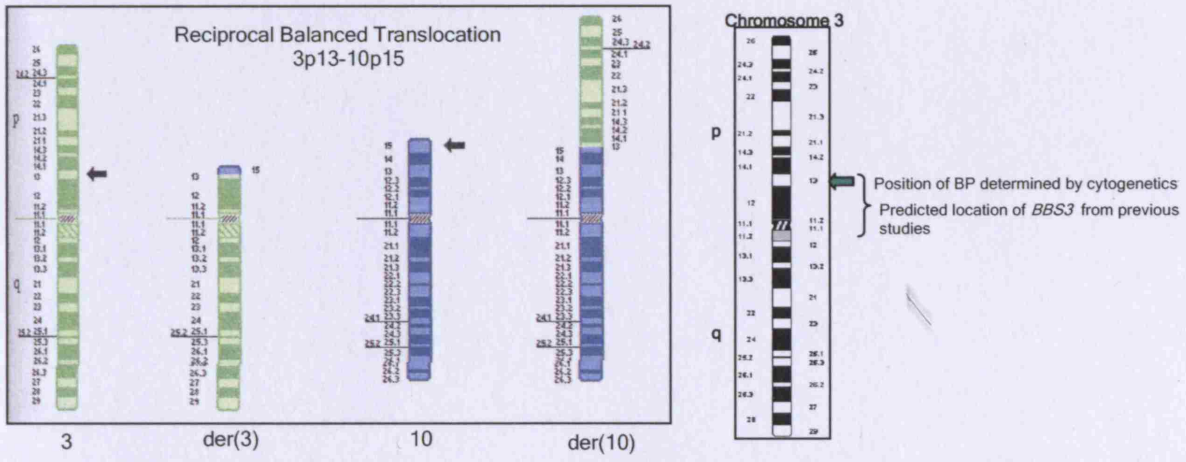

Figure 3.2: Karyotype of BBS patient showing breakpoint and predicted position of BBS3. Fluorescent in situ hybridisation analysis was performed on EBV transformed PBL from II-1 to determine if breakpoints were associated with any gene disruption.

An example of the successful use of this approach has been shown by the identification of the gene responsible for Alström syndrome, *ALMS1*. An individual with Alström syndrome was identified carrying a maternally inherited balanced reciprocal translocation t(2;11)(p13;q21) which disrupted *ALMS1* on 2p13. A frameshift mutation was detected in the paternal copy of the gene (Hearn *et al.*, 2002). It is believed that ALMS1 was the first human disease gene, characterised by autosomal recessive inheritance, to be identified as a result of a balanced reciprocal translocation.

3.2 Materials and Methods

3.2.1 Preparation of chromosomal probes

Bacterial Artificial Chromosomes (BACs) surrounding the predicted breakpoint were identified using the UCSC Genome Browser. They were obtained from BACPAC (California) and DNA was prepared using the techniques described in section 2.2.1.4. BAC DNA was then nick translated (see section 2.2.1.4-5), to incorporate a fluorescent label (SpectrumGreen or SpectrumOrange), and subsequently precipitated with herring sperm DNA and human Cot-1 DNA (see section 2.2.1.6), to inhibit competitive binding.

3.2.2 Preparation of metaphase spreads from patient cells

An EBV-transformed patient B-cell lymphoblastoid cell line was cultured as described in 2.2.1.1. Metaphase spreads and slides for fibre FISH were prepared as in section 2.2.1.2 and 2.2.1.3 respectively.

3.2.3 Preparation of genomic DNA from EBV cell lines

DNA was extracted from an EBV cell culture using the PUREGENE DNA Purification kit (Gentra) following manufacturers instructions. Informed consent was obtained.

3.2.3 Fluorescent *in situ* Hybridisation

Hybridisation of the metaphase spreads or fibre slides with BAC probes and known control probes was performed as described in section 2.2.1.5. Slides were viewed under a Zeiss Axioskop fluorescent microscope and images were taken using a Photometrics camera with SmartCapture software.

3.2.4 Sequencing

Primers were designed, and PCR amplification and sequencing was carried out as described in sections 2.2.2 and 2.2.3 Sequencing. Analysis was performed using Sequencher version 4.0.5 software.

3.2.5 Other methods

RT-PCR was performed on cDNA generated from mRNA extracted from patient cells, using exonic primers (see section 2.2.6). To verify a sequence change identified by direct sequencing, restriction digests were carried out on the PCR product in cases where the base change introduced or ablated a digest site (see section 2.2.5).

3.2.6 Websites

Genome Browsers: http://genome.ucsc.edu/
http://www.ensembl.org/Homo_sapiens

Protein Predictions: http://smart.embl-heidelberg.de/
http://www.sanger.ac.uk/Software/Pfam/
http://blocks.fhcrc.org/sift/SIFT.html

Sequence Alignments: http://searchlauncher.bcm.tmc.edu/multi-align

3.3 Results

3.3.1 Analysis of known BBS genes in Iranian patient

The patient was screened for mutations in all BBS genes cloned at that time, *BBS1*, *BBS2*, *BBS4* and *BBS6* by direct sequence analysis. No pathogenic sequence changes were identified. Sequence analysis is discussed in more detail in chapter 4.

3.3.2 Breakpoint on chromosome 3

Various BACs around the predicted breakpoint identified from the sequence databases (Ensembl and UCSC), were used as probes for FISH analysis of metaphase spreads from the patient and controls. Chromosome 10 centromeric control probes of a different colour to that of the BAC probes were simultaneously hybridised.

BACs hybridising proximal to the breakpoint (below) were identified by the presence of four spots, two of the same colour on both chromosome 3 and derivative 3 (der 3), and two for the centromeres of chromosome 10 and derivative 10 (der 10). An example is seen in figure 3.3.

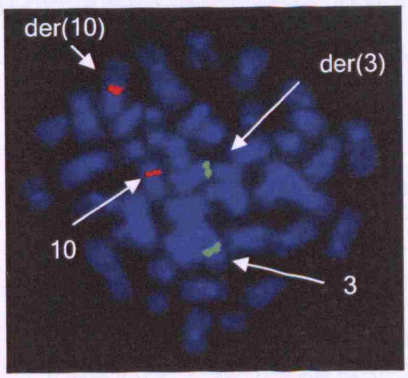

Figure 3.3: Metaphase spread from Iranian patient (II-1) with balanced reciprocal translocation t(3;10)(p13;p15.3) hybridised with chromosome 10 centromeric control probe (red) and RP11-1113O9 BAC probe (green) localising to chromosome 3. This shows that this BAC is located proximal to the breakpoint.

BACs hybridising distal to the breakpoint (above) were also identified by the presence of four spots, but this time distributed in a different pattern; with the normal 3 and 10 chromosome having a single spot, each a different colour and the der 10 chromosome also having two spots, a centromeric one as well as a BAC one of the other colour due to the chromosomal rearrangement. An example is seen in figure 3.4.

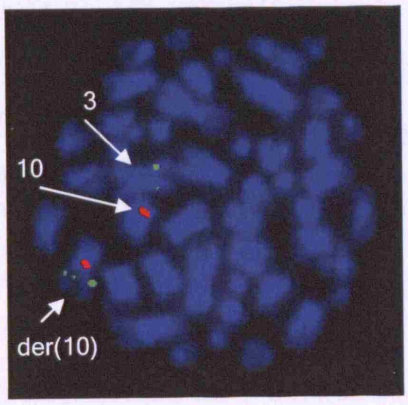

Figure 3.4: Metaphase spread from Iranian patient (II-1) with balanced reciprocal translocation t(3;10)(p13;p15.3) hybridised with chromosome 10 centromeric control probe (red) and RP11-1072F12 BAC probe (green) localising to chromosome 3. This shows that this BAC is located above the breakpoint.

A total of 19 BACs were hybridised in this way, and their location assigned as either proximal or distal to the translocation breakpoint (Fig 3.5).

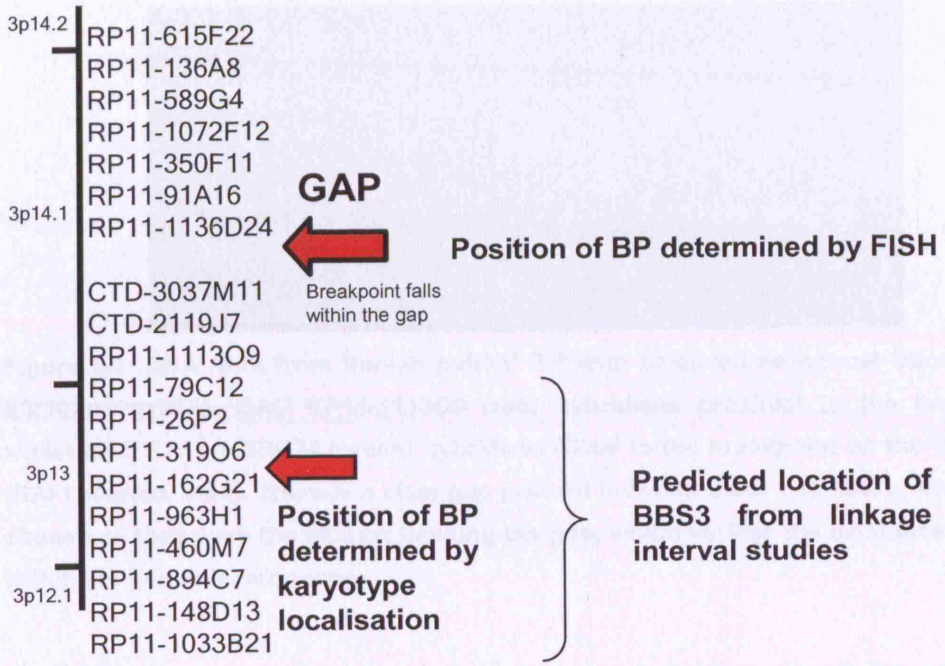

Figure 3.5: The position of 19 BAC probes, the predicted breakpoint by G-banding karyotype localisation and the linkage interval for *BBS3*, in relation to the translocation breakpoint in patient II-1.

Unfortunately, it transpired that the breakpoint predicted by cytogeneticists using G-banding karyotype localisation, was misleading. This is potentially due to the fact that there could possibly be a certain degree of ambiguity at this fragile site. The 3p breakpoint actually mapped distal to the predicted region and outside the locus for *BBS3*. The breakpoint mapped to within an, as yet, incomplete region of the genome sequence.

The gap in the genome sequence was ~250kb in size. The instability of this region may account for the presence of a breakpoint. The presence of the gap was verified by fibre FISH (Fig 3.6).

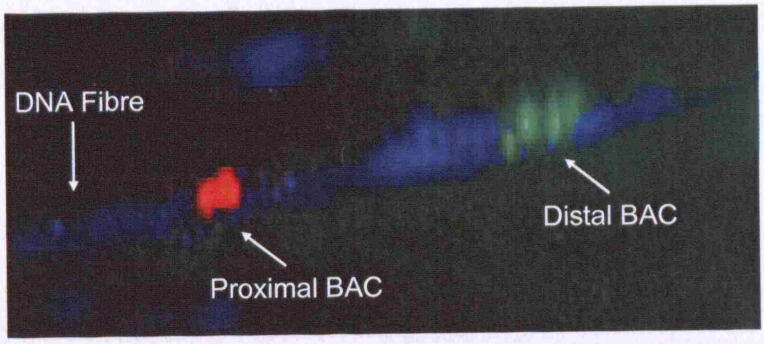

Figure 3.6: DNA fibre from Iranian patient II-1 with balanced reciprocal translocation t(3;10)(p13;p15.3). BAC RP11-1113O9 (red) hybridises proximal to the breakpoint, whilst BAC RP11-1136D24 (green) hybridizes distal to the breakpoint on the DNA fibre (DAPI stained, blue). There is a clear gap present between these two BACs, which were chosen as they were the closest flanking the gap, which verifies the existence of a gap within the genomic sequence.

A BAC spanning the breakpoint would hybridise to three separate chromosomes, 3, der 3 and der 10. Unfortunately the translocation breakpoint fell within a gap in the sequence databases, therefore a BAC spanning the breakpoint could not be identified.

This region of the human chromosome was compared to that of the mouse where there was no gap present. There was homology of synteny group on either side of the gap, but no genes were identified within the region (Fig 3.7).

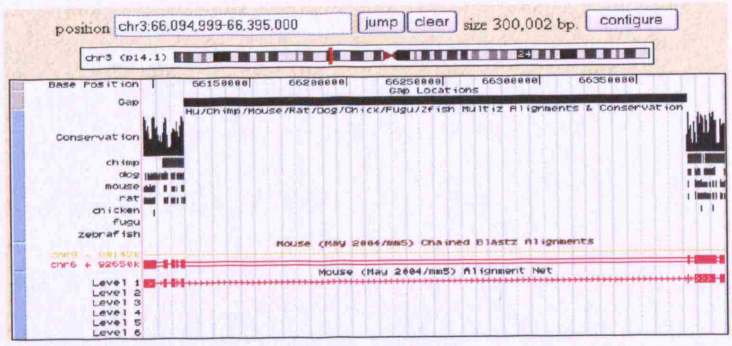

Figure 3.7: Region of human genome sequence in which a gap was identified, showing conservation of surrounding sequence in other genomes.

During the course of this study, *BBS3* was identified to be a member of the Ras superfamily of GTP-binding proteins located on 3q11.2, within the previously mapped interval for the gene (see section 3.1). Patient II-1 was screened for any sequence changes within this gene, but none were identified. Analysis of the breakpoint in this patient was continued, as it could identify further potential *BBS* gene candidates.

3.3.3 Breakpoint on chromosome 10

Although there was no evidence that a BBS gene might exist on chromosme 10, the mapped loci only account for 25% of all BBS patients (Stoetzel *et al.*, 2007). Therefore it is entirely possible that there may be a disruption to a novel BBS gene on chromosome 10. For this reason it was of interest to locate the translocation breakpoint on chromosome 10 in this patient. Nine BACs were screened as described in the previous section, and a BAC that spanned the breakpoint was identified (Fig: 3.8).

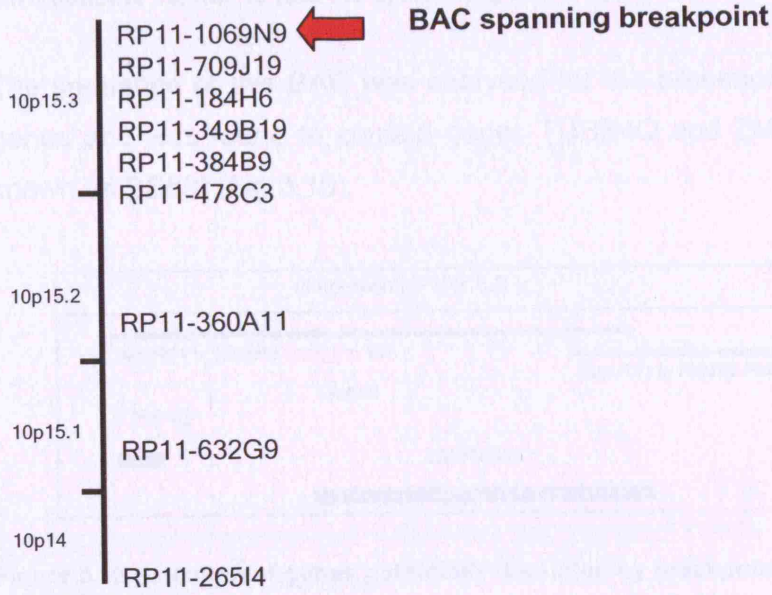

Figure 3.8: The position of the 9 BAC probes analysed in relation to the translocation breakpoint on chromosome 10 of patient II-1. BAC RP11-1069N9, which maps to 10p15.3, spanned the breakpoint.

Figure 3.9 shows the breakpoint-spanning BAC RP11-1069N9 hybridised to a metaphase spread prepared from the Iranian patient II-1. The BAC hybridises to three chromosomes: chromsome 10, derivative 10 and derivative 3.

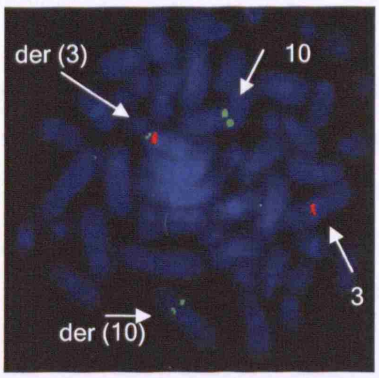

Figure 3.9: Metaphase spread from Iranian patient with balanced reciprocal translocation t(3;10)(p13;p15.3) hybridised with chromosome 3 centromeric control probe (red) and RP11-1069N9 BAC probe (green). This BAC probe hybridises to chromosome 10, der 10 and der 3, showing that it spans the translocation breakpoint.

The sequence of this BAC was analysed for the presence of candidate BBS genes and was found to contain genes TUBB4Q and ZMYND11 (previously known as BS69) (Fig 3.10).

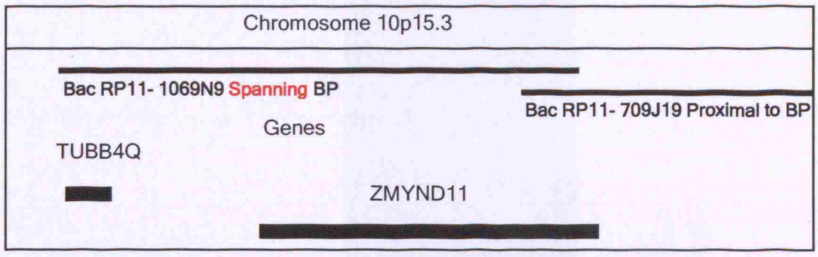

Figure 3.10: Location of genes potentially disrupted by breakpoint on chromosome 10.

TUBB4Q encodes a protein named beta-tubulin 4Q which contains 444 amino acids. It has more recently been renamed and is now referred to as TUBB8 (tubulin-beta 8). It belongs to the tubulin family and is a major constituent of microtubules. Its predicted structure is a dimer of alpha and beta chains and it is predicted to bind GTP at a site on the beta chain and on the alpha-chain (UniProtKB/TrEMBL entry). As the internal structure of cilia consists of a '9+2' axoneme that contains nine outer doublet microtubles, made up of alpha and beta tubulin, and cilia have been implicated to play a significant role in BBS, this gene was therefore potentially interesting.

Genomic DNA from patient II-1 and an unrelated control sample were prepared and analysed for the presence of any possible intragenic mutations in the maternal allele. The premise being that patient II-1 had disruptions to both copies of this gene, on the paternal allele due to the translocation and on the maternal a further pathogenic sequence variation. PCR primers were designed to amplify the entire coding region and intron/exon boundaries of TUBB4Q. Primer sequences and PCR conditions for the amplification of this gene can be found in the appendix. However, no sequence anomalies were identified compared to the control sample. RT-PCR was performed on cDNA generated from mRNA extracted from patient cells, using exonic primers (see appendix), but there was no difference between the patient and control, indicating that the TUBB4Q transcript was still expressed in the patient (Fig 3.11).

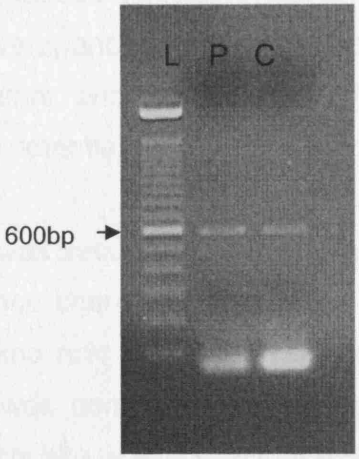

Figure 3.11: Gel showing the RT-PCR product for TUBB4Q in patient II-1 and control. RT-PCR product was generated from mRNA extracted from patient and control cells, using exonic primers. L= 100bp ladder, P= patient and C= control.

The gene ZMYND11 encodes a protein named Zinc finger, MYND domain containing 11, isoform b. Little is known about this gene, but it was initially classified as BS69 and is relatively large, comprising of 35 exons. The protein (527 amino acids) encoded by this gene was first identified by its ability to bind the adenovirus E1A protein. It is thought to contain a bromodomain, MYND-type zinc finger, PHD-type zinc finger, and a PWWP domain. The protein localises to the nucleus. It functions as a transcriptional repressor, and expression of E1A inhibits this repression. This protein is not expressed in tissue relevant to BBS and this, coupled with its large size, means it has assumed a low priority for screening.

3.3.4 Re-analysis of the breakpoint on chromosome 3

Several months after the analysis of the breakpoint on chromosome 3 had been completed, the incomplete region in the genome sequence was modified. New annotations included a gene, BAIAP1, which appeared to extend into the gap. The proposed function of this gene is that it may play a role as a scaffolding protein at cell-cell junctions. The protein contains guanylate kinase-like domains, WW domains and multiple PDZ domains. It is membrane-associated and localises to epithelial cell tight junctions. Some planar cell polarity (PCP) proteins contain PDZ domains and it is believed that BBS proteins may be involved in the PCP pathway (discussed in following chapters). There are seven different isoforms, which are widely expressed with the exception of skeletal muscle. A high level of expression is seen in the colon, kidney, lung, liver, pancreas, brain and heart. Many of these tissues are affected in BBS patients, and the presence of PDZ domains in the protein meant that this was a potentially interesting candidate gene.

As before, the gene was sequenced to find a possible intragenic mutation. A heterozygous sequence change was detected at the beginning of exon 16, which caused an amino acid substitution of proline for alanine (P835A) (Fig 3.12). This change was confirmed by restriction digest, as the sequence change eliminated a cut site when cut with the enzyme Hpy118III (Fig 3.13).

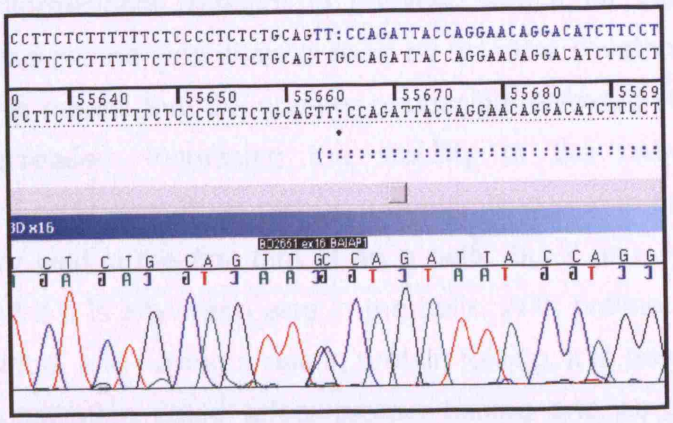

Figure 3.12: Chromatogram showing the sequence change at the beginning of exon 16 in BAIAP1 within patient II-1. The sequence change causes a missense substitution TTG (proline) > TTC (alanine).

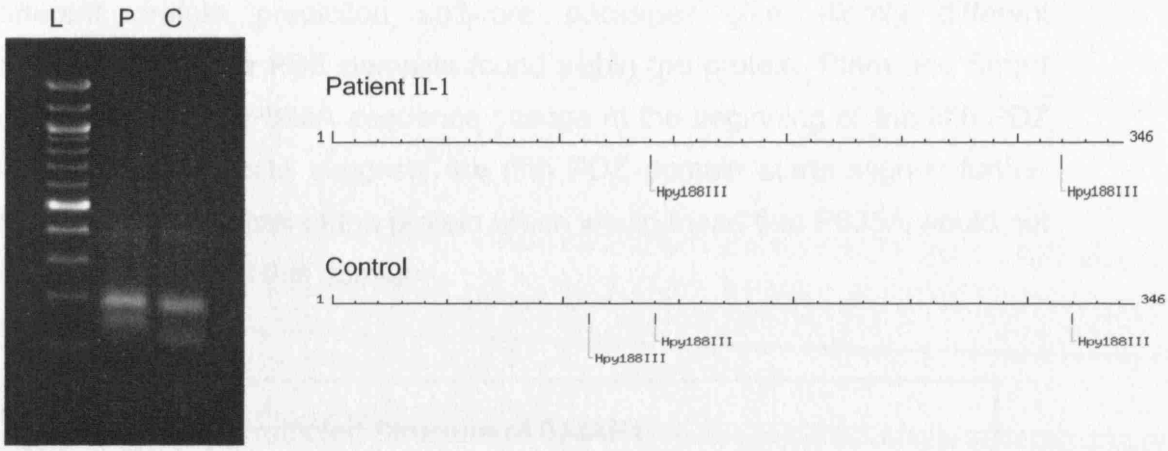

Figure 3.13: BAIAP1 exon 16 cut with Hpy188III in patient II-1 and an unrelated control. Hpy188III eliminates a cut site in the patient, so that when the products are separated on an agarose gel, fragment sizes vary compared to that of control. Confirming the heterozygous sequence change. L = 100bp ladder, P= patient II-1, C= control.

This sequence change was not seen in 204 control chromosomes, however it was not possible to sequence ethnically matched controls. This particular sequence change was not reported on SNP databases.

Proline and alanine are both hydrophobic amino acids, yet they are a different size and shape. Alanine has a single methyl group as a side chain, whilst proline, a cyclic secondary amino acid, has conformational constraints imposed by the cyclic nature of its pyrrolidine side group. Proline residues have less conformational freedom in unfolded structures than any other residue since the proline side chain is fixed by an extra covalent bond to the main chain. This means that the number of possible unfolded structures of a protein is decreased, increasing the stability of the native structure. Isomerisation of proline residues can be a rate-limiting step in protein folding. Proline fits very well in the first turn of an α helix, but it usually produces a significant bend if it is anywhere else in the helix. With proline being such a conserved residue, and having a role in protein folding, it is possible that this amino acid substitution could affect protein folding and as such putative protein-protein interactions (Biochemistry, Voet and Voet; Molecular Biology of the Cell, Alberts).

Different protein prediction software packages give slightly different localisations for the PDZ domains found within the protein. Pfam and Smart analysis place the P835A sequence change at the beginning of the fifth PDZ domain, whilst prosite suggests the fifth PDZ domain starts slightly further towards the N terminal of the protein which would mean that P835A would not be positioned within this domain.

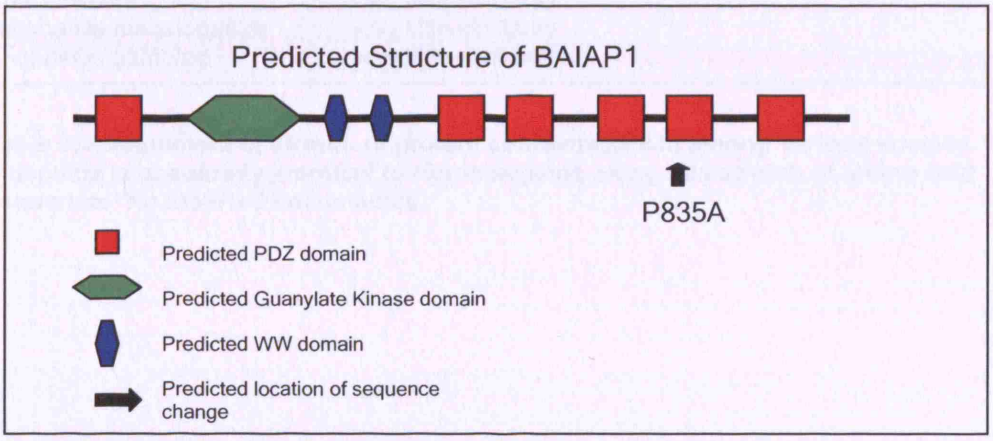

3.14: Predicted structure of BAIAP1, drawn as an amalgamation of the results from Pfam, Smart and prosite.

PDZ domains are well-known globular fold modules of many scaffolding proteins. The domains are involved in protein-protein interactions and play a central role in organising diverse cell signalling assemblies (Brone and Eggermont, 2005). To predict the effect of the amino acid substitution (P835A) on the protein function, SIFT (Sorting Intolerant From Tolerant) analysis was performed. The SIFT program uses sequence homology between related proteins to predict whether an amino acid substitution will affect protein function. Using this program the alanine to proline change at position 835 was predicted to be a tolerated substitution.

P835 is conserved among several species which contain the same sequence of amino acids, such as *Tetraodon nigroviridis*, *Danio rerio*, *Fugu rubripes* and *Mus musculus*. In *Xenopus tropicalis* and *Canis familiaris* the stretch of sequence is interrupted by additional amino acids (Table 3.1).

Homo sapiens	SRSMYENRL	PDYQEQ
Xenopus tropicalis	SRSMYENRLFIYCPLSGQERGFLSENISTHFQRECPV	PDFQEH
Canis familiaris	SRSMYENRPMSPSPASGLSKGERERE INSTSFGECQI	PDCQEQ
Tetraodon nigroviridis*	SRSMYESRL	PDFQEQ
Danio rerio*	SRSMYESRL	PDYQEQ
Fugu rubripes*	SRSMYESRL	PDFQEQ
Mus musculus*	SRSMYENRL	PDYQEQ
Gallus gallus	almost identical, but particular 'domain' missing	
Rattus norvegicus	almost identical, but particular 'domain' missing	
Apis mellifera	very little similarity	
Drosophila melanogaster	very little similarity	
Anopheles gambiae	very little similarity	

Table 3.1: Alignment of stretch of protein containing P835 among various species. Mus musculus is absolutely identical to Homo sapiens along this stretch of amino acid sequence. *No inserted amino acids

3.4 Discussion

The premise that balanced reciprocal translocations might reveal gene disruptions has been illustrated by the prior identification of ALMS1 and more recently by CGH array gene discoveries such as CHARGE syndrome (Hearn *et al.*, 2002; Vissers *et al.*, 2004).

Prior karyotyping initially placed the 3p breakpoint in this BBS patient, II-1, within the BBS3 interval providing a potential for positional cloning of this gene. However, a recent comparative genomics approach has identified BBS3 on 3q11.2 and found it to be a member of the Ras superfamily of GTP-binding proteins (Fan *et al.*, 2004). The 3p breakpoint actually mapped telomeric to the predicted region and outside the locus for *BBS3*. Unfortunately the translocation breakpoint in the Iranian patient mapped within an, as yet, incomplete region of the genome sequence. The gap in the genome sequence was ~250kb in size and the instability of this region may account for the presence of a breakpoint.

BAIAP1, a potential candidate, might be disrupted by the breakpoint on chromosome 3 as it lies near the edge of the gap, and could possibly be involved in BBS. The heterozygous sequence change identified in patient II-1 within the gene could be a polymorphism. However this particular sequence change has not been registered on SNP databases. Its absence from 204 control chromosomes is promising, but these were not ethnically matched. Whilst the sequence change is heterozygous, we have no way of knowing whether it lies on the maternally or paternally inherited chromosome. If the father, I-2, is also seen to carry the sequence change, the likelihood of BAIAP1 being involved in BBS decreases. However, there are cases where unaffected parents of BBS patients are homozygous for the most common BBS mutation M390R in *BBS1.* Cells from the father (I-2) are available to obtain genomic DNA to see whether he also carries the P835 sequence change in BAIAP1. Unfortunately, cells from the mother I-1 are not available for analysis. It is interesting that the particular amino acid that is affected is

conserved in several organisms, including *Mus Musculus, Fugu* and *Danio Rerio*, implicating its position as important to the proteins function. Screening this gene in further BBS patients could also be rewarding.

Further work is required to narrow down this breakpoint on chromosome 3p14.1, however this is hampered by the fact that this particular region of the human genome remains unsequenced.

The breakpoint on chromosome 10 was also further refined to 10p15. The TUBB4Q gene was identified as a potentially interesting target as it is located within the genomic region spanned by the breakpoint-spanning BAC. Sequence analysis was performed on the patient II-1, but no sequence changes were identified and RT-PCR product was no different in the patient than in the control, indicating that the TUBB4Q transcript is still expressed in the patient. The level of expression of the TUBB4Q transcript could possibly be measured by Real-time PCR, which may indicate whether there are any regulatory mutations that alter expression levels. ZMYND11, also found within the sequence of the BAC spanning the breakpoint on chromosome 10, still remains to be excluded.

Whilst BAIAP1 and ZMYND11 are not present in the Ciliary proteome, a data set enriched for proteins involved in ciliary function (see chapter 4), TUBB4Q is, further implicating this as a possible BBS candidate.

It is possible that the breakpoint on either chromosome interrupts regulatory elements, which are notoriously difficult to locate and may reside at considerable distances from the transcription units on which they operate. There is evidence to suggest that position effects can influence a gene from a distance of 1Mb (Lettice *et al.*, 2003).

It is likely that the patient has other chromosomal rearrangements or micro deletions, as it has become increasingly evident that such alterations occur collectively. A recent study revealed that a third of patients investigated had genomic imbalances that did not appear to be directly related to their

translocations. Up to 60% of patients with apparently balanced translocations also had additional rearrangements and karyotype complexity (Gribble *et al.*, 2005). In light of these findings and the advent of array based genome-wide scanning, high resolution analysis using CGH with 1 Mb or higher resolution tiling path clone sets, followed by further FISH and parental origin studies is recommended, in order to fully elucidate the range and complexity of genomic rearrangements in this patient.

Given the high degree of heterogeneity already observed in BBS and the fact that a large percentage of patients remain unlinked, it is possible that further disease related genes will be identified on chromosome 3 or 10. The gene TUBB4Q is the most interesting candidate to be identified during this study and it would be of interest to screen this gene in a pool of BBS patients.

3.5 Summary

Fluorescent *in situ* hybridisation was used to map the breakpoints of a balanced reciprocal translocation in an Iranian BBS patient. Unfortunately the breakpoint of chromosome 3 localised to an as yet incomplete region of the genome sequence. The breakpoint on chromosome 10 was mapped to a region containing two genes, which remain to be further validated as BBS causing genes. TUBB4Q is the most promising as it is contained in the ciliary proteome.

Chapter 4: Mutational analyses

Aims: To screen candidate *BBS* genes (*BBS3*, *BBS5* and *MGC1203*) in BBS patients.

4.1 Introduction

4.1.1 *BBS5*

Cilia and flagella are ancient, evolutionarily conserved eukaryotic organelles that project from cells and have been adapted by organisms to carry out diverse biological functions. They are microtubule-based structures nucleated by modified centrioles termed basal bodies (see section 1.3). The assembly, maintenance and function of cilia and flagella depend upon intraflagellar transport (IFT), and defects in this microtubule-based transport process and the function of cilia are associated with several human diseases, including BBS (see sections 1.3.3 and 1.3.4). Basal bodies can convert to centrioles that serve as the microtubule-organising centre (MTOC) in animal and algae cells. However, land plants, fungi and diatoms do not contain centrioles, which suggests that these organisms may have evolved other structures to organise microtubules (Pickett-Heaps, 1971). In order to identify proteins involved in ciliary and basal body biogenesis one of our collaborative groups undertook a comparative genomic approach that subtracted the nonflagellated proteome of *Arabidopsis* from the shared proteome of the ciliated/flagellated organisms *Chlamydomonas* and human (Li *et al.*, 2004). This identified 688 genes which were present exclusively in organisms with flagella and basal bodies, termed the flagellar apparatus-basal body (FABB) proteome (Fig 4.1).

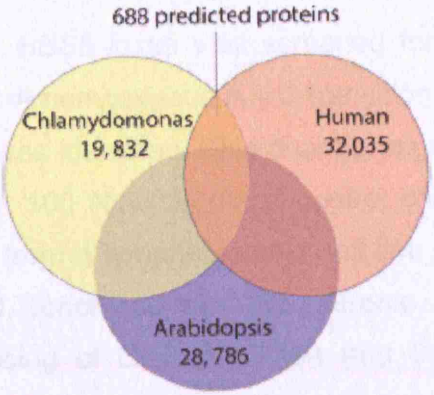

Figure 4.1: Diagram of the comparative approach to identify flagellar and basal body proteins. The proteome of *Chlamydomonas* (ciliated organism) was compared to the proteome of human (ciliated organism), from which the proteome of *Arabidopsis* (non-ciliated organism) was subtracted. The resulting 688 proteins were termed the flagellar apparatus-basal body (FABB) proteome (reproduced from Li *et al.* 2004).

The FABB proteome contained 52 of the 58 known flagellar and IFT genes (90%). At the time of creating the data set (in 2004), five of the then six known genes that when mutated, resulted in BBS in humans were included; *BBS1, BBS2, BBS4, BBS7* and *BBS8*. It was therefore hypothesised that genes in the dataset might be useful candidates for identifying novel BBS genes. This data set has since been updated, incorporating more recent ciliary and basal body proteomics data and can be accessed via www.ciliaproteome.org. Of the now known 12 BBS genes, 8 are found in the cilia proteome (see discussion).

At the time of identification of the FABB proteome, eight loci for the disease had been identified (*BBS1-BBS8*), six of which had been cloned. However *BBS3* and *BBS5* had not yet been identified. *BBS5* was the fifth BBS locus to be mapped in a large inbred family of European ancestry. Young *et al.* (1999) mapped the gene to a locus at chromosome 2q31 between markers D2S156 and D2S1238; the region spanned 14Mb and contained approximately 230 predicted genes. Two genes in this interval were present in the FABB proteome. FLJ11457, which encodes IFT139 and DKFZp762I194, which encodes a well-conserved, novel protein of unknown function. The complete open reading frame and intron-exon boundaries of FLJ11457 were sequenced in a patient from a family that defined the *BBS5* locus, but no pathogenic mutations were identified. Subsequently the Newfoundland family that

originally defined the *BBS5* locus was screened for mutations in the novel gene DKFZp762I194. A homozygous A→G transition at the +3 position of the exon 6 splice donor was identified. This change segregated with the disease and was not found in 100 Newfoundland control chromosomes. Analysis of RNA splice isoforms from a lymphoblastoid cell line from one of the patients compared to control concluded that the intronic mutation was found to compromise the splicing of DKFZp762I194 and therefore alter its protein product. As this gene also contains an X-box sequence upstream of the start ATG, it was a strong candidate for *BBS5* (Li *et al.*, 2004).

This previous work had been carried out by our collaborators. Whilst it was highly likely that this gene was in fact *BBS5*, more evidence was needed. It is for this reason that our patient cohort was screened for DKFZp762I194, to try and identify further mutations which could confirm the identification of *BBS5*.

4.1.2 *BBS3*

A locus for *BBS3* was initially mapped in 1994 and subsequent linkage analysis narrowed down the critical region to 6-cM between 3p12-13(Sheffield *et al.*, 1994; Young *et al.*, 1998; Ghadami *et al.*, 2000). (See chapter 3 for more details on the mapping of *BBS3*.) Further analysis at the time was problematic, as this critical interval contained >90 genes.

As previously mentioned, the BBS phenotype is thought to arise due to ciliary dysfunction. Notably, all known *C. elegans bbs* genes are expressed exclusively in ciliated cells. All contain a DAF-19 RFX transcription factor binding site (X-box) in their promoters approximately 100bp upstream of the translation start site (ATG) (Ansley *et al.*, 2003; Li *et al.*, 2004) (see fig 4.2).

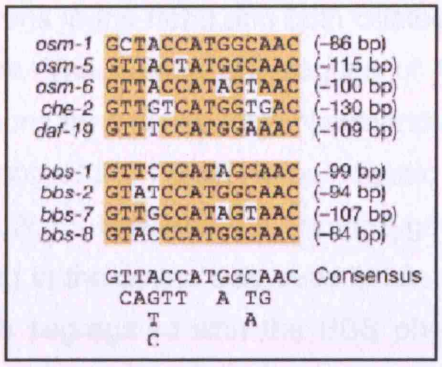

Figure 4.2: Alignment of X-boxes. The top panel shows the alignment of X-boxes from *C.elegans* genes expressed in ciliated neurons. The bottom panel shows the aligment of X boxes found in *C.elegans bbs* orthologues. The consensus sequence is given at the bottom. Distances in base pairs after the X-boxes are from the translation start site (ATG) of each gene. (Table taken from Ansley, Bandano et al 2003).

It was hypothesised that the *C. elegans* orthologue of human *BBS3* would also contain this regulatory element, which would allow prioritisation of candidates from the >90 genes that map to the BBS3 critical interval. In *C. elegans* 368 genes were identified with an X-box sequence within 1.5 kb of the start codon, 168 of which had a *bona fide* human orthologue. Three of these fell within the *BBS3* critical interval. The first gene, *ESRRBL1*, is most likely the human orthologue of *C. elegans che-13* which is expressed exclusively in ciliated neurons and has an important role in IFT. The second gene encodes the hypothetical protein *DKFZp761H079*, a member of the ARL family of small GTP-binding proteins (Takai *et al.*, 2001; Pasqualato *et al.*, 2002). As its sequence is similar to that of ARL2, it was named ARL2-like protein 1 (ARL2L1). The third gene encodes ARL6, another ARL family member. ARL proteins (so termed because they are ADP-ribosylation factor (ARF)-like), are small GTPases that undergo a GDP/GTP nucleotide exchange cycle, and are thought to be important regulators of cellular trafficking (Kahn *et al.*, 2006).

The expression patterns of the *C.elegans* orthologues of these three genes (*ESRRBL1, DKFZp761H079*, and *ARL6*) in *C. elegans* were virtually identical to those of the five known *C.elegans bbs* orthologues, (Ansley *et al.*, 2003; Li *et al.*, 2004). Namely, in a small subset of sensory cells that are ciliated, the

ciliated amphid neurons in the head and both ciliated phasmid neurons (PHA and PHB) in the tail. The human orthologues of these three genes were examined for mutations in a family from Newfoundland which was linked to the BBS3 locus (Young *et al.*, 1998). No pathogenic mutations were found in *ESRRBL1* or *ARL2L1.* However, a homozygous missense mutation (c.859G→C, resulting in the amino acid substitution G169A) was identified in *ARL6.* This mutation segregated with the BBS phenotype and was absent from 100 control chromosomes. For this reason, *ARL6* was hypothesised as a strong candidate for *BBS3.*

To validate this hypothesis, more evidence for the involvement of *ARL6* in BBS was required. Consequently it was decided to screen this gene in our patient cohort to look for the presence of pathogenic mutations.

4.1.3 *MGC1203*

As with many complex syndromes, the phenotypic variability observed amongst BBS patients cannot be explained by mutations at a single locus. For this reason it is plausible to assume that sequence variations at multiple loci exert a synergistic effect, modifying disease transmission and severity. As the interactions between known BBS genes are not enough to explain the degree of phenotypical variation among BBS patients (Katsanis, 2004), it was predicted that other mutant alleles might modify the disease manifestation. Yeast two-hybrid screens, using various BBS proteins as bait, have identified many possible interacting proteins.

In two separate yeast two-hybrid screens, both using BBS4 as bait, the protein MGC1203 (also known as CCDC28B; GenBank accession number NM_024296) was identified as a candidate interactor. This computationally predicted polypeptide is composed of 241 amino acids and bears no recognisable motifs. Amongst the other proteins identified, MGC1203 was of particular interest, as it was the only protein also present in the FABB proteome (flagellar apparatus-basal body proteome, see section 4.1.1).

Interactions between MGC1203 and most of the BBS proteins (BBS1/2/4/5/6/7/8) was confirmed by co-immunoprecipitations (Badano *et al.*, 2006). Furthermore, immunohistochemistry using a polyclonal antibody against MGC1203 in HeLa and IMCD3 cells showed staining near centrosomes and basal bodies, matching that of BBS4, BBS6 and BBS8. *In vivo* (mouse tissue), the expression pattern of MGC1203 was spatially coincident with BBS1 and BBS4 in tissues affected by the disorder (e.g. retina, pericardium and limb epithelium) (Badano *et al.*, 2006).

Because of the expression pattern, and the interactions between MGC1203 with the known BBS proteins, it was considered that this newly identified protein might also be associated with the BBS phenotype. For this reason, our cohort of patients were screened for the presence of mutations in this gene.

Even though to date 12 *BBS* genes have been identified (*BBS1-12*), many of the BBS patients (roughly 25%) remain unlinked (Stoetzel *et al.*, 2007). This, coupled with the observed clinical variability among BBS patients, which is not fully reconciled by interactions of known genes, has led to the conclusion that other genes may be associated with the disease. Whilst mutations in *MGC1203* might not directly cause BBS, it is possible that the protein is involved in the BBS functional circuit. As such it could be a strong candidate to contribute modifying alleles, enhancing the severity of the phenotype.

4.2 Materials and Methods.

4.2.1 Amplification of DNA by Polymerase Chain Reaction (PCR)

DNA was amplified by polymerase chain reaction as described in section 2.2.2. Primer sequences are given in the appendix. DNA samples were collected with full consent from BBS patients all over the world via clinicians, or personally collected by Prof. P. Beales.

4.2.2 Sequencing of PCR Products

PCR products were sequenced, desalted using Sephadex, run on a MegaBACE1000 capillary DNA fragment analyser and finally analysed using Sequencher version 4.0.5. Detailed protocols can be found in section 2.2.3.

4.3 Results

4.3.1 *BBS5*

A cohort of 125 BBS patients was screened for possible intragenic mutations. Primers were used to amplify the entire coding region and intron/exon boundaries of DKFZp762I194. In a family of Kurdish descent, PB127, a homozygous nonsense mutation c.177G>A in exon 3 was identified, which by conceptual translation leads to premature termination W59X (Fig: 4.3). The chromatogram for the identified sequence change is shown, alongside the corresponding chromatogram from a control sample. Unfortunately DNA from the parents was not available, so they remain un-sequenced.

The presence of this pathogenic mutation confirmed that DKFZp762I194 was *BBS5*. Taking into account data resulting from other screens by our collaborators, it is suggested that *BBS5* contributes approximately 3% to the BBS mutation pool; which is low compared to the contribution of most other *BBS* loci (Katsanis, 2004).

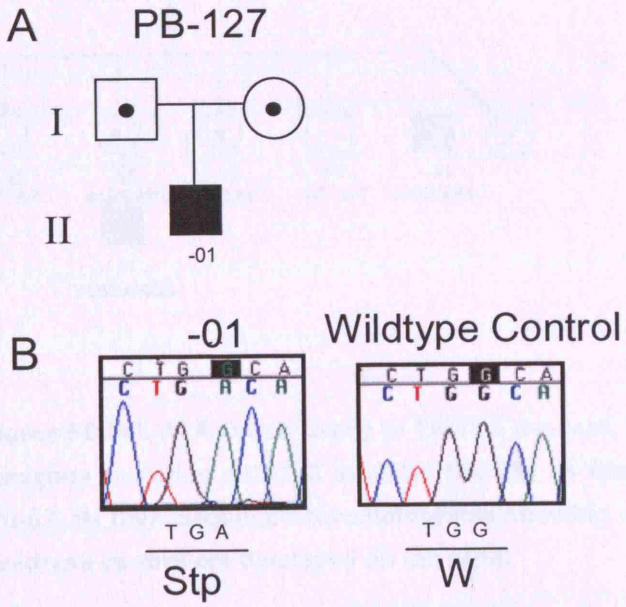

Figure 4.3: Pedigree PB127. A) A family of Kurdish descent, the index case II-01 is homozygous for a nonsense mutation. B) The G→A nucleotide change results in the introduction of a stop codon in exon 3 (W59X) in *BBS5*.

4.3.2 *BBS3*

Forty BBS patients were screened for possible intragenic mutations in *ARL6*, the strongest candidate for *BBS3*. Primers were used which amplified the entire coding region and intron/exon boundaries of *ARL6*. Affected members of a consanguineous Dutch family of Turkish descent, PB140, were found to carry a homozygous c.445C>G mutation that segregated with the phenotype. This mutation affects the Thr31 residue and results in the amino acid substitution T31R (Fig: 4.4). Initial numbering of the gene began at the start of exon 1, however subsequent analysis indicated the most likely start ATG to be at the beginning of exon 3. This accounts for the discrepancy between the numbering of affected nucleotide and amino acid.

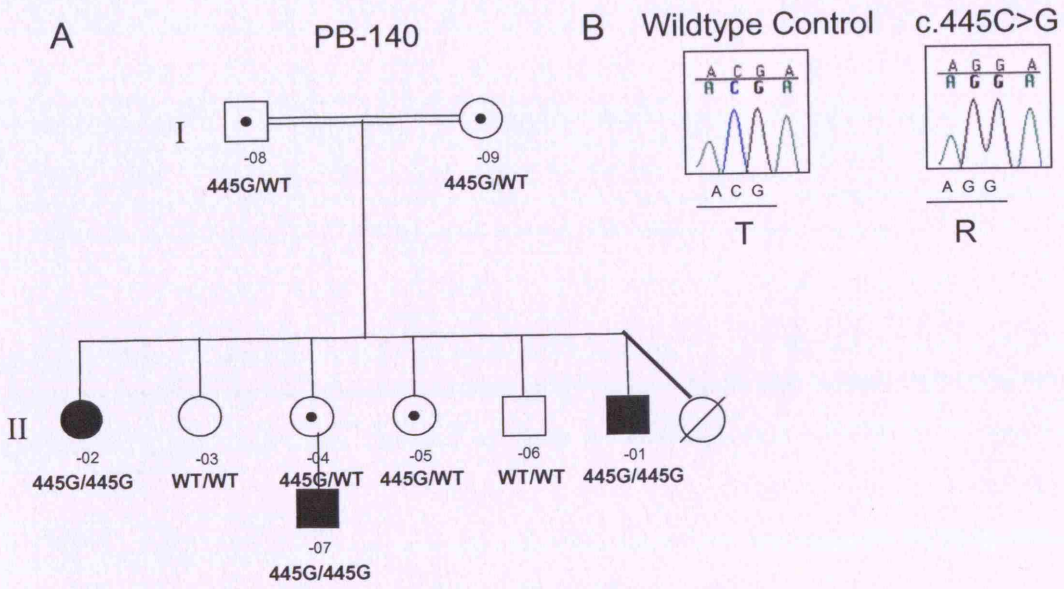

Figure 4.4: Pedigree PB140. A) A Dutch family of Turkish descent. The index case II-01 carries a homozygous mutation 445C>G in *ARL6* (*BBS3*), as does his less severely affected sister II-02. B) DNA sequence chromatograms showing a homozygous C→G transition and wildtype control are displayed on the right.

The index case in this family is a severely affected BBS patient (II-01) whose twin sister died at the age of 15 months of unknown causes. His older sister (II-02) is also affected and carries the same homozygous mutation, but has a

much milder phenotype. Clinical information regarding individual II-07 is not available.

Thr31 is a highly conserved amino acid with a hydroxyl side chain (threonine favoured strongly over serine) in the ARL6 amino acid sequence from 12 organisms(Fan *et al.*, 2004). Additionally, this residue lies in the highly conserved P loop motif of GTP-binding proteins. This change was not detected in 184 ethnically matched control chromosomes.

Combined with data from our collaborators that identified pathogenic mutations in the coding region of *ARL6* in three further families, our results have confirmed *ARL6* as the gene for *BBS3*.

4.3.3 *MGC1203*

Sixty-four BBS patients in our cohort were screened for possible intragenic MGC1203 mutations. Primers were used which amplified the entire coding region and intron/exon boundaries of *MGC1203.* No sequence changes causing coding variations were identified. However, a heterozygous C>T transition at the penultimate base of exon 3 (c.430C>T) was identified in seven individuals (7/64; 10.9%). Although this sequence variation is a silent change, its position at the end of exon 3 suggests it may affect splicing of the mRNA.

Further analysis of the pedigrees in which this sequence change was identified was carried out on as many samples as were available. In a family of European descent, PB029, the presence of the *MGC1203* 430T allele segregates with a penetrant phenotype. Both affected individuals (II-01 and II-02) are homozygous for the most common mutation in *BBS1* M390R, as well as harboring the heterozygous C>T transition in *MGC1203.* Interestingly, the unaffected father (I-03) is also homozygous for M390R but does not have the heterozygous C>T transition in *MGC1203.* At this locus he is homozygous C/C instead (Fig. 4.5 A). The combination of carrying the homozygous M390R mutation with the C>T substitution in *MGC1203* was identified in another individual in a separate pedigree (PB-139 I-01) (Fig. 4.5 B), along with a further individual carrying the conversion plus two compound heterozygous mutations in BBS1 (PB-153 I-01) (Fig. 4.5 C).

These data support the hypothesis that this allele is causally related to BBS or is in linkage disequilibrium with another mutation. They also support the proposed theory of oligogenic inheritance implicated in BBS disease transmission (section 1.2).

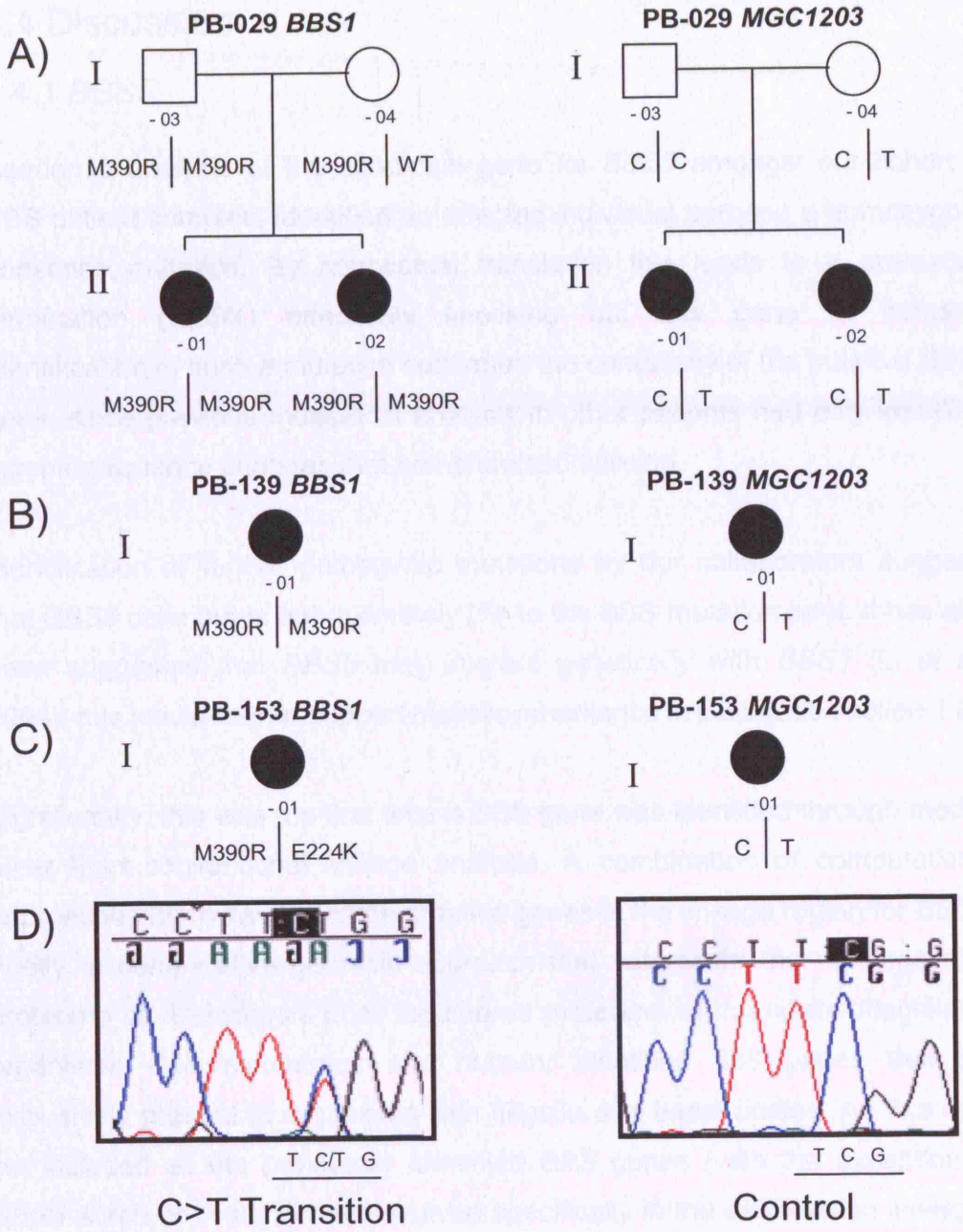

Figure 4.5: Sequence analysis of *MGC1203*. A) Pedigree PB029: The *MGC1203* 430T allele segregates with a penetrant phenotype. Both affected individuals (II-01 and II-02) are homozygous for the common M390R mutation in *BBS1* and are heterozygous for C340T in *MGC1203*. The unaffected father (II-03) also shares the homozygous M390R mutation, but not the heterozygous C340T allele. B) Individual PB139 II-01 is homozygous for M390R and heterozygous for C340T, implicating triallelic inheritance. C) Individual PB153 II-01 is heterozygous for C340T and compound heterozygous for two missense alleles in BBS1, M390R/E224K. D) DNA sequence chromatogram showing the C→T transition. On the left is the heterozygous change C/T on the right is control DNA C/C.

4.4 Discussion

4.4.1 *BBS5*

Sequence analysis of the candidate gene for *BBS5* amongst our cohort of BBS patient samples, identified an affected individual carrying a homozygous nonsense mutation. By conceptual translation this leads to a premature termination (W59X) effectively knocking out this gene in humans. Identification of such a mutation confirmed the candidacy of the putative *BBS5* gene, since previous mutational analysis in other patients had only identified intronic sequence changes that compromised splicing.

Identification of further pathogenic mutations by our collaborators suggests that *BBS5* contributes approximately 2% to the BBS mutation pool. It has also been suggested that *BBS5* may interact genetically with *BBS1* (Li *et al.*, 2004), this would further support triallelic inheritance in BBS (see section 1.2).

Significantly, this was the first time a BBS gene was identified through means other than conventional linkage analysis. A combination of computational approaches narrowed down the putative genes in the linkage region for *BBS5.* Firstly, a comparative genomic approach that subtracted the nonflagellated proteome of *Arabidopsis* from the shared proteome of the ciliated/flagellated organisms *Chlamydomonas* and human, identified 688 genes that are exclusively present in organisms with flagella and basal bodies. As this data set included all the previously identified *BBS* genes (with the exception of *BBS6* which appears to have evolved specifically in the mammalian lineage), it was hypothesised that many of these genes might be good candidates for identifying novel *BBS* genes. As such the candidate gene for *BBS5* was chosen as it was contained in this data set.

Secondly, the presence of a functional motif, an X-box, found upstream of this candidate gene highlighted it for further analysis. This nucleotide sequence has been identified in *C. elegans,* in which several genes needed for functional cilia have this specific 14 nucleotide sequence situated in the first

150 bp upstream of the ATG initiation codon (discussed in section 4.1.2 *BBS3*). This motif is thought to be the binding site for the RFX transcription factor DAF-19. *C. elegans* homologs of human *BBS1*, *BBS2*, *BBS7* and *BBS8* all contain such an X-box (shown in the paper by Ansley *et al.*, 2003), as did the homologue of the candidate *BBS5* gene. Adding further weight to the validity of the candidate gene.

On affirmation that the candidate gene was indeed *BBS5*, it was subjected to expression analysis. The following work was carried out by Li *et al.*, 2004 and has shed light on the functional aspects of this newly identified protein. The presence of an X-box in the promoter of *bbs-5* suggested that it was specifically expressed in ciliated cells and regulated by DAF-19. This was confirmed by GFP fluorescent studies in transgenic worms where a transcriptional reporter construct that consists of 500 bp of upstream sequence and the first two exons of *bbs-5* was fused in-frame to the *gfp* coding region. GFP fluorescence was detected in basal bodies at the base of cilia in all ciliated sensory neurons but not in any other cell types, implying that the BBS5 protein localises specifically to the base of the cilium. Immunohistochemistry in mice using an antibody raised against Bbs5 showed localisation of the protein to basal bodies at the apical surface of multiciliated ependymal cells lining the ventricles of the brain. Further studies in *C. elegans* showed that in the absence of DAF-19, expression of the bbs-5::gfp reporter was markedly reduced. RNA interference of *BBS5* in *Chlamydomonas* led to complete and partial aflagellation, strongly supporting a role for BBS5 in flagellar and basal body function and assembly/maintenance.

This was the first example of a gene associated with BBS to be identified through a comparative genomic approach. Its gives rise to the possibility of using unconventional methods to further isolate loci associated with the disease. This is especially important in light of the fact that many of the possibilities for large familiar linkage analyses have been exhausted. As such it is becoming more difficult to isolate the more elusive BBS genes. With roughly 25% of BBS patients remaining unlinked to any of the known loci

(Stoetzel *et al.*, 2007), identification of further genes associated with the disease is expected.

Also the two data sets (the FABB proteome and X-box containing genes) used in the identification of *BBS5* were the basis of the Ciliary proteome database which has now been assembled and contains all existing ciliary and basal body proteomics data (www.ciliaproteome.org). The Ciliary proteome has integrated results of several overlapping proteomics investigations involving mass spectroscopy, comparative genomics, transcriptional profiling and promoter analyses and so comprises of proteins required specifically for ciliary biogenesis and function in eukaryotes. This information is universally available and it is hoped that it will aid further investigations into the role of the cilium in disease and the mechanisms underlying ciliary biology. As ~25% of BBS patients still remain unlinked to any of the known loci (Stoetzel *et al.*, 2007), it is highly likely that this data set contains further proteins implicated in disease pathogenesis.

4.4.2 *BBS3*

Mutations identified in the candidate *ARL6* gene in this study helped to identify it as the *BBS3* gene. A homozygous 445C>G sequence change in a consanguineous Dutch family of Turkish descent was uncovered. This sequence change results in the amino acid substitution T31R, and is likely to be pathogenic. It was absent from 184 control chromosomes (sequencing of controls was carried out by our collaborator N. Katsanis). Interestingly this exact residue had previously been implicated with the disease. Our collaborators had identified a Saudi Arabian family in which a homozygous 445C>T transition segregated with the affected individuals (Fig 4.6 A). This mutation resulted in the non conservative amino acid change T31M (Fan *et al.*, 2004).

As T31 is a highly conserved amino acid, lying in the highly conserved P loop of GTP-binding proteins, the substitution probably affects the GTP-binding

activity and thus the function of ARL6, implicating this sequence change as a pathogenic mutation. Further homozygous missense mutations in highly conserved regions of the protein were identified in two further families (859G>C resulting in the amino acid substitution G169A, and 862T>G culminating in the non conserved amino acid substitution L170W (Fig 4.6.A)) (Fan *et al.*, 2004). Similarly the position of these residues implicates them in affecting the proteins activity.

ARL6 is a member of the ARL protein family, (so termed because they are ADP-ribosylation factor (ARF)-like). These proteins are small GTPases that undergo a GDP/GTP nucleotide exchange cycle, and are thought to be important regulators of cellular trafficking (Kahn *et al.*, 2006). Thr31 is a highly conserved amino acid with a hydroxyl side chain (threonine favoured strongly over serine)(Fig 4.6). This can be seen on comparison of amino acid sequences of ARL6 from 12 divergent organisms (Fig 4.6B). Additionally, this residue lies in the highly conserved P loop of GTP-binding proteins. The analogous T31N mutation in ARF1 completely abrogates GTP binding *in vitro* (Dascher and Balch, 1994). Furthermore, over expression of several small GTP-binding proteins mutated at the corresponding Thr31 residue produces cellular phenotypes consistent with loss of, or reduced function (Cuvillier *et al.*, 2000; Lu *et al.*, 2001; Engel *et al.*, 2004). The substitutions observed in the BBS patients probably affect the GTP-binding activity and thus the function of ARL6. All this evidence strongly suggest that this sequence change is a pathogenic mutation. Potentially protein binding assays from proteins isolated from patient derived lymphoblastoid cell lines could be carried out, in order to confirm whether GTP-binding activity is affected.

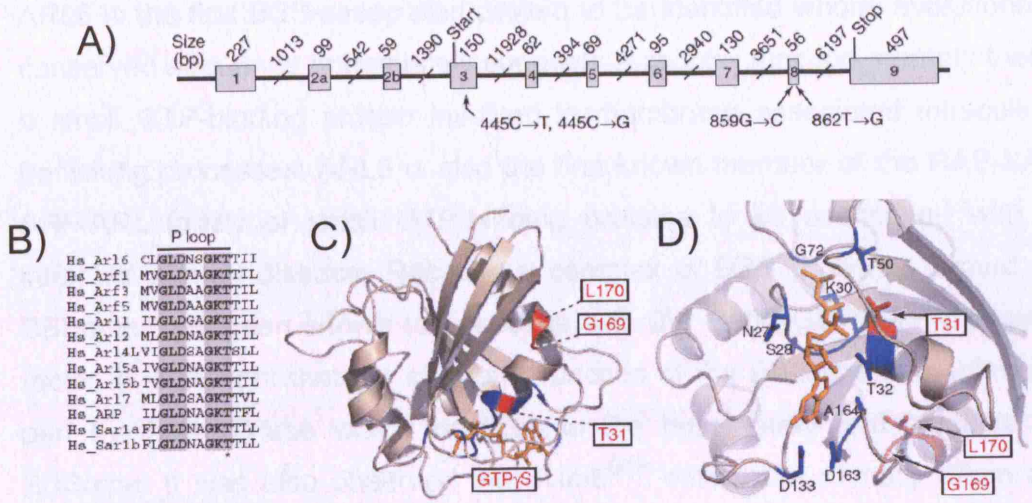

Figure 4.6: Diagram showing residues mutated in *ARL6* in BBS patients. Mutated residues in *ARL6* cluster in or close to the GTP binding site in a structure modeled after ARF6. A) Schematic of the gene *ARL6* showing the locations of mutations found in affected individuals from four families with *BBS3* mutations. B) Sequence conservation of the nucleotide binding site (P loop) in small GTP-binding proteins. Thr31 is marked by an asterisk. C,D) Homology modeling of ARL6 based on the crystal structure of ARF6. Taken from (Fan *et al.*, 2004).

RAB, ARF and ARL proteins are implicated in various aspects of biomembrane trafficking (Takai *et al.*, 2001; Pasqualato *et al.*, 2002). Haemagglutinin-tagged ARL6 is predominantly cytosolic, and associates with membranes *in vitro* in the presence of the nonhydrolysable GTP analog GTPγS (Ingley *et al.*, 1999). Transgenic *C. elegans* lines expressing GFP-tagged ARL6 were generated. These showed that ARL6-GFP is cytosolic, as it was found in the cell bodies, dendrites, transition zone regions (akin to basal bodies found at the base of cilia) and ciliated structures in sensory neurons (Fan et al., 2004). Its cell localisation is therefore similar to that of GFP alone expressed in sensory neurons. Using time-lapse microscopy, GFP-tagged ARL6 underwent IFT in the ciliary axoneme. Movement occurred in both retrograde and anterograde directions along the cilium at 0.82 and 0.64 μm s^{-1}, respectively. These rates are comparable to those of other dynein- and kinesin-associated IFT proteins (Fan *et al.*, 2004).

ARL6 is the first BBS-associated protein to be identified whose evolutionarily conserved sequence immediately suggests a cellular function, namely that of a small GTP-binding protein involved in membrane associated intracellular trafficking processes. ARL6 is also the first known member of the RAB-SAR-ARF-ARL family of small GTP-binding proteins to be associated with an inherited human disease. Recently a complex of BBS proteins, termed the BBSome, has been shown to associate with the Rab8 GDP/GTP exchange factor. It is thought that the ciliogenic function of the BBSome is mediated in part by this GTPase which localizes to the basal body and contacts the BBSome. It was also observed that $Rab8^{GTP}$ enters the primary cilium and promotes extension of the ciliary membrane. Prevention of $Rab8^{GTP}$ production blocked ciliation in cells and produced BBS phenotypes in zebrafish (Nachury *et al.*, 2007). Although BBS3 was not shown to be part of the BBSome, these findings demonstrate a ciliary function for GTP-binding proteins, and could shed light on the mechanistic properties of BBS3.

ARL6 was initially selected as a possible candidate as it mapped to the critical interval for *BBS3* and its *C.elegans* homologue contained an X box (a DAF-19 RFX transcription factor binding site found upstream of all known *C.elegans* bbs genes). Mutations in *ARL6* were seen to segregate with BBS in four independent families and it is thought that mutations in this gene contribute approximately 0.4% to the BBS mutation pool (Fan *et al.*, 2004). One family was identified in which two affected sisters were homozygous for the most common BBS mutation among Caucasians, M390R in *BBS1*; and one of them was heterozygous with respect to the mutation 895G>C in *BBS3*. Clinical assessment indicates that the sister with three mutations was more severely affected with respect to some clinical features of BBS, suggesting that the additional mutation in *BBS3* may act as a modifier (Fan *et al.*, 2004). This strengthens the argument that triallelic inheritance may be implicated in the disease (Badano et al., 2003).

Interestingly, work by another group independently verified that *ARL6* was *BBS3* (Chiang *et al.*, 2004). Comparative genomic analysis was performed to prioritise BBS candidate genes for mutation screening. Known BBS proteins

were compared with the translated genomes of model organisms to identify a subset of organisms in which these proteins were conserved. By including multiple organisms that have relatively small genome sizes, the number of candidate genes was reduced, and a few genes mapping to the BBS3 interval emerged as good candidates. Among these was *ARL6*, which was found to contain a homozygous nonsense mutation in exon 7 (R122X) that segregates completely with the disease in the Bedouin kindred originally used to map the *BBS3* locus.

4.4.3 *MGC1203*

Although no pathogenic sequence variations were identified in this gene, a heterozygous C>T transition at the penultimate base of exon 3 was identified in 10.9% (7/64 patients) of our patient cohort. Combined with sequencing data from other patient cohorts, overall the 430T variant of *MGC1203* is present in 6.2% of BBS patients compared to 1.4% of controls, showing significant association with BBS (Fischer's exact test $P<0.006$). Furthermore, a subsequent transmission disequilibrium test (TDT), screening transmission distribution of *MGC1203* in all available parents, showed that the 430T allele is transmitted to patients in 74% of cases, deviating significantly from the expected 50:50 distribution ($P<0.007$).

As no patients were identified with homozygous or compound heterozygous *MGC1203* mutations it is likely that *MGC1203* mutations alone are insufficient to cause BBS. This is supported by the identification of an unaffected parent homozygous for the 430T allele, as discussed in the following paragraph. However an epistatic relationship (the interaction of multiple loci on phenotypic variation,) between the 430T allele and BBS might be observed and the current study identified several sequence variations which strengthen this hypothesis.

Firstly, this study identified two heterozygous 430T patients, each harboring two further mutations at known BBS loci. More definitive evidence of the

involvement of *MGC1203* in BBS is provided by pedigree PB029, in which the presence of the *MGC1203* 430T allele segregates with a penetrant phenotype. Both affected individuals are homozygous for the common M390R mutation in *BBS1*, as well as having the heterozygous C>T transition in *MGC1203.* The unaffected father is also homozygous for M390R, but does not have the C>T transition in *MGC1203.*

Further evidence for an epistatic relationship between *MGC1203* and BBS has been observed in families harbouring the 430T allele. Several pedigrees have been identified in which some, but not all, affected individuals inherited the *MGC1203* mutation. In each case, the unbiased clinical view was that the 430T-bearing individuals were more severely affected (Badano *et al.*, 2006).

As this allele appeared to be involved in disease manifestation to some extent, further analysis was carried out by our collaborators. Although the 430T allele results in a silent change, its position in the penultimate base of exon 3 raised the possibility that it might affect splicing. Therefore quantitative RT-PCR was performed on patient derived cell lines with either the 430C/C or 430C/T genotype. A reduction of ~20% in *MGC1203* mRNA levels in the 430C/T cells suggested that a larger fraction of mRNA from the 430C/T genotype contains a premature termination codon (PTC). Construction of a series of minigenes by collaborators, showed a marked increase in mis-spliced mRNA production with the 430T allele. Further analysis involving the suppression of SC35 and ASF/SF2 (Serine/Arginine-rich (SR) proteins, involved in regulating and selecting splice sites) showed an increase in mis-spliced transcript from the 430T minigene, suggesting that this allele enhances the effect of SR proteins to potentiate the cryptic splice site (Badano *et al.*, 2006).

To investigate the epistatic effect of a hypomorphic *MGC1203* mutation on BBS mutations *in vivo*, antisense morpholinos were injected into zebrafish. Injection of a splice-blocking morpholino against *mgc1203* resulted phenotypes similar to *bbs4* and *bbs6* injected zebrafish. Namely shorter body axes, widened and kinked notochords and abnormally shaped somites.

Double morpholino injections with *mgc1203* and *bbs1, bbs4* or *bbs6* respectively heightened the severity of the observed phenotype, implicating an interaction between the morpholinos (Badano *et al.*, 2006). Notably, co-injection of mgc1203 RNA with the two morpholinos rescued the double-morphant phenotype, further suggesting that the synthetic phenotype was due to the interaction between the morpholinos, as opposed to potentially non-specific morpholino effects.

Combined, these studies indicate that the MGC1203 protein is involved in the pathogenesis of BBS most likely by contributing hypomorphic mutations to an already sensitised genetic background. The 430T mutation exerts its effect at the RNA level by enhancing the use of a cryptic splice junction in a suboptimal context that is probably stabilised by SR proteins such as SC35 and ASF/SF2.

Establishing the effect of epistatic variants is always going to be a challenging prospect. The identification of *MGC1203* and its effects on BBS demonstrated for the first time how the combined use of biochemical, genetic and *in vivo* tools can be applied to the dissection of epistatic phenomena. With the high degree of phenotypic variability observed amongst BBS patients, it is becoming increasingly important to use such combined approaches to study the effects of variants, enabling a better understanding of the relationship between genotype and phenotype.

4.4.4 General Discussion

We know that further BBS genes are yet to be identified, as 25% of patients, mostly of Middle-Eastern or Asian origin, remain unlinked (Stoetzel *et al.*, 2007). Whilst the genes that are directly responsible for the disease itself remain to be identified, searching for loci that may contribute to the severity of the phenotype, and so may be indirectly involved, is also necessary. As with the overwhelming majority of genes associated with Mendelian traits, knowledge of the genotype at a single locus can neither predict nor

satisfactorily explain the phenotypic manifestations in any given patient or family. This observation is leading to the identification of second-site modifications (such as in *MGC1203*) in which alleles at additional loci can influence the phenotypic outcome of mutations at a single locus, essentially de-Mendelising monogenic traits.

Despite now having access to the complete human genome sequence, it still remains difficult to select relevant genes for screening. The use of comparative genome approaches have enabled us to identify novel BBS loci and hopefully will continue to do so. However, they are not without their limitations as the very nature of the search criteria, whereby genes with additional extraciliary functions are excluded, means non-ciliary genes are excluded. Nothertheless this approach is especially useful for the identification of genes involved in rare (ciliary) disorders in which the putative linkage region is large.

4.5 Summary

The identification of pathogenic mutations in candidate genes for *BBS3* and *BBS5* confirmed these to be disease causing genes. Sequence variations at a novel locus, *MGC1203*, were shown to contribute epistatically to the phenotype of Bardet-Biedl syndrome.

Chapter 5: Yeast two-hybrid screen using murine Bbs6 as bait

Aim: To identify novel protein interactors of Bbs6 using the yeast two-hybrid system.

5.1 Introduction

5.1.1 The theory behind the yeast two-hybrid system

The yeast two hybrid system is a molecular genetic tool that is commonly used to study protein-protein interactions. It can be used to investigate whether two proteins interact with one another and can also be applied to isolate and identify proteins that interact with a known protein of interest. A reporter gene (usually *gal1-lacZ*- the *beta*-galactosidase gene) is transcriptionally activated, when two proteins interact.

The yeast two-hybrid system was devised by Stanley Fields and Ok-kyu Song in 1989 as an additional biochemical technique to crosslinking, co-immunoprecipitation and co-fractionation for studying protein-protein interactions (Fields and Song, 1989). They initially tested the system using two proteins known to interact, SNF1 and SNF4, but it has since been used to screen cDNA and genomic fusion libraries (Chien *et al.*, 1991).

The basic principle of the system utilises the fact that the intact GAL4 protein (a transcriptional activator) has two separate functional domains, a DNA binding domain (DBD) and a DNA activation domain (AD). The DBD binds to specific upstream activating sequences (UASs) within yeast promoters (GAL1 promoter) and transcription is activated by the acidic regions of the AD. The GAL4 DBD remains inactive and does not activate transcription if these domains are separated. However, if the two separate domains are brought within close proximity of one another, the activity of the protein can be regained (Fig. 5.1). This can be utilised to test whether two proteins interact. Two chimeric proteins, where each of the separate GAL4 domains are translationally fused to one of the

proteins that are thought to interact, are generated. Chimeric proteins are expressed in yeast as translation gene fusion plasmids. When two known proteins are being tested, the plasmids (one transcribing the first protein of interest fused to the GAL4 binding domain, and the other fused to the activation domain) are transformed together into yeast. If the proteins interact, the two GAL4 domains are brought together at the GAL4 promoter, activating transcription of the reporter gene (for example lac Z), turning the colonies blue in the presence of X-α-gal.

A fusion protein of interest can be used as 'bait' to screen a library of cDNA clones that are fused to the opposed domain (the 'prey'). If the library contains cDNA clones that encode proteins capable of interacting with the bait and activating the reporter gene, they can be isolated and identified. In such a way potential interacting proteins can be identified.

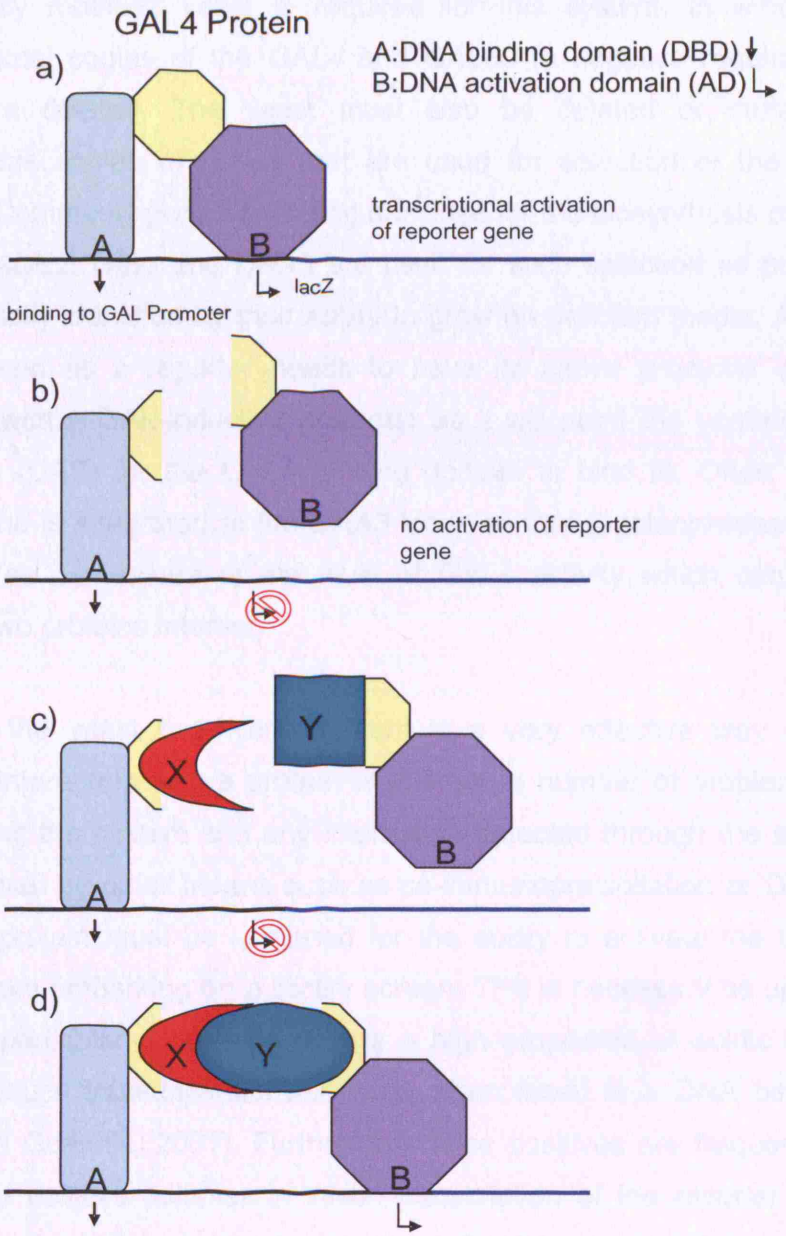

Figure 5.1: The Yeast two-hybrid system. a) The native GAL4 protein is a yeast transcriptional activator containing separate DNA-binding and activation domains which induce transcription of a reporter gene (typically GAL1-lacZ). b) When these two domains are separated, transcription of the reporter gene is prevented. c) Each of the separate GAL4 domains can be translationally fused to two seperate proteins ie X and Y. d) When there is an interaction between the two proteins the GAL4 domains are brought into close proximity resulting in transcriptional activity.

A specially modified yeast is required for this system, in which the yeast chromosomal copies of the *GAL4* and *GAL80* (a negative regulator of *GAL4*) genes are deleted. The yeast must also be deleted or mutated for any endogenous copies of genes that are used for selection of the bait or prey plasmid. Commonly genes encoding enzymes for the biosynthesis of amino acids such as *ADE2*, *HIS3* and *URA3* are used for such selection as positive clones can be easily identified by their ability to grow on deficient media. Any gene that will be used as a reporter needs to have its native promoter removed and replaced with a GAL-inducible promoter as it will need the upstream activating sequence (UAS) for the GAL4 binding domain to bind to. Often a GAL1-lacZ fusion gene is integrated at the *URA3* locus so that β-galactosidase activity can be used as a measure of the level of GAL4 activity which can predict how strongly two proteins interact.

Although the yeast two-hybrid system is a very effective way of identifying potential interactors with a protein of interest, a number of problems can occur when using the system and any interaction detected through the screen should be confirmed by other means such as co-immunoprecipitation or GST pulldown. The bait protein must be screened for the ability to activate the GAL4 system alone before embarking on a library screen. This is necessary as up to 5-10% of proteins, particularly those containing a high proportion of acidic residues, are able to induce transcriptional activation when fused to a DNA binding domain (Toby and Golemis, 2001). Furthermore false positives are frequently detected. These are positive colonies in which transcription of the reporter gene occurs even when the bait and prey don't interact. For this reason it is necessary to test the prey construct separately for autoactivation.

A list of commonly occurring false positives detected in screens using a variety of different proteins can be found online at:
www.fccc.edu/research/labs/golemis/InteractionTrapInWork.html

5.1.2 Previous yeast two-hybrid screens involving BBS proteins

Previous yeast two-hybrid screens using BBS4 as bait, have helped elucidate the role of the BBS4 protein (Kim *et al.*, 2004) Through identification of proteins with which it interacts, it has been possible to establish a putative function for the protein. Interaction with both PCM1 and p150 ^{glued} suggested that BBS4 is involved in the transport of PCM1 to centriolar satellites of cells by the dynein associated machinery (Kim *et al.*, 2004). Following the identification of the interaction between BBS4 and PCM1, it was confirmed by co-immunoprecipitation and colocalisation of BBS4 with PCM1 at centrosomes and at the basal bodies of ciliated cells indicating that BBS4 may also be involved in intraflagellar transport (Kim *et al.*, 2004). A number of nuclear receptor interacting proteins were also identified as potential BBS4 interactors, but these have yet to be verified (B. Hoskins, PhD Thesis, 2004).

Recent work involving a yeast two-hybrid screen using BBS2 as bait also identified several candidate interactors. These included the aryl hydocarbon-receptor interacting protein (AIP), a cytosolic chaperone involved in folding of mitochondrial pre-proteins, and RFX3, a transcription factor essential for cilia formation and maintenance (unpublished data). Significantly two other BBS proteins, BBS6 and BBS9 were pulled out of the library screen and their interaction with BBS2 was verified by co-immunoprecipitation. More detailed analysis of these interactions, through the use of truncated copies of BBS2 as bait, suggest that discrete domains within BBS2 are required for binding to the two other BBS proteins as separate complexes. Furthermore, introduction of BBS-associated amino acid substitutions into the BBS constructs, and consequent analysis of the interaction between BBS2, BBS6 and BBS9 using quantitative liquid ß-galactosidase assays, showed disruption of the interaction. Analysis of further possible direct interactions between other known BBS proteins, was carried out by subcloning and pairwise testing of a panel of full-length BBS1-12 bait and prey proteins. This approach identified yeast two-hybrid interactions between BBS8 and BBS9 and between BBS5 and BBS6 and BBS9. It was also shown that both BBS6 and BBS11 can self- associate in this model system. These data show convincing evidence of interactions between BBS

proteins and suggest a mechanism to explain the phenomenon of oligogenic inheritance in BBS (A. Ross, unpublished).

5.1.3 The BBS6 protein

BBS6 was the first BBS gene to be cloned. Following the identification of several Newfoundland samples that were unlinked to *BBS1-5* (Woods *et al.*, 1999) it was evident that other loci exist. By DNA pooling, Katsanis *et al.* (2000) were able to identify a critical interval of 1.9cM on chromosome 20p12. At around the same time, the gene for McKusick-Kaufman syndrome (MKKS) (OMIM #236700) had been identified in the same region (Stone *et al.*, 2000). MKKS comprises hydrometrocolpos, polydactyly, and congenital heart defects. Given the clinical overlap between these two syndromes, and the concordant mapping position of the two genes, it was hypothesised that *MKKS* was a good candidate gene for BBS6. Identification of a number of mutations in the *MKKS* gene in BBS patients confirmed this hypothesis (Katsanis *et al.*, 2000; Slavotinek *et al.*, 2000). It was suggested that most mutations in *MKKS* cause BBS whereas milder, less severe mutations cause MKKS. Mutations in this gene are the third most common of all the BBS gene mutations, and are seen in 5.8% of cases (Katsanis, 2004). The official name for the protein the *MKKS* gene encodes is MKKS/BBS6, however for reasons of simplicity I will refer to it as BBS6.

The BBS6 protein shows similarity to type II chaperonins, which aid the folding and structural modification of other proteins (Stone *et al.*, 2000). The protein has been shown to be expressed in a wide range of tissues including heart, brain, liver, skeletal muscle, kidney and retina (Slavotinek *et al.*, 2000). It is thought that the complete loss of function of the BBS6 product, and thus an inability to fold a range of target proteins, is responsible for causing some of the clinical features of BBS (Katsanis *et al.*, 2000).

Recent studies show that BBS6 is predicted to be a Group II chaperonin-like protein that has recently evolved in animals from a subunit of the eukaryotic chaperonin CCT/TRiC, and diverged rapidly to acquire distinct functions. Cytosolic BBS6 does not oligomerise, unlike other chaperonins, and the majority

of BBS6 resides within the pericentriolar material (PCM), a proteinaceous tube surrounding centrioles (Kim *et al.*, 2005). During interphase BBS6 is confined to the lateral surfaces of the PCM but during mitosis it relocalises throughout the PCM and is found at the intercellular bridge (Kim *et al.*, 2005). Its predicted substrate-binding apical domain is sufficient for centrosomal association and consistent with centrosomal function. Silencing of the *BBS6* transcript by RNA interference in different cell types leads to multinucleate and multicentrosomal cells with cytokinesis defects. Restricted tissue distribution of Bbs6 in mice brain, kidney, retina, olfactory epithelium and ependymal layer of ventricles, detected BBS6 only in regions containing or bordering ciliated cells, suggesting it may play a role in ciliated epithelial tissues (Kim *et al.*, 2005).

Antibody staining using an anti-BBS6 antibody to stain paraffin-embedded tissue sections of mice brain, kidney, retina, olfactory epithelium and ependymal layer of ventricles, detected BBS6 only in regions containing or bordering ciliated cells

The more recently identified *BBS10* and *BBS12* genes also encode vertebrate-specific type II chaperones (Stoetzel *et al.*, 2006; Stoetzel *et al.*, 2007), yet the only other link between the known BBS proteins is their involvement in the function of basal bodies and cilia (Ansley *et al.*, 2003).

To date there are no confirmed interactors of BBS6 (with the exception of BBS2; A Ross, unpublished). For this reason a yeast two-hybrid screen was carried out to try and identify possible interactors and shed light on the potential function of this protein. The yeast two-hybrid system was selected as a method as the BBS2 and BBS4 screens had been successful and the system was up and running in the laboratory. Mouse Bbs6 was selected as there was a murine E9.5/E10.5 cDNA library in prey plasmid already available to screen. Additionally a $Bbs6^{-/-}$ mouse had recently been generated in our laboratory.

5.2 Materials and Methods

5.2.1 Cloning

Full length murine Bbs6 cDNA was cloned in-frame into the GAL4 DNA binding domain vector pGBDU-c3 (using the *Eco*R1 and *Sal*1 sites of the multiple cloning site) as described in section 2.2.6. The pGBDU plasmid contains an Ampicillin resistance gene (*Amp*^{r}) for selection in bacteria and a nutritional marker (*URA3*) for selection in yeast.

5.2.2 Yeast two-hybrid screen

A yeast two-hybrid screen using murine Bbs6 as bait to screen an E9.5/E10.5 embryonic mouse cDNA library in the pVP16 vector (In house, courtesy of P. Ataliotis) was carried out as described in 2.2.7, using the PJ69-4A strain of *S. cerevisiae*. Initial transformation of *S.cerevisiae* with pGBDU-Bbs6 was carried out using lithium acetate and selection in dropout medium lacking uracil. This was followed by transformation with 250 µg prey library cDNA (Leu+). Resulting transformations were spread on medium stringency selective dropout medium lacking uracil, leucine and histidine (one of the reporters used in our system) supplemented with 5 mM 3-aminotriazole (3-AT). Colonies that had grown within 5 days were re-streaked onto higher stringency selection plates lacking uracil, leucine and adenine (a second reporter) and supplemented with X-α-gal. Positive colonies grew and turned blue due to the activation of the third reporter lac-z. Transfection efficiency was tested as described in 2.2.7.4.

The genotype of PJ69-4A and vector maps for pVP16 and pGBDU are given in the appendix.

5.2.3 Identification of positive clones

Prey plasmids were extracted from positive clones as described in section 2.2.7.7. Subsequently inserts were amplified by PCR and sequenced using the 509 VP16 forward and 510 VP16 reverse primers as described in section 2.2.7.8 Amplification and identification of the prey cDNA sequence. Sequences were subjected to BLAST analysis for identification and verification that they were in-frame to known or predicted protein-coding regions or ESTs.

5.2.4 Confirmation of positive clones

To confirm the interaction was reproducible and bait specific, prey clones were isolated by electroporation of yeast plasmid DNA into *E.coli* DH10B^{TM}-T1^{R} electrocompetent cells (Invitrogen) and independently co-transformed into fresh yeast with the bait clone and with an empty plasmid, as described in section 2.2.7.9.

5.3 Results

5.3.1 Autoactivation test

To test the ability of the pGBDU-Bbs6 to activate the system alone, the plasmid was singly transformed into PJ69-4A. The absence of growth on either SD-Ura-Ade or SD-Ura-His+3AT plates indicated that there was no autoactivation of the system by the pGBDU-BBS6 protein. 3AT is an inhibitor of the histidine pathway and is added to the media to suppress leaky expression of *HIS3*.

5.3.2 Transformation efficiency

The transformation efficiency of the library plasmids was calculated to be $8.47x10^6$ cfu/µl, indicating that coverage of the whole cDNA library was likely to be achieved. This number was calculated by serially diluting the transformed yeast and counting the number of colonies grown on the respective plates.

Serial dilution of transformation	N. of colonies grown on plate
1 in 10	663
1 in 100	67
1 in 1000	7

Transformation efficiency: (n. of colonies) x (serial dilution) x (total volume of transformation/volume of serial dilution)

(7) x (10^3)x (12100µl/10 µl) = 8.47 x 10^6

Table 5.1: Calculations for transformation efficiency for the yeast two-hybrid transformation.

5.3.3 First round of selection

For the first round of selection, cells were plated on SD-Ura-Leu-His+3AT agar following the introduction of both the bait and prey plasmids into the yeast. If the two clones interacted, the *GAL1-HIS3* reporter was activated to transcribe *His3* and the yeast cells would be able to survive on the media, in the absence of histidine. After six days incubation at 30°C, 198 colonies had grown on the plates.

5.3.4 Second round of selection

Positive clones that had grown during the first round of selection were transferred to SD-Ura-Leu-Ade+X-α-gal plates for a second, more stringent round of selection, as *HIS3* is a 'leaky' reporter. Following the addition of the X-α-gal, positive colonies should turn blue, demonstrating the ability to transactivate β gal. Of the 198 colonies identified during the first round of selection, 86 failed to grow in the absence of adenine. One colony grew, but developed a red colour. Red colonies are false positives, able to synthesize adenine through an alternative pathway. For identification of the remaining 111 positive colonies, the prey plasmid was isolated and the insert amplified by PCR and sequenced for identification.

5.3.5 Identification of positive clones

Of the 111 positive clones identified after the second round of selection, 77 were able to be sequenced. BLAST analysis identified 44 different possible interacting proteins. 26 of the clones were exact duplicates of another clone and on four occasions more than one clone was identified for the same protein.

Stage of screen	N. of clones
1st round of selection	198
2nd round of selection	111
Sequence analysis successful	77
Duplicated clones	26
Identified interactors	44

Table 5.2: Number of clones remaining at various stages of the yeast two-hybrid screen.

The majority of the clones appeared to be in frame with the GAL4 AD (activation domain) and therefore presumed to generate a functional polypeptide. In seven cases sequence analysis was not able to verify whether they were in frame and only two clones appeared not to be in frame, namely the clones encoding NUMA1 and PGEA1. Table 5.3 shows a summary of the proteins encoded by the positive clones. Clones are listed in the order that they were picked after the first round of selection. Amongst the proteins identified was BBS2, this served as a good internal control, as a previous yeast two-hybrid screen using BBS2 as bait

had pulled out BBS6 as prey. Of note is the identification of the chromodomain helicase DNA binding protein 7 (CHD7), chromodomain helicase DNA binding protein 8 (CHD8) and chromodomain helicase DNA binding protein 9 (CHD9).

Interactor	In Frame with GAL4 AD	N. different clones	N. total clones
Eukaryotic translation initiation factor 4 gamma	Yes	2	2
Chromodomain helicase DNA binding protein 7 (CHD7)	Yes	2	6
ATM/ATR-Substrate Chk2-Interacting Zn2+-finger protein	Yes	1	1
Semaphorin cytoplasmic domain-associated protein 3B (Semcap3)	Yes	1	3
Spectrin, beta, erythrocytic (includes spherocytosis, clinical type I) (SPTB), transcript variant 2	Yes	1	2
Jumonji, AT rich interactive domain 1A (RBBP2-like) (JARID1A)	Yes	1	1
Spectrin, beta, non-erythrocytic 1 (SPTBN1), transcript variant 2	Yes	1	3
Nesprin-2	Yes	1	2
Chromodomain helicase DNA binding protein 8 (CHD8)	Yes	1	1
Breast cancer metastasis suppressor 1 (BRMS1),transcript variant 3	Yes	1	2
Translocase of outer mitochondrial membrane 70 homolog A (yeast) (TOMM70A)	?	1	1
CD320 antigen (CD320)	?	1	1
GATA zinc finger domain containing 2B (GATAD2B)	Yes	4	7
Mus musculus 2 days neonate thymus thymic cells cDNA, RIKEN full-length enriched library, clone:E430013O10	?	1	1
Bromodomain containing 3 (BRD3)	Yes	1	1
Meiosis-specific nuclear structural 1 (MNS1)	Yes	1	2
Elongation factor Tu GTP binding domain containing 1	Yes	1	3
KIAA1005 protein (KIAA1005)	Yes	1	1
F-box protein 5 (FBXO5)	Yes	1	4
Cytoplasmic linker 2 (CYLN2), transcript variant 2	?	1	2
Nuclear casein kinase and cyclin-dependent kinase substrate 1 (NUCKS1)	?	1	1
EH-domain containing 2 (EHD2)	Yes	1	2
Mus musculus RIKEN cDNA 2410004L22 gene (2410004L22Rik)	Yes	1	1
CDK5 regulatory subunit associated protein 3 (CDK5RAP3), transcript variant 3	Yes	1	3
Cerebellar degeneration-related protein 2	?	1	1
Chaperonin containing TCP1, subunit 6A (zeta 1), transcript variant 1	Yes	1	1
Rho guanine nucleotide exchange factor (GEF) 12 (ARHGEF12)	Yes	1	1
DNA (cytosine-5-)-methyltransferase 1 (DNMT1)	Yes	4	4
Chromodomain helicase DNA binding protein 9 (CHD9), transcript variant 1	Yes	1	1
Bromodomain containing 2 (BRD2)	Yes	1	2
Ring finger protein 41	?	1	1
Nuclear mitotic apparatus protein 1 (NUMA1)	No	1	1
PKD2 interactor, golgi and endoplasmic reticulum associated 1 (PGEA1), transcript variant 2	No	1	1
Cytoskeleton associated protein 5 (CKAP5), transcript variant 2	Yes	1	1
Rearranged L-myc fusion (RLF)	Yes	1	1
Hypothetical protein FLJ10569	Yes	1	1
Bardet-Biedl syndrome 2 (BBS2)	Yes	1	1
Myeloid/lymphoid or mixed-lineage leukemia 3 (MLL3) transcript variant 1	Yes	1	1
GATA zinc finger domain containing 2A	Yes	1	1
Fibronectin leucine rich transmembrane protein 1 (FLRT1)	Yes	1	1
Microtubule-actin crosslinking factor 1 (MACF1), transcript variant 2	Yes	1	1
Fibroblast growth factor receptor 3 (achondroplasia, thanatophoric dwarfism) (FGFR3), transcript variant 2	Yes	1	1
Kinesin family member 1A (KIF1A)	Yes	1	1
Mus musculus chromosome 6, clone RP23-25K2	Yes	1	1

Table 5.3: Summary of the 44 proteins predicted to interact with Bbs6, identified through a yeast two-hybrid screen. Sequence analysis indicated that the majority of the clones were in frame with the GAL4 activation domain. A question mark denotes that the sequence at this region was not good enough to determine if in frame or not. Clones are listed in the order that they were picked after the first round of selection.

5.3.6 Further analysis of positive clones

Of the 44 possible interactors identified, 11 were chosen for further analysis. These were chosen for various reasons (outlined below) and on the basis of their relevance to BBS.

Clones chosen for further analysis (in alphabetical order):

- Bardet-Biedl syndrome 2 (BBS2): This clone was chosen as it served as a positive internal control. A previous yeast two-hybrid screen using BBS2 as bait had identified BBS6 as an interactor (A. Ross, unpublished).

- Chaperonin containing TCP1, subunit 6A (zeta 1): CCT 6a is one of the seven subunits that makes up the type II chaperonin CCT. This chaperone is a hetero-oligomeric complex that assists the folding of actins, tubulins and other proteins in an ATP dependent manner (Valpuesta *et al.*, 2002). It was chosen as Bbs6 is a putative chaperone.

- Chromodomain helicase DNA binding protein 7 (CHD7), 8 (CHD8) and 9 (CHD9): These clones were chosen on the basis that it was interesting to have identified three members of a protein family. Additionally, CHD7 has particular relevance, as mutations in this gene have been shown to cause CHARGE syndrome (Vissers *et al.*, 2004). CHARGE syndrome is an autosomal dominant disorder affecting several tissues in a non-random fashion. Observed in 1:10,000 live births, the main features associated with the disease are coloboma, heart malformations, atresia of choanae, retardation of growth and development, genital hypoplasia and ear abnormalities including deafness (Blake and Prasad, 2006; Sanlaville and Verloes, 2007).

- DNA (cytosine-5-)-methyltransferase 1 (DNMT1): This protein appears to show strong affinity to Bbs6, as four separate clones encoding different parts of the same protein, and collectively spanning the entire length of the protein, were pulled out during the screen. DNMT1 regulates the

- DNA (cytosine-5-)-methyltransferase 1 (DNMT1): This protein appears to show strong affinity to Bbs6, as four separate clones encoding different parts of the same protein, and collectively spanning the entire length of the protein, were pulled out during the screen. DNMT1 regulates the expression of cell-cycle proteins and could be involved in cancer development (Hermann *et al.*, 2004; Luczak and Jagodzinski, 2006).

- EH-domain containing 2 (EHD2): EHD2 is one of four highly homologous C-terminal EH-domain-containing proteins. The Eps 15-homology (EH) domain is a highly conserved motif comprising of approximately 100 residues, and proteins with this domain can carry out a variety of crucial cellular functions including regulation of the actin cytoskeleton, signal transduction and transcriptional regulation of the endocytic pathway (Naslavsky and Caplan, 2005). In particular, EHD2 has been shown to interact with the insulin-responsive glucose transporter GLUT4, and may participate in insulin-induced GLUT4 recruitment (Park *et al.*, 2004).

- Kinesin family member 1A (KIF1A): This protein is a member of the Kinesin-3 family of kinesin-like proteins, which are motor proteins that mediate transport of axonal vesicles.

- Microtubule-actin crosslinking factor 1 (MACF1): This cytoskeletal linker protein can associate with both actin filaments and microtubules. Association with this protein could help explain some of the more subtle phenotypes of BBS, for example the hearing abnormalities (see chapter 6-9). Of note is the possible association of BBS6 with CCT 6a, a subunit of type II chaperonin that assists the folding of actins and tubulins.

- PKD2 interactor, golgi and endoplasmic reticulum associated 1 (PGEA1): This protein, more commonly known as chibby, is a beta-catenin transcriptional activator and oncoprotein involved in the development of several cancers. It was chosen for further analysis because of its association with PKD2, which regulates its intracellular location (Hidaka *et al.*, 2004). Mutations in *PKD2* have been found to be responsible for

autosomal dominant polycystic kidney disease (ADPKD) (Tsiokas *et al.*, 2007), the most common hereditary disease affecting kidneys which clinically overlaps with BBS.

- Translocase of outer mitochondrial membrane 70 homolog A (yeast) (TOMM70A): This protein is a molecular chaperone thought to help target certain proteins to the mitochondria (Young *et al.*, 2003). It was chosen for its role as a molecular chaperone.

Of the above mentioned clones, unfortunately two were lost during the process of further analysis. It was not possible to isolate the clone encoding part of the PGEA1 protein by electroporation, and re-transformation of the clone for KIF1A was unsuccessful.

The clone encoding CHD7 autoactivated the yeast reporter in the absence of bait, as when transformed alone it grew on the SD-Ura-Leu-Ade+X-α-gal plates. The clones for CHD8 and CHD9 were unable to grow on the SD-Ura-Leu-Ade+X-α-gal plates when transformed with BBS6. These results are difficult to explain but it was assumed that interaction with CHD proteins were false positives.

However, reproducible interactions were observed with all other clones. Of note was the interaction between BBS6 and MACF1. Yeast co-transformed with both plasmids grew particularly quickly compared to all other clones, implicating a strong interaction between these two proteins. A liquid β-gal assay would be needed to quantify this qualitative observation. Table 5.4 and figure 5.2 summarise the interactors after further analysis.

Interactor	Length of Transcript (bp)	bp present in clone	Accesion Number
Bardet-Biedl syndrome 2 (BBS2)	2166	868-1290	NM 031885
Chaperonin containing TCP1, subunit 6A (zeta 1), transcript variant 1 (CCT6A)	1599	565-995	BC 106942
DNA (cytosine-5-)-methyltransferase 1 (DNMT1)	4884	1-550	NM 001379
EH-domain containing 2 (EHD2)	1632	916-1391	NM 014601
Microtubule-actin crosslinking factor 1 (MACF1)	15987	9654-10216	NM 33044
Translocase of outer mitochondrial membrane 70 homolog A (yeast) (TOMM70A)	1836	208-654	NM 14820

Table 5.4: Bbs6 interactors remaining after further analysis. Including base pairs (bp) present in the clone correlating to the full length transcript.

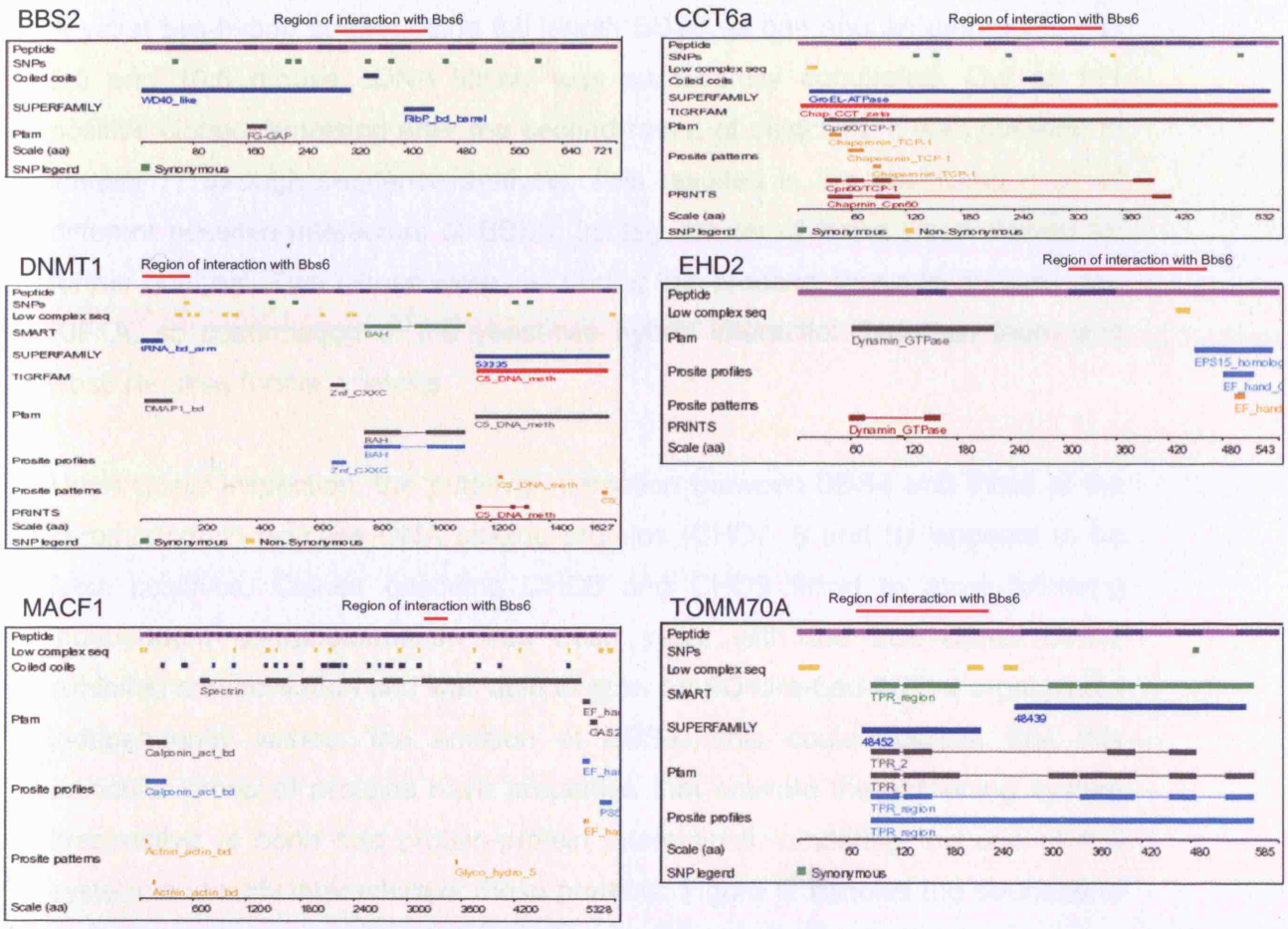

Figure 5.2: Peptide information for Bbs6 interactors. Protein features as found on Ensembl. Red bar across the top of each schematic represents the region of interaction with Bbs6.

5.4 Discussion

A yeast two-hybrid screen using full length BBS6 as bait and an embryonic day 9.5 and 10.5 mouse cDNA library was successfully completed. Out of 111 positive clones remaining after the second round of selection, it was possible to identify 77 through sequence analysis. This resulted in the identification of 44 different possible interactors of BBS6. Initially eleven of these were chosen for further analysis. Two clones were lost during this process, those for PGEA1 and KIF1A, so confirmation of the yeast-two hybrid interaction between them and Bbs6 requires further analysis.

Upon closer inspection, the putative interaction between BBS6 and three of the chromodomain helicase DNA binding proteins (CHD7, 8 and 9), appears to be false positives. Clones encoding CHD8 and CHD9 failed to grow following independent co-transformation into fresh yeast with the bait clone. CHD7 exhibited autoactivation and was able to grow on SD-Ura-Leu-Ade+x α-gal plates independently without the addition of BBS6. This could suggest that this particular group of proteins have properties that activate the screening system irrespective of *bona fide* protein-protein interactions, hindering the use of this system to identify interactors of these proteins. Figure 5.3 shows the structure of these three proteins and the location of clones identified.

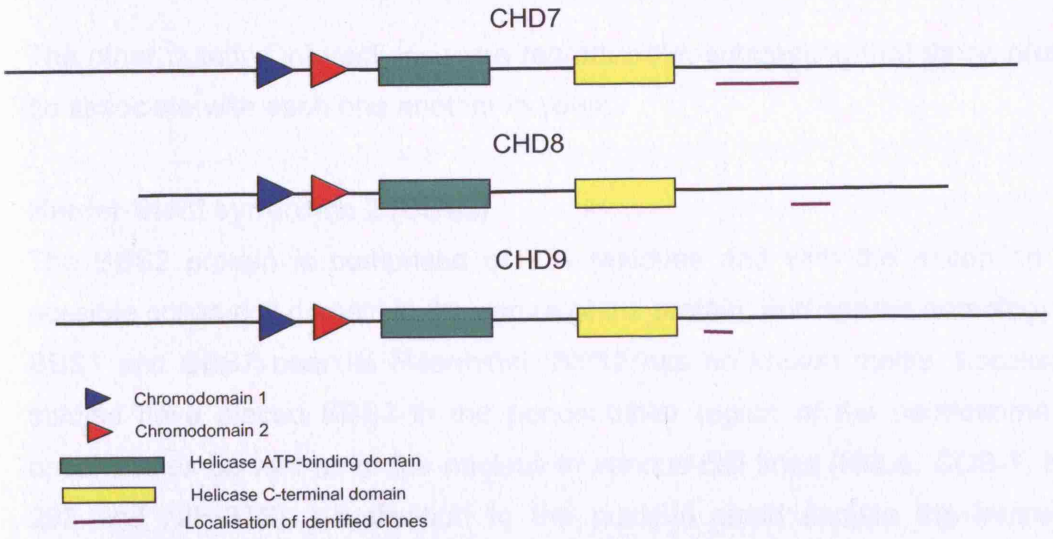

Figure 5.3: Schematic representation of the CHD7, 8 and 9 proteins showing the position of the known domains and the identified clones. (Not to scale)

It is strange that they all interact in non-overlapping regions. There was no sequence homology amongst the interacting regions. CHD (chromo-ATPase/helicase-DNA-binding) proteins are ATP-dependent chromatin remodelling factors implicated in RNA polymerase II transcription regulation. Structurally they all encode double chromodomains which always occur N-terminal to a conserved SNF2 domain. SNF2-containing proteins are thought to perform ATP-dependent protein translocation on DNA and promote chromatin remodelling (Flaus *et al.*, 2006). Phylogenetic classification of CHD proteins according to their chromodomains has classified four distinct subfamilies (Flanagan *et al.*, 2007). Interestingly the three chromodomains pulled out in this yeast 2 hybrid screen are all class D CHD proteins, of which there are only six in total. CHD7 is implicated in CHARGE syndrome (Vissers *et al.*, 2004), whilst CHD8 is associated with beta catenin mediated gene expression (Sakamoto *et al.*, 2000) and CHD9 is associated with ligand-dependent transcription by nuclear receptors (Surapureddi *et al.*, 2002). Although the clones identified in this screen do not appear to be located in structurally comparable domains, it is interesting that CHD7, 8 and 9 all fall within the same class of CHD proteins and one could assume that this might account for them initially being isolated during the screen. However there is nothing reported in the literature about CHD proteins as common false positives in yeast.

The other putative interactions were reproducible, suggesting that these proteins do associate with each one another in yeast.

Bardet-Biedl syndrome 2 (BBS2)

The BBS2 protein is comprised of 721 residues and with the exception of a possible coiled-coil domain in the centre of the protein, and shared homology with BBS1 and BBS7 near its N-terminal, BBS2 has no known motifs. Localisation studies have placed BBS2 in the pericentriolar region of the centrosome and basal bodies as well as in the nucleus in various cell lines (HeLa, COS-7, HEK-293 and NIH-3T3). Localisation to the nucleus could explain the interaction between the protein's ciliary function and transcriptional regulation. A yeast two-

hybrid screen using BBS2 as bait identified both BBS6 and BBS9 as interactors and it is thought that it does so by forming separate complexes with each protein.

The identification of BBS2 as an interactor with BBS6 in the current yeast two-hybrid screen, not only confirmed the validity of their association, but also served as an internal positive control.

EH-domain containing 2 (EHD2)

EH (Eps15 homology) domain proteins contain a highly conserved motif comprised of around 100 residues. These proteins carry out a variety of cellular functions including the regulation of the actin cytoskeleton, signal transduction, and transcriptional regulation of the endocytic pathway. Most EH domains are found at the N-terminus, but four highly homologous C-terminal EH-domain-containing paralogs are expressed in mammalian cells (EHD1-EHD4). Along with their EH domain, they also contain a central coiled coil region involved in oligomerisation and an N-terminal nucleotide-binding motif. In particular these proteins have been implicated in vesicle trafficking and appear to regulate several key endocytic steps including internalisation and recycling (Naslavsky and Caplan, 2005). In particular EDH2 has been shown to interact with the insulin-responsive glucose transporter GLUT4 and may participate in insulin induced GLUT4 recruitment (Park *et al.*, 2004).

The association with BBS6 and EHD2 could further implicate the role of the BBS6 protein in the structure and maintenance of the cytoskeleton and cellular trafficking (see chapter 8 and 9). Furthermore the specific interaction between EDH2 and GLUT4 could provide an explanation the cause of the type 2 diabetes observed among BBS patients.

Chaperonin containing TCP1, subunit 6A (zeta 1)

CCT6A is a subunit of the group 2 eukaryotic cytosolic chaperone CCT (Chaperonin Containing TCP-1; also termed TRiC). Built like other chaperones it is composed of two superimposed rings, each ring consisting of eight different subunits (CCT1-8) which have approximately 30% identity (Grantham *et al.*, 2000; Valpuesta *et al.*, 2002). This chaperone predominantly folds actin and

tubulin proteins, however it has also been shown to interact with 9-15% of newly synthesised proteins (Thulasiraman *et al.*, 1999). Interaction between its unfolded substrates occurs between specific CCT subunits and the binding of ATP generates large conformational rearrangements, assisting the folding of the bound proteins (Schoehn *et al.*, 2000).

The identification of this protein through the yeast two-hybrid screen is of interest as Bbs6 is a putative chaperone based on its predicted structure. As the interaction appears to be with subunit CCT6A, it is plausible that Bbs6 is either aiding the folding of this subunit or that Bbs6 is binding to this subunit to be modified itself. The preference of CCT to fold actin or tubulins is noteworthy in the context that another protein identified in this screen is MACF1, a microtubule and actin cross linking protein. Furthermore, one of the other proteins identified, EHD2, belongs to a class of proteins (EH domain proteins) that carry out a variety of cellular functions including the regulation of the actin cytoskeleton.

DNA (cytosine-5-)-methyltransferase 1 (DNMT1)

DNA methylation is a stable, but not irreversible, epigenetic signal which silences gene expression and is carried out by DNA methyltransferase enzymes. It plays a role in many cellular processes including control of gene expression, cellular differentiation and development, preservation of chromosomal integrity, parental imprinting and chromosome inactivation (Hermann *et al.*, 2004). DNA methylation has also been implicated in brain function and the development of the immune system. Alteration of genomic methylation patterns have been associated with cancer and aging. Dnmt1 was the first mammalian DNA methyltransferase to be discovered (Gruenbaum *et al.*, 1982) and there have been three more identified since (Dnmt3a, Dnmt3b, Dnmt2) (Hermann *et al.*, 2004). They all appear to have a common structure, being divided into an N-terminal regulatory part and a C-terminal catalytic part. The catalytic domain is characterised by ten conserved amino acids motifs. The Dnmt1 and Dnmt3 enzymes contain large N-terminal regulatory domains. It is thought that this N-terminal part of Dnmt1 seems to be involved in the intracellular delivery and regulation of its catalytic activity. Dnmt1 is essential in normal embryonic development, and as a result any knockout

animals die very early on in development (Li *et al.*, 1992) and have significantly reduced levels of DNA methylation.

BBS6 could potentially be the chaperone for this protein.

Translocase of outer mitochondrial membrane 70 homolog A (yeast) (TOMM70A)

Mitochondria require up to 1000 proteins to function properly, the majority of which are synthesised as precursors in the cytoplasm. These mitochondrial preproteins are initially chaperoned to the mitochondria by the cytosolic heat shock protein cHSP70 and are then pursued by Translocators of the Outer Membrane (TOMs). This is followed by transient interactions of the unfolded proteins with Translocators of the Inner Membrane (TIMs). TOMM70A is a mammalian gene orthologous to the yeast Tom70 import component. It localises to the outer mitochondrial membrane and could play a significant role in the import of nuclear-encoded mitochondrial proteins (Edmonson *et al.*, 2002). Young *et al.* have observed a dual function for Tom70: not only does it act as a preprotein receptor, but also as a co-chaperone that aids other chaperones in the targeting of pre-proteins to mitochondria (Young *et al.*, 2003).

Again of note is the association of BBS6 with another potential chaperone particulary a mitochondrial chaperone. Taken together with the results of the BBS2 yeast two-hybrid screen, which identified the aryl hydocarbon-receptor interacting protein (AIP) a cytosolic chaperone involved in folding of mitochondrial pre-proteins, as a potential interactor of BBS2 (A.Ross, unpublished) , this finding becomes more significant.

Microtubule-actin crosslinking factor 1 (MACF1)

MACF1 (microtubule actin crosslinking factor) is a multidomain protein that associates with microfilaments and microtubules. This protein is also referred to as ACF7 (actin crosslinking family 7) and belongs to a family of proteins called plakins. Plakins are linker proteins that connect the cytoskeletal network to membrane associated junctional complexes, and are important in maintaining tissue integrity (Lin *et al.*, 2005). MACF1$^{-/-}$ mice die at gastrulation stage and

display developmental retardation at E7.5 with defects in formation of the primitive streak, node and mesoderm (Chen *et al.*, 2006). Endodermal cells derived from MACF1$^{-/-}$ mice exhibit defects in microtubule (MT) dynamics and the MTs themselves are bent parallel to the plasma membrane near the cell periphery. Near the cortex of these cells, MTs fail to track along actin cables, suggesting that MACF1 is important for guiding MTs on actin filaments (Kodama *et al.*, 2003). More recently MACF1 has been shown to play a role in the Wnt signalling pathway, where it functions as a positive regulator in the translocation of Axin and its associated complex from the cytoplasm to the cell membrane. This is seen to be an indispensable step for signal transmission upon Wnt stimulation(Chen *et al.*, 2006).

Association of Bbs6 with MACF1 could allude to its role in the maintenance of the microtubule network and its involvement in intracellular trafficking. Also the association of Bbs6 with actin is of interest given the identification of a subunit of the CCT chaperone, which predominantly folds actins.

In summary, many of the proteins identified through this study, are in some way associated with cytoskeletal proteins, particularly actin and microtubules (summarised in table 5.5). These findings could aid the determination of the BBS6 protein's function, expanding the theory of BBS proteins being solely cilial and basal body proteins. A further point of interest is that two of the identified interactors are involved in chaperoning (CCT6A and TOMM70A). With BBS6 being a putative chaperone, this could be more than a coincidence, and it is possible that BBS6 is being chaperoned, or is chaperoning these proteins. A point to remember when analysing these results is that in total 44 possible interactors were identified. Only a quarter of these were chosen for further analysis and, as they were selected for relevance to BBS, there was a certain degree of bias in their selection. Further analysis of the remaining clones identified could enrich our understanding of the BBS proteins' function. It is possible that some of the candidates could be further BBS proteins, however, of the six interactors isolated for further analysis, only BBS2 is found in the ciliaproteome (http://www.ciliaproteome.org).

Identified Interactor	Predicted Cellular Function
Bardet-Biedl syndrome 2 (BBS2)	Basal body & cilium function
Chaperonin containing TCP1, subunit 6A (zeta 1)(CCT6A)	Chaperone (actin & tubulin)
DNA (cytosine-5-)-methyltransferase 1 (DNMT1)	DNA methylation
EH-domain containing 2 (EHD2)	GLUT4/actin interactor
Microtubule-actin crosslinking factor 1 (MACF1)	Cytoskeletal linker protein
Translocase of outer mitochondrial membrane (TOMM70A)	Mitchondrial chaperone

Table 5.5: Summary of confirmed Bbs6 interactors and their predicted cellular functions.

Further work must be carried out to support the interaction of these proteins with BBS6 and to elucidate their biological relevance. Direct interaction studies include co-immunoprecipitation, GST pulldowns and analysis of co-localisation of protein expression in relevant cell lines and mouse tissues. Chapter 8 contains expression data from proteins identified during this screen. Liquid β-galactosidase activity assays can be carried out to measure the strength of the interactions. Deletion analysis of Bbs6 and/or prey constructs could further refine the domain of interaction. Modelling BBS6 mutations found in human patients could further allude to the proteins function. Animal models could be used to further test for genetic interactions between BBS6 and its interactors. Examples could include crossing knockout mice or double gene knockdown in zebrafish embryos. Repeating the screen using an alternative library would be useful for the identification of further possible interacting proteins, as well as confirming the results from the current screen. If an interactor is identified through two separate screens carried out using different prey libraries, its association with the bait is more likely to be real. Additionally, the 33 remaining clones that were also isolated during the screen have yet to be confirmed. It is highly likely that the proteins these encode are involved in BBS6 function.

One protein we might have expected to emerge from this screen was BBS5, as direct yeast two-hybrid interactions have been observed between BBS6 and BBS5 whilst pairwise testing a panel of full-length BBS1-12 bait and prey proteins (A. Ross, unpublished). That this was not the case can easily be explained primarily through the possible absence of BBS5 in the cDNA library, but also further through the lack of necessary post-translational modifications, indirect interactions requiring the presence of intermediary proteins or low protein

expression levels that may miss transient or weaker interactions between the proteins.

Of note is that the murine version of BBS6 was chosen as bait against a murine cDNA prey library. Although the mouse and human BBS6 protein are almost identical, the mouse and human proteome may vary slightly, and so potential human-specific protein-protein interactions might have been missed. As the mouse and human BBS6 protein are so similar, it would be possible to use the current bait plasmid to screen a human library.

Recently a complex composed of seven of the BBS proteins (BBS1, BBS2, BBS4, BBS5, BBS7, BBS8 and BBS9) was identified. This has been termed the BBSome and has been shown to localise to centriolar satellites in the cytoplasm and to the ciliary membrane where it is required for ciliogenesis (Nachury *et al.*, 2007). This finding implicates that the BBS proteins function in part in tandem and could explain the phenotypic overlap between patients with different gene mutations. Interestingly BBS6 was not part of this complex, although BBS2, which interacts with BBS6 is. Further members of the BBSome could potentially be candidates identified through our yeast two-hybrid screen.

The yeast two-hybrid system is a useful method to identify and evaluate protein-protein interactions, but it does have its limitations. As the process is done in a yeast model system the effect of post-translational modifications cannot be accounted for. Additionally, indirect interactions requiring intermediary proteins aren't identified and weaker or more transient interactions between proteins can easily be missed. However, these points should not undervalue the usefulness of such a screen as the first steps in the functional analysis of a novel protein.

5.5 Summary

A yeast two-hybrid screen using full length murine BBS6 as bait, successfully identified 44 potential interacting proteins. Further analysis of an initial cohort of these interactors, (BBS2, EHD2, TCP1 subunit 6A, DNMT1, TOMM70A and MACF1) verified the findings in the yeast system. The remaining 33 clones have yet to be confirmed but could also yield interesting candidates. The strong association of BBS6 with proteins associated with the cytoskeleton, particularly actin and microtubules, implicate a role for BBS6 beyond cilial and basal body function.

Chapter 6: Phenotypic analysis of the *Bbs6*$^{-/-}$ mouse

Aim: To assess the phenotype of *Bbs6*$^{-/-}$ mice in relation to the clinical features seen in BBS patients.

6.1 Introduction

Mus musculus is a good model organism in which to study human diseases. It is a mammalian species with similar anatomy, embryology and physiology to humans. As its genome has been sequenced, genetic manipulation is relatively straightforward. The gestation period is only 21 days and offspring are fertile after four to seven weeks. It was for these reasons that a mouse model of BBS was considered as a good way to further study the disease. A mouse null for *Bbs6* was generated from ES cells in which gene disruption had occurred following insertion of a trapping cassette into intron 1 of the *Bbs6* gene.

A *Bbs4* knockout mouse had been previously generated by another research group, and shown to display major components of the human phenotype, including obesity and retinal degeneration and a deficit in olfaction. However, polydactyly and renal anomalies, two of the other primary features of the disease in humans were not reported. The observed retinopathy involved apoptotic death of photoreceptors, which contain a modified primary cilium. Mice were born runts but became obese at 12 weeks. *Bbs4*-null mice were shown to develop both motile (trachea) and primary cilia (kidney), demonstrating that *Bbs4* is not required for global cilia formation. The investigators report that male *Bbs4*-null mice fail to form spermatozoa flagella (Mykytyn *et al.*, 2004; Eichers *et al.*, 2006).

Similarly, a *Bbs2* knockout mouse has also been reported. Not only do these mice become obese and develop retinal degeneration, they also develop renal cysts and show a deficit in olfaction. As with the *Bbs4*-null mice, retinopathy involves normal retina development followed by apoptotic death of

photoreceptors. It was additionally observed that photoreceptor death was preceded by mislocalisation of rhodopsin, indicating a defect in intraflagellar transport. Again null mice were shown to develop both motile and primary cilia, demonstrating that *Bbs2* is not required for global cilia formation. As with the *Bbs4* knock out mouse, the investigators report that male *Bbs2*$^{-/-}$ mice fail to form spermatozoa flagella. Interestingly it is reported that both *Bbs4*$^{-/-}$ and *Bbs2*$^{-/-}$ mice have a defect in social function (Nishimura *et al.*, 2004).

In a recent paper highlighting the loss of BBS proteins as a cause of anosmia in humans, mice with deletions of *Bbs1* and *Bbs4* were examined to test whether this phenotype was caused by ciliary defects. Loss of function of either protein affected the olfactory, but not the respiratory epithelium, causing severe reduction of the ciliated border, disorganisation of the dendritic microtubule network and trapping of olfactory ciliary proteins in dendrites and cell bodies. *Bbs1* and *Bbs4* null mice had considerable phenotypic variability. Neither had polydactyly, renal or liver malformations. All mice were runts at birth and by week 10 ~10% of the mice became obese and 30% developed retinal degredation (Kulaga et al.,2004).

The following table gives an overview of the *Bbs* null mice published to date.

Mouse	*Bbs1*-null	*Bbs2*-null	*Bbs4*-null	*Bbs4*-null
Generation	Trapping cassette (between x11-12)	Targeted deletion (x5-14)	Targeted deletion (x6-11)	Trapping cassette (between x1-2)
Background	Mixed 129Sv/Ev:C57BL/6J	Not stated	Back crossed 2 generations to enrich for C57BL/6J	Mixed 129Sv/Ev:C57BL/6J
Embryonic lethality	40-50%	+ (value not stated)	48%	40-50%
Obesity	Runts at birth, ~10% become obese	Runts at birth, become obese at 12 weeks	Runts at birth, become obese at 12 weeks	Runts at birth, ~10% become obese
Polydactyly	-	-	-	-
Renal cysts	Not reported	+	Not reported	+?
Retinal degeneration	+ (in ~30% of mice)	+	+	+ (in ~30% of mice)
Fertility	Decreased	Males infertile	Males infertile	Decreased
Flagella	Not reported	-	-	+
Olfactory deficits	+	+	+	+
Reference	Kulaga et al., 2004	Nishimura et al., 2004	Mykytyn et al., 2004	Kulaga et al., 2004 Eichers et al., 2006

Table 6.1: Over view of the phenotypes observed in mice null for *Bbs* genes.

Bbs6-null mice generated by gene disruption due to insertion of a trapping cassette into intron 1, were generated by our group. These animals were examined for phenotypical abnormalities including; polydactyly, obesity, renal cyst development, fertility and olfactory deficits. A further *Bbs6* knockout mouse targeted at exon 3 has been generated by another research group and will be discussed further on (Fath *et al.*, 2005).

6.2 Materials and Methods

6.2.1 Generation of *Bbs6*$^{-/-}$ mice

129Sv/Ev embryonic stem cell lines targeted for *Bbs6*, where gene disruption had occurred following insertion of a trapping cassette into intron 1, were selected (Omnibank® Clone 367255, Lexicon Genetics) (see Fig 6.1). Chimeras were generated by microinjection of ES cells into blastocysts (Genoway, France). Male transmitters were crossed with wild-type C57BL/6J females and bred to homozygosity. All analyses were performed on a mixed 129Sv/Ev:C57BL/6J background.

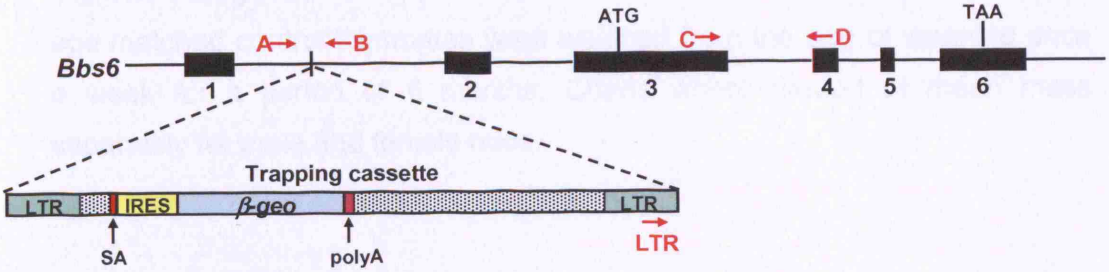

Figure 6.1: Schematic representation of the site of gene disruption by insertion of a trapping cassette into the *Bbs6* genomic region. The red arrows A, B and LTR indicate the position of the primers used for genotyping by PCR, C and D those used in RT-PCR. LTR, long terminal repeat; IRES, internal ribosomal entry sequence; SA, splice acceptor; polyA, polyadenylation signal sequence.

6.2.2 Genotyping of pups

Pups were tail tipped at an age of 9-13 days and the genomic DNA isolated (see section 2.2.8.1). Genotyping by PCR was performed using three primers. Primer positions are shown in Fig 6.1. PCRs were carried out as described in section 2.2.2, the only difference being the addition of a third primer. All primers were used at a final concentration of 5 pmol. The annealing temperature was 65°C.

6.2.3 RT-PCR

RT-PCR analysis was performed to find out if there was complete loss of *Bbs6* mRNA. Total RNA was extracted from dissected organs using Trizol reagent (Invitrogen) following manufacturers instructions. RNA was then reverse transcribed into first strand cDNA and RT-PCR performed using intron-crossing primers specific to *Bbs6*, as described in section 2.2.5. RT-PCR was also performed using primers specific for β-actin as a control.

6.2.4 Analysis of weight gain

Eight homozygous *Bbs6* -/- (n = 4 male, n = 4 female) and an equal number of age matched control littermates were weighed from the age of weaning once a week for a period of 6 months. Charts where plotted of mean mass separately for male and female mice.

6.2.5 Histology and immunofluorescence

Desired organs were dissected, fixed and either wax embedded and sectioned on a microtome at room temperature, or OCT embedded and sectioned on a cryostat at -22°C. Sections were mounted onto either TESPA coated slides or positively charged SuperFrost + slides (BDH). OCT sections were stored at -80°C. Wax embedded kidney and testes sections were subsequently stained with hematoxylin and eosin. Immunohistochemistry was performed on OCT embedded snout sections. Primary antibody was mouse anti acetylated α-tubulin diluted 1 in 800 (Sigma) and secondary antibody was donkey anti-mouse Alexa594 diluted 1 in 200 (Molecular Probes). Nuclei were counter stained with Dapi, using a mounting medium containing Dapi (Vectashield containg Dapi; Vector Labs). For more details see sections 2.2.8.2-2.2.8.4.

6.2.6 Hearing and olfaction analysis

The Preyer's reflex was initially used to asses the hearing ability of the mice using a click box (MRC, Harwell). Assessment was made in a group of age-matched *Bbs6*$^{-/-}$ (n=24) and wild-type littermate controls (n=20). Subsequently DPOAEs were measured in twelve mutant mice and five age-matched controls. DPOAEs (distortion product otoacoustic emissions) are measurable sounds of coclear origin, caused by the reflex motion of sensory hair cells as they energetically respond to auditory stimulation, and are highly sensitive to cochlea pathology in a frequency dependent manner (Kemp *et al.*, 1990). A buried food pellet recovery test was employed to assess olfactory deficiencies among the mice. A group of age-matched *Bbs6*$^{-/-}$ (n=8) and wild-type littermate controls (n=8) were tested. Details of these procedures are given in 2.2.8.6-2.2.8.7 in the materials and methods section.

6.2.7 Analysis of fertility

Mating pairs (n=3) aged 6, 8, 10, 12 and 14 weeks, were set up with both *Bbs6*$^{-/-}$ male and female mice crossed with controls and *Bbs6*$^{-/-}$ male and female mice crossed with each other. Testes were removed from three *Bbs6*$^{-/-}$ and *Bbs6*$^{+/-}$ 8-week-old male mice, weighed, wax embedded and stained with haematoxylin and eosin as described in section 2.2.8.4. Testes weights were measured as a percentage of body weight. Spermatids were extracted from sacrificed homozygous animals and wild type controls, diluted in PBS and visualised under light microscopy.

Bbs6 expression analysis via the *β-galactosidase* reporter gene was performed in the testis. As the inserted trapping cassette contained a *β-galactosidase* reporter gene, it would be expected that *β-galactosidase* would be expressed only in cells where the *Bbs6* promoter was active and so the normal expression pattern of the *Bbs6* transcript could be examined in animals carrying the trapping cassette. *β-galactosidase* assays were performed on adult testes from heterozygous animals, no *β-galactosidase*

activity was detected in wild-type animals. Assays were carried out as described in section 2.2.8.5.

6.3 Results

6.3.1 Generation of mice with disruption of *Bbs6*.

Mice null for *Bbs6* were created through gene disruption following insertion of a trapping cassette into intron 1 (Fig 6.1). A three primer PCR assay confirmed correct targeting of *Bbs6* (Fig 6.2 A). Heterozygous mice were crossed to generate *Bbs6*$^{-/-}$ homozygotes. RT-PCR analysis using mRNA extracted from brain, kidney, lung, liver and spleen confirmed that there was complete loss of *Bbs6* mRNA, showing that this insertion creates a *Bbs6* null mutation (Fig 6.2 B). Genotyping of pups from F1 heterozygous crosses gave F2 ratios that did not differ significantly from predicted Mendelian ratios (n=200, chi-square=1.87, p>0.1 (Table 6.2 C)), indicating that the gene disruption is not embryonic lethal.

A

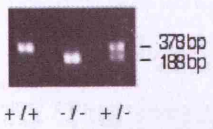

B

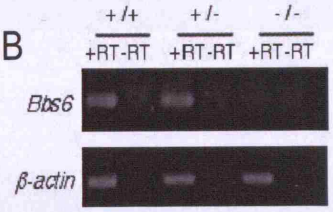

C

	Bbs6$^{+/+}$	Bbs6$^{+/-}$	Bbs6$^{-/-}$	Total
Observed	57	91	52	200
Expected	50	100	50	200

Figure 6.2: Generation of the Bbs6$^{-/-}$ mouse. A) Genotype analysis by PCR using primers A, B and LTR (see Fig 6.1) amplifies a wild-type fragment of 378 bp, a homozygous knock out fragment of 188. B) RT-PCR analysis of cDNA generated with or without reverse transcriptase (+/-RT) from total RNA extracted from brain using exonic Bbs6 primers and β-actin control primers. Genotypes are shown above the panels. C) Genotyping results of pups from F1 heterozygous crosses. Chi-square value is 1.87, which gives a p value of >0.1 with 2 degrees of freedom between the observed and expected ratios. There appears to be no embryonic lethality for the Bbs6 homozygotes.

6.3.2 Analysis of primary features of BBS.

Obesity:

Bbs6$^{-/-}$ mice were initially runty at birth compared to their wild-type litter mates. On average both the male and female *Bbs6*$^{-/-}$ mice remained smaller, however there were large variations in weight. Charts of mean mass are given in Fig 6.3. Raw data is given in appendix C.

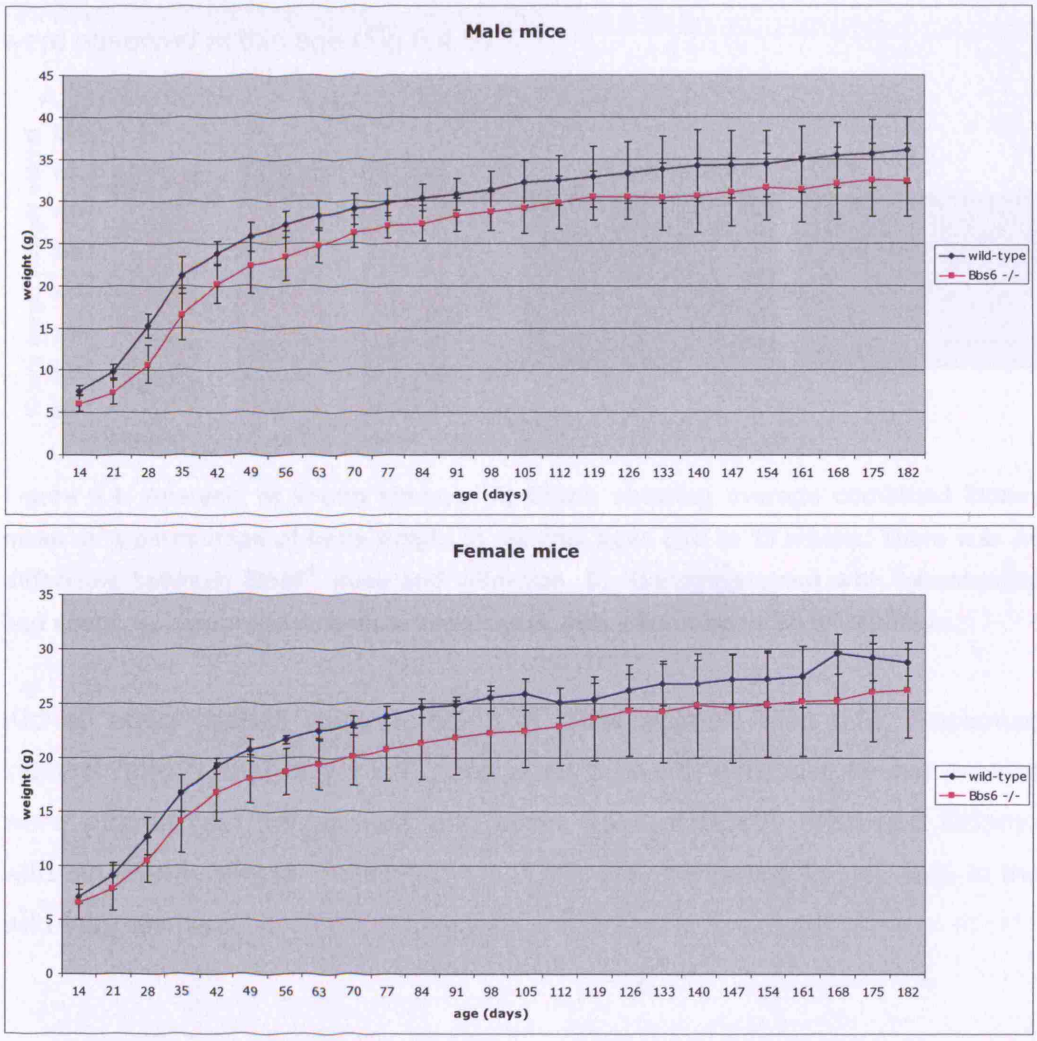

Figure 6.3: Mouse weights over a period of six months from birth. *Bbs6*$^{-/-}$ mice weigh on average slightly less than wild-type litter mates but there is a large degree of variation. Standard error of the mean shown by error bars. (n = 4 Male *Bbs6*$^{-/-}$, n = 4 Male wild-type, n = 4 Female *Bbs6*$^{-/-}$, n = 4 Female wild-type)

Kidney abnormalities:

Kidney masses were recorded in mice aged from two to thirteen weeks. To account for the mice being different sizes, kidney mass was recorded as a percentage of body mass. No differences were observed between *Bbs6*$^{-/-}$ and control animals (Fig 6.4 A). These kidneys were sectioned and stained with hematoxylin and eosin to visualise any structural differences or the presence of cysts. Hematoxylin stains negatively charged nucleic acids (nuclei and ribosomes) blue, and eosin stains proteins pink. No structural abnormalities were observed at this age (Fig 6.4 B).

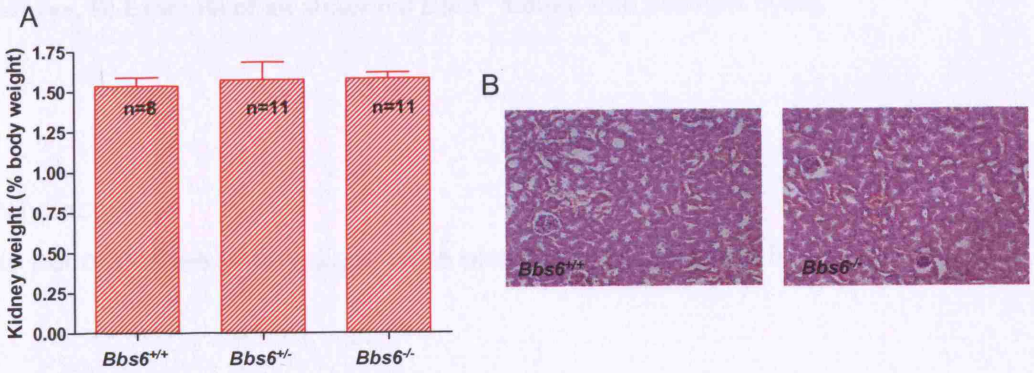

Figure 6.4: Analysis of young kidneys. A) Graph showing average combined kidney mass as a percentage of body weight in animals aged two to 13 weeks. There was no difference between *Bbs6*$^{-/-}$ mice and wild-type. B) Kidneys stained with hematoxylin and eosin. No structural defects or renal cysts were observed in *Bbs6*$^{-/-}$ kidneys.

Kidney abnormalities were detected in older animals (Fig 6.5). Sectioned kidneys from a total of thirteen mice aged between nine and twelve months were stained with hematoxylin and eosin. 75% of *Bbs6*$^{-/-}$ mice had kidneys with structural defects, possibly cysts. This was compared to just 33% in the wild-type animals.

A

	Bbs6$^{+/+}$	*Bbs6*$^{+/-}$	*Bbs6*$^{-/-}$
Total n. animals	3	2	8
Normal kidneys	2	1	2
Abnormal kidneys	1	1	6
% Abnormal	33%	50%	75%

B

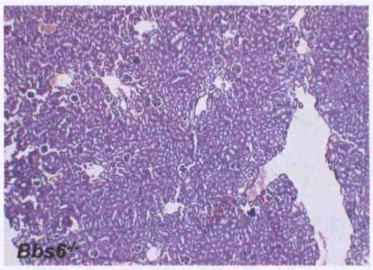

Figure 6.5: Analysis of mature kidneys. A) Table summarising analysed mature kidneys. B) Example of an abnormal *Bbs6*$^{-/-}$ kidney with possible cysts.

Polydactyly:

No abnormalities of any digits were observed in any of the Bbs6$^{-/-}$ mice.

6.3.3 Analysis of secondary features of BBS.

Olfactory deficiencies:

A buried food pellet recovery test was employed to assess olfactory deficiencies among the mice. In a group of age-matched *Bbs6*$^{-/-}$ (n=8) and wild-type littermate controls (n=8), *Bbs6*$^{-/-}$ mice displayed significantly longer latencies in their ability to retrieve the buried treat than their control littermates. The Mann-Whitney U test was used to analyse the data in which the latencies from each group (*Bbs6*$^{-/-}$ vs *Bbs6*$^{+/+}$) were jointly ranked and then the ranks summed and averaged for each group for each day the animals were tested (Fig 6.6). Raw values are given the appendix C.

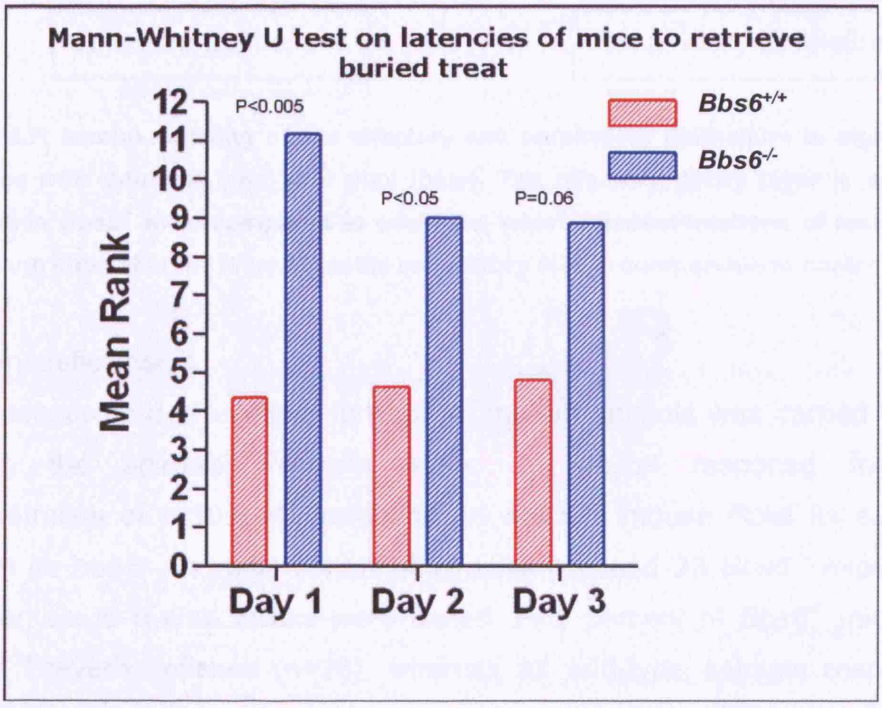

Figure 6.6: Graph showing the results of the Mann-Whitney U test carried out on latencies of mice to retrieve buried food treat. *Bbs6*$^{-/-}$ mice ranked significantly higher than wild-type mice, which reflects their increased latencies in retrieving the treat.

Examination of the olfactory epithelium by staining for the ciliary-specific marker, acetylated α-tubulin, revealed marked thinning of the olfactory ciliary layer in *Bbs6*$^{-/-}$ mice compared to wild-type controls, potentially indicative of short ciliary structure. Staining of the respiratory epithelium from adjacent sections showed that motile cilia were preserved (Fig 6.7).

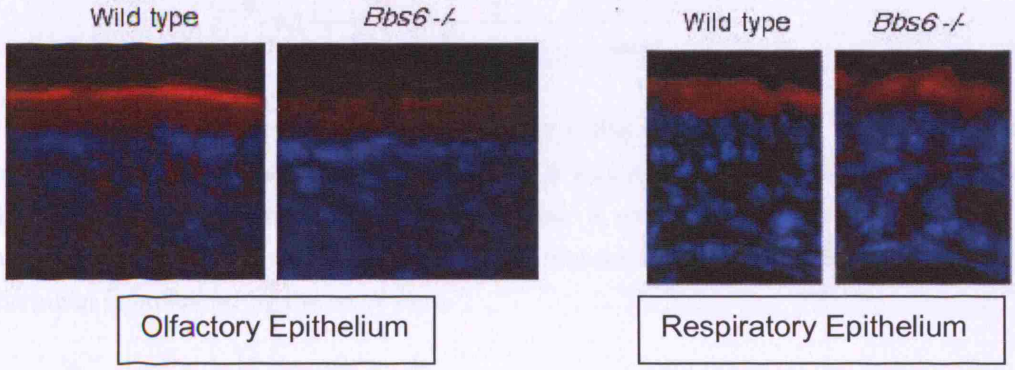

Figure 6.7: Immunostaining of the olfactory and respiratory epithelium in eight-week old mice with α-tubulin (red) and dapi (blue). The olfactory ciliary layer is severely reduced in *Bbs6*$^{-/-}$ mice compared to wild-type, whist adjacent sections of respiratory epithelium show that the layer of motile respiratory cilia is comparable to control.

Auditory deficiencies:

Initial assessment of auditory function of mutant animals was carried out by judging the animals Preyer's reflex, a natural response following administration of a 19.5 Hz toneburst, in which a mouse flicks its ears flat against its head. An initial cohort of 20 wild-type and 23 *Bbs6*$^{-/-}$ mice aged between six to twelve weeks were tested. Fifty percent of *Bbs6*$^{-/-}$ mice had absent Preyer's reflexes (n=23), whereas all wild-type animals responded (n=20) (Fig 6.8).

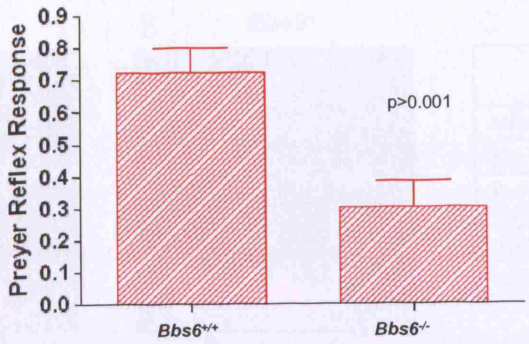

Figure 6.8: Graph to show the average Preyer reflex score of *Bbs6* null mice (n=23) versus wild-type controls (n=20). A score of 1.0 was awarded if the mouse responded well by flicking its ears flat against the head, a score of 0.5 if there was a mild response, and a score of 0.0 if there was no response whatsoever. Standard error of the mean is indicated by the error bars.

The elicitation of the Preyer reflex provides a global measure of hearing function. To further locate the origin of hearing deficit, distortion product otoacoustic emissions (DPOAEs) were examined. These are measurable sounds of coclear origin, caused by the reflex motion of sensory hair cells as they energetically respond to auditory stimulation, and are highly sensitive to cochlea pathology in a frequency dependent manner (Kemp *et al.*, 1990). Intensity of emission was examined in wild-type mice (n=5; age range 12-31 weeks) with normal Preyer reflexes and compared to age-matched *Bbs6*$^{-/-}$ mutant mice (n=12). Fifty percent of *Bbs6* null mice yielded no response above the ambient background noise and 66.6% displayed either no response or a low response, compared with 100% response rate in wild-type mice, significantly indicative of a severe impairment to cochlea function (Fig 6.8). Emissions could only be recorded for a small range of frequencies ~3.5-kHz-7-kHz owing to the nature of the mouse cochlea and the limitations of the equipment available. Mice did not respond below 3.5-kHz.

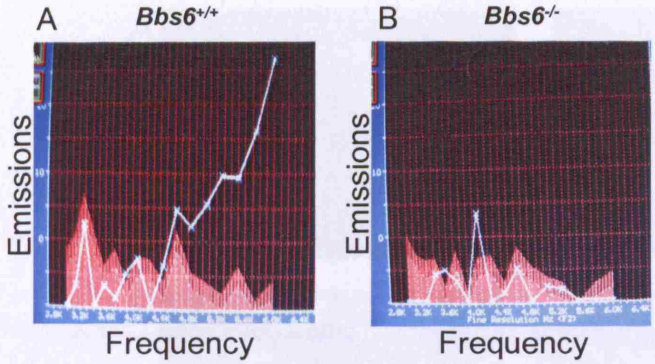

C

	Bbs6 $^{+/+}$	*Bbs6* $^{-/-}$
Animals Tested	5	12
High Response	2	2
Medium Response	3	2
Low Response	0	2
No Response	0	6

Figure 6.9: Distortion product otoacoustic emissions in *Bbs6*$^{-/-}$ mice. A,B) Typical graphs resulting from DPOAE emissions for Wild-type and *Bbs6* null mice. Red bars represent ambient background noise. Figure A) is representative of a high response and figure B) of no response. C) Table of results. All Wild-type animals had either a high or medium response. 50% of *Bbs6*$^{-/-}$ animals had no response and 66% had no or low response.

Analysis of fertility:

Fertility among *Bbs6*$^{-/-}$ males and females did not differ from controls. Mating pairs set up as described in the materials and methods section showed that *Bbs6*$^{-/-}$ animals sired litter numbers comparable to controls. Testes weights were slightly lower than wild-type controls (average combined testes weight as percentage of body weight for wild-types was 0.87% (n=3) compared to 0.66% (n=3) in *Bbs6*$^{-/-}$ animals). Hematoxylin and eosin staining of sectioned testes revealed the developing spermatids to be more densely packed in the control animals (Fig 6.10 A), which could explain the difference in weight. Expression of *Bbs6* in the adult male testis, as indicated by the β-gal reporter gene, was shown to be in the developing spermatids, predominantly in the nucleus (Fig 6.10 B). Flagella were present and on observation did not differ from controls (Fig 6.10 C).

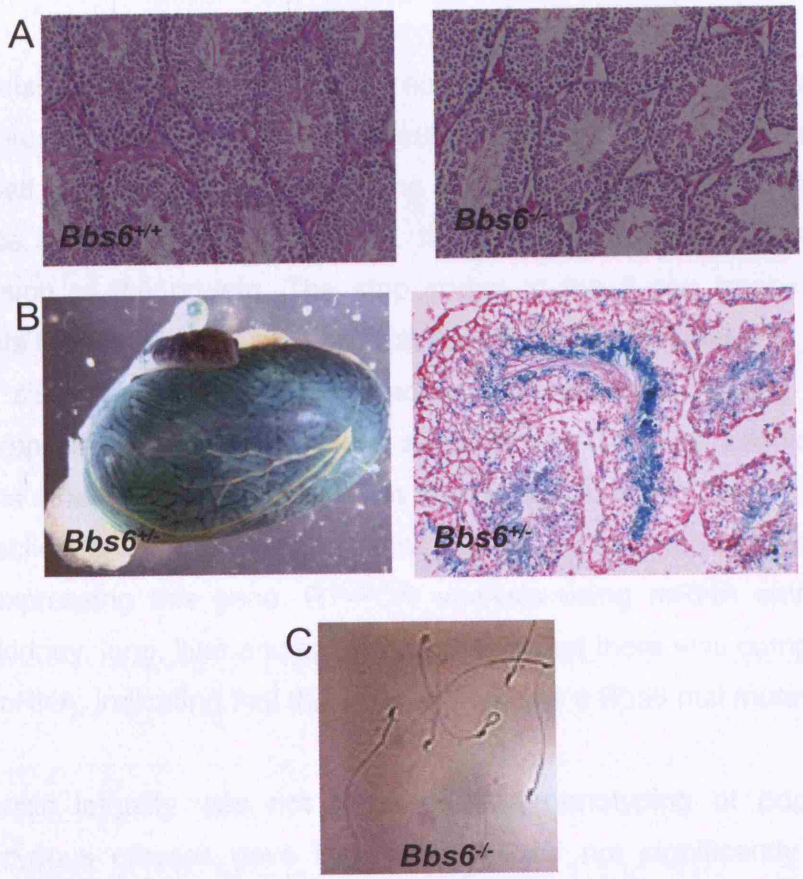

Figure 6.10: Analysis of testes from *Bbs6*$^{-/-}$ mice and wild-type controls. A) Sections from eight week old hematoxylin and eosin stained testes show that in *Bbs6*$^{-/-}$ animals developing spermatids are less densely packed. B) Staining for *β-galactosidase* activity in whole mount testis from an eight week old heterozygous mouse shows that there is prominent *Bbs6* testicular expression, predominantly in the nucleus of the developing spermatids. c) Light microscopy imaging of spermatids extracted from *Bbs6*$^{-/-}$ mice. Spermatids were observed to be structurally and functionally normal.

6.4 Discussion

Gene disruption by insertion of a trapping cassette into the *Bbs6* genomic region successfully generated mice null for *Bbs6*. Although the start ATG for the Bbs6 protein is at the beginning of exon 3 and the inserted trapping cassette is between exons 1 and 2, its insertion affects splicing and hence expression of the protein. The stop codon in the β-geo trapping cassette prevents formation of a fusion protein. A poly-A signal follows this and serves as the site where A poly-A tail attaches. This prevents splicing around the gene trap or initiation of translation at the Bbs6 ATG. The trapping cassette contains a neomycin resistance gene and by definition this gene is expressed, as selection for the ES cells containing this gene trap is made by selecting for cells expressing this gene. RT-PCR analysis using mRNA extracted from brain, kidney, lung, liver and spleen confirmed that there was complete loss of Bbs6 mRNA, indicating that this insertion creates a Bbs6 null mutation.

Embryonic lethality was not observed and genotyping of pups from F1 heterozygous crosses gave F2 ratios that did not significantly differ from predicted Mendelian ratios. Analysis of the *Bbs6* null mouse enabled us to observe the effect of a single *Bbs* gene in a mammalian organism.

A second group published data on an independently generated *Bbs6* knock out mouse, which was generated using a gene-targeting construct designed to knock out exon 3 of the gene (Fath *et al.*, 2005). As with our mice all analyses were performed on a mixed 129Sv/Ev:C57BL/6J background. Phenotypic differences between the two mice can be observed. This *Bbs6* knock out mouse exhibits a small degree of embryonic lethality, the mice become obese and have high leptin levels and it is reported that they fail to form spermatozoa. Similarly both mice display photoreceptor degeneration, fail to exhibit polydactyly. The following table gives a summary of the phenotypic findings of the current study, and compares them to the data from the other *Bbs6*$^{-/-}$ mouse.

Mouse	*Bbs6*-null (current study)	*Bbs6*-null (other study)
Generation	Trapping cassette (between x1-2)	Targeted deletion (x3)
Background	Mixed 129Sv/Ev:C57BL/6J	Mixed 129Sv/Ev:C57BL/6J
Embryonic lethality	-	23.6%
Obesity	Runts at birth, ~10% become obese	Runts at birth, become obese
Polydactyly	-	-
Renal cysts	Possible	-
Retinal degeneration	+	+
Fertility	+	Males infertile
Flagella	+	-
Olfactory deficits	+	+
Reference	Ross et al. 2005	Fath et al., 2005

Table 6.2: Summary of phenotype displayed by the *Bbs6* null mice. The two separately generated mouse models exhibit similar features to the other mouse models for *BBS* genes. The major difference between the two models is the lack of spermatozoon flagella.

As obesity is one of the primary features of the disease, it would have been expected that mice null for *Bbs6* would become obese. At birth *Bbs6*$^{-/-}$ mice were runty compared to their litter mates, and on average they remained smaller as they got older. This is in contrast to the other reported *Bbs6*$^{-/-}$ mouse model, where both male and female knock out mice became obese and had higher leptin levels than controls. *Bbs2*$^{-/-}$ and *Bbs4*$^{-/-}$ mice have also been reported as being runts at birth, but becoming obese at ~12 weeks. Analysis of fat distribution in older animals demonstrates that the increased weight corresponds to an increase in centrally deposited adipose tissue (Mykytyn *et al.*, 2004; Nishimura *et al.*, 2004).

More recently it has been observed amongst our cohort of *Bbs6*$^{-/-}$ mice, that roughly 10% of homozygous and heterozygous mice become obese, though not in the group that we originally weighed. This variability may be due to the mixed genetic background. We were unable to weigh more numbers of mice over a six month period. Ideally we would have had higher n numbers for this study.

Polydactyly was not observed in either of the *Bbs6* mouse models, nor was it reported for any of the BBS mouse models generated so far. As polydactyly features so heavily in the diagnosis of the disease, it is of considerable interest that it is not observed in any of the single gene knock out mice reported to date. It is questionable whether this could be due to differential developmental processes between mice and humans, or whether the occurrence of polydactyly is associated with oligogenicity (see section 1.2.9). This second theory could be verified by the generation of triallelic or double knockout mice and observing if they have extra digits. The majority of BBS patients do display polydactyly, in contrast triallelism amongst BBS patients is not widespread. Hence it is not likely that this theory holds true in humans.

Whilst the kidneys of the younger *Bbs6* null animals were no different from control, structural abnormalities were seen in the more mature animals. These have yet to be examined more closely, but it is most probable that with time the kidneys of *Bbs6*$^{-/-}$ mice do become cystic. Whilst it is possible that the observed 'holes' in the kidney tissue cold be due to preparation artefact, this is unlikely as the surrounding cells appear intact. The development of kidney cysts in the mature animals is unsurprising, as the development of the kidney phenotype in patients is often later in life. The other *BBS* mouse to develop renal cysts so far has been the *Bbs2* knock out model reported by Nishimura et al.(2004) by the age of five months. The *Bbs4* knockout mouse has also been shown to develop renal cysts by six months (P.Beales, unpublished data). The emergence of the renal phenotype appears to be variable amongst the different mouse models, highlighting the variability between the *Bbs* genes.

Retinal degeneration is also one of the primary features of BBS. Analyses of retinas from *Bbs6*$^{-/-}$ mice was carried out by Alison Ross, and showed that loss of *Bbs6* does not prevent initial formation of photoreceptors, but does cause age-related progressive degeneration associated with apoptosis in the outer nuclear layer (ONL) of photoreceptors (Ross *et al.*, 2005). This similar finding is reported in all other *Bbs* gene mouse mutants. The transport of rhodopsin is impaired in *Bbs6*$^{-/-}$ retina, similar to *Bbs2*$^{-/-}$ mice, and consistent

with an IFT defect (see section 1.3.2). In the *Bbs6*$^{-/-}$ mouse retinal degeneration is milder than in the other mouse models, with a slower progression of degeneration.

The olfactory deficiencies identified in *Bbs6*$^{-/-}$ mice, which likely result from the severe depletion of cilia and microtubules from the dendrites of the olfactory epithelium, support recent similar data from *Bbs1*, *Bbs2* and *Bbs4* null animals (Kulaga *et al.*, 2004; Mykytyn *et al.*, 2004; Nishimura *et al.*, 2004). It also corroborates recent data identifying partial or complete anosmia in human BBS patients (Kulaga *et al.*, 2004). Whilst marked thinning of the olfactory ciliary layer is observed in the mice, the adjacent respiratory cilia (motile cilia) layer is always intact. This could represent the difference between motile vs primary (non motile) cilia. It has been stated that BBS is caused by a defect of primary cilia function (see section 1.3).

Although deafness is not a primary feature of the human BBS phenotype, it has been reported that ~3% of patients have sensorineural deafness (Burn, 1950; Beales *et al.*, 1999). In an initial cohort of *Bbs6*$^{-/-}$ mice, auditory function was assessed using a click box to judge the animals response to a 19.5 kHz toneburts. 50% *Bbs6*$^{-/-}$ mice were non responsive, compared to 100% of the wild type litter mates. With the use of DPOAE analyses the source of this defect was further localised to the cochlea. Further analysis of the auditory phenotype of these animals is discussed in the subsequent chapters.

Although *Bbs6* expression was seen in the developing spermatids, fertility was not affected in either male or female *Bbs6*$^{-/-}$ mice that were generated by us. Null mice successfully produced offspring with comparable litter sizes to controls. In male nulls, fully functional flagella were observed. However the other *Bbs6*$^{-/-}$ mouse is reported to have absent flagella similar to the male *Bbs2* and *Bbs4* null mice reported by the same investigators (Mykytyn *et al.*, 2004; Nishimura *et al.*, 2004). However these investigators had not looked at the sperm directly, but had only completed histological examinations of the testes. It was also reported that two adult male patients with *BBS2* mutations, homozygous for the mis-sense mutation V75G, had abnormal spermatozoa

(oligoteratoastenozoospermia with severe necrozoospermia and severe abnormalities of the sperm acrosome, nucleus, and axonemal structures) (Nishimura *et al.*, 2004).

Whole-mount *in situ* analyses of developing (E10.5-E12) embryos with an RNA probe specific to the *BBS6* transcript had previously revealed prominent staining in the heart, brain, retina and limb buds and developing neural tube (Kim *et al.*, 2005). Antibody staining using an anti-BBS6 antibody to stain paraffin-embedded tissue sections of mice brain, kidney, retina, olfactory epithelium and ependymal layer of ventricles, detected BBS6 only in regions containing or bordering ciliated cells (Kim *et al.*, 2005). The expression pattern of *Bbs6* was analysed via the *β-galactosidase* reporter gene inserted into the trapping cassette during generation of the mouse knock out. This work was carried out by a fellow member of the lab. Between E11.5-E13.5, there was prominent *β-galactosidase* activity in the developing eyes, snout and forebrain and in the dorsal root sensory nerves along the developing neural tube. At E11.5-12.5 there was also prominent expression in the apical ectodermal ridge (AER) of the limb buds, with expression at E13.5 in the epithelium between the forming digits and in the mesenchymal layer of the zeugopod. At E13.5, *β-galactosidase* activity became prominent in the pinna of the ear. Sectioning of an E13.5 embyro revealed expression in the sensory epithelium of the otocyst and in the sensory layer of the retina and the lens of the eye (Ross *et al.*, 2005).

The embryonic expression analysis of *Bbs6* via the *β-galactosidase* reporter gene is comparable to the previous *in situ* analyses. This expression reflects the known organs that are affected in BBS patients. Of note is the expression in the developing limb buds, which is consistent with the polydactyly seen in patients, even if this full blown phenotype is not observed in the mice.

The variability between the other *Bbs6*$^{-/-}$ mouse and ours, could be explained by the difference in generation of the mice. Ours were created using a gene trapping cassette between exon 1 and 2, whist they used a gene-targeting

construct designed to knock out exon 3. However RT-PCR analysis does not detect mRNA in our model, so it is highly unlikely that it is hypomorphic. Phenotypic differences are most likely due to the mixed backgrounds and the influence of modifier genes. Initially all mice were on a 50:50 129Sv/Ev:C57BL/6J background but after several generations of breeding experiments, the relative contribution of each background are now unknown. An example of this is the tubby mouse, its auditory phenotype is modified by the genetic background (Ikeda *et al.*, 2002). The wildtype alleles of the modifier of tubby hearing 1 gene (*moth1*) from certain strains protect tubby mice from hearing loss.

Interestingly the *BBS* mice show a degree of variation in regard to phenotype compared to each *BBS* gene. This is in contrast to the patients, in which no significant genotype-phenotype between the various BBS loci has been observed (see section 1.1.4). Explanations for this include the presence of modifiers and interactions between the BBS genes themselves (see section 1.2.9). It is important to note that if background plays such a big part in the development of a phenotype as has been observed among the mice, it would explain the degree of phenotypic variation and lack of genotype-phenotype relationship among patients, considering that humans are on a 'mixed background'. Back-crossing the mice onto a pure background might decrease the observed variability in phenotype and may help to identify modifier genes, since complex inheritance in the form of oligenicity is thought to be involved with the disease. Candidate modifiers include the other *BBS* genes, and it is therefore of interest to generate multi allelic mice to observe the effect this would have on the phenotype.

Whilst the phenotype of the *Bbs6*$^{-/-}$ mouse is not as severe compared to the other BBS mouse models, its increased fertility (compared to the others) makes it is easier to generate animals for further analysis. There remain many further aspects of the *Bbs6*$^{-/-}$ mice phenotype to examine. It would it be of significant interest to do a more in depth study into the obesity and kidney defects observed. This could be aided by metabolic analysis of blood chemistry testing for example for abnormal lipid profiles, insulin and leptin

levels. Behavioural assessment of the *Bbs6*$^{-/-}$ mice compared to their wild-type litter mates would also be of interest, and could aid investigations into the genetics of behavioural disturbances. On a functional level, cell lines would be derived from *Bbs6*$^{-/-}$ tissue for *in vitro* evaluation and experimentation. One of the phenotypes I chose to focus on was the emerging auditory phenotype which is discussed in the following chapters.

6.5 Summary

A *Bbs6* null mouse was successfully generated by gene disruption due to insertion of a trapping cassette into intron 1. These mice phenotypically resembled the other *Bbs1,Bbs2* and *Bbs4* null mice displaying age related retinal degeneration, obesity, renal and olfactory defects. The emergence of an auditory phenotype amongst the *Bbs6*$^{-/-}$ mice raised awareness of an auditory component of the disease in humans, and has lead to more detailed analyses.

Chapter 7: Evaluation of Bbs6 in the organ of Corti

Aims: To assess the origin of the hearing deficit in the *Bbs6*$^{-/-}$ mouse and analyse the expression pattern of the Bbs6 protein during development of the cochlea.

7.1 Introduction

During the phenotypic analysis of the *Bbs6*$^{-/-}$ mouse, it became clear that there was an auditory component to the disease. An initial screen to assess auditory function by measuring the Preyer's reflex response to a 19.5 kHz tone burst, showed that fifty percent of the mice tested were non-responsive. Subsequently distorted DPOAEs, measurable sounds of cochlear origin, implicated the cochlea as the origin of hearing deficit (see previous chapter for more details).

This cochlear association with the disease may appear inconsistent with regard to the other basal body/cilia associated symptoms of BBS. However upon further inspection a connection becomes apparent. An important aspect of the developing cochlea is under the control of a primary cilium. This microtubule containing cilium, referred to as the kinocilium, is responsible for the establishment of stereociliary hair bundles protruding from the apical end of hair cells. Although confusingly termed stereocilia, these hair bundles are comprised mostly of actin filaments and not microtubules as in true cilia.

The cochlea hair cells are so called because of the hair-like appearance of the stereociliary bundles. They transduce sound energy collected by the outer and middle ear and prepare it for neural transmission. The uniform orientation of the stereociliary hair bundles is vital for the transmission of sound (Raphael and Altschuler, 2003; Frolenkov *et al.*, 2004).

7.1.1 The cochlea

The cochlea is the auditory portion of the inner ear in mammals. It is a spiralled, hollow chamber, encased in bone (the otic capsule), which is embedded in the temporal bone. Within it lies the organ of Corti, the sensorineural organ for hearing (Fig 7.2 A). The organ of Corti is comprised of polarised epithelial cells, sensory and non-sensory cells of placodal origin, which are spatially organised in an orderly pattern, spiralling from the base of the cochlea to the apex (Fig 7.1). There are two distinct types of sensory cells in the cochlea, inner hair cells and outer hair cells, so called because of their morphology. In addition there are a range of non-sensory cell types, referred to collectively as supporting cells, which play auxiliary and supportive roles. Support cells have been suggested to function by monitoring a homeostatic environment in which the hair cells function (Raphael and Altschuler, 2003).

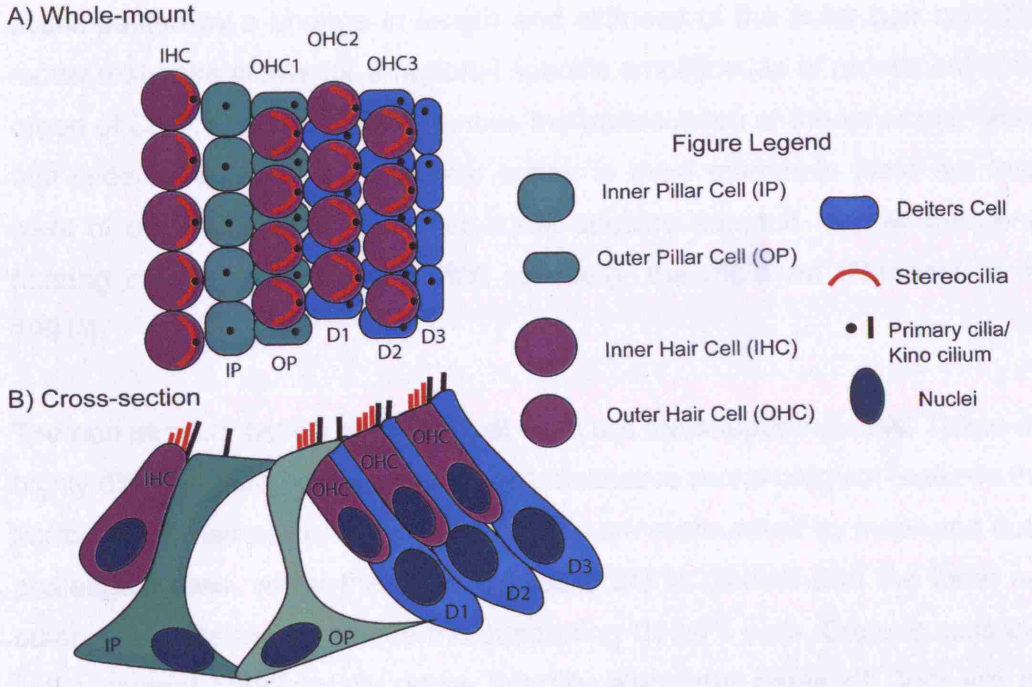

Figure 7.1: The arrangement of sensory hair cells and non-sensory supporting cells in the mammalian cochlea. A) Schematic representation of a whole-mount of the developing organ of Corti. Stereociliary bundles (red) are located on the apical surface of hair cells. Primary cilia are located on all cells, at the apical surface. Stereociliary bundles appear as a flattened "C"-shape on inner hair cells, and as a "V"-shape on outer hair cells. B) Schematic representation of key cell-types in a cross-section of the developing organ of Corti.

The hair cells are responsible for converting sound waves into electrical signals that are relayed to the auditory brainstem (Raphael and Altschuler, 2003). Hair cells have an excess of negatively charged ions inside and an excess of positively charged ions outside. Slight movement of the stereocilia opens transduction ion channels allowing K^+ and Ca^{2+} into the cell, causing depolarization. This causes the hair cell to release neurotransmitters at the base, allowing signaling towards the brain. The inner hair cell is the true sensory cell type and sends impulses via the auditory nerve upon stimulation. One row of inner hair cells runs along the entire length of the organ of Corti. The inner hair cells are separated from the outer hair cells by the supporting pillar cells. The outer hair cells enhance the performance of the cochlea by increasing the selectivity and sensitivity of its response. Often referred to as the cochlear amplifier, the outer hair cells display a dual response upon stimulation. The release of neurotransmitter at the base of the cell is accompanied by a change in length and stiffness of the outer hair cell. This motile response allows for a regional specific amplification of movement in the organ of Corti, which in turn enhances the transduction of the inner hair cell at that specific region of the cochlear spiral. In most mammals there are three rows of outer hair cells, however some species adapted for low frequency hearing can have a fourth or fifth row (e.g. the mole rat (Raphael *et al.*, 1991)).

The non-sensory cells in the organ of Corti are the supporting cells. These are highly differentiated epithelial cells with distinctive morphological features that surround the hair cells. The inner hair cells are surrounded by inner and outer phalangeal cells, whilst the outer hair cells are in contact with the inner and outer pillar cells and lie above the supporting Deiter's cells. Dieter's cells also make contact basolaterally. More laterally along the organ of Corti are the Hensen's cells. It is thought that the support cells' functions go beyond that of structural support as there is evidence that they participate in regulating the ionic environment within and around the organ of Corti (Raphael and Altschuler, 2003).

7.1.2 Stereocilia

It is the stereociliary bundles at the apical ends of hair cells that enable these particular cell types to carry out such a diverse and specialised role. Their deflection as whole entity opens ion channels, depolarising the cell, producing an electrical signal or receptor potential.

The hair bundle is comprised of many stereocilia. These are membrane bound cellular projections comprised of actin and arranged in a staircase-like array at the lateral edge of hair cells (Fig 7.2) (Frolenkov *et al.*, 2004). The inner hair cells usually have two main rows of stereocilia, whilst outer hair cells have three. They are arranged in rows of increasing height with the tallest positioned laterally. Collectively the stereocilia form a 'W' or 'V' shaped bundle. At the base of each stereocilium is an electron-dense rootlet embedded in the cuticular plate. The staircase arrangement of actin-containing stereocilia is maintained by a complex array of protein links (Nayak *et al.*, 2007). Tip links, horizontal top connectors, shaft connectors and ankle links connect adjacent stereocilia. Kinocilial links connect the kinocilium to the tallest row of stereocilia. Upon stimulation, movement of the stereocilia in the direction of the tallest row opens transduction ion channels. K^+ and Ca^{2+} enter the cell, changing the ionic potential and generating a transduction current. This transduction current activates voltage sensitive calcium channels along the hair cell lateral wall and base as well as Ca^{2+} activated K^+ channels. The end result is the release of neurotransmitter at the base of the hair cell. It is thought that the transduction channels, possibly located in the proximity of the tip link filaments, are mechanically gated and that a spring like mechanism transmits forces for opening and closing these channels (Fettiplace, 2006). The exact composition of the tip links, and the properties and function of the transduction channel are unknown. Recently cadherin 23 and protocadherin 15, defects of which cause the sensorineural disease Ushers syndrome, have been shown to be components of the tip links (Lagziel *et al.*, 2005; Ahmed *et al.*, 2006; Kazmierczak *et al.*, 2007). A number of candidates have been considered as the transduction ion channel, including epithelial sodium channel (ENaC) and acid-sensing ion channel (ASIC) members of the

DEG/ENaC superfamily of amiloride-sensitive sodium channels. However it is most likely thought to consist of TRP channels, such as TRPN1, TRPV4, TRPML3 and TRPA1 (Corey, 2006).

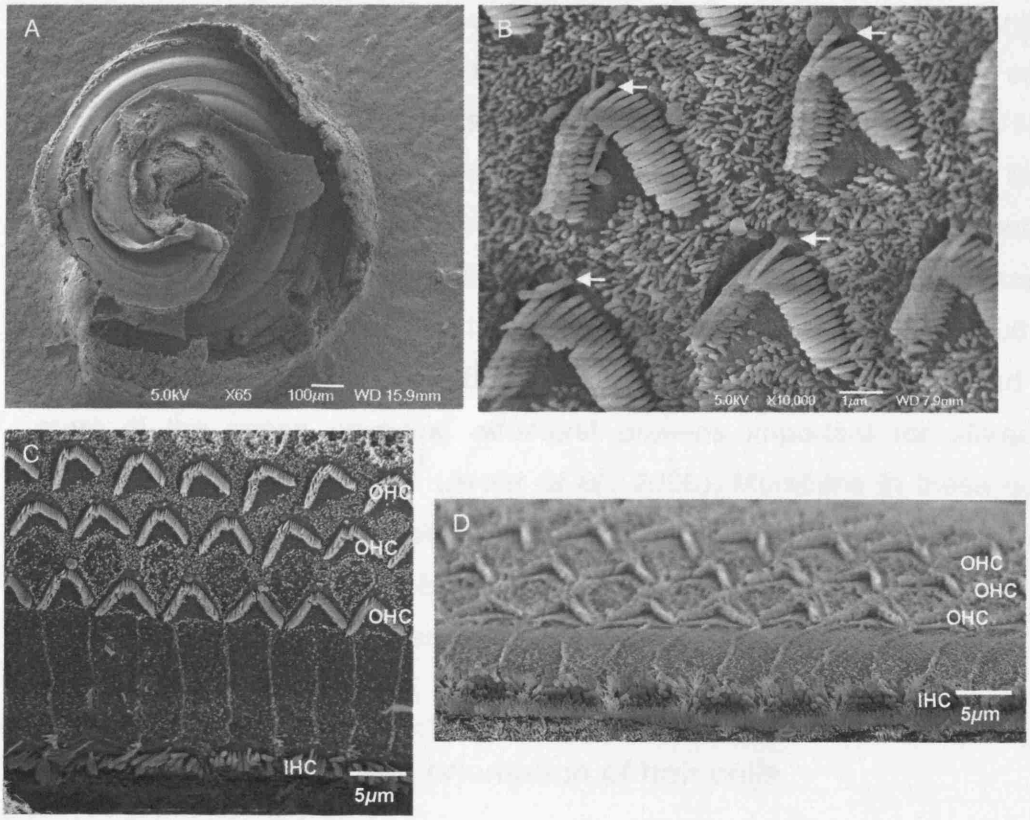

Figure 7.2: Scanning electron microscopy (SEM) images of mammalian auditory sensory cells. Images were obtained from a post natal day 10 (P10) wild type mouse. A) A low power magnification of the whole organ of Corti dissected down to the sensory epithelium. B) Magnification of an almost mature hair bundle that consists of three rows of individual stereocilia and a true cilium, the kinocilium (white arrow), which is always positioned at the lateral vertex of the bundle. C, D The three rows of outer hair cells with uniformly orientated stereocilia. The vortexes with a single kinocilium of the 'v/w' shaped stereocilia point to the lateral side. The stereocilia on the inner hair cells are less tightly packed. Images were taken by Prof. A. Forge, UCL Ear Institute, UK.

Although stereocilia are not true cilia, their arrangement is under the control of a true tubulin based cilium, the kinocilium, which moves across the hair cell during its development and lies behind the row of the tallest stereocilia. In mammals the kinocilium disappears soon after birth, whilst in reptiles it is maintained throughout life (Frolenkov *et al.*, 2004).

Hair cell transduction and auditory perception are dependent on the uniform orientation of the stereociliary bundles and disruption to these can cause hearing and/or balance defects such as in Usher Syndrome (Self *et al.*, 1998; Alagramam *et al.*, 2001; Di Palma *et al.*, 2001; Johnson *et al.*, 2003). Usher syndrome, an autosomal recessive condition involving sensorineural hearing impairment and progressive retinal dystrophy, is the most common cause of deaf-blindness in humans and is estimated to affect 3-6.2 per 100,000 live births (Cohen *et al.*, 2007). So far eight of the 11 loci have been cloned with most of the genes encoding structural proteins important for stereocilia structure and maintenance (Kremer *et al.*, 2006). Mutations in these genes cause disorganised stereociliary bundles. This led us to consider whether defects in the stereociliary bundles of *Bbs6*$^{-/-}$ mice could contribute to the observed auditory deficiencies.

7.1.3 The kinocilium and orientation of hair cells.

A single tubulin-based primary cilium known as the kinocilium, is thought to be important for hair cell stereociliary bundle development during cochlear maturation (Denman-Johnson and Forge, 1999; Frolenkov *et al.*, 2004) (Fig 7.2 B). Although in mammalian auditory hair cells, the kinocilium degenerates after bundle formation (at ~8 days post-natal), the residual basal body may be required to maintain bundle orientation, structure and function. The unique organisation of stereocilia rows that is required for mechanotransduction, and their precise arrangement appears to be evolutionarily conserved (Wiederhold, 1976). Formation is dependent on the kinocilium, a true tubulin based primary cilium, which emerges on the apex of all hair cells roughly midway through gestation. It migrates to the apical edge of the cell from

where subsequently the stereocilia elongate to form their staircase-like bundle (Frolenkov *et al.*, 2004). This migration of the kinocilium is thought to determine the eventual orientation of the bundle. This morphological polarity defines a functional polarity, as deflections of the stereocilia along the line of polarity optimally stimulate the hair cell (as described above).

Polarity of hair-bundles on different hair cells with respect to each other is not random. They show a distinct 'orientation' related to that of their immediate neighbours and their position in the sensory patch (Fig 7.2 C,D). The signalling processes that control hair bundle orientation are thought to be similar to those that control planar cell polarity (PCP), which are simultaneously controlling the morphological patterning of the organ of Corti (Dabdoub *et al.*, 2003; Kelly and Chen, 2007).

In mouse, the auditory hair cells are not discernable until mid gestation at around E13. As they arise from surrounding support cells they differentiate and reorient to their final arrangement. The correct coordination of these reorientation events is essential for hearing. Orientation defects can be caused by genes that affect planar cell polarity (PCP). Mice with defects in PCP genes have shortened cochlea ducts and misoriented stereociliary bundles, causing hearing defects (Wang *et al.*, 2005). These include mice with mutations in *Vangl2*, *Scrib1* and *PTK7/CCk-4* (Montcouquiol *et al.*, 2003; Lu *et al.*, 2004) .

Planar cell polarity refers to the organisation of cellular structures within the plane of an epithelium such that the structures are all orientated the same way. It is a fundamental aspect of development in both vertebrates and invertebrates and has been extensively studied in Drosophila. Along with misorientated stereociliary bundles, mice with mutations in PCP genes have a whole range of symptoms arising from defects in convergent extension such as neural tube defects (Montcouquiol *et al.*, 2003; Wang *et al.*, 2005).

7.1.4 Expression analysis of Bbs6

Because the *Bbs6*$^{-/-}$ mouse exhibits an auditory phenotype, one would predict that the Bbs6 protein is involved in development and/or function of the wild type cochlea. For this reason we were interested in analysing the expression pattern of Bbs6 in the developing cochlea. Generation of the *Bbs6*$^{-/-}$ mouse incorporated a *β-galactosidase* reporter gene in the inserted trapping cassette. Thus *β-galactosidase* assays could be used to determine the expression pattern of the *Bbs6* transcript in animals carrying the trapping cassette. *β-galactosidase* should only be expressed in cells where the Bbs6 promoter is active.

Additionally, immunohistochemistry using an antibody against Bbs6 enables a more detailed analysis of expression of the *Bbs6* gene product in an *in vivo* model system. The antibody directly localises the protein whilst *β-galactosidase* assays visualise mRNA promoter activity. Previous analysis of protein expression has predominantly been on cultured cell lines, although these have enabled us to gain valuable insights into the role of the BBS6 protein, they have their limitations.

Cellular localization of BBS6 by fluorescence immunocytochemistry using an affinity-purified anti-BBS6 antibody in cultured cells shows that BBS6 appears to be a core centrosomal protein as it remains associated with centrosomes during the cell cycle (Kim *et al.*, 2005). In cells bearing primary cilia it is associated with the basal bodies, but excluded from the ciliary axoneme. More detailed expression analysis places cytosolic BBS6 within the pericentriolar material (PCM), a proteinaceous tube surrounding centrioles. During interphase BBS6 is confined to the lateral surfaces of the PCM, whilst during mitosis it relocalises throughout the PCM and is found at the intercellular bridge during cytokinesis (Kim *et al.*, 2005). Although centrosomes serve as nucleation and organising sites for cytoplasmic microtubules, centrosomal assembly of BBS6 appears to be independent of microtubules or the dynein motor, unlike BBS4 (see chapter 5 and 6) (Kim *et al.*, 2005). Whole-mount in situ analyses of developing (E10.5-E12) mouse

embryos with an RNA probe specific to the *Bbs6* transcript reveals staining in the heart, brain, retina, limb buds and developing neural tube (Kim *et al.*, 2005). Antibody staining on paraffin-embedded tissue sections of murine brain, kidney, retina olfactory epithelium and the ependymal layer of ventricles, reveals that Bbs6 is only detected in restricted regions of these tissues, namely in those areas that contain or border ciliated cells (Kim *et al.*, 2005). This expression pattern is similar to that observed for Bbs4 and Bbs8 and reflects the known organs affected in BBS patients (Ansley *et al.*, 2003; Kim *et al.*, 2004).

The affinity purified anti-BBS6 antibody used in the above mentioned localization studies was available to us for immunohistochemistry. This antibody was used to localise the Bbs6 protein in developing cochlea in order to further elucidate the role of the Bbs6 protein in the auditory system.

7.1.5 Auditory deficiencies in BBS patients.

Although deafness is not a primary feature of the human BBS phenotype, it has been reported that ~3% of patients have sensorineural deafness (Burn, 1950; Beales *et al.*, 1999). Recent clinical findings have also implicated an auditory defect as a further component of the disease. Audiometric assessments in 19 BBS patients at 1kHz and 4 kHz showed that 53% and 84% of subjects respectively, had a threshold that was >2 S.D. above the expected value for their age, indicative of a subclinical hearing loss (Ross *et al.*, 2005). Currently a study is underway to further examine auditory function in a cohort of British BBS patients. Furthermore a non-syndromic deafness locus (*DFN* B48) has been mapped to region containing *BBS4* as a candidate gene (Ahmad *et al.*, 2005). If this is the case it provides further evidence for a link between BBS and deafness.

These findings implicate BBS proteins in the normal development and functioning of the auditory system. As such they require more detailed analysis in the cochlea model system. As the *Bbs6*$^{-/-}$ mouse was shown to

have aberrant auditory function, we began by investigating this more closely. We examined the organ of Corti, the potential origin of hearing deficit in these animals, in more detail. Subsequently we sought the expression pattern of the Bbs6 protein in wild type cochlea both in adult mice and during development.

7.2 Materials and Methods

7.2.1 Further analysis of hearing deficit in *Bbs6* mutant animals.

For a more detailed analysis for the development of the auditory phenotype amongst the *Bbs6*$^{-/-}$ mice, a cohort of 19 *Bbs6*$^{+/-}$ and 12 *Bbs6*$^{-/-}$ animals from four different litters were assessed for auditory function by judging their Preyer reflex response to a 20 kHz tone burst using a standardised click box (MRC) at onset of hearing, three and six months. The investigator was blind to the genotype of the animal tested. For more details refer to section 2.2.8.6.

7.2.2 Analysis of the organ of Corti in Bbs6 mutant animals.

Whole-mount preparations from wild-type and *Bbs6*$^{-/-}$ organ of Corti were prepared and stained with phalloidin to visualise the stereociliary bundles as described in section 2.2.9. Confocal immunofluoresence with an antibody against acetylated tubulin and double staining with phalloidin was carried out on E18.5 embryos to localise the kinocilium. Scanning electron microscopy on whole-mount preparations was carried out by Prof. Andy Forge at the Center for Auditory Research, UCL Ear Institute, UCL, London.

7.2.3 Analysis of Bbs6 expression in the developing cochlea.

Expression of *Bbs6* in a P0 and adult (older than eight weeks) cochlea was examined, as indicated by the *β-galactosidase* reporter gene on sectioned cochleas. X-gal assays were carried out on *Bbs6*-/+ cochlea, animals as described in section 2.2.8.5, prior to sectioning. Protein expression of Bbs6 in the developing murine cochlea was visualised by confocal immunofluoresence on whole mount preparations and frozen cryosections using an antibody against the Bbs6 protein. Imaging was carried out using a Zeiss LSM500 confocal scanning microscope. Detailed methods are described in section 2.2.9. BBS6 antibody was generated by M. Leroux and had been previously published (Kim *et al.*, 2005). Further antibody information can be found in the appendix.

7.3 Results

7.3.1 *Bbs6*$^{-/-}$ mice show progressive hearing loss.

A cohort of *Bbs6*$^{-/-}$ mice and *Bbs6*$^{+/-}$ mice were assessed for their response to a 20 kHz tone burst using a standardised click box at onset of hearing (P14), three and six months. In total 12 *Bbs6*$^{-/-}$ and 19 *Bbs6*$^{+/-}$ mice from four different litters were tested. The animals' response was scored by judging their Preyer's reflex, a natural response in which the mouse flicks its ears flat against its head in response to a tone burst. A score of 1.0 was awarded if the mouse responded well by flicking its ears flat against its head. A score of 0.0 was awarded for no response and a score of 0.5 for a minimal response. Regarding the other phenotypes *Bbs6*$^{+/-}$ mice showed no indication of partial disease manifestation and so for this study we made the assumption that heterozygote animals were not affected and could be substituted for wild type litter mates.

At onset of hearing all animals scored 1.0, however at three months almost half (41.6%) of *Bbs6*$^{-/-}$ animals had no response, compared to just 5.26% of *Bbs6*$^{+/-}$ animals. Degeneration of hearing was clearly progressive as at six months only 25% of *Bbs6*$^{-/-}$ animals scored 1.0 whilst 57.89% of the *Bbs6*$^{+/-}$ mice displayed a Preyer's reflex response (Table 7.1).

A) Bbs6 +/-	Onset of hearing	3 months	6 months
Score 1.0	100% (19/19)	78.94% (15/19)	57.89% (11/19)
Score 0.5	0%	16% (3/19)	26.31% (5/19)
Score 0.0	0%	5.26% (1/19)	15.79% (3/19)

B) Bbs6 -/-	Onset of hearing	3 months	6 months
Score 1.0	100% (12/12)	58.3% (7/12)	25% (3/12)
Score 0.5	0%	0%	8.3% (1/12)
Score 0.0	0%	41.6% (5/12)	66.6% (8/12)

Table 7.1: Summary of results for progressive hearing study. *Bbs6*$^{+/-}$ and *Bbs6*$^{-/-}$ Animals from four different litters were tested at onset of hearing, three and six months for their response to a 20 kHz tone burst. A full Preyer's reflex response was awarded with the score 1.0, no response with 0.0 and a mild response 0.5.

These results suggest a progressive degeneration of auditory function in the *Bbs6*$^{-/-}$ animals at a higher rate than the control group. Interestingly at the onset of birth auditory function appears normal. Previous analysis of distortion product otoacoustic emissions (DPOAEs; sound responses generated when the cochlea is stimulated (see chapter 6 for more detail) of *Bbs6*$^{-/-}$ animals had isolated the sensory hair cells on the organ of Corti as one of the origins of the auditory dysfunction, for this reason these cells were analysed more closely.

7.3.2 Stereociliary bundle abnormalities are observed in the cochlear outer hair cells of *Bbs6*$^{-/-}$ mice.

Phalloidin staining of stereociliary bundles on P2 sensory hair cells, showed bundle abnormalities in the organ of Corti of *Bbs6*$^{-/-}$ mice (Fig. 7.3). In the knockout animals abnormally shaped and/or flattened bundles were observed. Outer hair cells appeared to be more affected than inner hair cells.

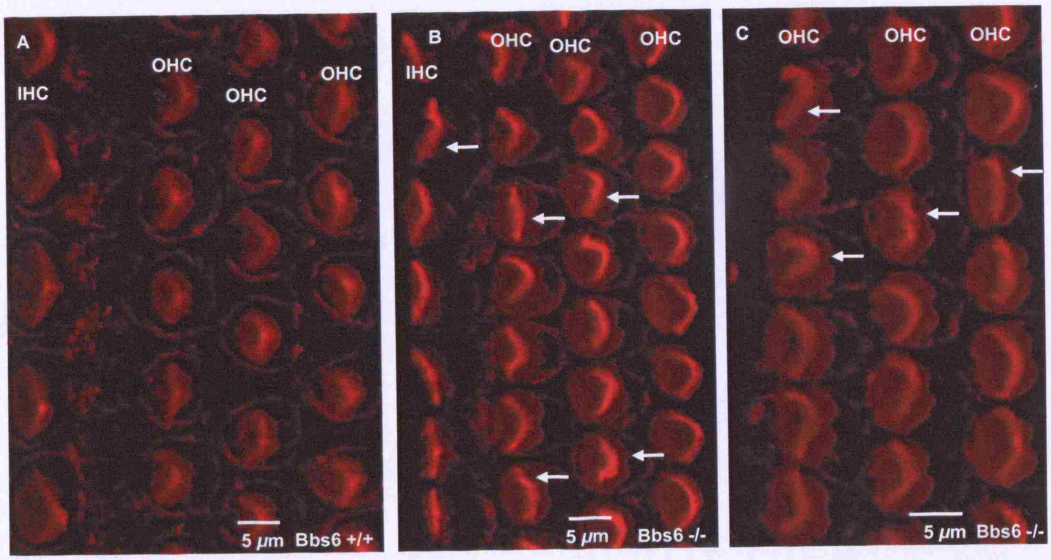

Figure 7.3: Phalloidin staining on organ of Corti of P2 *Bbs6*$^{+/+}$ and *Bbs6*$^{-/-}$ mice. Abnormally shaped or flattened stereociliary bundles (white arrows) can be observed in the mutant animals (B and C) as opposed to the more uniform bundle arrangements in the wild-type animal (A).

To examine the abnormally shaped stereociliary bundles in more detail, scanning electron microscopy (SEM) was performed on adult cochlea dissected from *Bbs6*$^{-/-}$ and wild-type mice. Images were taken by Prof. Andy Forge at the Center for Auditory Research, UCL Ear Institute, UCL, London. This gave a more detailed view of the morphology of the stereociliary bundles and confirmed that in the *Bbs6*$^{-/-}$ animals several were misoriented and/or abnormal in shape.

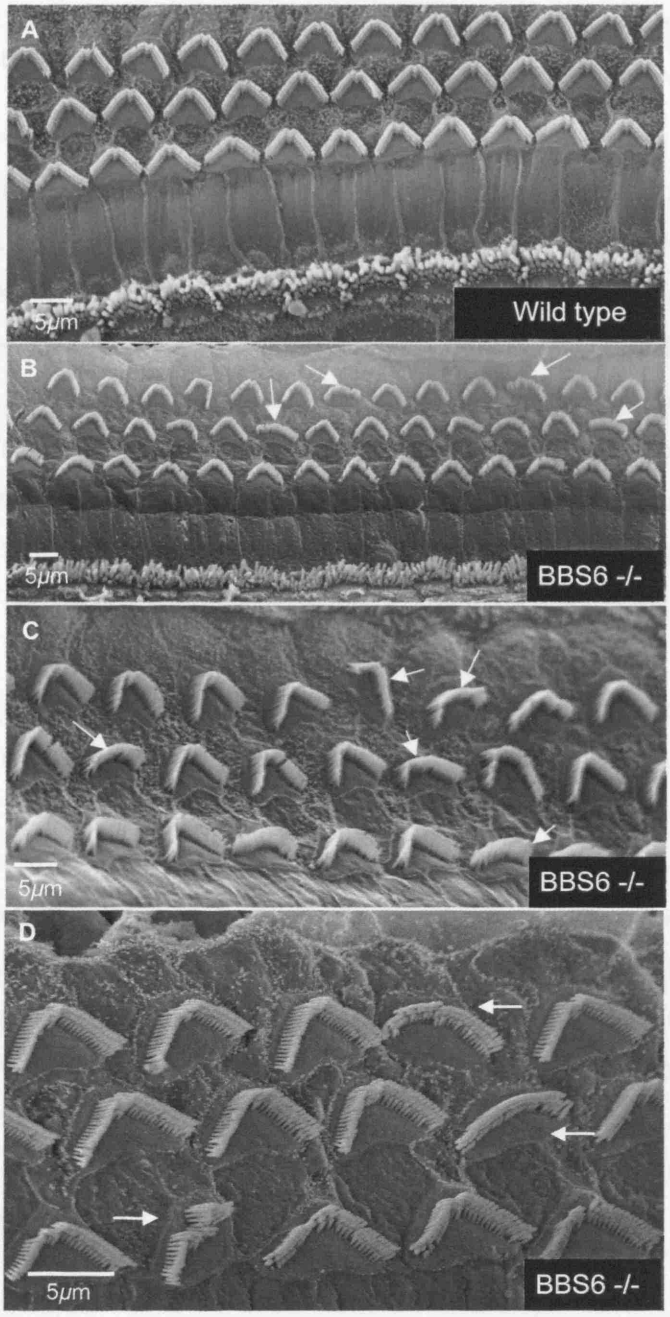

Figure 7.4: Scanning electron microscopy of organ of Corti of adult *Bbs6*$^{+/+}$ mice. (A) and *Bbs6*$^{-/-}$ (B,C,D) mice confirms stereociliary defects as seen with phalloidin staining in the younger animals. The abnormally shaped and flattened bundles are clearer to see than with the phalloidin staining. In the *Bbs6*$^{-/-}$ animals, several are misoriented and/or abnormal in shape (indicated by arrows). Images were produced by Andy Forge, UCL, Institute of Hearing Research.

7.3.3 Abnormal stereociliary bundles still have a kinocilium, but its association is perturbed.

To assess whether the abnormal stereociliary bundles in the *Bbs6*$^{-/-}$ mice are still associated with kinocilia, organ of Corti were double stained with phalloidin and an anti-acetylated-α tubulin antibody. Anti-acetylated-α tubulin labels microtubules and is commonly used for visualising primary cilia. This staining showed that even in hair cells with misshapen bundles, *Bbs6*$^{-/-}$ mice (E18.5) still have kinocilia (Fig 7.5 A). However more detailed analysis using SEM reveals a dissociation of the kinocilium from mis-shapen bundles (Fig 7.5 B). Normal bundles, such as the one on the right, are situated tightly adjacent to their kinocilium. In comparison the abnormally flattened bundles, like the one on the left, are seen distinctly separated from their kinocilium.

This abnormal placement may be caused by a lack of adhesion between the kinocilium and the tallest row of stereocilia, demonstrated by the disassociation of bundles from their basal body. The kinocilium, normally at the vertex of the bundle, is anchored in the cell by its basal body. Double staining with phalloidin and an antibody against γ-tubulin, a basal body marker in slightly older animals (P9 as opposed E18.5), reveals that stereociliary bundles of some *Bbs6*$^{-/-}$ hair cells are misorientated relative to their basal body (Fig 7.5 C). The basal bodies in affected cells retain their position in the cell relative to those in other cells, suggesting kinocilia migration is normal in all cells and that the kinocilium of these bundles has physically detached from the lateral vertex of the bundles, resulting in misplacement.

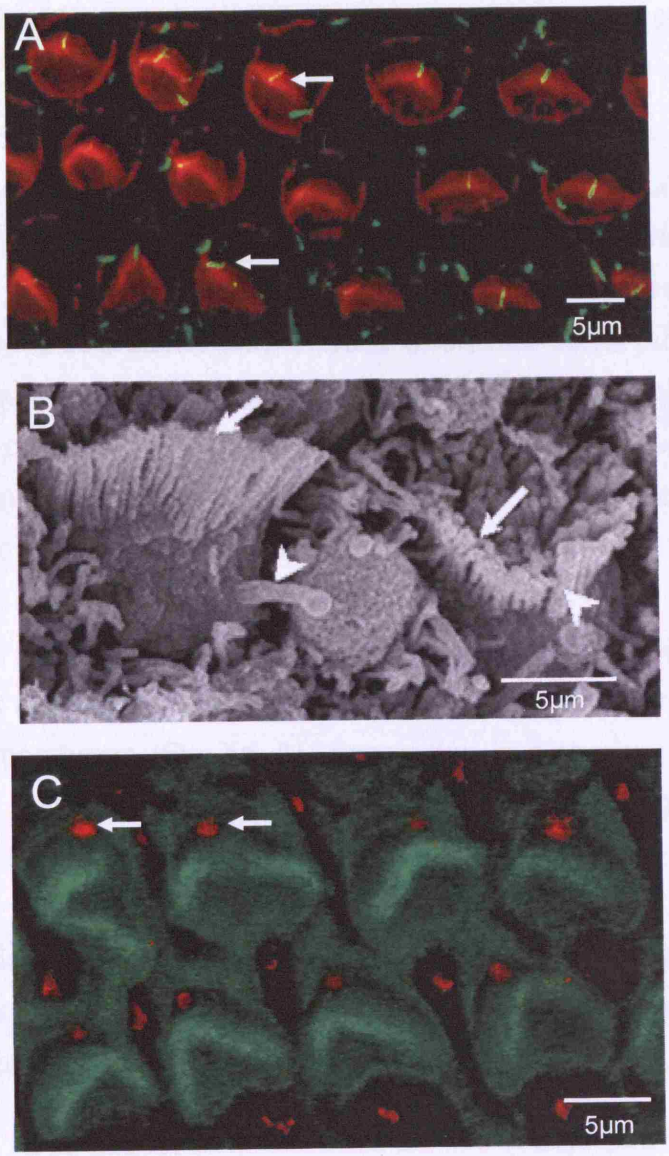

Figure: 7.5 Cochlear stereociliary bundle examination in *Bbs6*$^{-/-}$ mice. A) Double labelling with phalloidin (red) and acetylated tubulin (green) of E18.5 animals shows that even OHCs with mis-shapen bundles have a kinocilium (white arrows). B) SEM examination of E18.5 cochlear reveals a physical separation of the kinocilium (arrow head) from mis-shapen bundles (white arrows). C) In P9 *Bbs6*$^{-/-}$ OHCs double staining with phalloidin (green) and an antibody against γ-tubulin (red) reveals that stereociliary bundles of some *Bbs6*$^{-/-}$ hair cells are misorientated relative to the basal body (white arrows).

7.3.4 X-gal assays reveal differential expression pattern of *Bbs6* in the adult compared to the developing organ of Corti.

Expression of *Bbs6* in the adult cochlea, as indicated by the *β-galactosidase* reporter gene was examined on sectioned cochleas. *Bbs6* mRNA is detected via X-gal staining in $Bbs6^{+/-}$ cochlea. As the inserted trapping cassette contains a *β-galactosidase* reporter gene, it would be expected that *β-galactosidase* is expressed only in cells where the *Bbs6* promoter is active and so the normal expression pattern of the *Bbs6* transcript can be examined in animals carrying the trapping cassette. *β-galactosidase* assays were performed on cochlea from heterozygous animals, no *β-galactosidase* activity was detected in wild-type animals.

In the adult, light microscopy reveals strong *Bbs6* expression in the spiral ganglion, as well as at the bottom of the inner and outer hair cells and in the Reissner's membrane (Fig 7.6 A). Expression is also seen in the cochlear nerve fibres and the interdental cells of the spiral limbus (bone), and outer sulcus.

In P0 animals, *Bbs6* mRNA expression is more extensive (Fig 7.6 B). Not only is it notable in hair cells but also supporting cells, Köllikers organ, spiral ganglion neurons and the stria vascularis.

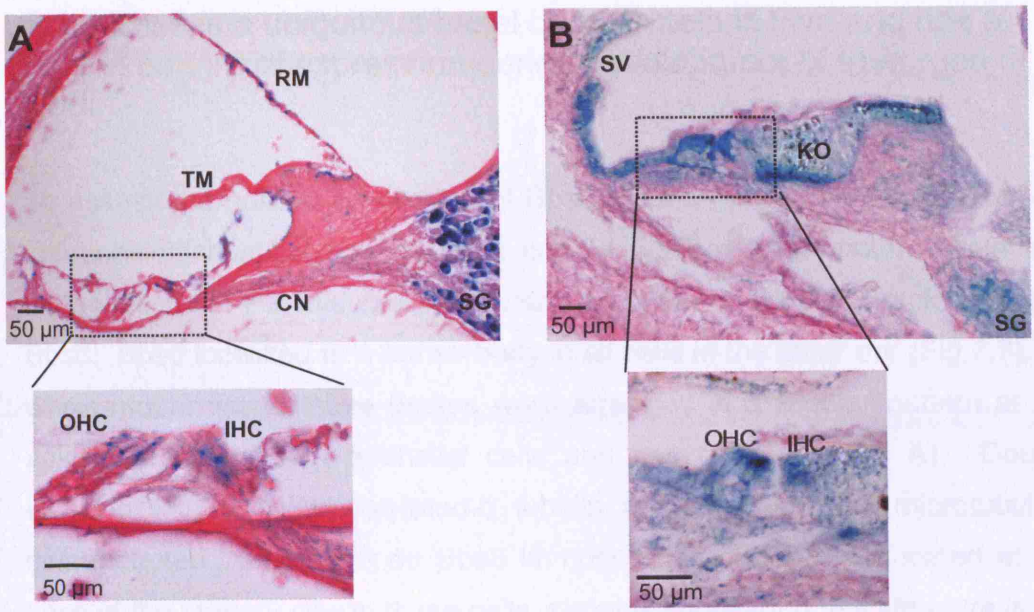

Figure 7.6: Staining for *β-galactosidase* activity in *Bbs6*$^{+/-}$ cochlea counterstained with eosin. A) Light microscopy of a cochlear cross-section from an adult mouse shows expression predominantly in the spiral ganglion, as well as at the bottom of the inner and outer hair cell and in Reissner's membrane. B) Staining in the younger animal (P0) shows strong *Bbs6* expression in the inner and outer hair cells, spiral ganglion, stria vascularis and Köllikers organ. SG, spiral ganglion; IHC, inner hair cell; OHC, outer hair cell; TM, tectorial membrane; CN, cochlear nerve fibres; RM, Reisner's membrane, SV, stria vascularis.

7.3.5 Bbs6 is a ubiquitous basal body protein in vivo and has a unique pattern of expression during development of the organ of Corti.

To assess the normal distribution of Bbs6 protein in the developing cochlea, immunohistochemical analysis was carried out on whole-mount tissue and cryo-sections in P2 wildtype mice, using a primary antibody directed against Bbs6. Bbs6 localized to a dense body in all cells in the inner ear (Fig 7.7). In whole-mount tissue these bodies were arranged in a regular pattern at the apical/lumenal pole of epithelial cells and hair cells (Fig 7.7 A). Double labelling with an anti-acetylated-α tubulin antibody (labelling microtubules) demonstrated that the dense Bbs6 immunofluorescence was located at the base of the primary cilia in these cells, strongly suggesting this structure is the basal body. Cryo-sections confirmed the close association of Bbs6 with the kinocilia of hair cells (Fig 7.7 B), and also primary cilia of supporting cells (Kölliker's cells Fig 7.7 C,D). Kölliker's cells are columnar cells medial to inner hair cells found only in the developing cochlea. Bbs6 labelling was observed at the proposed basal body, and the anti-acetylated-α tubulin antibody also revealed apico-basal cytoplasmic microtubules emanating from the basal body (Figure 7.7 C). On closer inspection, expression of Bbs6 was also observed in discrete microtubule-rich regions at the base of inner and outer hair cells, corresponding to developing innervation (Fig 7.7B).

To confirm Bbs6 as a basal body protein in the developing cochlea, an anti-γ-tubulin antibody (a marker of peri-centriolar material) was co-localized with Bbs6 in P2 wildtype mice. Kölliker's cells labelled with anti-acetylated-α tubulin and Bbs6 (Fig 7.8 A) gave an almost identical expression pattern to Kölliker's cells labelled with anti-acetylated-α tubulin and anti-γ-tubulin (Fig 7.8 B). Co-localisation of Bbs6 with anti-γ-tubulin confirmed Bbs6 as a basal body protein in all cell types studied (Fig 7.8 C,D).

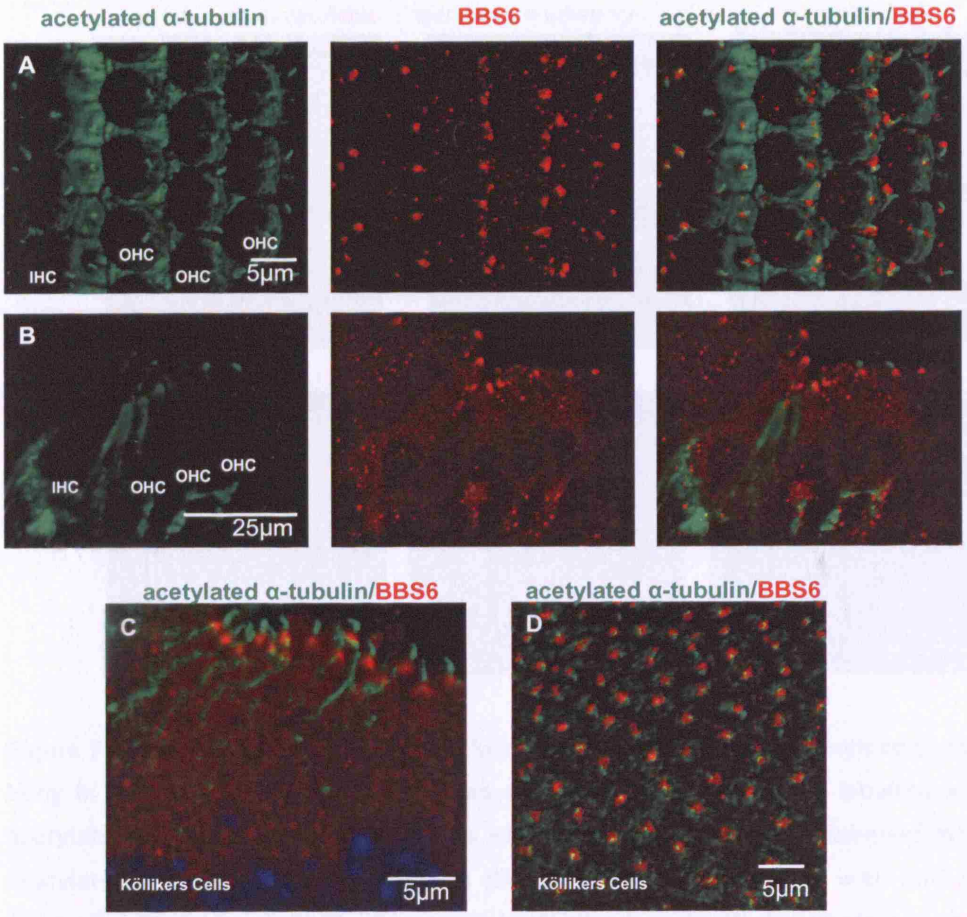

Figure 7.7: Bbs6 localises to a dense body at the base of primary cilia. P2 wildtype mice immunolocalised with Bbs6 (red) and anti-acetylated-α tubulin (green). A) Whole mount view of the surface of the organ of Corti showing one row of inner hair cells (IHC) and three rows of outer hair cells (OHC). Bbs6 localises to a dense body at the base of each primary cilium (on hair cells and supporting cells). This is confirmed on cross-section analysis B), where Bbs6 is also seen in discrete microtubule-rich regions at the base of inner and outer hair cell. C,D) Cross section and whole mount staining of Köllikers cells, developmental support cells with prominent primary cilia.

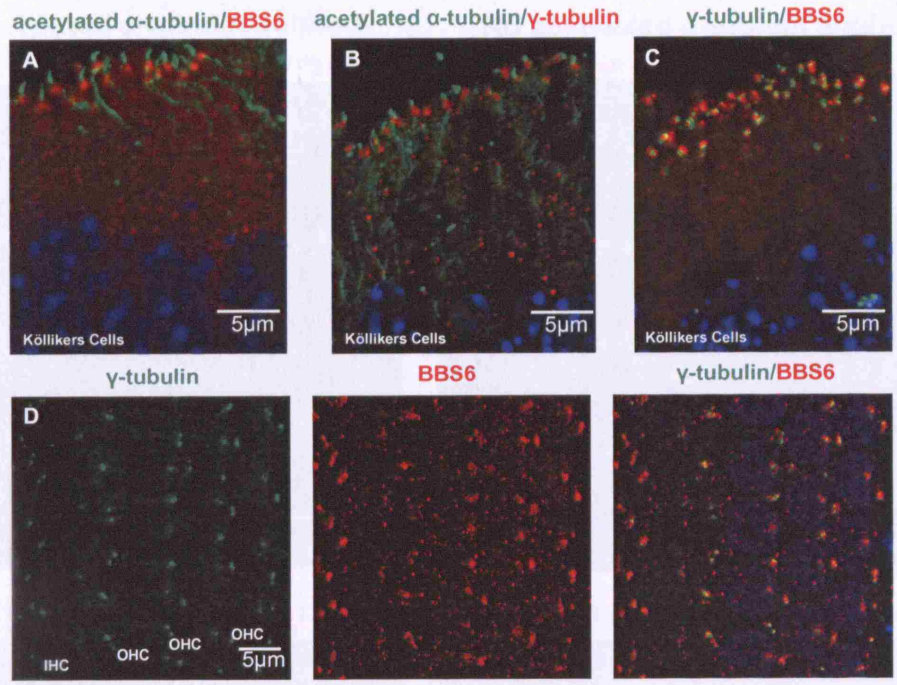

Figure 7.8: Bbs6 is a ubiquitous basal body protein in vivo. Bbs6 localises to the basal body in P2 wildtype mice. A,B,C: Cross sections of Kölliker's cells labelled with anti-acetylated-α tubulin and Bbs6 (A) is similar to Kölliker's cells labelled with anti-acetylated-α tubulin and anti-γ-tubulin (B). Co-localisation of Bbs6 with anti-γ-tubulin confirmed Bbs6 as a basal body protein in Kölliker's cells (C). D) Whole mount view of the surface of the organ of Corti showing one row of inner hair cells (IHC) and three rows of outer hair cells (OHC). Co-localisation of Bbs6 and anti-γ-tubulin confirmed Bbs6 as a basal body protein in all cell types.

To ensure specificity of the BBS6 antibody and no cross talk from the secondary antibody, a series of 'no primary' control immunohistochemical analyses were performed. Test conditions were performed simultaneously and image settings were unchanged between imaging. Omission of the primary antibody for BBS6 resulted in no detectable fluorescence (Fig 7.9).

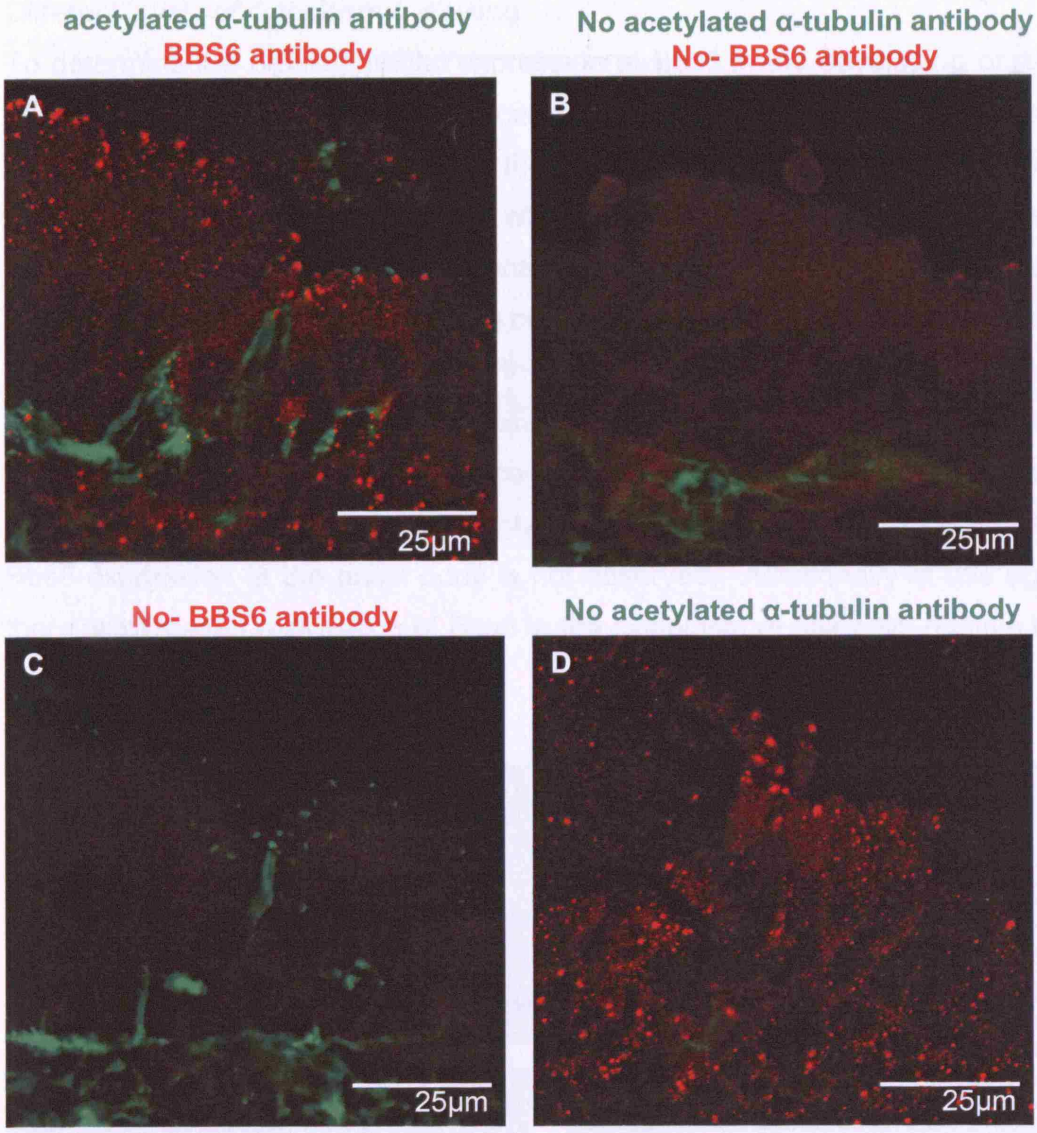

Figure 7.9: Bbs6 immunohistochemistry analysis is 'specific'. Cross section of P2 wildtype cochlea simultaneously processed with A) primary antibody for Bbs6 (red) and anti-acetylated-α tubulin (green), B) Neither primary antibody, C) Omission of primary antibody for Bbs6 and D) omission of primary antibody for acetylated-α tubulin. Omission of the Bbs6 antibody leads to no detectable Bbs6 fluoresence.

Different levels of cytoplasmic labeling.

To determine the developmental expression of Bbs6 in the developing organ of Corti, cryo-sections were taken from wild-type mice at E13.5 to P9. Bbs6 can be detected in the basal body at the apical pole of cells in the otic capsule at E13.5 (Fig: 7.10 A). At E17.5, by which time differentiated inner and outer hair cells can be identified, Bbs6 localises to basal bodies of both hair cell types and their respective supporting cells (Fig: 7.10 B). A comparable pattern of expression is maintained through the first postnatal week (Fig: 7.10 C). As development progresses Bbs6 expression at the basal body in the outer hair cells diminishes. In the outer hair cells at P9, Bbs6 just weakly stains the basal body (Fig: 7.10 D). Interestingly in the inner hair cells this decline in Bbs6 expression at the basal body is not observed. Additionally at this age there is increased expression of Bbs6 in the cytoplasm of hair cells relative to supporting cells.

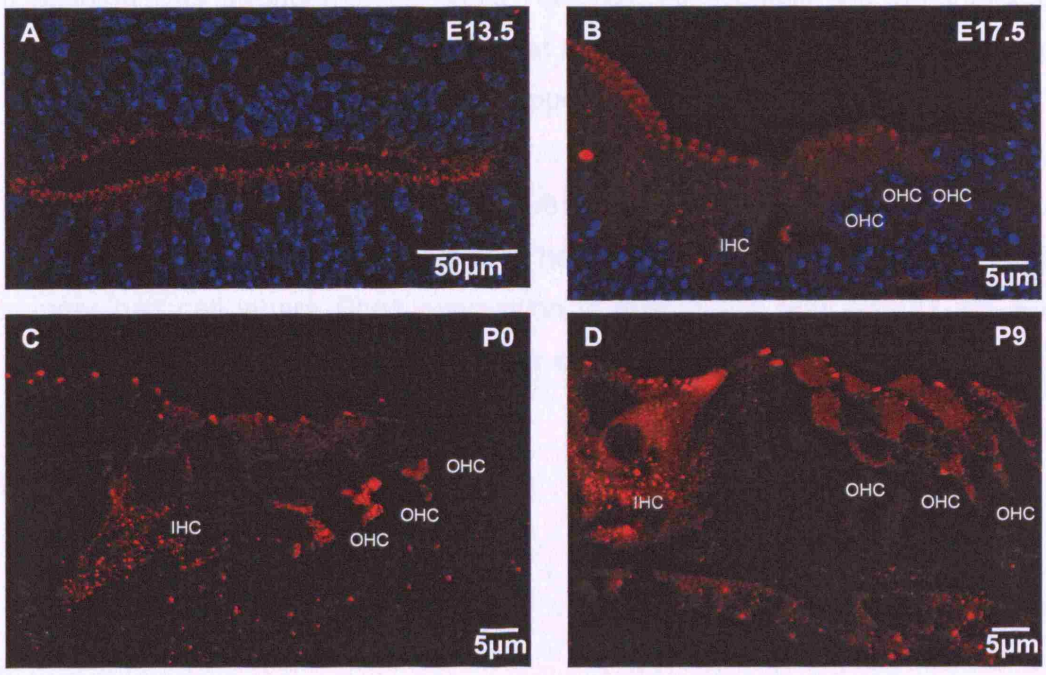

Figure 7.10: Expression pattern of Bbs6 in the developing organ of Corti. Cross-section immunostaining of developing organ of Corti with an antibody against Bbs6. A) At E13.5 Bbs6 (red) can be detected at the apices of cells in the early otocyst. Nuclei are labelled with DAPI. B) By E17.5 Bbs6 is localised more specifically to basal bodies of hair cells and supporting cell. C) This expression pattern is maintained during the first

week of life, with an increase in cytoplasmic labelling of Bbs6 in the hair cells. D) By P9 basal body expression in the outer hair cells is diminished, whilst cytoplasmic expression of the hair cells relative to the support cells is increased.

Bbs6 expression in the adult organ of Corti.

The expression pattern of Bbs6 in the cochlea as indicated by the *β-galactosidase* assays revealed a difference between adult and developing tissue (See Fig 7.6). Therefore one would expect such a result to be reflected in immunolocalisation of the Bbs6 antibody on adult tissue. At the onset of hearing at P12 (Fig 7.11 A) Bbs6 expression was similar to P9 (compare with Fig 7.10 D). Basal body expression in the outer hair cells continued to diminish but there was increased strong cytoplasmic expression in inner and outer hair cells relative to the support cells. In adult, anti-Bbs6 continued to label both inner and outer hair cell cytoplasm (Fig 7.11 B,C). This cytoplasmic staining was stronger in the inner hair cell. Additionally the inner hair cell continued to retain an accumulation at the basal body, in contrast to the outer hair cells where such accumulation appears to be completely lost.

Co-localisation with anti-γ-tubulin revealed a marked difference of γ-tubulin expression between the two types of hair cells, with more accumulation in the inner hair cell where Bbs6 expression is maintained (Fig 7.11 D, E). Even though Bbs6 is lost from the outer hair cell, its basal body structure remains.

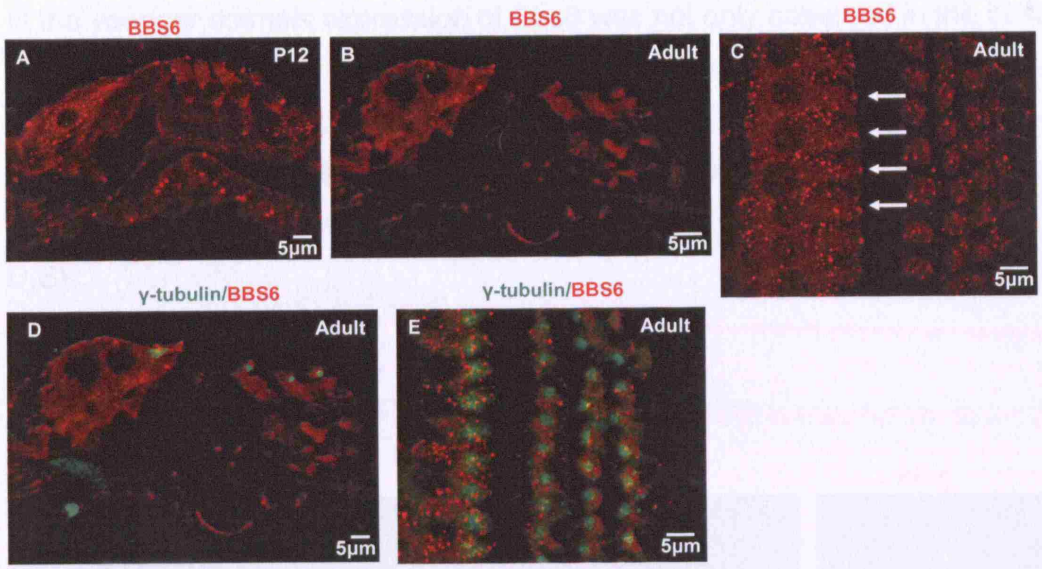

Figure 7.11: Bbs6 expression in the adult organ of Corti. Cross sections and wholemounts of adult organ of Corti labelled with anti-Bbs6 (red) and anti-γ-tubulin (green). A) At onset of hearing cytoplasmic labelling of hair cells is at its strongest. B,C) Adult labelling of Bbs6 reveals dense cytoplasmic expression in the inner hair cell with accumulation at the basal body (white arrows) whilst cytoplasmic expression in the outer hair cells is diminished and no basal body accumulation is detected. D,E) Anti-γ-tubulin labelling reveals differences in size between the basal body structure in inner hair cells compared to outer hair cells.

Neuronal staining:

The comparatively strong staining of the spiral ganglion in the adult X-gal assays (see Fig 7.6) gave rise to the possibility of BBS6 being involved in neuronal processes. Immunostaining using an antibody against Bbs6 shows high levels of Bbs6 expression throughout the spiral ganglion on a low power magnification of P9 cross section through the cochlea (Fig 7.12 A,B). Higher magnification of this staining localizes Bbs6 predominantly to the cytoplasm of the ganglion cells, excluding the nucleus (Fig 7.12 C).

In the younger animals expression of Bbs6 was not only observed in the basal body region of the hair cells, but also in discrete microtubule-rich regions at the base of inner and outer hair cells, corresponding to developing innervation (see Fig 7.7). Localisation of Bbs6 to neuronal structures was confirmed by double labelling with an anti-neurofilament antibody (anti-NF200) (Fig 7.12 D,E).

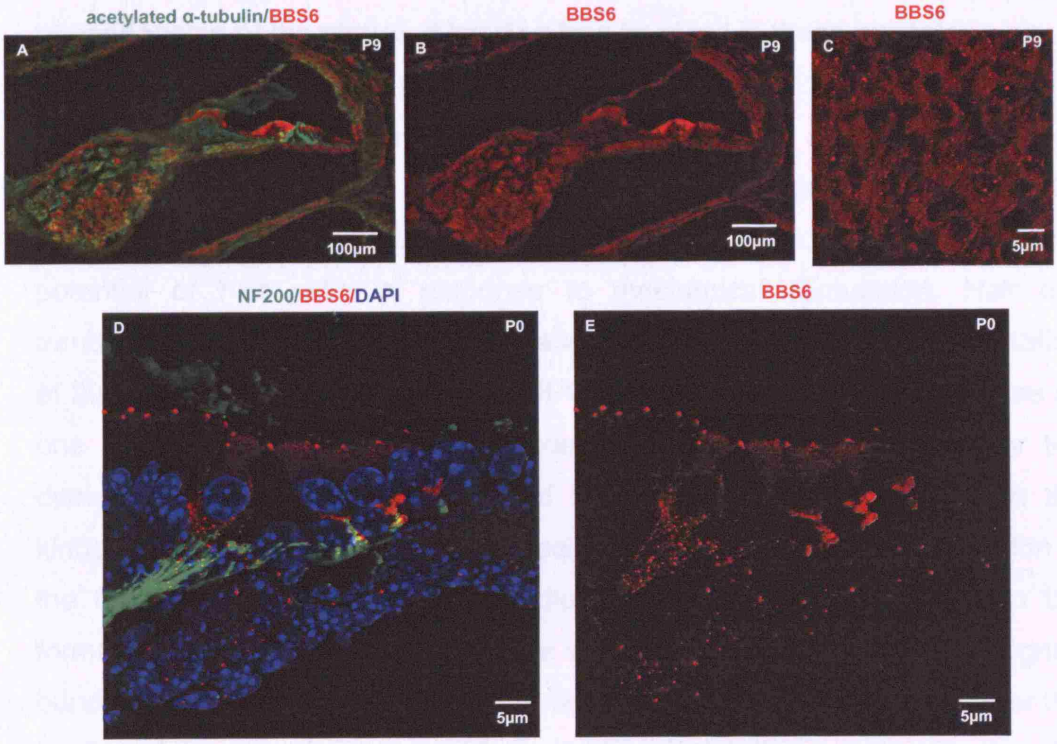

Figure 7.12: Neuronal expression of Bbs6. Cochlear cross sections labelled with anti-Bbs6 (red) and anti-neurofilament (anti-NF200) (green). A,B) Low power magnification reveals strong expression of Bbs6 in the spiral ganglion. C) Higher power magnification localises this staining to the cytoplasm. D) Co-localisation of Bbs6 with anti-neurofilament.

7.4 Discussion

Mouse hearing deficit

Whilst fifty percent of the adult population of *Bbs6*$^{-/-}$ mice have auditory deficits as tested by their lack of a startle response to a 20 kHz tone burst and DPOAEs, the animals' auditory function appears normal at onset of hearing. This implies that hearing loss is progressive and that the Bbs6 protein is principally involved in the maintenance of hearing function rather than its establishment. Ideally auditory brain stem responses are needed for a better understanding of the nature of hearing loss involved in these animals.

Upon closer examination we observed malformed and/or mis-oriented sterociliary bundles on the apices of hair cells on the organ of Corti in *Bbs6*$^{-/-}$ mice. Stereociliary bundles are responsible for modulating the receptor potential of hair cells in response to mechanical stimulation. Hair cell transduction and auditory perception are dependent on the uniform orientation of the stereociliary bundles. Absent DPOAEs had already implicated these as one of the sources of the hearing deficit in these mice. A cause for the disrupted stereociliary bundles could be a lack of adhesion between the kinocilium and the tallest row of stereocilia, as we see a physical separation of the kinocilium from misshapen bundles. The kinocilium is involved in the formation of the bundles. Furthermore we see a disassociation of misaligned bundles from their basal body. As the development of the bundles is under the control of the kinocilium (a modified primary cilium), it is perceivable that the cause of the misshapen bundles is due to a defect of kiniocilial function. Particularly in light of the fact that BBS is classified as a ciliopathy and the BBS proteins identified so far have all been implicated in basal body or cilia function.

Observational analysis alone is not sufficient to verify the bundle defects as a cause of the auditory deficit, as not all hair cell bundles are affected and there appears to be a large variation in degree of malformation/misorientation.

Further investigation to assess the function of the stereocilary bundles in the *Bbs6*$^{-/-}$ mutant animals is needed.

The stereocilia in each hair bundle are connected together by a filamentous process, the tip link, which passes obliquely between the distal end of one stereocilium and the side of the longest adjacent one. Tip links are thought to connect directly to transduction channels, so that deflections of a hair bundle opens these channels. FM1-43, is a styryl dye and is thought to load into hair cells via these transduction channels (Gale *et al.*, 2001). A simple test to see whether these transduction channels are working in our mutant animals would be to load the dye for a short period of time and see if it enters the hair cell.

Not only do we see flattened and misshapen bundles, but we also see a degree of misrotation of some of the bundles in *Bbs6*$^{-/-}$ mice. This phenotype is reminiscent of mice with mutations in the evolutionary conserved planar cell polarity (PCP) pathway. PCP drives cellular processes such as epithelial cell polarization, cell migration and mitotic spindle orientation (Klein and Mlodzik, 2005). Mutations of the PCP signalling pathway in mice cause a variety of phenotypes including severe neural tube closure defects, extension of the organ of Corti and misorientation of stereocila (Montcouquiol *et al.*, 2003; Dabdoub and Kelley, 2005; Wang *et al.*, 2005; Wang and Nathans, 2007). More recently, defects in the PCP pathway have also been linked to polycystic kidney disease (Fischer *et al.*, 2006). BBS proteins have been implicated in the PCP pathway due to phenotypic overlap between BBS and PCP mutants, including abnormalities of the arrangement of sensory hair cells of the cochlea and defects in neural tube closure (Ross *et al.*, 2005). Furthermore a genetic interaction between BBS genes and the PCP pathway has been demonstrated by the interaction between *Bbs6* and *Vangl2* (a known PCP gene), as double heterozygotes display bundle abnormalities comparable to knockouts, whilst single heterozygotes do not (Ross *et al.*, 2005).

Not all the hair cells in the organ of Corti are affected in *Bbs6*$^{-/-}$ mice. This is not as atypical as one would expect. Even among 'core' PCP mutants there is a large amount of variation between the severity of defects and subset of hair

cells affected (Wang and Nathans, 2007; Zallen, 2007). The genetic background also appears to play a role in the severity of the phenotype. There appears to be a definite progression in terms of PCP defects such that third row outer hair cells are almost always the most affected and to date, none of the reported PCP mutants have any defects in the first row outer hair cells. This could be seen as an anomaly as all the cells have the same gene mutation. An explanation could lie in terms of a developmental gradient across the organ of Corti, with the polarising signal being derived more closely to the inner hair cell or first row of outers. Rotation of the hair bundle could be triggered by stimulation of the PCP pathway. Vangl2, one of the proteins implicated at the beginning of the molecular PCP pathway, encodes a membrane protein comprising four transmembrane domains and a large intracellular domain with a PDZ-domain-binding motif at its carboxy terminus (Kibar *et al.*, 2001). This protein has been localised to the ciliary axoneme and basal bodies of ciliated cells (Ross *et al.*, 2005), so it is possible that it is also found within the membrane of the kinocilium. In this context it could be in part responsible for triggering downstream intracellular events that eventually lead to the rotation of the hair bundle.

The concept of planar cell polarity depending on a single genetic pathway is coming into question; it is possible that this idea could be replaced by two (at least) independently acting processes (Lawrence *et al.*, 2007). It is likely that whilst not directly a PCP gene, the BBS genes could be indirectly involved in the processes of regulating tissue polarity.

Furthermore the observed differences amongst this population of cells may reflect participation of additional and partially redundant family members. This brings into question the role of other genes compensating for Bbs6 in the knockout animals. In particular BBS10 and BBS12 have been shown to have partial sequence homology to BBS6 (see chapter 1 for more details).

Whilst trying to gain a better understanding of the role of Bbs6 in the inner ear, its important to note that the abnormal shape of the stereociliary bundles and their rotation are potentially two separate unrelated processes. In light of

this Bbs6 possibly has its affect much further down stream in both of these pathways. Furthermore, it is not clear whether the bundle defects alone are the cause of the auditory deficit, as not all hair cells are affected. This could explain the variation amongst the animal population as only 50% appear affected. The percentage of affected hair cells in an individual could correlate to its hearing ability with a certain threshold being required for auditory perception. More detailed auditory characterisation is required.

Expression of BBS6

Analysis of the expression pattern of Bbs6 in the inner ear gives us further indications as to a possible cause of the hearing defect. Cochlear expression of Bbs6 as indicated by the β-galactosidase reporter gene showed strong expression in the hair cells (as would be expected from the phenotype), but also strong expression in the spiral ganglion. Interestingly relative expression in the spiral ganglion is stronger in the adult which ties in with when we observe the measurable outcome, namely hearing loss.

To gain a more detailed view of the expression pattern, immunolocalisation of Bbs6 was performed. From this data we see that, as expected from previous cell line work, Bbs6 localises to the basal body. During development it associates with the basal body in all cell types studied, confirmed by co localisation with the known basal body marker γ-tubulin. In the adult, basal body expression is lost from all cell types except the inner hair cell. These data are consistent with the observed abnormalities in the bundles, as the basal body, being the anchor of a cells' primary cilium, is particularly important in the first few days of development. The kinocilium moves across the apex of the hair cell and initiates the formation of the bundle, but then retracts at about P8 (Frolenkov *et al.*, 2004). Importantly in *Bbs6*$^{-/-}$ mice misaligned bundles show dissociation from the basal body relative to surrounding hair cells.

Inconsistent with this is that the *Bbs6*$^{-/-}$ mice are phenotypically normal when it comes to auditory function at the onset of hearing at around P12. This implies that the lack of Bbs6 does not affect the mechanism of hearing at this point in development. Further to this, the cytoplasmic labelling of Bbs6 in hair cells

comes on at around p9 when the kinocilium is retracting, is strongest at p12, the onset of hearing and then diminishes in the outer hair cells in the adult, when the hearing loss occurs.

This anomaly could be explained by the association of Bbs6 with neuronal function, and that the auditory deficit is potentially caused by neuronal dysfunction. Strong expression of Bbs6 in the spiral ganglion (particularly in the adult) as well as association of Bbs6 with neuronal filaments in regions at the base of inner and outer hair cells, corresponding to developing innervation, give rise to this theory. In addition, the strong cytoplasmic labelling of the adult inner hair cell could be due to its involvement in inner hair cell transduction or innervation, both vital for the transmission of sound. This hypothesis is further supported by co-localisation of Bbs6 with anti-neurofilament to the microtubule-rich regions at the base of inner and outer hair cells, corresponds to developing innervation, in developing animals (P0).

With BBS6 being a putative chaperone based on its predicted protein structure, it is plausible that not only is it acting as a chaperone for proteins involved in ciliogenesis at the basal body, but also as a chaperone for proteins involved in neuronal transport up and down axons. Taken together, one could argue that BBS6 is possible a chaperone for motor proteins in general and that intra flagellar transport (the movement of proteins up and down the primary cilium, vital for its maintenance and function; explained in more detail in chapter 1), and axonemal transport share similar processes.

The BBS6 antibody used in this study was supplied by one of our collaborators and it had been previously published (Kim *et al.*, 2005). To ensure specificity of this BBS6 polyclonal anibody, which was raised in rabbit, a series of 'no primary' control immunohistochemical analyses were performed. Test conditions were performed simultaneously and image settings were unchanged between imaging. Omission of the primary antibody for BBS6 resulted in no detectable fluorescence (Fig 7.9). A more robust control would haven been to substitute the primary antibody for pre-immune serum.

The limitations of the use of fluorescent in-situ hybridisation to identify protein localisation, is that the identity of the protein can not be corroborated. Thus this antibody might possibly be localising to similar proteins such as BBS10 or BBS12. Whilst this is unlikely, doing a western blot, preferentially using proteins isolated from cochlear preparations, would strengthen our findings. Firstly this would confirm that we are seeing BBS6 expression in the cochlea, and secondly this method of detection could specify more precisely the size of the protein being picked up by the antibody. In addition, using this antibody on *Bbs6*$^{-/-}$ tissue would be the ideal control as this should not show any staining.

To further study the function of the BBS6 protein a yeast two-hybrid screen was carried out to identify potential protein interactors (chapter 5). It was possible to obtain antibodies to several of the identified proteins, and the next chapter assesses the localisation of these proteins in the developing inner ear in an attempt to further understand the role of these proteins in an *in vivo* model system.

7.5 Summary

In summary, we have seen that the auditory impairment observed in *Bbs6*$^{-/-}$ mice is progressive as hearing is normal at onset. The hearing loss could potentially be due to malformations of the stereociliary bundles on the apices of hair cells. Immunolocalisation of the Bbs6 protein at the basal body can help explain this phenotype and also shows for the first time Bbs6 localising to basal bodies *in vivo*. Bundle defects alone do not fully explain the phenotype, but the observed neuronal association of Bbs6 could offer an explanation. Linking the two could be the role of BBS6 as a chaperone for motor proteins involved in both processes.

Chapter 8: Expression of BBS6 interacting proteins in the cochlea

Aim: To assess the expression pattern of proteins identified through a yeast two-hybrid screen using Bbs6 as bait, in the murine cochlea.

8.1 Introduction

To further investigate the function of the BBS6 protein, a yeast-two-hybrid screen using murine Bbs6 as bait and an embryonic mouse library as prey, was carried out to identify possible interactors (see chapter 5). The table below shows a list of proteins pulled out during the screen.

Identified Interactor	Predicted Cellular Function
Bardet-Biedl syndrome 2 (BBS2)	Basal body & cilium function
Chaperonin containing TCP1, subunit 6A (zeta 1)(CCT6A)	Chaperone (actin & tubulin)
DNA (cytosine-5-)-methyltransferase 1 (DNMT1)	DNA methylation
EH-domain containing 2 (EHD2)	GLUT4/actin interactor
Microtubule-actin crosslinking factor 1 (MACF1)	Cytoskeletal linker protein
Translocase of outer mitochondrial membrane (TOMM70A)	Mitchondrial chaperone

Table 8.1: Summary of confirmed Bbs6 interactors and their predicted cellular functions.

Significantly, another BBS protein BBS2 was isolated validating the results previously obtained from a yeast-two-hybrid screen using BBS2 as bait, which isolated BBS6 as an interactor. This interaction has been extensively studied (see below). As an antibody against Bbs2 was available, it was used on murine cochlea to see if the expression pattern matched that of Bbs6.

It was possible to obtain antibodies against two other proteins on the list MACF1 and CCT6A. MACF1 (Microtubule-actin crosslinking factor 1) showed strong interaction with Bbs6, suggesting a role for BBS6 as a cross-linker between microtubules and actin. CCT6A (Chaperonin containing TCP1, subunit 6A) is a true chaperonin, predominantly folding actin and tubulin.

A further protein, KIF1A, implicated in axonal vesicle transport, was also isolated during the screen. Although it was not possible to verify this interaction presently, its proposed function in light of the outcome of the previous chapter (possibly implicating BBS6 in neuronal transport), makes it particularly interesting. In light of this an antibody against this protein was acquired and immunolocalised in the developing inner ear.

8.1.1 The BBS6:BBS2 interaction

BBS2 is the third most common locus for BBS. It encodes a 721 amino acid protein with no known motifs with the exception of a possible coiled-coil domain between residues 332 and 365. The protein also has a region of shared homology with BBS1 and BBS7 near its N-terminal (see Fig 1.2). Localisation studies have placed it around the centrosome/basal body in cultured cells. A yeast two-hybrid screen using BBS2 as bait identified BBS6 and BBS9 as interacting ptoteins. These interactions were confirmed by co-immunoprecipitations. The domain of interaction between BBS2 and BBS6 was further defined by testing BBS6 prey vectors against yeast two-hybrid baits expressing a series of truncated forms of BBS2. This narrowed down the region of interaction to between residues 231-402. The reverse screen (using BBS6 as bait) identified BBS2 as an interactor, isolating a positive prey clone encoding amino acids 299-415. Taken together this narrows down the region of interaction to 299-402, within which lies the predicted coiled coil domain (332-365). Introduction of mutant variants of known mutant alleles found in BBS patients, into the bait vectors, significantly disrupts the protein interaction (A. Ross, unpublished data).

8.1.2 Additional interactors of BBS6.

Chaperonin containing TCP1, subunit 6A (zeta 1)

CCT6A is one of the seven subunits that makes up the type II chaperonin CCT. This chaperone is a hetero-oligomeric complex that assists the folding

of actins, tubulins and other proteins in an ATP dependent manner (Valpuesta *et al.*, 2002). For more information about this protein see section 5.4.

Microtubule-actin crosslinking factor 1 (MACF1)

This cytoskeletal linker protein can associate with both actin filaments and microtubules. It belongs to a family of proteins (plakins) that connect the cytoskeletal network to membrane associated junctional complexes, and are important in maintaining tissue integrity (Lin *et al.*, 2005). Loss of MACF1 has been shown to affect microtubule form and function (Chen *et al.*, 2006), and it has been suggested that MACF1 is important for guiding microtubules on actin filaments (Kodama *et al.*, 2003). For more information see section 5.4.

Kinesin family member 1A (KIF1A)

KIF proteins (kinesin superfamily proteins) are microtubule dependent molecular motors that are key players in intracellular transport, which is essential for cellular function and morphology. They can be divided into two classes depending on their expression pattern (Nakagawa, 1997 #774). The KIF superfamily is the first large protein family in mammals whose constituents have been completely identified and confirmed *in silico* and *in vivo* (Miki, 2005 #775). KIF1A was cloned in 1995 and was shown to be a novel neuron-specific kinesin (Okada, 1995 #773). This monomeric globular protein contains its motor domain in the N-terminal region, and as such is classified as an N-Kinesin. It displays the fastest reported axonal anterograde transport (transport from the cell body to the synaptic terminal) at 1.2 μm/s. It is predicted that membrane proteins are sorted into different classes of transport organelles in the cell body and transported by specific motor proteins through the axon. KIF1A is thought to predominantly transport the synaptic vesicle proteins synaptotagmin, synaptophysin and Rab3A (Okada, 1995 #773).

KIF1A knockout mice die mostly within a day of birth, displaying motor and sensory disturbances (Yonekawa, 1998 #776). There appears to be a significant and specific decrease of synaptic vesicle precursor transport in the nervous system. Synaptic vesicle density is dramatically decreased with an

accumulation of small clear vesicles in cell bodies. Neuronal degeneration and death is also observed in the mutant animals, and also in neuronal cultures from mutant animals. The death of neuronal cultures is blocked by coculture with wild type neurons or exposure to a low concentration of glutamate. This suggests that mutant neurons are not receiving sufficient afferent stimulation such as neuronal contacts or neurotransmission, resulting in cell death. These data demonstrate that KIF1A transports synaptic vesicle precursors and KIF1A mediated axonal transport is crucial for the viability, maintenance and function of neurons (Yonekawa, 1998 #776).

These proteins were shown to potentially interact with BBS6 (see chapter 5). As antibodies to these three proteins became available to us, they were tested on cochlear tissue to see if they had a similar expression pattern to that of Bbs6. Possibly implicating novel roles for these proteins in the auditory system.

8.2 Materials and Methods

8.2.1 Confocal immunoflurosecence

Immunohistochemistry using antibodies against proteins identified through the Bbs6 yeast two-hybrid screen was carried out on murine cochlea preparations. Animals older than eight weeks were assigned as adult. Whole mounts or frozen cross sections were prepared from mice (CD1 or 50:50 129Sv/Ev:C57BL/6J background) as described in section 2.2.8.3, immunolocalisation was carried out as described in section 2.2.9. See appendix D for antibody concentrations and suppliers.

All staining experiments were repeated on a minimum of three different tissue samples to ensure true representation of antibody localisation.

8.3 Results

8.3.1 Expression of BBS2 in the developing murine cochlea

8.3.1.1 BBS2 associates with the actin cytoskeleton and microtubules in postnatal pillar cells.

Immunostaining with BBS2 initially showed expression in epithelial support cells and subsequently in hair cells. Whole mount staining at P2 showed Bbs2 localising in a distinct punctate pattern in areas between the heads of the inner pillar cells (Fig 8.1 A). Co-labeling with phalloidin highlighted this actin rich boundary. Further association of Bbs2 with actin-rich elements in epithelial cells was observed in the inter-cellular boundaries of Reissner's membrane cells that face the scala media (Fig 8.1 B).

As the tissue develops, the levels of Bbs2 expression increased. By P4 Bbs2 was evident as a dense ring around the apex of the inner pillar cell and also as a beam across the region of the outer pillar cell (Fig 8.2 A). Co-localisation with acetylated tubulin indicated that this pattern matched that of microtubules at this developmental age, which migrate to actin-rich regions in inner and outer pillar cells (Mogensen *et al.*, 2000). A cross section at this age reveals that the Bbs2 expression in the inner pillar cell was coincident with the actin cytoskeleton, which forms a tubular core at the apical pole of the cell (Fig 8.2 B).

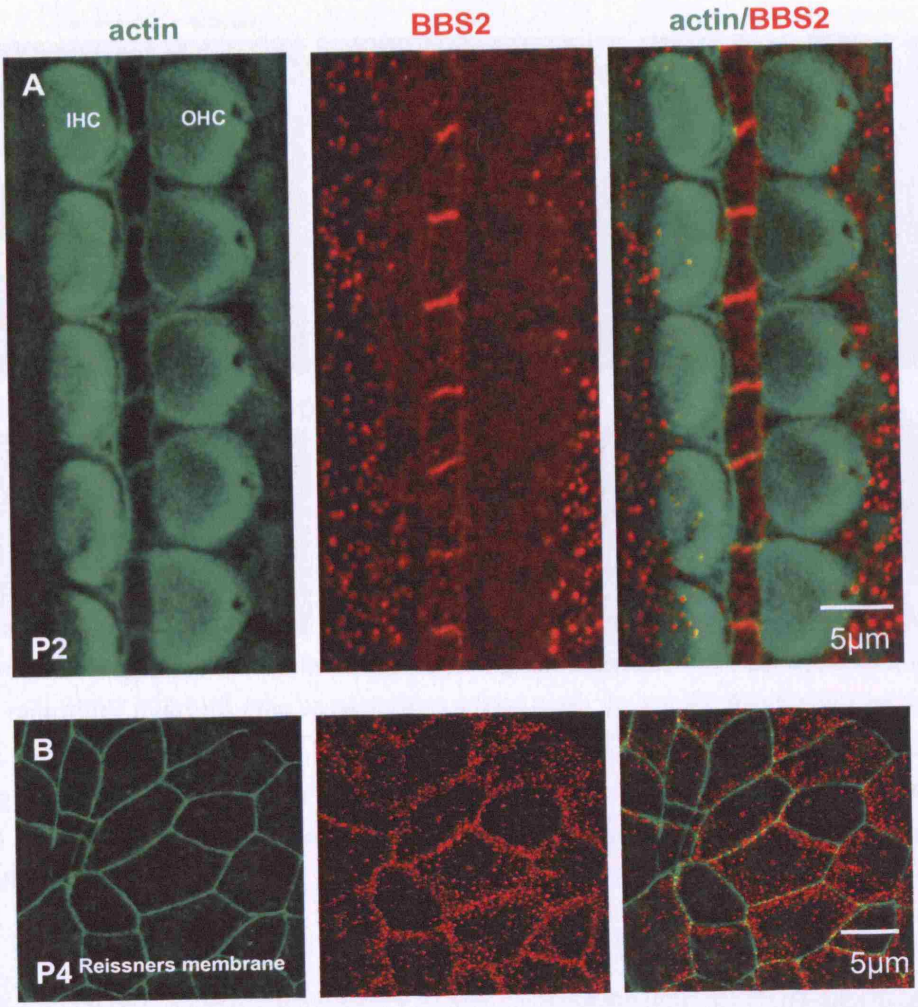

Figure 8.1: Bbs2 associates with actin-rich regions in early posnatal pillar cells. A) In the P2 organ of Corti Bbs2 (red) expression is seen at the apical intercellular boundaries between inner pillar cells as marked by actin (green). B) The actin rich inter-cellular boundaries between mesenchymal cells of Reissner's membrane also co-localise with Bbs2.

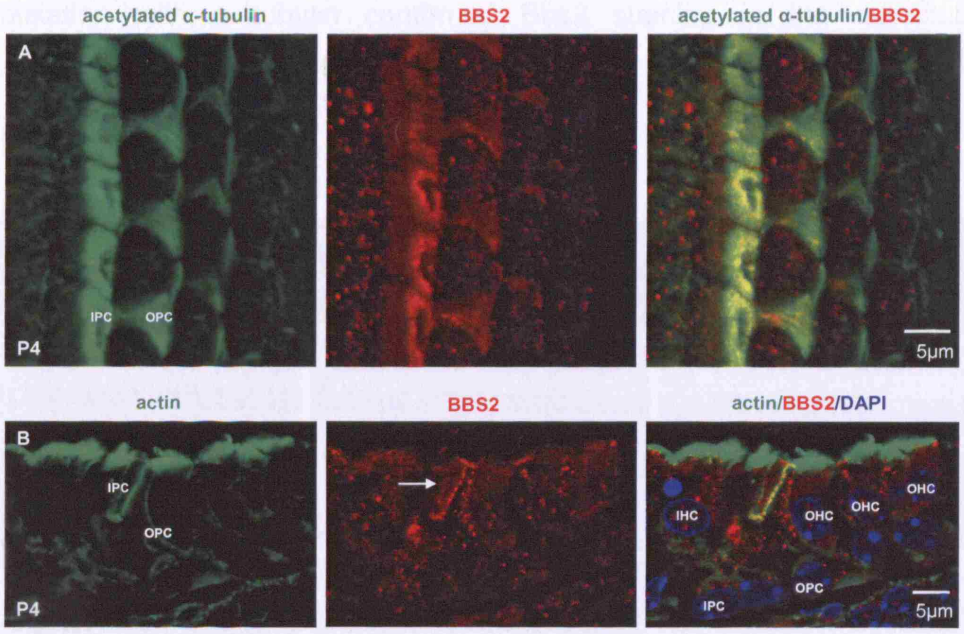

Figure 8.2: Bbs2 expression increases with age and associates with actin cytoskeleton and migrating microtubules in postnatal pillar cells. A) By P4 Bbs2 (red) co-localises with microtubules (green) at the heads of inner and outer pillar cells (IPC)(OPC). B) Cryo-section of the P4 organ of Corti confirmed that Bbs2 (red) localises to a tubular core of actin (green) at the apical pole of inner pillar cells (white arrow). Nuclei are labelled with DAPI.

8.3.1.2 Bbs2 associates with actin cytoskeleton in non-sensory supporting cells, stereocilia and basal bodies in sensory hair cells prior to the onset of hearing.

In slightly older animals, at P9, we saw expression of Bbs2 localising to the stereociliary bundles of inner and outer hair cells (Fig 8.3). As in earlier development there was continued expression of Bbs2 in the actin-rich apices of supporting cells (Fig 8.3A), but additionally we saw punctuate Bbs2 expression within stereocilia of inner and outer hair cells. Higher magnification of the inner hair cell apex revealed Bbs2 strongly decorating each individual stereocilium as well as localising beneath the bundle at the level of the cuticular plate (Fig 8.3C,D). Focusing slightly below the apex of the cell, at the level of the cuticular plate, Bbs2 expression was evident at the cell membrane and as a dense accumulation at the region of the basal body (Fig 8.4A). Co-

localisation with γ tubulin confirmed Bbs2 staining in the microtubule organising centre (MTOC) (Fig 8.4B).

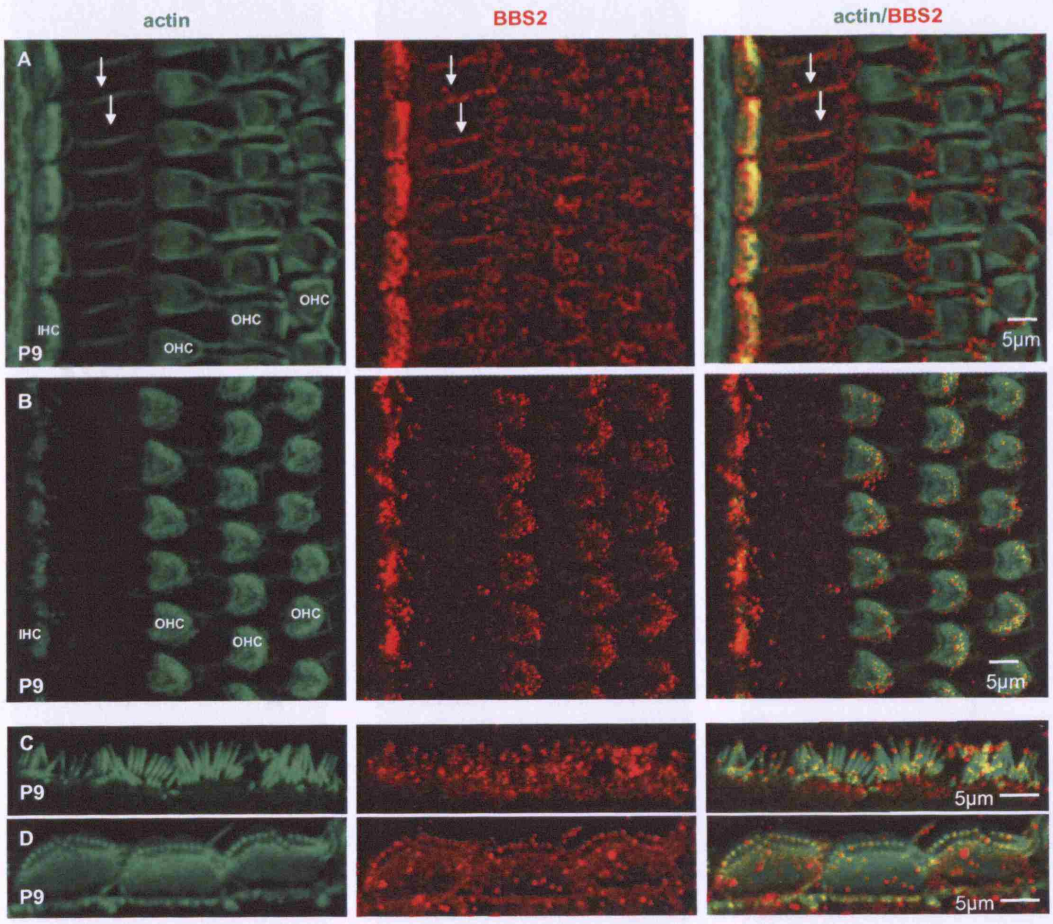

Figure 8.3: Bbs2 expression in P9 organ of Corti. A) At P9 there is continued punctuate Bbs2 (red) expression between the actin rich boundaries (green) of adjacent pillar cells (white arrows). B) Focusing on the stereociliary bundles of inner and outer hair cells, we see punctuate staining within the actin containing stereocilia bundles of inner and outer hair cells. C,D) Detail of inner hair cell apex. The stereocilia are strongly decorated with Bbs2. Bbs2 is also detected within the cuticular plate.

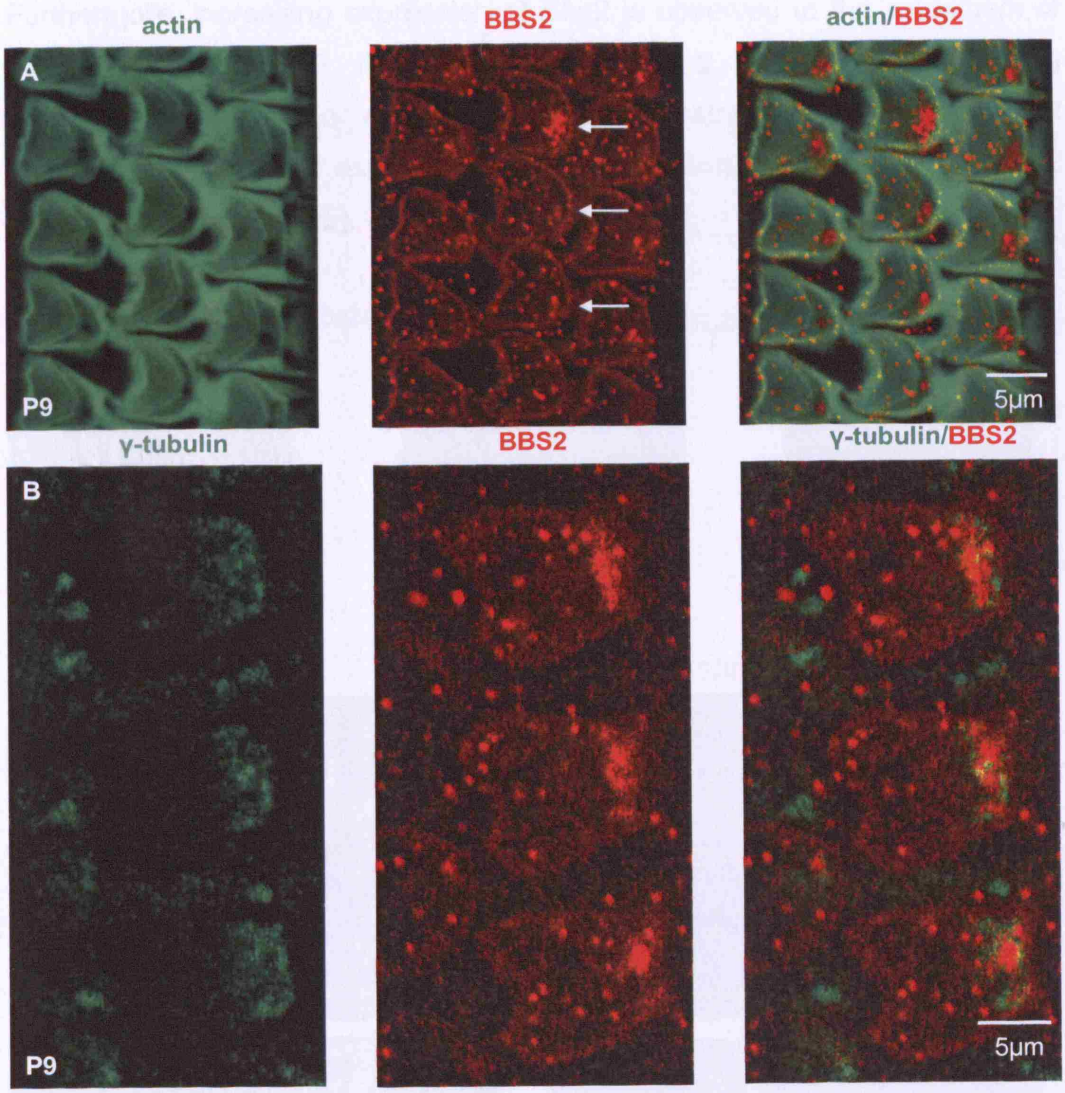

Figure 8.4: Bbs2 expression in P9 outer hair cells. A) In P9 mice, just prior to onset of hearing, Bbs2 (red) is detected within the focal level of the cuticular plate (white arrows) where actin (green) is absent. B) Double staining with γ-tubulin (green) and Bbs2 (red) demonstrates that Bbs2 is expressed in the pericentriolar region (MTOC) of outer hair cells at this age.

Furthermore, increasing expression of Bbs2 is observed in the cytoplasm of outer hair cells at P9. Its expression increasing towards the apex (Fig 8.5A,B,C). Comparable cross sections demonstrate the developmental gradient of cytoplasmic expression, and also confirm the expression of Bbs2 in stereocilia (Fig 8.5D,E).

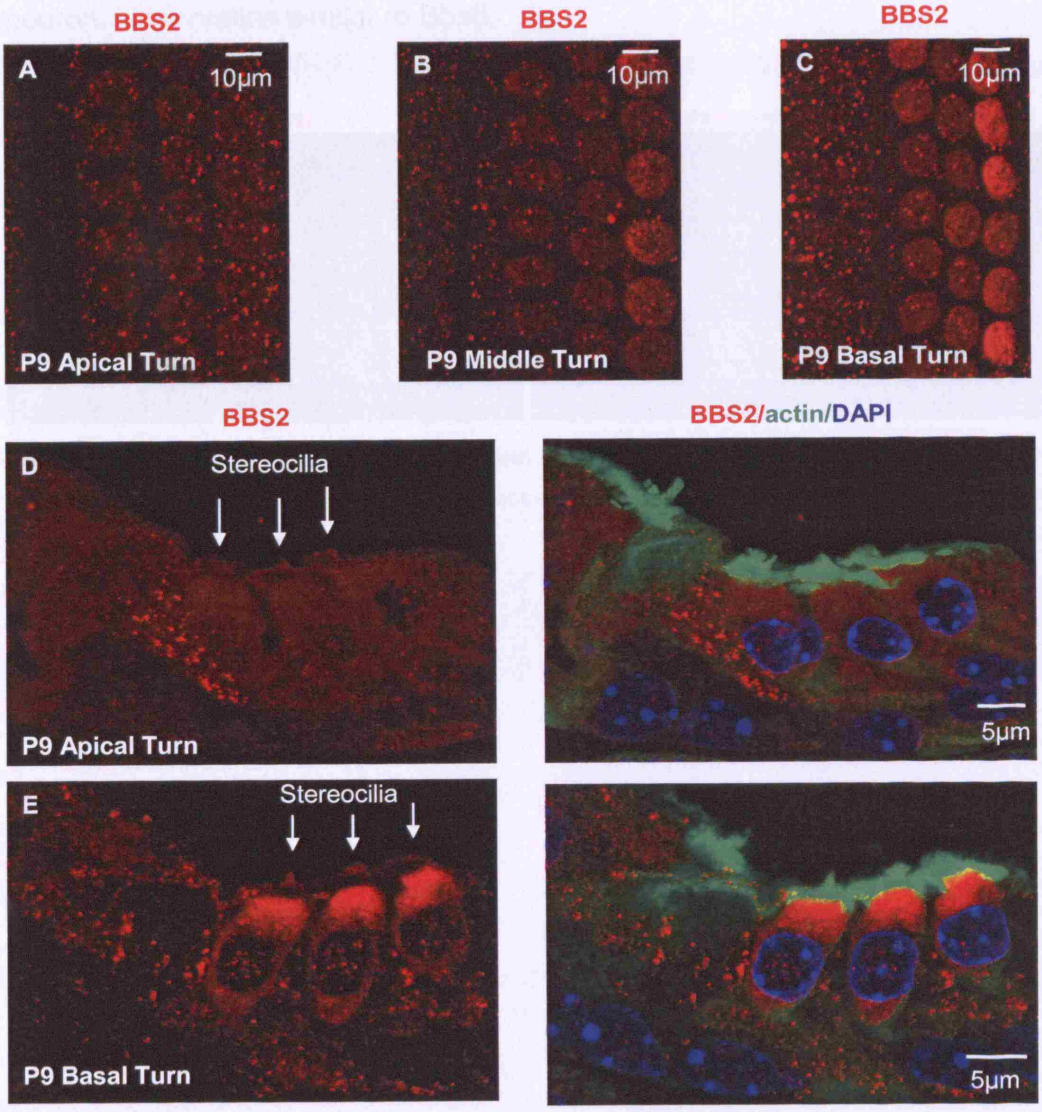

Figure 8.5: Progressive accumulation of Bbs2 expression in P9 outer hair cells. A,B,C) In P9 mice, just prior to onset of hearing, Bbs2 (red) accumulates in the outer hair cells, expression appears in a developmental pattern, appearing first in the base and progressing to the apex. D,E) The same pattern is observed on cross sections, where it is also possible to confirm the stereociliary association of Bbs2 (white arrows).

In the adult we observed continued cytoplasmic expression of Bbs2 in the hair cells, with the inner hair cell exhibiting stronger expression relative to the outer hair cells (Fig 8.6). We also saw slight accumulation of Bbs2 in the cytoplasm of the inner and outer pillar cells. Interestingly, we also observed staining at the base of inner and outer hair cells, corresponding to regions of neuronal innervation similar to Bbs6.

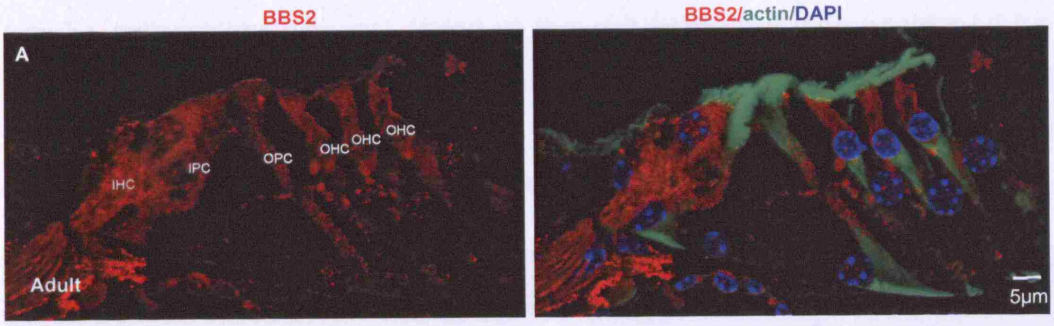

Figure 8.6: Bbs2 expression in adult organ of Corti. Hair cells retain their cytoplasmic expression into adulthood. Bbs2 also accumulates at the base of hair cells around regions of neuronal innervation.

8.3.1.3 Basal body mislocalistion of Bbs2 in *Bbs6* mutant OHC

To test the functional interaction of Bbs2 with Bbs6, we examined the localisation of Bbs2 in *Bbs6*$^{-/-}$ mice. In *Bbs6*$^{-/-}$ mice (P9), the expression of Bbs2 was still evident in the stereociliary bundles of all outer hair cells. However in cells whose stereociliary bundles were mis-oriented the accumulation of Bbs2 at the focal level of the basal body was not apparent (Fig 8.7A,B). Further inspection of outer hair cells with misaligned bundles revealed that in some instances, the basal body/MTOC (as denoted by γ-tubulin expression) was not found at the cell apex, but was positioned just above the nucleus, at the basal pole of the cell (Fig 8.7C1-C4). The degree of stereociliary bundle mis-orientation could not be correlated with the positioning of the basal body/MTOC along the apico-basal axis of the cell.

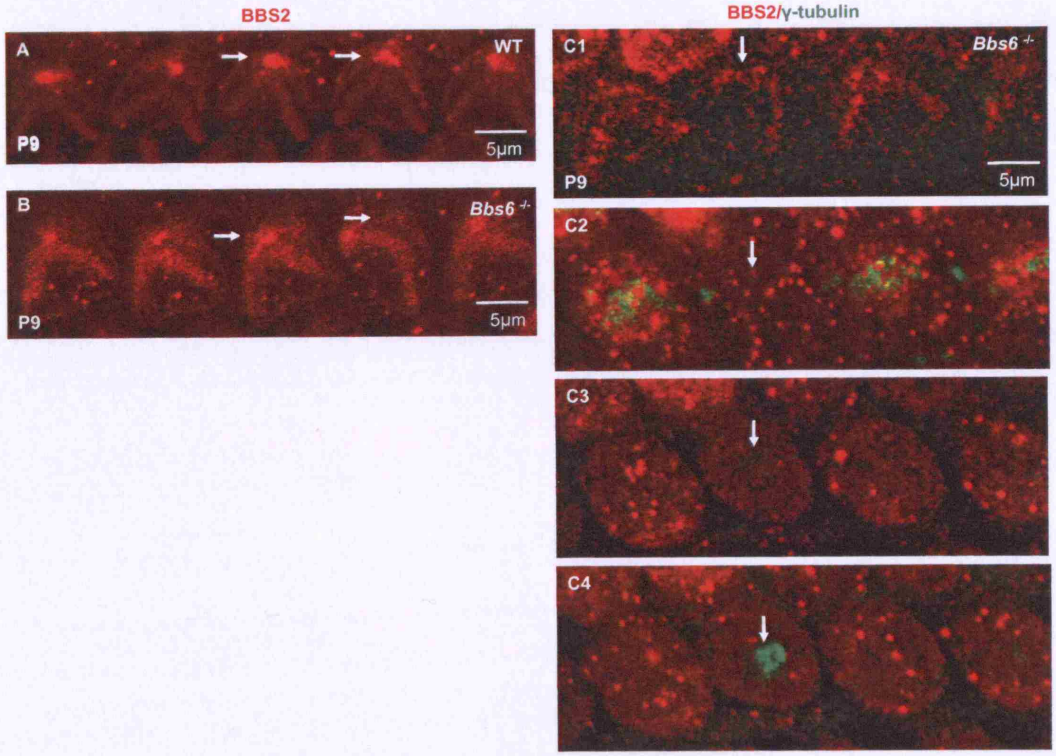

Figure 8.7: Bbs2 expression in Bbs6$^{-/-}$ outer hair cells. A,B) Bbs2 (red) expression is still observed in the sterociliary bundles of P9 outer hair cells. In *Bbs6*$^{-/-}$ mice however, cells with mis-oriented bundles the accumulation at the basal body was not observed (white arrows). C) Further inspection revealed that in these cells the basal body (green) was positioned more basally within in the cell. Focus C1 z=1.1μm, C2 z=3.3μm, C3 z=5.0μm, C4 z=6.0μm.

8.3.3 Expression of MACF1, CCT6A and KIF1A in the developing murine cochlea.

MACF1

Because of the strong association between BBS6 and MACF1 observed during the yeast two-hybrid screen, the expression pattern of this protein was analysed to see if it matched that of Bbs6. A commercial antibody against this protein was obtained from Abnova, Taiwan, and was tested on wild-type P4 cochlear. This tissue was chosen as that is what was available at the time and it is known that at this age, the basal bodies of the hair cells show strong expression of Bbs6.

In contrast to Bbs6, immunohistochemistry using an antibody against MACF1 showed no evidence of basal body staining or neuronal staining between the Deiters' cells at the base of the outer hair cells (Fig 8.8). There was labelling in Deiters' phalangeal processes, which was absent in the no-primary control. Possible expression of MACF1 was observed in the inner and outer pillar cells.

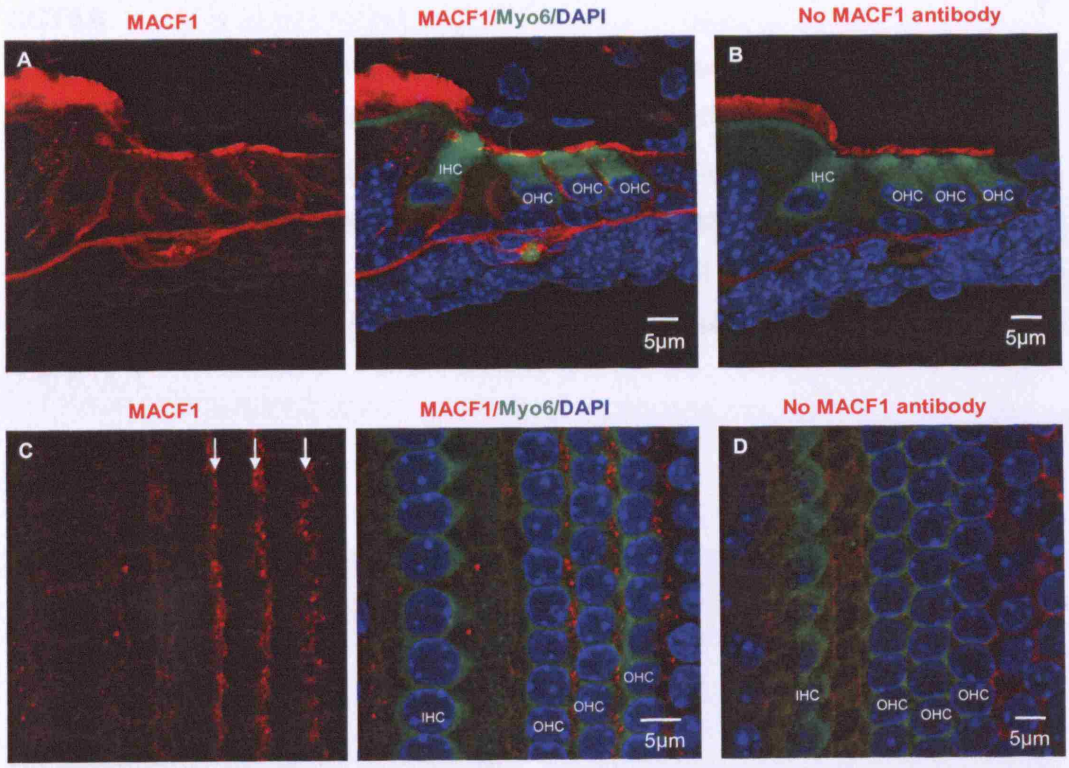

Figure 8.8: MACF1 expression in P4 cochlear. A) Tranverse section labelled with MACF1 (red), Myo6, a marker for hair cells (green) and DAPI (blue). There is no evidence of basal body staining. We do see evidence of labelling in Deiters' phalangeal processes which is absent in the 'no primary antibody' control (B). C) This staining is confirmed using whole mounts, with speckled labelling down to the level of outer hair cell nucleus (10 μm from the top of the outer hair cell) (white arrows). D) This labelling is absent in the 'no primary antibody' control.

CCT6A

In the adult cochlea staining was observed in the outer hair cells underneath the nucleus, possibly in regions corresponding to efferent neurons (Fig 8.9A). This was reminiscent of Bbs6 expression at onset of hearing (P9-P12). CCT6A was also localised to the spiral ganglion, similar to Bbs6 at this age however basal body staining of the inner hair cell as seen using the Bbs6 antibody, was absent (Fig 8.9B). Staining was absent in 'no primary' control (Fig 8.9C).

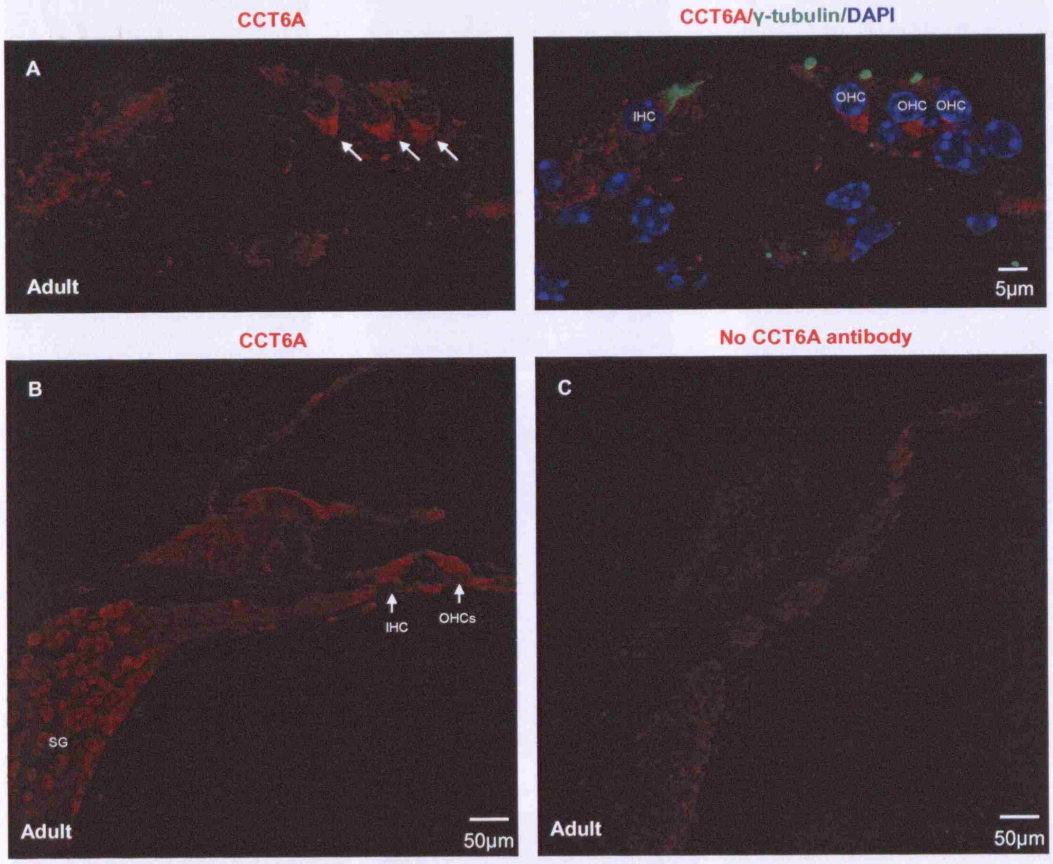

Figure 8.9: CCT6A expression in adult cochlea. A) CCT6A (red) is observed on the underside of the outer hair cells, suggestive of neuronal tissue (white arrows). Basal body expression was absent. B) Low power magnification of the adult cochlea shows expression in the spiral ganglion (SG), which is absent in the 'no-primary' control (C).

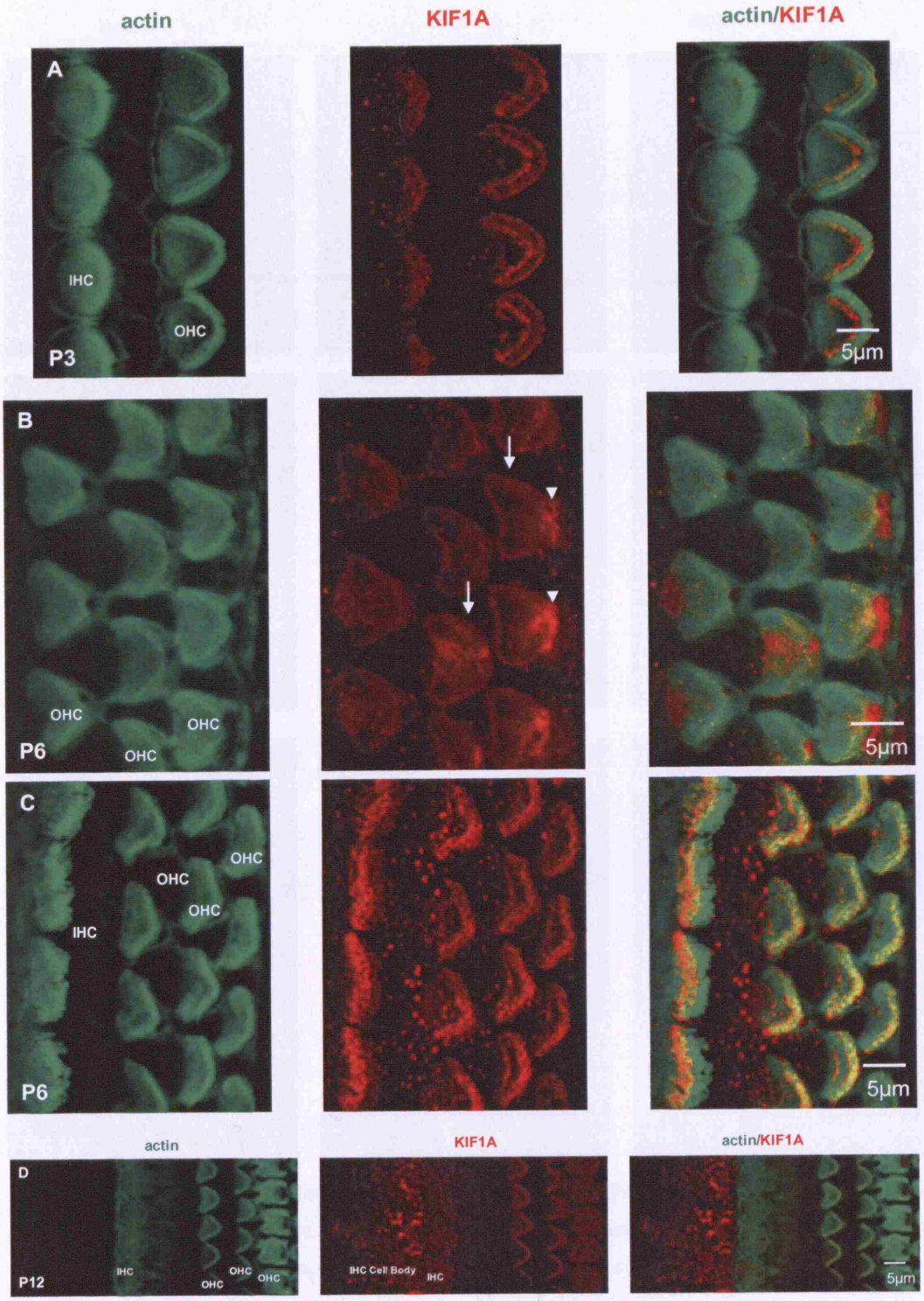

Figure 8.10: KIF1A localizes specifically to the apex of hair cells. A) At P3 KIF1A is expressed at the base of the IHC and OHC stereociliary bundles. B,C) At P6 the pattern of expression was continued in IHC and OHC, but KIF1A was also observed at the centrosome. D) By p12 apical hair cell expression of KIF1A is reduced but replaced by dense granular expression in the cytoplasm of the inner hair cell.

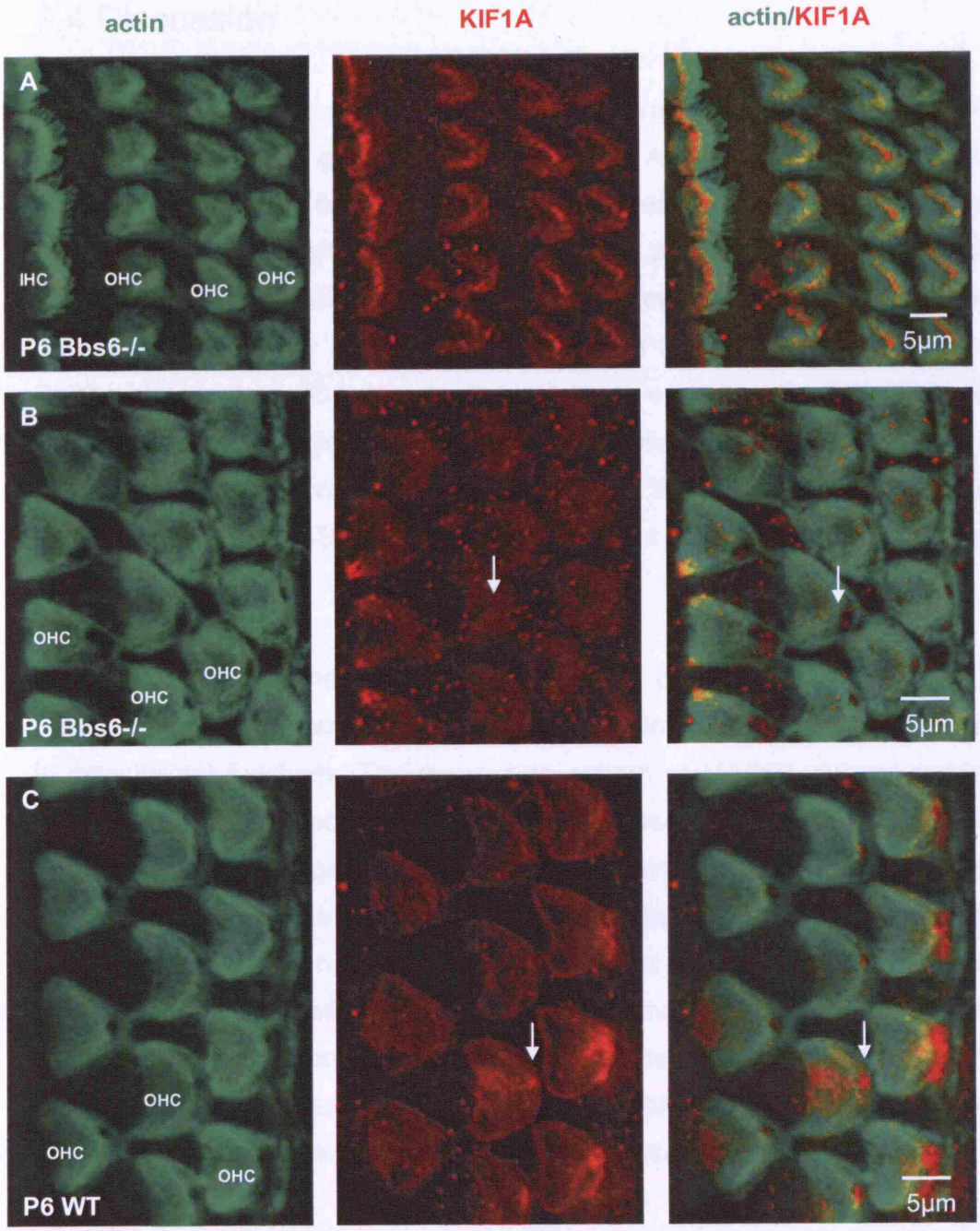

Figure 8.11: KIF1A expression in *Bbs6*$^{-/-}$ hair cells. A) At P6 KIF expression at the base of the stereociliary bundles is evident in *Bbs6*$^{-/-}$ mice. B,C) Expression at the centrosome (white arrows) appears reduced in comparison to wild-type.

8.4 Discussion

Immunohistochemistry using antibodies against proteins identified as interactors with BBS6 gave unexpected results. As Bbs6 was predominantly localised to the basal body, we would have expected to see this expression pattern repeated. In early development, the Bbs2 protein localized to the actin cytoskeleton and microtubules. Only at P9, just prior to the onset of hearing do we see basal body accumulation of Bbs2. At this time the association of Bbs2 with the sterociliary bundle is much more apparent. As the stereocilia are comprised of actin, opposed to the tubulin containing kinocilium, it strengthens the observed alliance of BBS2 with the actin cytoskeleton. This could implicate the BBS proteins in cell processes other than cilia/basal body function.

In support of this theory is the association of BBS6 with MACF1, a microtubule and actin cross-linking factor, again implicating the BBS proteins in cytoskeletal functions. The expression pattern of MACF1 did not overlap that of Bbs6. It was predominantly localized to a region between the hair cells in the Deiters' phalangeal processes. These microtubule rich structures are long appendages of the Deiters' cells which run between the outer hair cells. The cytoskeletal decompression in the phalangeal processes of Deiter's cells provides the visco-elastic coupling between the motile outer hair cell and the elastic basilar membrane which runs beneath the organ of Corti. A second antibody to MACF1 has recently become available, immunolocalisation with this antibody might reveal alternate expression pattern of the protein.

Interestingly staining with an antibody against the chaperone CCT6A suggests a neuronal function for this protein. In the adult we see CCT6A densely accumulating at the bottom of the outer hair cells but not the inner hair cells. This staining is reminiscent of the efferent nerve endings found predominantly at the bottom of outer hair cells. In contrast, the inner hair cell is innervated by a high proportion of afferent nerve fibres. Double staining with a neurofilament marker is needed to confirm this association. Furthermore localisation of this protein in younger animals is necessary to evaluate its role

in development. Adult tissue was used for these experiments as it is what was available at the time. Of note is that specifically in adult tissue we see BBS2 accumulating at the base of outer, as well as inner hair cells, much in the same location at CCT6A, further implicating BBS proteins in possible neuronal function.

This putative neuronal association of BBS is further supported by the localisation of KIF1A to the apical region of hair cells in the developing cochlea. As with BBS2, CCT6A and MACF1, KIF1A was identified during a yeast two-hybrid screen using BBS6 as bait. Being a microtubule dependent molecular motor protein, predominantly thought to transport synaptic vesicle proteins, such localisation was unusual. This microtubule plus end-directed kinesin motor has only been described previously in neuronal tissues, where it is responsible for the trafficking of synaptic vesicle precursors (Okada *et al.*, 1995; Yonekawa *et al.*, 1998). KIF1A preferentially associates with polyglutamylated tubulin, which has been observed specifically at the apex of hair cells (Ikegami *et al.*, 2007). Whilst the localisation within the hair cells could be justified on the basis of internal vesicular transport, association of KIF1A with the actin based stereociliary bundles was particularly intriguing. At P3 and P6 KIF1A expression was concentrated at the base of stereociliary bundles. The KIF1A immunofluorescence did not coincide with that of actin at the distal ends of the stereocilia, suggesting that there was no direct interaction between the motor and the actin core of stereocilia. It is possible that KIF1A is transporting cargo required for bundle formation and function, in a microtubule-dependent manner to the cuticular plate where the microtubule "fuzzy caps" enmesh with the actin matrix at the stereocilia base (Jaeger *et al.*, 1994). This hypothesis is supported by the identification of MACF1 through our yeast two-hybrid screen, reinforcing the link between microtubules and polarized F-actin. Transiently, KIF1A was also seen to localise to the centrosome, potentially aiding intraflagellar transport? Additionally, the relative shift of expression pattern at the onset of hearing from the inner hair cell apex to the cytoplasm is possibly consistent with a role for KIF1A in release of neurotransmitter during hearing. At P6, KIF1A expression in the *Bbs6*$^{-/-}$ animals was still observed at the base of the

stereociliary bundles. Suggesting that such expression is not entirely dependent on the Bbs6 protein. Centrosomal expression at this age appeared to be reduced in the knockout animals. This was only qualitatively and not quantitatively observed and would need further investigation. Specifically real-time PCR could be employed to measure this differential expression. This observation could be explained on the basis of the putative role for the Bbs6 protein as a chaperone (see previous chapter). Bbs6 could possibly be responsible for the correct folding of KIF1A at this cellular location. In its absence, BBS10 or BBS12, further putative chaperons, might substitute. These results implicate a role for the KIF1A protein in organ of Corti function and more detailed analysis could shed new light on the current understanding of how streocilia are formed and maintained.

The centrosomal localization of Bbs2 and KIF1A computes with the involvement of BBS proteins with basal body/cilia function. Further to this the mis-localisation of these proteins in hair cells with misaligned bundles in *Bbs6*$^{-/-}$ animals strongly implicates them in bundle formation and suggests that Bbs6 could be required for their centrosomal localization. These findings could explain bundle abnormalities in BBS mutant animals. However it must be noted that bundle misalignment alone is not sufficient to cause the observed degree of hearing loss (see previous chapter).

Taken together these data reflect alternative roles for BBS6. With the strong association of Bbs6 with the basal body we would have expected to see more of an association of the BBS6 interacting proteins with the basal body and a more overlapping expression pattern to that of Bbs6. Whilst the possible neuronal expression of Bbs6 is mirrored in these data, basal body staining is not as evident. However low abundance of these proteins at the basal body at any one time might make detection via immunohistochemistry difficult. Further more we see the striking labeling of the streociliary bundles. This staining is not observed with Bbs6, but animals lacking this protein do have bundle abnormalities (see previous chapter) implicating its role in formation/function of these bundles. It is possible that Bbs6 is chaperoning proteins with a structural role or possibly supporting neuronal transport. The site of this

chaperoning is possibly at the basal body. Whilst Bbs6 is there permanently, the other proteins might just visit transiently for modification purposes and then relocate to where they are required. This transient localisation might not be enough to be detected using immunofluoresecnce.

8.5 Summary

Here we show that whilst Bbs6 is predominantly a ubiquitous basal body protein, basal body expression of BBS6 interacting proteins is limited. Whilst Bbs2 was shown to localise to the hair cell basal body during a critical window of hair cell development, its specific association with actin-containing structures in cochlear cells, including hair cell stereocilia was striking. Some of the proteins also associated with neuronal structures, further implicating BBS proteins in neuronal function. It was noted that in mis-oriented hair cells from *Bbs6*$^{-/-}$ mice Bbs2 was perturbed and KIF1A expression at the centrosome of *Bbs6*$^{-/-}$ knockout hair cells was possibly reduced, potentially implicating these proteins in hair cell function.

Chapter 9: Evaluation of Bbs4 in the organ of Corti

Aims: To analyse the expression pattern of Bbs4 and associated proteins in the developing cochlea. To assess the auditory phenotype of $Bbs4^{-/-}$ mice.

9.1 Introduction

In light of the previous expression analysis of BBS proteins in the developing cochlea, we thought it would be instructive to examine a further BBS protein in the same model system. Of all the BBS proteins, BBS4 has been most extensively studied. This meant that both an antibody against Bbs4 and a *Bbs4*$^{-/-}$ mouse was available and allowed us to further investigate this protein in the murine cochlea.

9.1.1 The BBS4 Protein

BBS4 was mapped to chromosome 15q23 by Carmi et al (1995) and cloned in 2001 by Mykytyn *et al.* (2001). The gene is comprised of 16 exons, encoding a 519 amino acid protein. With the exception of partial sequence homology to BBS8 (Ansley *et al.*, 2003), the BBS4 polypeptide sequence showed no homology to any known proteins, so little was known about the function of the protein at the time of cloning. However, the predicted protein sequence shows strong homology to O-linked N-acetylglucosamine (O-GlcNAc) transferase (OGT)- which has been implicated in insulin resistance and may play a role in diabetes (Mykytyn *et al.*, 2001). The protein also contains 13 tetratricopeptide repeat (TPR) motifs, which are commonly involved in protein-protein interactions (Mykytyn *et al.*, 2001; Kim *et al.*, 2004). More recently identification of proteins that interact with BBS4 has enabled the function of the protein to be postulated.

Identified through a yeast two-hybrid screen and confirmed by co-immunoprecipitations and co-localisation in mammalian in cell lines, the

protein PCM-1 (pericentriolar material 1) was established as an interactor of BBS4 (Kim *et al.*, 2004).

PCM-1 is a 228kDa protein and is associated with centriolar satellites and the centrosomal matrix (Balczon *et al.*, 1994). It has a dynamic cellular distribution, localising to centrosomal satellites throughout the cell cycle except during metaphase and anaphase when it becomes cytosolic (Dammermann and Merdes, 2002). PCM-1 acts as a scaffold for several proteins, including centrin, pericentrin, kendrin/pericentrin B and ninein, and is transported to the centrosome in a microtubule dependent manner. It is thought to be involved in recruiting proteins necessary for centrosome replication and in organising or anchoring microtubules emanating from the microtubule organising centre (MTOC) (Dammermann and Merdes, 2002).

Cellular localisation studies in mammalian cell lines confirmed that BBS4 and PCM-1 co-localise to centriolar satellites and the basal body of ciliated cells. BBS4, unlike PCM-1, was consistently found to be associated with the centrosomes throughout the cell cycle, which suggests that it localises to centriolar satellites in a PCM-1-independent manner (Kim *et al.*, 2004). Loss of BBS4 function in cell lines leads to dispersal of PCM-1 in the cytosol coupled with disrupted microtubule networks. This phenotype was shown to be due to defective microtubule anchoring and not nucleation. Re-growth of microtubles in control cells and BBS4-depleted cells was essentially identical after transient treatment with nocodazole, which causes depolymerisation of microtubules (Kim *et al.*, 2004). Furthermore BBS4 has been implicated in cell cycle processes as BBS4 depleted cells show abnormal division and are prone to undergo apoptosis (Kim *et al.*, 2004).

Another protein shown to interact with BBS4 is the $p150^{glued}$ subunit of dynactin. Initially identified through a yeast two-hybrid screen, co-immunoprecipitation of the two proteins verified the interaction (Kim *et al.*, 2004). $p150^{glued}$ is one of the best characterised components of the dynactin complex, which has been found to interact with dynein and is required for dynein-mediated vesicle motility along retrograde minus end microtubules.

The p150^{glued} subunit itself binds directly to microtubules, centractin and the intermediate chains of cytoplasmic dynein (Vaughan and Vallee, 1995). This physical link between dynein and dynactin is a key factor in modulating the function and cargo binding of the dynein molecular motor (Vale, 2003).

Mislocalisation of BBS4 and PCM-1 in cells over expressing p50-dynamitin, an antagonist of dynactin, indicates that the dynein-dynactin machinery is responsible for transporting BBS4 to the pericentriolar material and that the BBS4 protein may function as an adaptor protein to transport PCM-1 to its appropriate cellular location (Kim *et al.*, 2004). More specifically, the region of p150^{glued} that interacts with BBS4 lies outside those required for binding microtubles and dynein intermediate chains, suggesting that BBS4 is transported to the pericentriolar region by the dynein-dynactin complex (Kim *et al.*, 2004).

The following model (Fig 9.1) highlights a proposed function of BBS4. In summary, BBS4 is thought to be a pericentriolar protein playing a central role in recruiting cargo to centriolar satellites and is thought to be involved in the formation of the centrosomal MTOC. BBS4 has been shown to form a stable complex with PCM-1, with both proteins co-localising to centriolar satellites of centrosomes. Loss of BBS4, leads to dispersal of PCM-1 to the cytosol accompanied with a range of microtubule related cellular defects. These defects are thought to be due to the loss of the BBS4-PCM-1 functional interaction. Direct interaction with the p150^{glued} subunit of dynactin-dynein microtubule-based molecular motor, suggests that BBS4 is directly involved in the transport of PCM-1 to the centrosomal satellites by acting as a dynein-associated adaptor protein. These data provided the first evidence for an intracellular role of a BBS protein and further implicated BBS4 in intraflagellar transport.

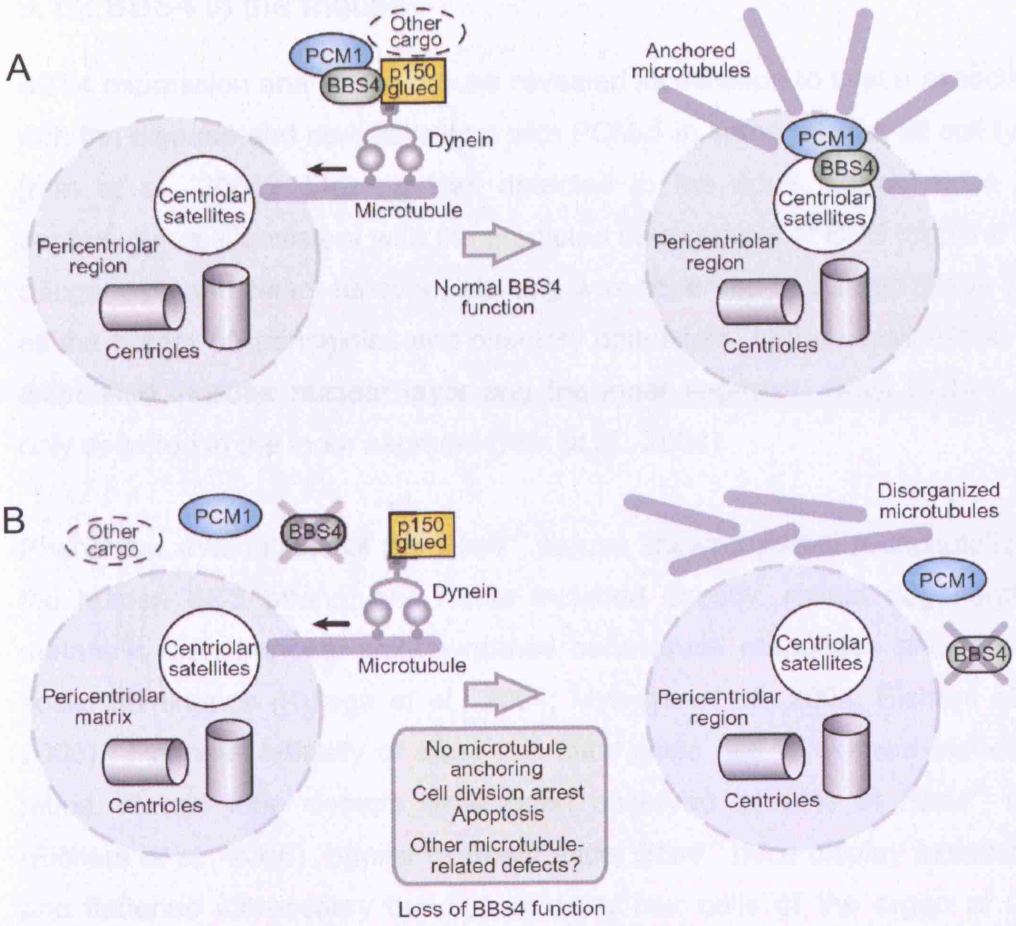

Figure 9.1: Model of BBS4 (dys)function. A) Normal BBS4 function. BBS4 recruits PCM-1 and associated cargo to the centriolar satellites in a dynein-dependent manner, probably through its interaction with $p150^{glued}$. B) In the absence of BBS4, PCM-1 and possibly its cargo do not localise to the centriolar satellites, leading to several cellular phenotypes. Figure taken from (Kim *et al.*, 2004).

9.1.2 BBS4 in the mouse

BBS4 expression analysis in mouse revealed localisation to tissue associated with the disease and co-localisation with PCM-1 in some but not all cell types (Kim *et al.*, 2004). Staining was detected in the adult hippocampus and dentate gyrus. Consistent with the predicted involvement of BBS proteins with ciliogenesis and ciliary function, staining was observed in ciliated tissue such as the border of bronchioles and olfactory epithelium. In the retina BBS4 was expressed in outer nuclear layer and the inner segment, whist PCM-1 was only detected in the inner segment (Kim *et al.*, 2004).

Phenotypic evaluations of the *Bbs4*$^{-/-}$ mouse showed partial recapitulation of the human BBS phenotype. These included obesity, retinal degeneration, metabolic disturbances, anxiety-related behavioural responses and reduced social dominance (Kulaga *et al.*, 2004; Mykytyn *et al.*, 2004; Eichers *et al.*, 2006). Perinatal lethality of *Bbs4* null mice gives rise to skewed Mendelian ratios. Neural tube defects have been observed in 14% of *Bbs4*$^{-/-}$ mice (Eichers *et al.*, 2006). Similar to *Bbs6*$^{-/-}$mice, *Bbs4*$^{-/-}$ mice display misoriented and flattened stereocilary bundles of outer hair cells of the organ of Corti (Ross *et al.*, 2005). These two features implicate BBS4 in the planar cell polarity (PCP) pathway as they are common features associated with PCP mutants (Montcouquiol *et al.*, 2003; Torban *et al.*, 2004; Wang *et al.*, 2005). Genetic interactions of *BBS4* and one of the core PCP genes, *vangl2,* in the zebrafish add weight to this hypothesis (Ross *et al.*, 2005).

BBS4 has been further implicated in microtubule organisation, as the cilia layer of olfactory epithelia appears to be nearly eliminated with disorganisation of the dendritic microtubule network in *Bbs4*$^{-/-}$ mice. Furthermore PCM-1 is mislocalised in this knockout tissue. Unsurprisingly this leads to reduced olfactory function, shown recently to be a further component of the disease in humans (Kulaga *et al.*, 2004).

None of the *Bbs4*$^{-/-}$ mice exhibit polydactyly or situs inversus. This, in conjunction with the considerable phenotypic variability observed amongst the

knockout animals, is consistent with an oligogenic causality of disease manifestation.

9.1.3 The microtubule aspect of BBS

Recent studies have highlighted a potential involvement of microtubule dysfunction in BBS. Suppression of *BBS4* mRNA causes marked disorganization of centrosomal microtubules *in vitro* (Kim *et al.*, 2004). In addition *Bbs1*$^{-/-}$, *Bbs4*$^{-/-}$ and *Bbs6*$^{-/-}$ mice have unstable microtubules in their olfactory cilia, and distorted microtubular organization of dendrites (Kulaga *et al.*, 2004) (Ross *et al.*, 2005). These observations raise the possibility that BBS proteins play a role in the establishment of microtubules, or may interact with microtubules during intracellular retrograde transport. This notion is supported by the interaction of BBS proteins with microtubule-associated proteins. As stated, BBS4 has been proposed to behave as an adaptor between PCM-1 and dynein molecular motors, implicating the BBS family in the retrograde translocation of subcellular cargo along microtubules (Kim *et al.*, 2004). In support of this, knockdown of *bbs* function in zebrafish causes significant delay in retrograde melanosome transport (mediated by the molecular motor protein dynein), whereas anterograde transport (mediated by kinesin II) was not affected (Yen *et al.*, 2006). As discussed previously, a yeast two-hybrid screen using Bbs6 as bait identified microtubule associated proteins namely MACF1 (Microtubule-actin crosslinking factor 1) and CCT6a. MACF1 is a cytoskeletal linker protein that associates with both actin filaments and microtubules. CCT6a is a subunit of the type II chaperonin that assists the folding of actins and tubulins.

In light of this we have investigated the expression of various BBS proteins in the organ of Corti, the sensory epithelium of the mammalian cochlea. The epithelial cells of this highly differentiated organ are uniquely enriched with cytoskeletal microtubules (Mogensen *et al.*, 1997), and so provide a 'high gain' model for the study of low abundance microtubule-associated proteins.

9.1.4 Microtubules in the cochlea.

Microtublues are polarized structures comprised of α and ß tubulin, usually radiating from the centrosome of a cell. These structures are essential for many cellular functions such as cellular transport, motility, polarity and division, they also confer structural integrity and cellular architecture. The centrosome is the largest non-membrane bound organelle in most cells and acts as a microtubule organizing centre (MTOC) by nucleating and anchoring microtubules (Zimmerman *et al.*, 1999). It has a complex structure consisting of a pair of centrioles surrounded by a matrix of amorphous material, referred to as the pericentriolar material. Additionally, electron-dense granules called massules or centriolar satellites associate peripherally with centrosomes (Andersen *et al.*, 2003). The centrioles are thought to organise the pericentriolar material and confer centrosomal stability (Bobinnec *et al.*, 1998). They are conserved, microtubule-based structures that localise not only to centrosomes but also to the basal bodies of cilia and flagella. Basal bodies, which anchor a cells cilium are modified centrosomes (see chapter one for more details).

The developing mammalian cochlea has a wide range of polarized tissue including both sensory and supporting cells. These cells posses a pair of closely adjacent centrosomal centrioles and are involved in the construction of microtubules. Initially one of these centrioles forms part of the basal body of a primary cilium, and is retained after the cilium retracts. A subset of these supporting cells, the inner and outer pillar cells, are of particular interest because they contain a vast amount of microtubules emanating from their apical surfaces where the basal body/centrosome is located (up to 4000 in mouse). These cells are particularly useful to examine the involvement of low abundance proteins in microtubule nucleation and growth.

The postnatal development of cytoskeletal microtubules in cochlear epithelial cells, particularly of inner and outer pillar cells, has been extensively documented (Tucker *et al.*, 1992; Tucker *et al.*, 1993; Henderson *et al.*, 1995; Tucker *et al.*, 1995; Mogensen *et al.*, 1998; Mogensen *et al.*, 2000). In

addition, the spatio-temporal distributions of associated basal body proteins and microtubule-associated proteins have been mapped (Mogensen *et al.*, 2000; Mogensen *et al.*, 2002). Consequently models for the assembly of the pillar cell architectural cytoskeleton have been proposed (Mogensen *et al.*, 1997; Mogensen *et al.*, 2000).

Recently, Mogensen proposed a theory in which epithelia cell microtubules grow from non-centrosomal sites. Observations from murine pillar cells implicate a process by which the pericentriolar regions function as microtubule-nucleating domains, whilst cell surface-associated sites operate as docking domains, capturing the minus ends of migrating nucleated microtubules. Short nucleated microtubules migrate along temporary microtubule tracts. Large microtubule arrays then align and extend in an apico-basal orientation from non-centrosomal sites (Mogensen *et al.*, 1997) (Fig 9.2).

Because of the ideal system for looking at low abundance microtubule associated proteins provided by the pillar cells, we chose this tissue to further investigate the possible links between BBS genes and microtubules.

The results of the expression analysis of the Bbs2 and Bbs6 proteins in the organ of Corti are detailed in the previous two chapters. This chapter focuses on expression analysis of the Bbs4 protein. The results are brought together for the discussion at the end.

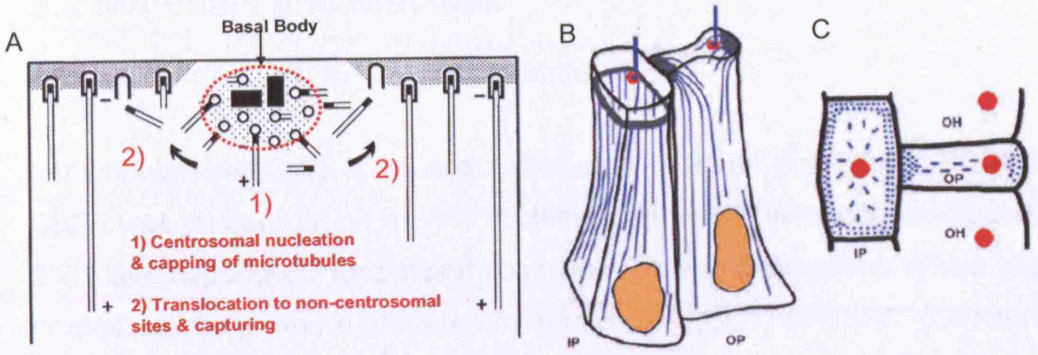

Figure 9.2: Schematic diagrams of microtubule organisation in pillar cells. A) Apical portion of a polarized cell showing how a microtubule-nucleating domain (lightly stippled) around the centrioles (black rectangles) and a cell surface-associated docking domain (densely stippled) may operate. Microtubules are nucleated by pericentriolar nucleating elements (circles) and their minus ends then capped (black squares). This is done at the basal body (red dotted line). Short capped microtubules are released from nucleating elements, translocated, and subsequently captured at their minus ends by docking elements in a docking domain. Microtubule elongation then follows. (Figure taken from Mogensen et al., 1997) B) 3-D representation of the inner pillar (IP) and outer pillar (OP) cells showing apically located centrosomes (red, with centriole and primary cilium in blue) and the majority of the microtubules associated with an aplical peripheral ring of dense material (grey) in the IP cell and two dense aggregates at either end of the apex in the outer pillar cell. B) Apical view of pillar cells showing location of the centrosomes (red), microtubule ends (blue dots) at the apical sites and the transient microtubule population (blue lines).

9.2 Materials and Methods

9.2.1 Confocal immunofluorescence

Immunohistochemistry using antibodies against BBS4 and PCM1, BBS1 and BBS5 was carried out on murine cochlea preparation as described in section 2.2.9 See appendix D for antibody concentrations and suppliers. Whole mount or cross sections where prepared from mice WT (CD1) or *Bbs4*$^{-/-}$ (C57BL/6J). All staining experiments were repeated on a minimum of three different tissue samples to ensure true representation of antibody localisation.

9.2.2 Animals

Whole mount or cross sections where prepared from mice WT (CD1) or *Bbs4*$^{-/-}$ (C57BL/6J). *Bbs4*$^{-/-}$ mice where given to us by Dr N. Katsanis and generated by insertion of a trapping cassette into intron 1 which resulted in aberrant splicing and complete loss of the mRNA message (as described in (Kulaga *et al.*, 2004)). Genotyping was preformed on DNA extracted from Tail tips, using the TD55 PCR conditions (see section 2.2.2), using the following primers.

Forward primer: GTAACTGGCTTTTTGCATCACTCA

Reverse primer: TCAGTTGGGGATACACAAATAAAC

LTR primer: AAATGGCGTTACTTAAGCTAGCTTGC

Similar to the genotyping of the Bbs6$^{-/-}$ a three primer PCR reaction was carried out. The forward and reverse primers amplify a ~500bp region from the wild-type chromosome, whereas the LTR-reverse primers detects an inserted trapping cassette and amplifies a ~300bp fragment.

9.3 Results

9.3.1 Bbs4 localises to microtubules of the epithelial cell cytoskeleton, basal bodies and primary cilia.

Whole-mount cochlea preparations from postnatal day 2 (P2) were labeled with an antibody against Bbs4. Qualitative analysis reveales a high abundance of Bbs4 at this developmental age. Co-labelling with an anti-acetylated-α tubulin antibody (a marker of microtubules) shows accumulation primarily to microtubules of the epithelial cell cytoskeleton. Bbs4 was detected homogeneously throughout the head of inner pillar cells and weakly in the apical microtubule beam in outer pillar cells (Fig 9.3 A). Double labeling with an anti-γ-tubulin antibody, a marker of peri-centriolar material used to identify basal bodies, confirmed Bbs4 as a basal body protein *in vivo* (Fig 9.3 B).

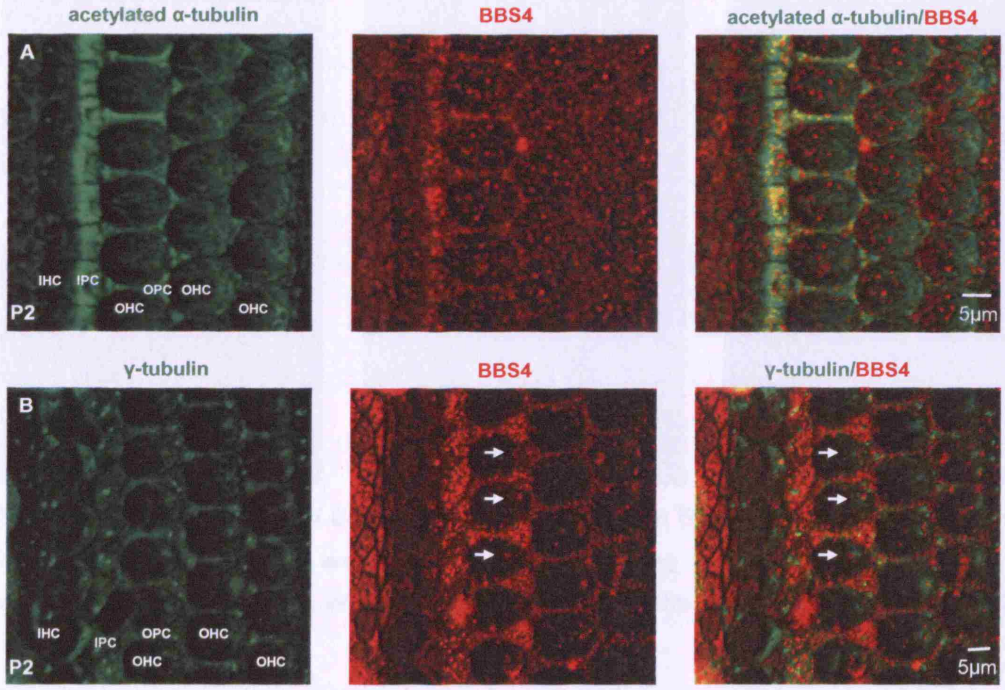

Figure 9.3: Bbs4 localisation in a P2 organ of Corti. A) Staining of a P2 whole mount cochlea shows association of Bbs4 (red) with regions of developing microtubules (green). Particularly dense accumulation is observed at the head of the inner pillar cell. B) Co-localisation of Bbs4 with anti-γ-tubulin (green) confirmed Bbs4 as a basal body protein in hair cells. inner hair cell (IHC), outer hair cells (OHC), inner pillar cell (IPC), outer pillar cell (OPC)

To see if Bbs4 localised to primary cilia, we co-labelled younger (E17.5) tissue, in which the kinocilia are active, with Bbs4 and acetylated-α tubulin. Focusing on the level of the kinocilium, we saw association of Bbs4 with these primary cilia (Fig 9.4). In some cilia we saw Bbs4 along the entire length of the cilium whilst in others we see granular accumulation.

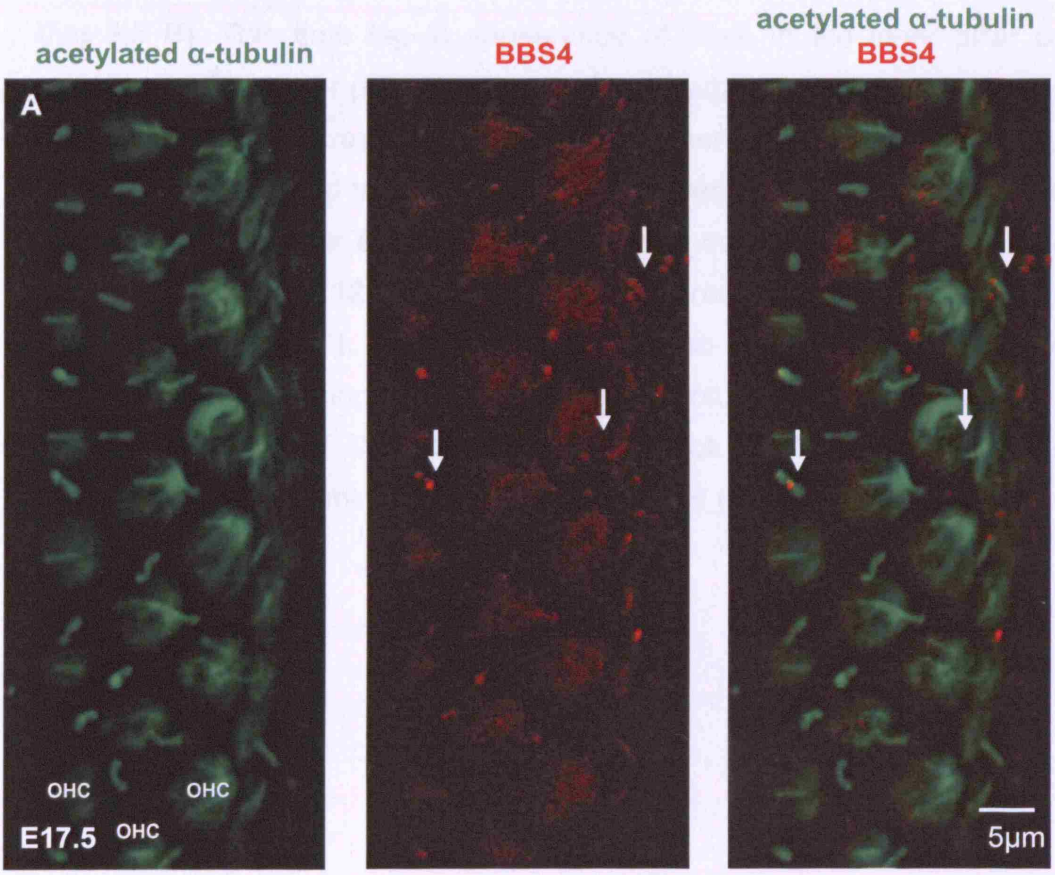

Figure 9.4: Localisation of Bbs4 to primary cilia. In an E17.5 whole mount preparation of outer hair cells (OHC) we see Bbs4 (red) localizing to the kinocilium labeled with acetylated tubulin (green). White arrows point to individual cilia associating with Bbs4.

9.3.2 Bbs4 localises along pillar cell microtubules as they develop, but expression is reduced in the mature organ of Corti.

Cryosections at P2 showed that Bbs4 was restricted to the apical pole of the inner pillar cell, consistent with an association with minus ends of microtubules extending in an apico-basal orientation (Fig 9.5 A). Bbs4 was first seen within the apico-basal microtubular array of outer pillar cells at P6 (Fig 9.5 B). This time lag in appearance of Bbs4 in the inner pillar cells compared to the outer pillar cells is consistent with the development of apico-basal microtubular arrays in these cells, as observed by the spatio-temporal pattern of α-acetylated tubulin labeling. Subsequently Bbs4 progressed further along the microtubular arrays of both inner and outer pillar cells in an apico-basal direction. By P12 Bbs4 was equally expressed throughout both pillar cell types (Fig 9.5 C). By this stage Bbs4 also appeared in Deiter's cells (support cells), localising selectively to their microtubular arrays. In contrast, in the mature organ of Corti, once all the microtubular bundles have been established, Bbs4 staining is significantly reduced (Fig 9.5 D).

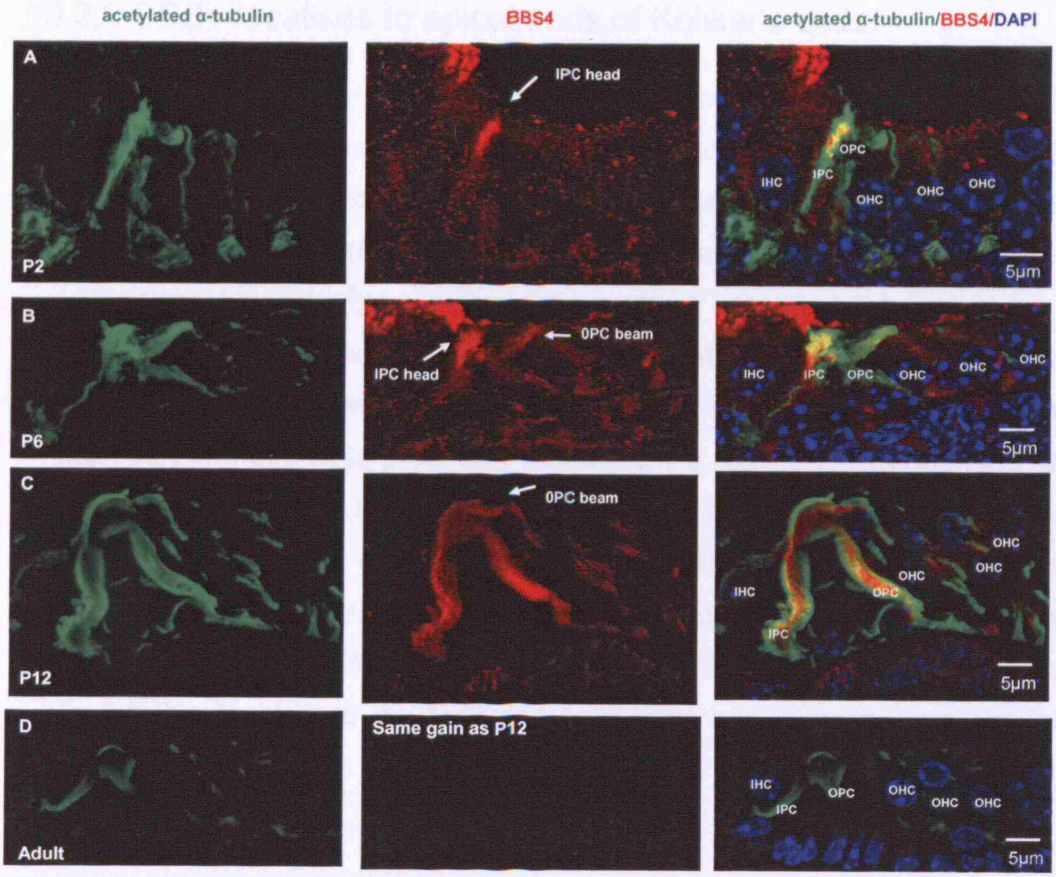

Figure 9.5: Bbs4 localisation in the developing organ of Corti. Transverse sections of the organ of Corti at different stages of development stained with an antibody against Bbs4 (red), acetylated α-tubulin (green) and DAPI (blue). Bbs4 localises to the developing microtubules in younger animals (A,B,C) but is absent in the mature organ of Corti. Inner hair cell (IHC), outer hair cells (OHC), inner pillar cell (IPC), outer pillar cell (OPC). White arrows point to the IPC head and OPC beam.

9.3.3 BBS4 localises to apical ends of Koliker's cells.

The Kollikers' organ is a sheet of epithelial support cells which extends over the organ of Corti during development. This structure is absent in the mature cochlea. In early development (P2), Bbs4 localises to the apical ends of cells in the Kolliker's organ (Fig 9.6 A). In each cell we saw a distinct region devoid of Bbs4 labelling, double labeling with γ-tubulin identified this region as the basal body. On a cross section it appeared that, as in the pillar cells, Bbs4 localised to minus ends of microtubules. It is known that microtubule nucleation in these cells proceeds within the 1-6 day period (Mogensen 1997 CMC). Consistent with this Bbs4 is expressed at the apical ends of these cells throughout this period of time (Fig 9.6 B, C). Although Kolliker's cells have fewer microtubules than the pillar cells, their bundles are also oriented parallel to their apicobasal axis. By P9 this staining in the Kolliker's cells was gone (Fig 9.6 D). At this age the Kolliker's cells have bent over to cover the inner hair cells.

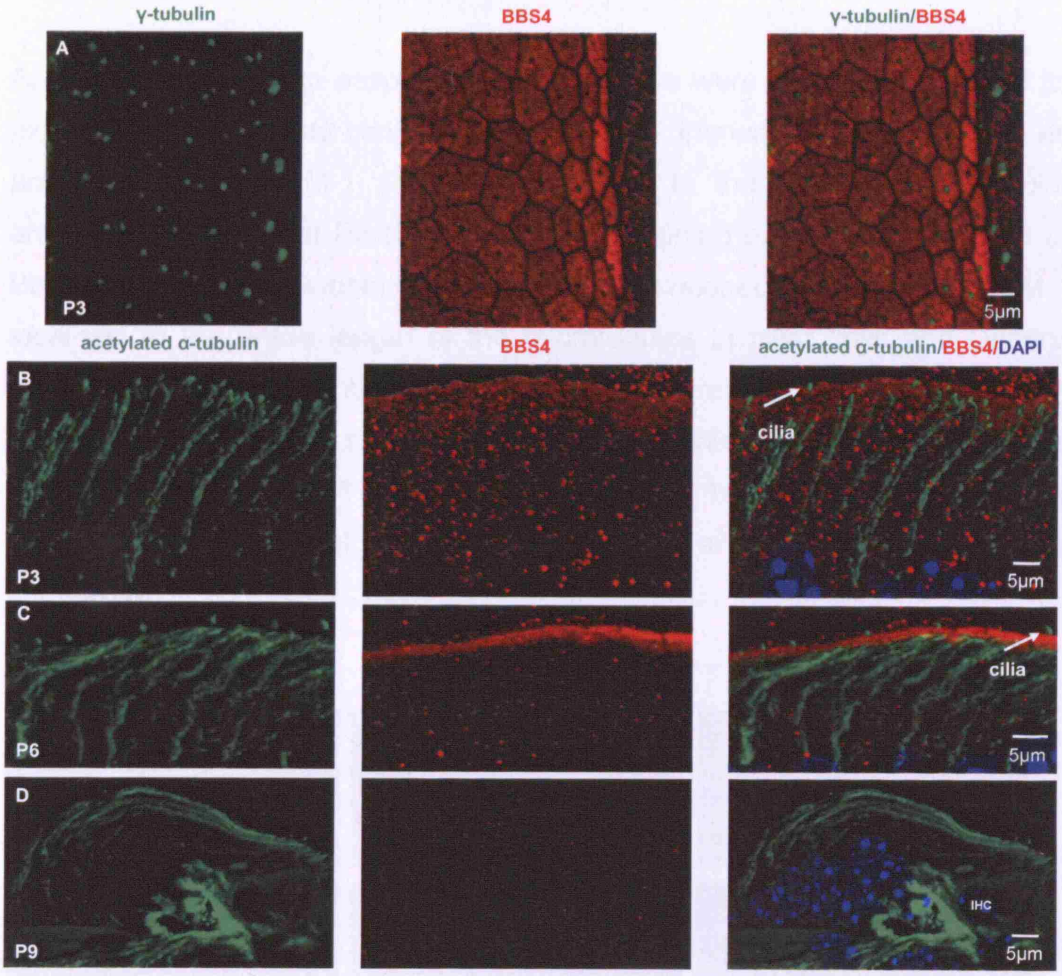

Figure 9.6: Bbs4 localises to the apical ends of Kolikers' cells. A) Whole mount staining of P2 cochlea shows association of Bbs4 (red) with the apical ends of Kollikers cells. B) Transverse sections reveal that this staining is restricted to the very apex of the cell were microtubules (green) are nucleated. C) At P6 expression is retained whilst the Kollikers' cells migrate over the inner hair cell (IHC). D) Once migration of the Kollikers' cells is complete, by P9, this expression is absent.

9.3.4 Expression analysis of PCM-1 in the organ of Corti.

As PCM-1 is known to associate with BBS4, we were interested to see if its expression pattern was similar in the cochlea. Immunolocalisation using an antibody against PCM-1 showed localization to the growing microtubular arrays of pillar cells at P6 (Fig 9.7 A). This staining pattern matched that of Bbs4 at this age. Subsequently in more developed tissue (P9), PCM-1 localised to the entire length of the microtubules in pillar cells and Deiters' cells (Fig 9.7 B). In contrast to Bbs4 staining, which is absent in the adult cochlea, PCM-1 was still evident in older animals (Fig 9.7 C). The accumulation of PCM-1 at the apical end of hair cells could possibly correspond to the basal body. Co-labeling with anti-γ-tubulin is needed to confirm this.

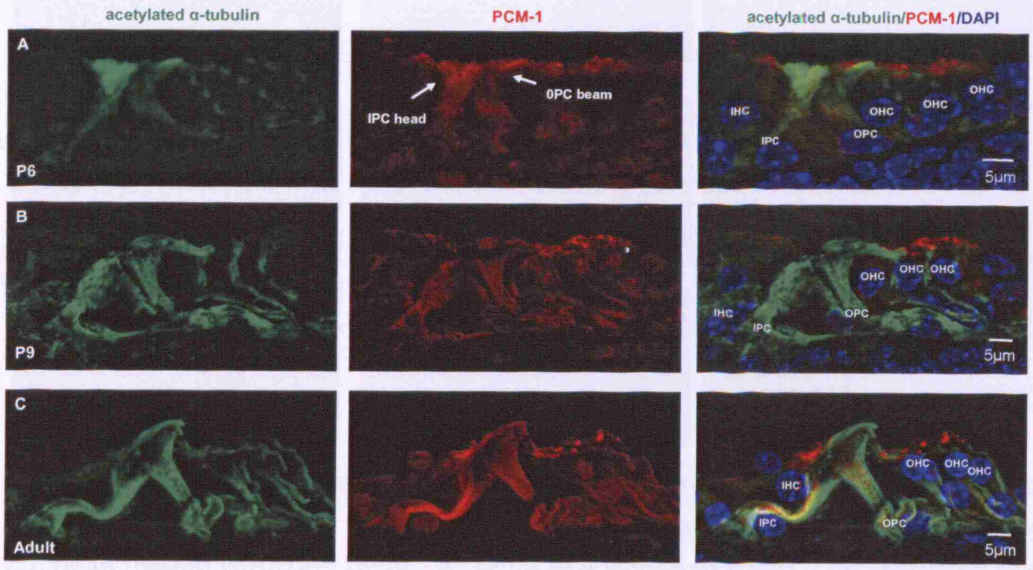

Figure 9.7: PCM-1 localisation in the organ of Corti. Transverse sections of the organ of Corti at P6, P9 and adult stained with an antibody against PCM-1 (red), acetylated α-tubulin (green) and DAPI (blue). A, B) In the developing cochlea the spatio-temporal expression pattern of PCM-1 closely matches that of Bbs4, localizing to the developing microtubules. C) In contrast to Bbs4, expression is maintained in the adult where we see PCM-1 associating with regions of dense microtubules as well as potential basal body regions. inner hair cell (IHC), outer hair cells (OHC), inner pillar cell (IPC), outer pillar cell (OPC). White arrows point to the IPC head and OPC beam.

9.3.5 Expression analysis of p150^{glued} in the organ of Corti.

A further protein known to associate with BBS4 is the p150^{glued} subunit of dynein. It is thought that BBS4 acts as an adaptor protein between this subunit and PCM-1. As an antibody to this protein was available, we studied its localization in the developing organ of Corti. Unlike Bbs4 and PCM-1 there is relatively limited staining at P6, with the exception of punctuate accumulation along the Deiters' cell microtubules (Fig 9.8 A). At P9, just prior to onset of hearing, p150^{glued} is seen in virtually all cell types throughout the entire cell (Fig 9.8 B). This expression is reduced in the mature organ of Corti with the exception of the pillar cells, which retain a high level of p150^{glued} expression (Fig 9.8 C).

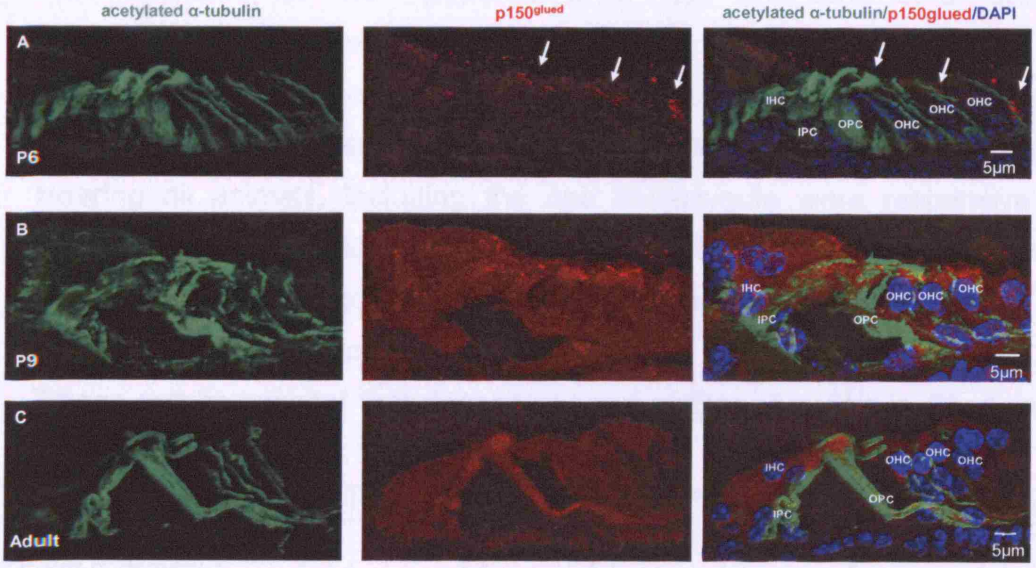

Figure 9.8: p150^{glued} localisation in the organ of Corti. Transverse sections of the organ of Corti at P6, P9 and adult stained with an antibody against p150^{glued} (red), acetylated α-tubulin (green) and DAPI (blue). A) At P6 expression of p150^{glued} is restricted to the Deiters' cell microtubules (White arrows). B) By P9 expression appears to be widespread throughout the organ of Corti. C) In the adult expression is more concentrated in the microtubule rich pillar cells. inner hair cell (IHC), outer hair cells (OHC), inner pillar cell (IPC), outer pillar cell (OPC)

9.3.6 Analysis of the *Bbs4*$^{-/-}$ cochlea.

Using *Bbs4*$^{-/-}$ mice, we were able to further investigate the function of BBS4 in the auditory system. Unfortunately breeding these animals was extremely difficult. This meant we had trouble repeating the experiments, and further analysis is required. We did not have enough animals to assess a large cohort of *Bbs4* $^{-/-}$ animals for their Preyers reflex (as we had been able to with *Bbs6*$^{-/-}$ mice), however it was noted that all knockout animals (n=4) tested prior to being culled had an absent startle response to a 19.5 kHz sound burst.

One litter which included two *Bbs4*$^{+/+}$, four *Bbs4* $^{+/-}$ and one *Bbs4*$^{-/-}$ animals, was assessed for their response to a 19.5 kHz tone burst using a standardised click box at onset of hearing, three and six months. The response was given a score of 1.0 for a positive reflex (ears flicked flat to the head), 0.5 for a mild response, and 0 for no noticeable response. At onset of hearing all animals, including the one homozygote were responsive and scored 1.0. At three months only the homozygote was non-responsive, whilst one of the heterozygotes had a reduced response. By six months both wildtype animals still scored 1.0, whilst only one heterozygote did (Table 9.1). These results suggest that degeneration of auditory function in *Bbs4* mutant animals is progressive.

Genotype	*Bbs4*$^{+/+}$	*Bbs4*$^{+/+}$	*Bbs4*$^{+/-}$	*Bbs4*$^{+/-}$	*Bbs4*$^{+/-}$	*Bbs4*$^{+/-}$	*Bbs4*$^{-/-}$
Animal ID	97.2.4	97.2.6	97.2.3	97.2.2	97.2.5	97.2.7	97.2.1
Onset of hearing	1	1	1	1	1	1	1
3 months	1	1	0.5	1	1	1	0
6 months	1	1	0	0.5	1	0	0

Table 9.1: Summary of results for progressive hearing study on one litter of Bbs4 mutant mice. Animals were tested at onset of hearing, three and six months for their response to a 19.5 kHz tone burst. A full Preyers reflex response was awarded with the score 1.0, no response with 0.0 and a mild response 0.5.

As the Bbs4 protein was associated with microtubular arrays in the organ of Corti, it is possible that it plays a role in its architectural development. For this reason electron microscopy was carried out on a *Bbs4*$^{-/-}$ cochlea. As in the *Bbs6*$^{-/-}$ mice, scanning electron microscopy of the organ of Corti displayed malformed and mis-oriented outer hair cell bundles (Fig 9.9 A). However the ultra-structure of the organ of Corti appeared normal, with rigid pillar cells and a patent tunnel of Corti formed (Fig 9.9 B). In transmission electron micrographs the pillar cells of the *Bbs4*$^{-/-}$ mouse showed no obvious abnormalities compared to its wild-type littermate (Fig 9.9 C,D). The apico-basal microtubular arrays in pillar cells appeared normal, with comparable microtubular numbers and orientation. This suggests that despite the absence of Bbs4, *Bbs4*$^{-/-}$ mice cochlear epithelial cells have normal cyto-architecture.

Figure 9.9: Electron microscopy of a *Bbs4*$^{-/-}$ cochlear. A) Scanning electron microscopy of the organ of Corti and B) the tunnel of Corti, show abnormal stereociliary bundles but intact pillar cells. C-F) Transmission electron micrographs of pillar cells from a *Bbs4*$^{-/-}$ cochlear (E, F) and wild type cochlear (C, D) show comparable microtubular arrangement. Images were taken by Prof. A. Forge, UCL Ear Institute, UK.

Next we analysed the expression pattern of PCM-1 in the *Bbs4*$^{-/-}$ animals. We had already observed that in wild type mice, PCM-1 showed association with microtubules in a similar fashion to Bbs4. In contrast, PCM-1 staining in *Bbs4*$^{-/-}$ animals (n=2) showed uneven expression and aggregation of the protein (Fig 9.10). At the head of the outer pillar cell, where microtubules are least concentrated, PCM-1 immunofluorescence was observed to occur in large granules. This pattern was distinct from that in *Bbs4*$^{+/+}$ mice, where PCM-1 was evenly distributed along microtubules.

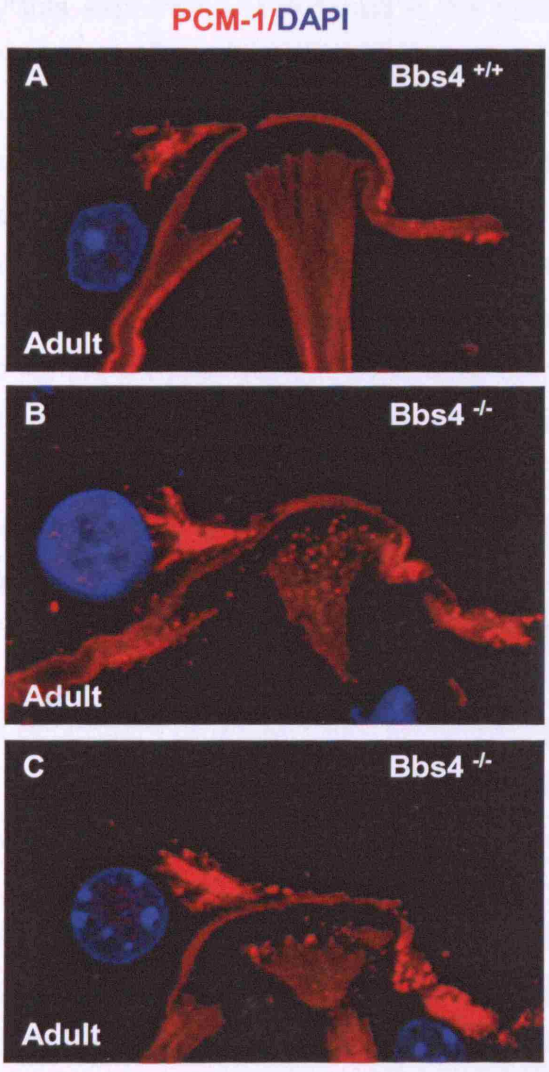

Figure 9.10: PCM-1 staining in *Bbs4*$^{-/-}$ mice. A) In *Bbs4*$^{+/+}$ mice PCM-1 (red) localizes to the microtubules (Fig 9.6) and we see microtubular array like staining at the head of the pillar cells. B, C) In *Bbs4*$^{-/-}$ mice we see accumulation and uneven distribution of PCM-1 at the head of the pillar cells.

9.4 Discussion

9.4.1 Bbs4

The Bbs4 protein was shown to be widely expressed in the murine organ of Corti. In the developing organ of Corti, immunohistochemistry using an antibody raised against Bbs4, showed localization to microtubules of the epithelial cell cytoskeleton, basal bodies and primary cilia. The most striking staining was observed along pillar cell microtubules as they develop. Interestingly this expression is reduced in the mature organ of Corti. During development, Bbs4 is also seen localizing to the apical ends of Kollikers cells.

The association of Bbs4 with cilia and basal bodies is unsurprising as previous localization studies have placed it there, and the association with intraflagellar transport has been described (Kim *et al.*, 2004). However the close association of Bbs4 with the developing microtubules is more intriguing, especially in light of the fact that this expression pattern is closely matched by that of PCM-1 and that PCM-1 is mislocalised in $Bbs4^{-/-}$ mice.

PCM-1 is a component of centriolar satellites within the pericentriolar material. The primary function of pericentriolar material is to nucleate microtubules, which are radially arranged from the centrosomal surface or subsequently released and anchored in other places of the cell. It is thought this microtubule anchoring is dependent on PCM-1 indirectly, through the recruitment of other proteins at the centrosome in a PCM-1 dependent manner (Dammermann and Merdes, 2002).

Another proposed role for PCM-1 is believed to be mediating transport of centrosmal components from the cytoplasm to the centrosome. In this role it is thought to be involved in recruiting proteins necessary for centrosome replication. This has been suggested following observation of the protein in cytoplasmic apical regions of epithelial cells where most of the minus end of microtubules are located. PCM-1 is transported to the centrosome in a microtubule-dependent manner by the dynein-dynactin molecular motor

(Dammermann and Merdes, 2002). As the expression pattern of the protein varies at different stages of the cell cycle, it is plausible that PCM-1 has more than one function (Kubo and Tsukita, 2003).

Kim et al. recently showed that BBS4 localizes to the centriolar satellites of centrosomes and basal bodies and is necessary to recruit PCM-1 to these structures. It is proposed that BBS4 is probably acting as an adaptor protein between PCM-1 and the dynein-dynactin molecular motors. Silencing of BBS4 in cell culture resulted in PCM-1 mislocalisation, loss of microtubule anchoring at the centrosome, defects in cytokinesis and apoptosis (Kim *et al.*, 2004). The mislocalisation of PCM-1 is consistent with findings in cochlea pillar cells, where PCM-1 is also mislocalised in $Bbs4^{-/-}$ mice.

As development of the organ of Corti progresses, Bbs4 is seen to localize to all along pillar cell microtubules as they mature. This staining pattern is mirrored by PCM-1. In adult tissue this is not the case. Expression of Bbs4 is diminished, whilst expression of PCM-1 remains strong. Implicating that whilst both proteins are important for the formation of the microtubule bundles, once established, Bbs4 may no longer be required for maintenance, whilst PCM-1 is required for continued maintenance and function.

Further evidence for the involvement of Bbs4 with microtubule maturation is evident from the staining in the Kollikers organ. In this structure, only found in the developing cochlea, Bbs4 localizes to the apical ends of cells. On a cross section it appears that, as in the pillar cells, Bbs4 is localizing to minus ends of microtubules. By P9 this staining in the Kolliker's cells is gone. Although Kolliker's cells have fewer microtubules than the pillar cells, their bundles are also oriented parallel to their apicobasal axis. It is known that microtubule nucleation in these cells proceeds within the 1-6 day period (Mogensen *et al.*, 1997). By day P9 the Kolliker's cells have bent over to cover the inner hair cells. It is probable that the microtubules in these cells are required for this dynamic cell morphogenesis. If this is so, the network of microtubules must be laid down early, once this process has occurred, proteins involved in the assembly of microtubules would no longer be required.

With the abundant expression of Bbs4 in the cochlea, it is not surprising that all the *Bbs4*$^{-/-}$ mice that we were able to study at were non responsive to a 19.5 kHz tone burst. As with the *Bbs6*$^{-/-}$ mice this hearing loss appears to be progressive as at onset of hearing the one *Bbs4*$^{-/-}$ animal we were able to test did respond. With the strong association with Bbs4 and microtubules we could have expected to see morphogenic abnormalities of these. However electron microscopy carried out on a *Bbs4*$^{-/-}$ cochlea showed that the ultra-structure of the organ of Corti appeared normal, with rigid pillar cells and a patent tunnel of Corti. Further transmission electron micrographs of the pillar cells showed that the apico-basal microtubular arrays appeared normal. Whilst the absence of Bbs4 does not affect the cyto-architecture of cochlea epithelial cells, it is still possible that the protein is involved in its function. Such as optimising/modulating intracellular transport or possibly signaling to neurons.

As with the *Bbs6*$^{-/-}$ animals, we observed malformed and mis-oriented outer hair cell bundles, implicating the involvement of BBS4 with the PCP pathway. The degree of affectedness is not sufficient to cause the auditory phenotype.

One insight into the mechanism of Bbs4 in the cochlea comes from the mislocalisation of PCM-1 in mature pillar cells of *Bbs4*$^{-/-}$ animals. At the head of the outer pillar cells, PCM-1 immunofluoresence occurs in large granules, as opposed to wild-type animals where PCM-1 is evenly distributed along microtubules. This implies, that as the predicted models suggested (see figure 9.1), BBS4 is required for correct PCM-1 localisation and hence function.

It would be interesting to see whether the localization of p150^{glued} subunit of dynein, a further protein known to associate with Bbs4 was also mislocalised in these animals. As opposed to PCM-1, expression of p150^{glued} in the cochlea with the antibody tested is relatively limited and does not correlate strongly with microtubules. However punctuate accumulation in the phalangeal processes of the Dieters cells is reminiscent of MACF1 staining and could contribute to the potential neuronal aspect of the disease (see

chapter 7), bearing in mind that dynein is a molecular motor associated with microtubules.

More detailed analysis of the auditory phenotype in the *Bbs4*$^{-/-}$ mice is required, but such work is hindered by the lack of availability of the animals. Ideally this would consist of auditory brain stem responses, DPOAEs, FM1-43 experiments to establish the function of the bundles, and further protein expression anlysis in knockout tissue. Additionally real-time PCR could be used to qualify any difference in protein expression, for example of PCM-1 in cochlea tissue.

9.4.2 BBS protein localization in the organ of Corti.

The expression of Bbs4 in the cochlea and its association with microtubules is of interest with regard to the observed expression of other BBS proteins in the same model system. In summary we observe that Bbs6 localizes to all basal bodies, and most likely acts as a chaperone (see chapter 7). Bbs2 is restricted to apical microtubules in supporting cells, its function is currently unknown (see chapter 8). And in this chapter we observe that Bbs4 associates with microtubules in the cell body and the cilium, and probably plays a role in protein trafficking (Fig 9.11).

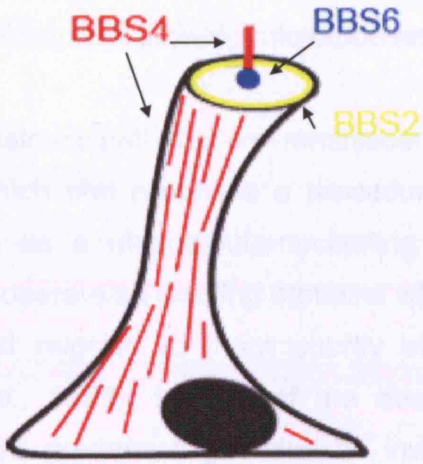

Figure 9.11: Schematic representation of the localisation of Bbs2, Bbs4 and Bbs6 in a mouse inner pillar cell. Bbs6 localizes to all basal bodies. Bbs2 is restricted to apical microtubules in supporting cells. Bbs4 associates with microtubules in the cell body and the cilium.

Such diverse staining patterns for the different BBS proteins suggests that whilst these are part of a similar process, they might have slightly different roles in this tissue. Bbs6 could potentially be part of the microtubule nucleation process, which occurs at the centrosome/basal body. Additionally, being a putative chaperone, and with the latest evidence of its interactions with BBS2, the Bbs6 protein could modify Bbs2 at the centrosome before it localizes to the outer edge of the pillar cells. Bbs4 could possibly act as a MAP (microtubule anchoring protein) to stabilize the microtubules, potentially in association with PCM-1. Furthermore with Bbs2 only localizing to the apical ends of epithelial cells it appears that this protein is not nucleating microtubules, but rather involved in anchoring their minus ends at non-centrosomal sites.

As mutations in any one of the BBS genes cause indistinguishable phenotypes, one would assume BBS proteins to be part of a similar process. Therefore it was surprising to observe varying expression patterns amongst the BBS proteins analyzed in this study. This discrepancy could be resolved if

the roles of these proteins were all interconnected in the same process, namely the stabilization of growing microtubules.

Our observed staining patterns are reminiscent of a model proposed by M Mogensen in which she proposes a procedure by which the pericentriolar region functions as a microtubule-nucleating domain, whilst cell surface-associated sites operate as docking domains which capture the minus ends of microtubules that migrate to them shortly after nucleation (see Fig 9.2) (Mogensen *et al.*, 1997). In light of the observed staining patterns, it is possible that BBS proteins might also be involved in this process. So far ninein has been implicated in this process as a non-nucleating microtubule minus-end stabilizing and anchoring protein (Mogensen *et al.*, 2000). It would be interesting to observe the staining pattern of ninein in the *Bbs4*$^{-/-}$ and *Bbs6* $^{-/-}$ animals to see if this protein is in some way disrupted. Although ninein was not isolated during the course of the BBS4 and BBS6 yeast two-hybrid screens, it would interesting to see if ninein does interact with any of the BBS proteins. Direct interaction studies could include direct interactions through the yeast two-hybrid system, co-immunoprecipitation, GST pulldowns and analysis of co-localisation of protein expression in relevant cell lines and mouse tissues.

A further explanation for the very different expression patterns between the various BBS proteins observed in the murine cochlea among different cell types, could be due to the varying types of microtube networks in different cell types. It is known that there is differential distribution of modified tubulin in the mammalian cochlea (Furness *et al.*, 2005). Post-translational modifications of tubulin suggest that dynamic microtubules are present in sensory cells (such as the inner and outer hair cells), whilst stable microtubules are found predominantly in the supporting cells (pillar cells and Dieter's cells)(Slepecky *et al.*, 1995). These differences contribute to the observed morphological and physiological differences between these cell types. The sensory hair cells are metabolically and mechanically dynamic, as seen in the transport of membranes and neurotransmitters and the changes of the outer hair cells' motility. In contrast the supporting cells contain a structural frame work and

scaffold, relaying stability and rigidity to this organ tissue. The further analysis of which specific types of modified tubulin (for example, tyrosinated, polyglutamylated, acetylated) associate with different BBS proteins could be performed *in vitro*. Such experiments could include co-immunoprecipitation analyses and yeast two-hybrid interactions. The yeast two-hybrid screen using Bbs6 as bait already implicated this protein with both microtubles and actin. And the strong association of Bbs6 with Bbs2, further associated Bbs2 in microtubular processes.

It is observed that BBS proteins are found in many cell types, in particular Bbs6 which appears to be ubiquitous to all cells. Interestingly Bbs6 and Bbs4 knockout animals are still viable and hearing appears normal at onset, leading to the conclusion that in the absence of these proteins other proteins may compensate. Identification of such proteins could lead to the identification of further disease causing genes.

Whist previous work on BBS protein localization has predominantly been on cell lines, here we show expression of these proteins in *in vivo* tissue during a period of dramatic growth and differentiation. It is hoped that these findings can help to establish the role BBS proteins play in other developmental processes. The last few years have seen an explosion in our understanding of many ciliary disorders and studies on BBS have vastly supported such research. The current findings could have implications beyond just that of BBS, such as other ciliary diseases or disorders involving microtubule function.

9.5 Summary

The Bbs4 protein was shown to be associate developing microtubules and basal bodies in the murine organ of Corti. Whilst the *Bbs4*$^{-/-}$ mice appear to have normal hearing at birth, they become non responsive to a 19.5 kHz tone burst over time. The gross cyto-architecture of the *Bbs4*$^{-/-}$ mice cochlear epithelial cells appears normal, but PCM-1 is mislocalised.

Taken together with data from previous chapters we see that Bbs6 is shown to localize to all basal bodies and most likely acts as a chaperone. Bbs2 localisation appears to be restricted to apical microtubules in supporting cells, potentially capturing nucleated microtubules. Bbs4 associates with microtubules and basal bodies, and plays a role in protein trafficking. The results of these studies suggest that BBS proteins play distinct roles in the processes of microtubule nucleation and growth, and are not just restricted to the function of the cilium or basal body.

Chapter 10: BBS and Zebrafish

Aim: To further assess the mechanisms of BBS pathogenesis using the zebrafish as a model organism.

10.1 Introduction

The zebrafish is one of the latest model organisms exploited by researchers as a model system for the study of development and human disease. It boasts many features suitable for both developmental and genetic analysis. Analysis of orthologous *BBS* genes in zebrafish has been carried out and we sought to continue this line of research.

10.1.1 Use of zebrafish as a model organism

The zebrafish (*Danio rerio*), is a fresh water fish originally found in slow streams and rice paddies and the Ganges river in East India and Burma. Since the early 1970's the zebrafish has been used as an excellent model for studies in vertebrate biology. George Streisinger, the 'founding father' of zebrafish developmental and genetic research first began using this organism as a model system in his laboratory at the University of Oregon. With the advent of functional genomics, the zebrafish model has proved itself as a valuable tool in the understanding of genes involved in development and disease. The explosion of both the number of zebrafish researchers and the generation of such genetic information has led to the establishment of a centralised database for the zebrafish community, ZFIN (http://zfin.org). This database includes information on zebrafish mutants, genetic maps, EST databases, publications and zebrafish laboratories.

The following factors contribute to the utility of this small fresh water fish in research. Externally developing embryos are transparent, allowing visual analyses of early developmental processes. The small size of the mature adult (average one inch) allows large numbers of these vertebrates to be maintained in a relatively small space and females can lay more than 200

eggs per week (Zon, 1999). *Danio rerio* is able to bridge the gap between *Drosophila/Caenorhabditis elegans* and mouse/human genetics, allowing work into the development and function of vertebrate-specific features such as kidney, multichambered heart, notochord and neural crest cells. Regions of synteny between human and zebrafish genomes facilitate candidate approaches towards cloning and large scale genetic screens have identified hundreds of mutant phenotypes in various aspects of early development (Driever *et al.*, 1996; Haffter *et al.*, 1996). These aspects provide a forward genetic approach for assigning function to genes, and positioning them in developmental and/or disease-related pathways (Dooley and Zon, 2000). The speed of development of zebrafish embryos (hours not days, compared to mouse), enables rapid turn around of experimentation. Finally, one of the best attributes of the zebrafish is the ease with which physical and genetic manipulations can be carried out. Examples include injection of genetic material, generation of transgenic GFP lines and the ability of analysing cell behaviour *in vivo*.

10.1.2 Using morpholinos to model disease

One of the most common forms of genetic manipulation used in this field of research is targeted gene knockdown. Injection of morpholinos (antisense, morpholino-modified oligonucleotides) has been shown to effectively and specifically inhibit translation in zebrafish (Nasevicius and Ekker, 2000). Morpholinos are chemically modified oligonucleotides with base-stacking abilities similar to those of natural genetic material (Summerton and Weller, 1997). They were initially used to bind to and block translation of mRNA *in vitro*, in tissue cultured cells, but now they have found widespread usage *in vivo*.

Morpholinos function via an RNAse-H-independent, steric block mechanism, and are most commonly used to hinder translation initiation, making *in vivo* targeting highly predictable and reducing non-specific effects (Summerton and Weller, 1997). Translation initiation is blocked in the cytosol by targeting the 5' UTR through the first 25 bases of coding sequence. This technology can also

be used to modify pre-mRNA splicing in the nucleus, by targeting splice junctions. More recently morpholinos have been designed to block miRNA activity, inhibiting maturation and activity of microRNAs. Determination of the specificity of any phenotype can be made either through targeting of the same gene by a second, non overlapping oligo or by RNA rescue. Unlike tissue-restricted limitations found with RNA-based interference, all zebrafish cells readily respond to this technique and it is completely penetrant throughout the first few days of development, during which the body plan is laid down (Nasevicius and Ekker, 2000).

Morpholinos were first used to model human disease when knockdown of the uroporphyrinogen decarboxylase gene by morpholino, recapitulated the phenotype of hepatoerythropoietic porphyria in the zebrafish (Nasevicius and Ekker, 2000). Since then thousands of papers have been published, demonstrating the usefulness of morpholinos for both single and multiple gene knockdown for the understanding of vertebrate embryonic development and disease (http://www.gene-tools.com/Publications/).

10.1.3 Zebrafish models of BBS

The use of zebrafish to study the effect of BBS genes was first described in 2005 (Ross *et al.*, 2005). *Bbs* genes had been implicated in the PCP signalling pathway in the mouse and further evidence of their developmental role was sought in another model organism. In the mouse, PCP genes play a vital role in convergent extension (CE) processes during gastrulation. Such defects also occur in zebrafish with mutations in PCP genes such as *trilobite* (*tri*, a mutation of *vangl2*), resulting in the phenotypic shortening and widening of the body axis. Defective neurulation and neural cell adhesion are also common phenotypes associated with disruption of the PCP pathway (Torban *et al.*, 2004). Homozygous *tri* mutants have defective gastrulation movements and posterior migration of hindbrain neurons (Jessen *et al.*, 2002). Disruption of the zebrafish *bbs* orthologs (*bbs4* and *bbs6*) in homozygous *tri* resulted in an enhanced convergents extension phenotype. Compared with uninjected homozygous *tri* mutants they had more severe body axis compression,

compressed somites, a wider presumptive neural tube and a shorter relative distance between rhombomere 5 and the first somite (Ross *et al.*, 2005). These data provided strong evidence that *bbs* genes interact genetically with *vangl2* in zebrafish further implicating the involvement of *BBS* genes in the PCP pathway.

Bardet-Biedl syndrome morpholinos in zebrafish (*bbs4, bbs6* and *bbs1*) also showed dosage dependent phenotypes during somitogenesis (Badano *et al.*, 2006). Severely affected embryos showed dorsal thinning and shorter body length. By 12 somite stage the notochord was kinked and sometimes twisted, accompanied by widening of the somites. Cell detachment was also observed along the neural tube, most frequently in the head and tail regions (Badano *et al.*, 2006). These defects were reminiscent of the neurulation and neural cell adhesion defects observed in PCP mutants, and were consistent with the previously observed genetic interaction between *bbs* genes and the PCP pathway. Similar results were observed with morpholinos against *bbs4, bbs6* and *bbs1* but with descending levels of severity (Badano *et al.*, 2006).

In the same study the epistatic effect of a genetic modifier of the disease *mgc1203* was ascertained. The identification of this gene and its involvement in BBS is discussed in chapter four. Morpholino injection against *mgc1203* resulted in a phenotype that overlapped that of the *bbs* gene knockdown. Double morpholino injections with *mgc1203* and any of the *bbs* genes (*bbs1*, *bbs4*, *bbs6*) enhanced this phenotype, however the most pronounced effect was seen with knockdown of *mgc1203* and *bbs1*(Badano *et al.*, 2006). Mutations in *mgc1203* alone have never been shown to be sufficient to cause BBS, suggesting that this gene behaves as a modifier of the disease (see chapter four for more details).

In continuation of this work, we chose to further investigate the effect of another *bbs* gene in zebrafish. *bbs8* was chosen as it is one of the better characterised bbs genes and because of its sequence homology to *bbs4,* the most extensively studied BBS gene to date.

10.2 Materials and Methods

10.2.1 Embryo culture and zebrafish stocks

Zebrafish, *Danio rerio*, were maintained by the UCL Fish Facility as described in section 2.2.10.1. Embryos were collected from matings, cultured and staged by developmental time and morphological criteria. TL wild-type, *trilobite* (*tri*) allele^{m209} and *smoothened* (*smo*) animals were used for analyses. Mutant embryos were obtained by incrossing heterozygous carriers.

10.2.2.Morpholino antisense oligonucleotide injection

Morpholino antisense oligonucleotides, designed and synthesised by Gene Tools (Oregon), were used to knock-down the function of *bbs5* and *bbs8*. For more details see section 2.2.10.2. Morpholinos were injected into the yolk just under the blastoderm of 1-2 cell stage embryos or into the centre of the yolk at midblastula stages. 1 nl volume of varying dilution was delivered using a micro-injector.

10.2.3 RNA *in situ* localisation and immunohistochemistry

For whole-mount *in situ* localisation, embryos were fixed in 4% paraformaldehyde prior to hybridisation. Riboprobes were synthesised from linearised DNA templates using a digoxygenin RNA-labeling kit (Roche). For more details see section 2.2.10.3. Probes were made from plasmid clones donated by Steve Wilson, UCL, or acquired from GeneService, Cambridge.

For immunohistochemistry of the Kupffer's vesicle, embryos were fixed at eight somite stage in 80%MeOH and 20%DMSO. Immunolocalisation of the cilia was performed using primary antibodies against α-acetylated tubulin. Primary antibodies were detected using a tagged anti-mouse secondary antibody conjugated with Alexa Fluor 488. Embryos were dissected to expose the Kupffer's vesicle prior to imaging. For more details see section 2.2.10.4.

10.2.4 Imaging

Embryos were imaged using a digital camera (Zeiss Axio Cam MRm) and images processed using Adobe Photoshop. Animals were oriented in 3% methyl cellulose or 70% glycerol for orientation. Images were processed using Adobe Photoshop. A Lecia Confocal microscope was used for confocal microscopy imaging of the Kupffer's vesicle. Images were processed using Volocity (Improvision) software. For more details see section 2.2.10.5.

10.3 Results

10.3.1 *bbs8* expression in wild-type embryos

In situ hybridisation using a probe against *bbs8* was used to determine the expression pattern of *bbs8* in developing wild-type embryos.

During earlier stages of development, we observe a gradual increase of ubiquitous *bbs8* expression (Fig 10.1). At tailbud stage this was relatively weak, and no specific localisation is detected (Fig 10.1 A). By 4 somites it was still fairly weak, however a possible increase of expression could be seen in the developing head region (Fig 10.1 B). At 18 somites the *bbs8* transcript hybridises throughout the embryo. We see stronger levels of transcript in the head region, specifically in the eye. The tip of the tail also appears to have slightly stronger expression than the rest of the embryo (Fig 10.1 C). Parallel control *in situs* carried out with a *bbs8* sense probe show no detectable background.

At 24 hpf *bbs8* transcripts appeared to be ubiquitously expressed, with accumulation along the tail, in particular around the tip, and in the head region of the embryo (Fig 10.2). We see upregulated expression of the somites and highest expression was detected in the eye. Higher levels are also detected in the brain. In comparison, hybridisation with the control *bbs8* sense probe was negative.

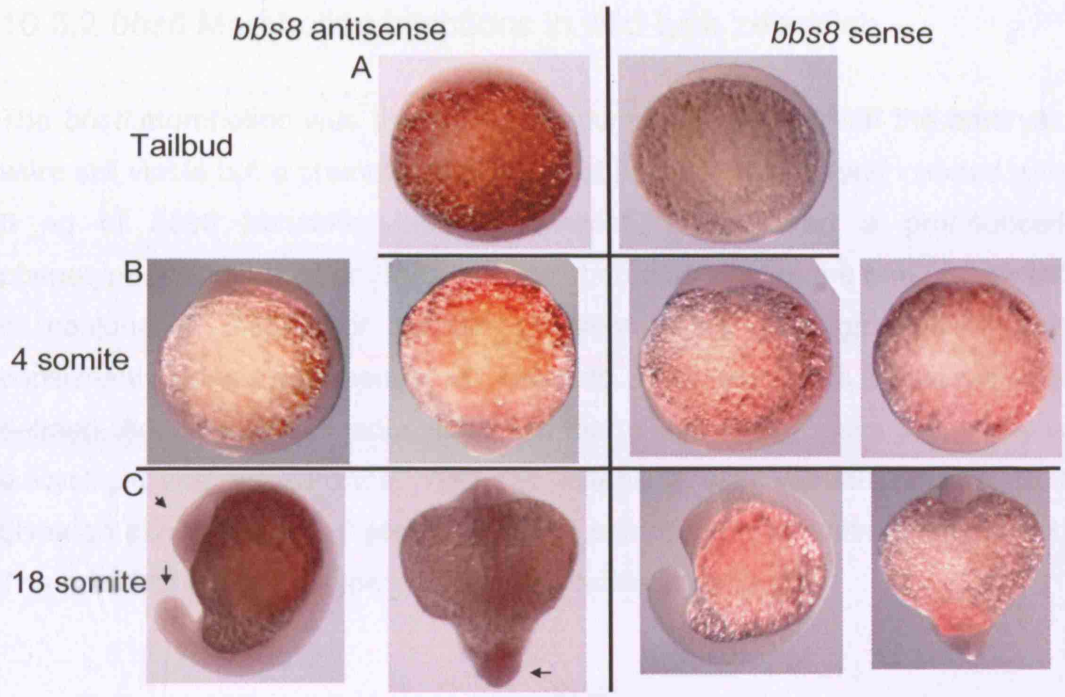

Figure 10.1: *In situ* hybridisation of *bbs8* in developing wild-type zebrafish. As development progresses *bbs8* becomes more ubiquitously expressed in the wild-type embryo. Accumulation around the head and tail region is detected in the later stages (C, arrows). Lateral view (left) and ventral view (right) of 4 and 18 somite stage embryos.

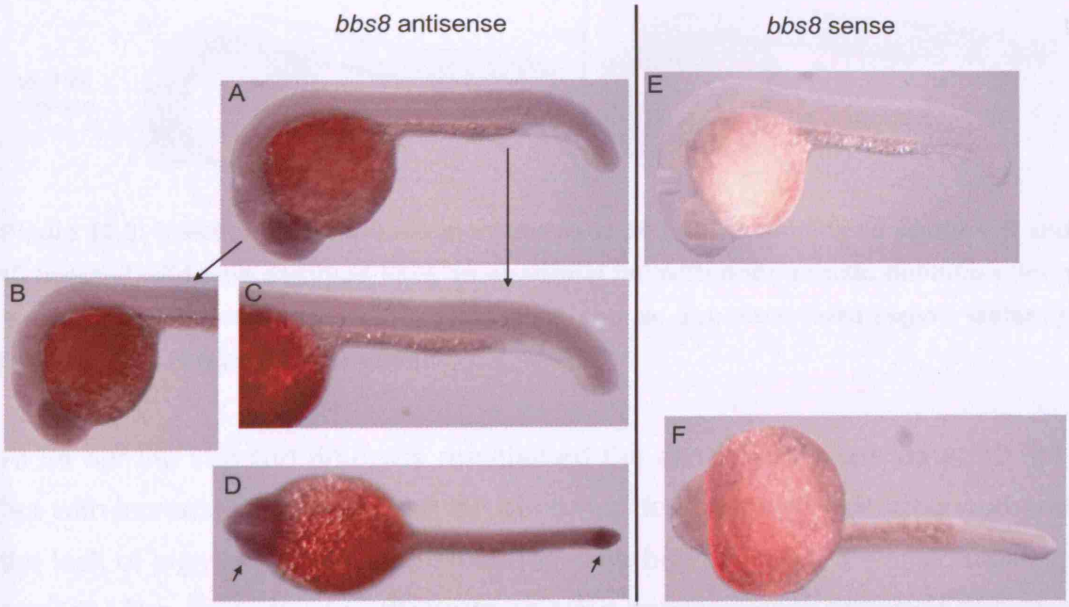

Figure 10.2: *In situ* hybridisation of *bbs8* in 24 hpf wild-type zebrafish. A,B,C,D) *bbs8* is ubiquitously expressed in the wild-type embryo. Stronger expression is observed in the head region (eye and brain) and in the tail (particulary the tip). E,F) Control *in situ* hybridisation using a *bbs8* sense probe is negative for *bbs8* expression. A,B,C,E lateral view, D,F ventral view, anterior is to the left.

10.3.2 *bbs8* Morpholino injections in wild-type zebrafish

The *bbs8* morpholino was titrated to an optimum dose at which the embryos were still viable but a phenotype could be observed. All embryos injected with 6 ng of *bbs8* translation-blocking morpholino exhibited a pronounced phenotype. At 30 hpf all embryos had an abnormal 'kink' at the end of their tail in conjunction with poor somitic definition. Lack of pigmentation was consistently observed amongst all embryos. Brain ventricles appeared less defined. Additionally the reduced size of the telencephalon gave the embryos a 'cyclopic like' appearance. Yolk sac extension was variable. Figure 10.3 gives an example of two injected embryos compared to an uninjected control. The extent of the phenotype was variable amongst embryos.

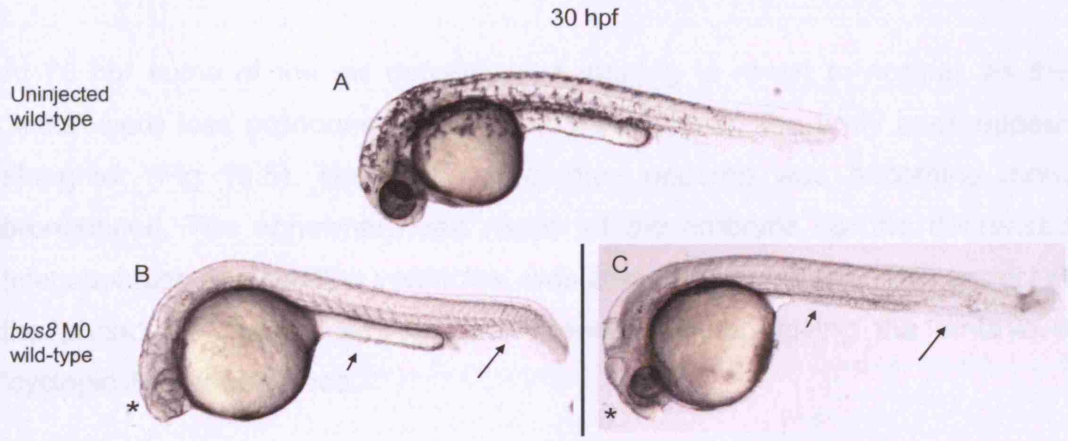

Figure 10.3: Injection of 6 ng *bbs8* morpholino at 30 hpf. A) Uninjected control. B and C) Injected wild-type embryos have an abnormal tail with poor somitic definition (long arrow), variable yolk extension (short arrow) and an abnormal head region (asterix). Pigmentation is markedly reduced.

At 54 hpf the injected embryos maintained the same phenotype as at 30 hpf, but with increased severity. The tail abnormalities were more pronounced and the lack of pigmentation was maintained. The brain ventricles were becoming swollen. The abnormal somitic segmentation became more apparent and was accompanied by a discontinued spinal chord. Additionally, cardiac oedema began to emerge (Fig 10.4).

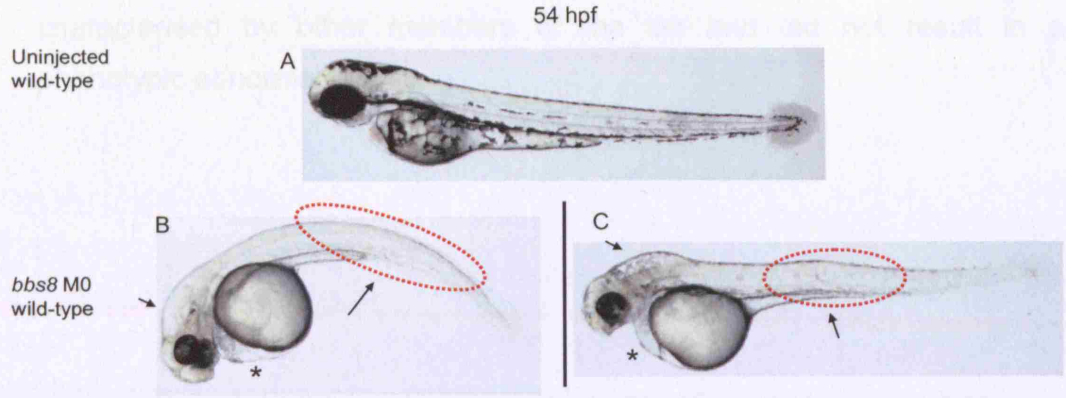

Figure 10.4: Injection of 6 ng *bbs8* morpholino at 54 hpf. A) Uninjected control. B,C) The phenotype of injected wild-type embryos is similar to before but with increased severity. Abnormal tail regions with poor somitic definition (long arrow), swollen ventricles (short arrow) and lack of pigmentation. Additionally cardiac oedema is beginning to emerge (asterix).

At 78 hpf some of the tail defects were starting to revert to normal, as the 'kinks' were less pronounced and in some embryos, the body axes appear straighter (Fig 10.5). However the cardiac oedema was becoming more pronounced. The abnormal head region of the embryos i.e. the decreased telencephalon and swollen ventricles, was also more apparent. This aspect of the phenotype made the eyes look closer together, giving the embryo a 'cyclopic like' appearance.

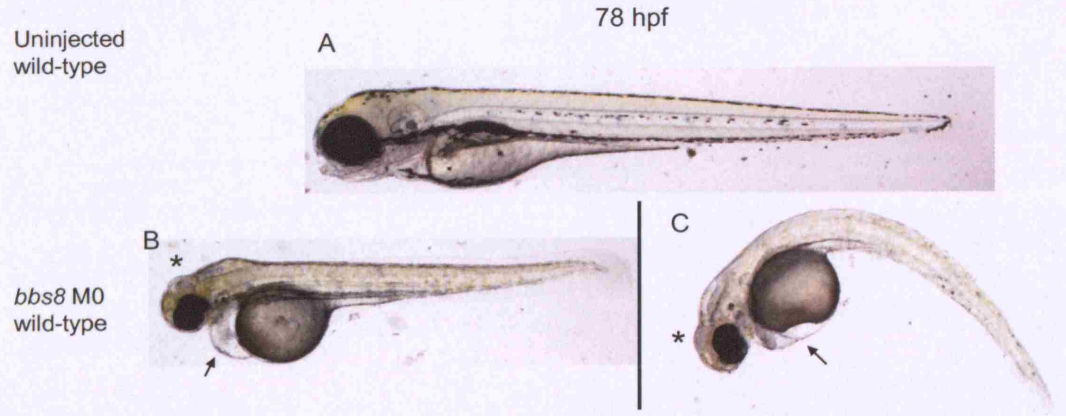

Figure 10.5: Injection of 6 ng *bbs8* morpholino at 78 hpf. A) Uninjected control. B,C) The cardiac edema is more pronounced (arrow), and the abnormal head region makes the embryo look 'cyclopic like' (asterix).

Injection of equal levels of scrambled morpholino (control) was previously characterised by other members of the lab and did not result in any phenotypic abnormalities.

10.3.3 Further analysis of *bbs8* in the zebrafish

To get a clearer picture of the extent of the abnormalities in the head region, expression of specific brain markers was analysed in the injected embryos. Since the phenotype of the *bbs8* morpholino resembled that of sonic hedgehog (shh) mutants, we tested for genetic interactions between *bbs* genes and the shh pathway. Previous studies had also demonstrated genetic interactions between *bbs* genes and the PCP pathway, these experiments were repeated using the *bbs8* morpholino.

10.3.3.1 *In situ* hybridization of *eng2a*, *shh* and *emx1* in wild-type vs *bbs8* morpholino injected embryos.

engrailed 2a (*eng2a*), is one of the best characterised homeoproteins involved in anterior/posterior patterning. It is used as a marker for the midbrain hindbrain boundary. Whilst the anterior line of this marker appears slightly diffuse and not as 'straight' in the *bbs8* mo (6 ng) injected 24hpf embryos compared to uninjected, the expression pattern is not dramatically different (Fig 10.6). Further staining of the muscle pioneers is not different between the injected and control embryos.

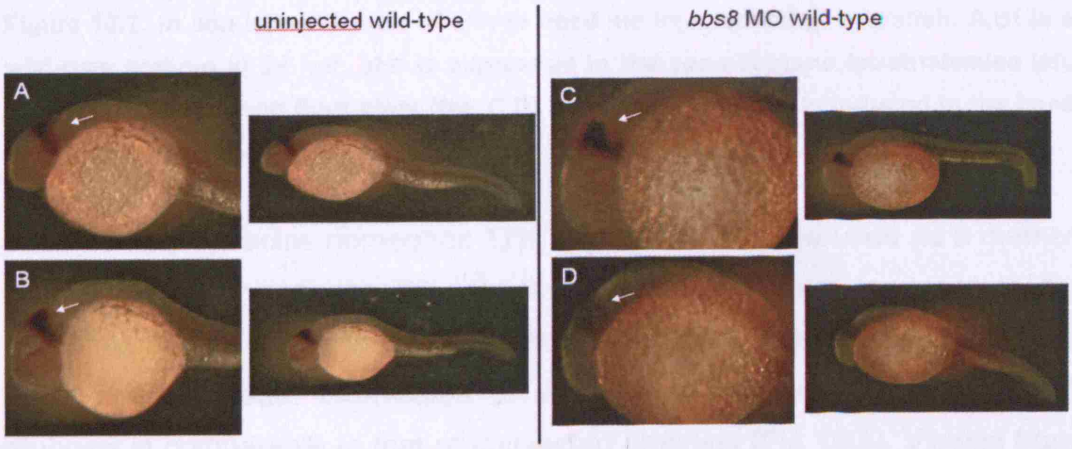

Figure 10.6: *In situ* hybridisation of *eng2a* in *bbs8* mo injected 24hpf zebrafish. Expression of *en2a* in *bbs8* mo injected embryos (C,D) is not obviously different from control (A,B). Arguably marker definition is slightly less pronounced in the injected embryos (white arrows).

In a wildtype 24 hpf embryo, the *shh* (sonic hedgehog) transcript is a marker for the hypothalamus and the zona limitans intrathalamica (zl) (Fig 10.7). This later structure refers to the border between the dorsal and ventral thalamus. This transcript is also expressed along the floor plate. Expression of *shh* in the *bbs8* mo (6 ng) injected 24hpf embryos is not markedly different from the control. However the level of expression at the zl appears reduced and does not extend as far as in the uninjected embryos.

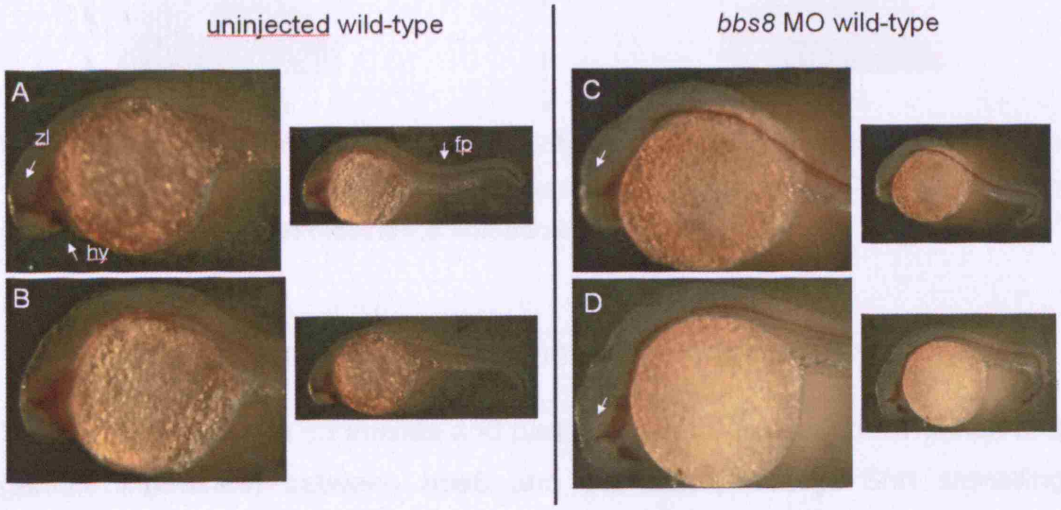

Figure 10.7: *In situ* hybridisation of *shh* in *bbs8* mo injected 24hpf zebrafish. A,B) In a wild-type embryo at 24 hpf, *shh* is expressed in the zona limitans intrathalamica (zl), hypothalamus (hy) and floor plate (fp). C,D) Expression at the zl is reduced in the bbs8 mo (6 ng) injected embryos (white arrows).

emx1 (empty spiracles homeobox 1) is a homoeobox gene used as a marker for the telencephalon. As this structure in the forebrain appeared to be misshapen in the *bbs8* morpholino injected animals, the expression pattern of *emx1* was analysed. Expression of *emx1*, from a lateral view of injected embryos is comparable to that of uninjected embryos (Fig 10.8). Viewed from the ventral side of the embryo *emx1* expression is still comparable, however, the disrupted head region means that the telencephalon is closer to the yolk sac in injected embryos. The additional staining in the injected embryo could possibly be localising to the hypothalamus.

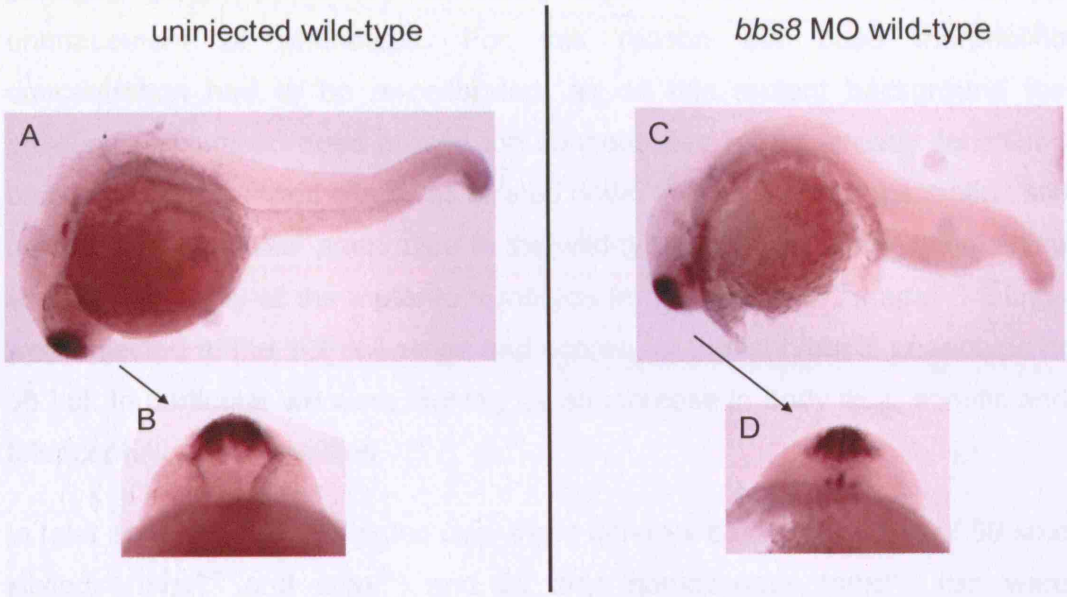

Figure 10.8: *In situ* hybridisation of *emx1* in *bbs8* mo injected 24hpf zebrafish. A,B) In a wild-type embryo at 24 hpf, *emx1* is expressed in the telencephalon. C,D) In a *bbs8* mo (6 ng) injected embryo expression is comparable.

10.3.3.2 Injection of *bbs8* morpholino into *smo* zebrafish.

In view of these brain anomalies and partial cyclopia, we sought evidence of a genetic interaction between bbs8 and the shh pathway. Shh signalling depends on the smoothened receptor (smo), which tranduces the signal intracellularly. Homozygous mutant *smo* zebrafish display characteristic phenotypes of a shh signalling deficiency, including U-shaped somites and curled body axis, cyclopia and cardiac oedema (www.zfin.org). These overlapped with the phenotypes arising from *bbs8* knockdown in wild-type zebra fish. Heterozygous *smo* fish are phenotypicaly indistinguishable from wild-type, but if *bbs8* interacts with the shh pathway, these should be discernable upon injection of the *bbs8* morpholino. Additionally on the homozygous *smo* background, injection of *bbs8* morpholino should enhance the phenotype.

bbs8 morpholino was injected into *smo* zebrafish to see if the phenotype of *smo* mutants was altered or enhanced. 6 ng *bbs8* morpholino, the original

concentration, resulted in the death of the majority of the embryos. All embryos looked particulary unhealthy after injection, but there was no enhnacement of phenotype. For this reason the *bbs8* morpholino concentration had to be re-calibrated, as on this mutant background the previously optimised dose proved too concentrated for an already sensitised background. The morpholino was titrated down to 3 ng. This concentration still produced a '*bbs8* like' phenotype in the wild-type embryos, whilst maintaining structural integrity of the mutants. Embryos from three $smo^{-/+}$ x $smo^{-/+}$matings were injected at the 1-2 cell stage and scored for the 'shh/bbs8' phenotype at 30 hpf. In particular we were looking for an increase in body axis, somitic and telencephalic abnormalities.

In total three batches, collected over three different days, consisting of 59 *smo* siblings ($smo^{+/+}$ and $smo^{-/+}$) and 25 *smo* homozygous ($smo^{-/-}$) fish were injected and cultured for 30 hours. After injection, both $smo^{-/-}$ and $smo^{-/+}$ showed an identical phenotype to that of *bbs8* morphants. There was no evidence of increased severity or penetrance of the bbs8 phenotype in the *smo* haploinsufficient embryos. Furthermore 25/25 $smo^{-/-}$ fish also showed no enhancement of the smoothened phenotype with the *bbs8* morpholino knock down (Fig 10.9). This suggests there is no epistasis between *bbs8* and the shh pathway.

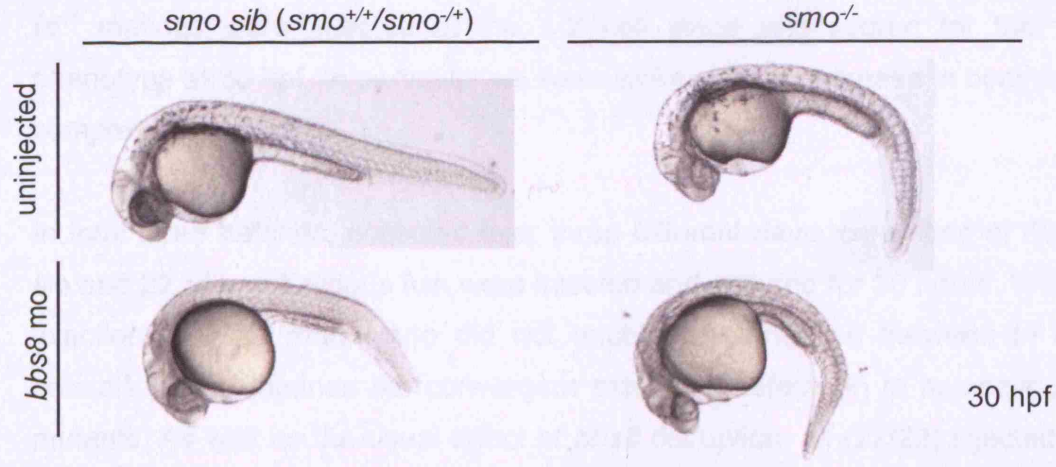

Figure 10.9: Injection of *smo* zebrafish with *bbs8* morpholino. Injection of 3 ng *bbs8* morpholino on the $smo^{+/+}/smo^{-/+}$ and $smo^{-/-}$ background does not enhance the phenotypic severity of the *smo* animals. Additional defects seen after injection are due to *bbs8* disruption, being additive and not synergistic.

10.3.3.3 Injection of *bbs8* morpholino into *tri* zebrafish.

Previous studies had implicated the *bbs* genes in the PCP pathway. PCP mutants in zebrafish display convergent extension defects. Trilobite (*tri)* zebrafish have a mutation of *vangl2*, the ortholog of *Ltap* (Looptail) in the mouse. Injection of *bbs4* and *bbs6* morpholino was shown to enhance the convergent extension defects in $tri^{-/-}$ zebrafish, increasing the severity of body axis compression, suggesting that these *bbs* genes interact genetically with *vangl2* in the zebrafish (Ross *et al.*, 2005).

As with the *smo* mutants, heterozygous (+/-) *tri* fish are phenotypically indistinguishable from wild-type (+/+), they are collectively referred to as *tri* 'sib', to distinguish them from *tri* homozygous (-/-) embryos. If *bbs8* interacts with the PCP pathway, *tri* sib embryos should be discernable upon injection of the *bbs8* morpholino. Additionally on the homozygous *tri* background, injection of *bbs8* morpholino should enhance the phenotype.

bbs8 morpholino was injected into *tri* zebrafish to see if the phenotype of *tri* mutants was altered or enhanced. The morpholino was titrated to 4 ng. This concentration produced a '*bbs8* like' phenotype in the wild-type embryos, whilst maintaining structural integrity of the mutants. Embryos from three $tri^{-/+}$ x $tri^{-/+}$ matings were injected at the 1-2 cell stage and scored for the '*tri*' phenotype at 30 hpf. In particular we were looking for an increase in body axis compression.

In total three batches, collected over three different days, consisting of 59 *tri* sib and 22 *tri* homozygous fish were injected and cultured for 30 hours. Whilst injection of *bbs8* morpholino did not enable differentiation between *tri* sib animals, it did enhance the convergent extension defects in *tri* homozygous mutants. As well as the usual effect of *bbs8* disruption, all (22/22) injected *tri* homozygotes had more severe body axis compression than usually observed (Fig 10.10).

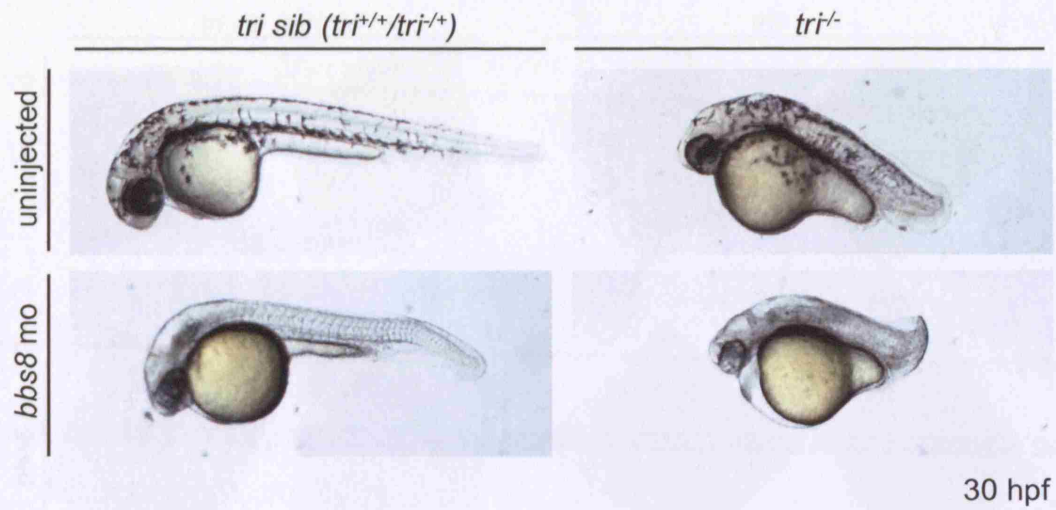

Figure 10.10: Injection of *tri* zebrafish with *bbs8* morpholino. Injection of 4 ng *bbs8* morpholino on the wild-type and *tri* background. Injected homozygous *tri* mutants had more severe body axis compression than usually observed.

Because this enhanced body axis compression could have arisen through a number of different processes, the somites and rhombomeres of early stage embryos (eight somites) were examined. Embryos were injected with two concentrations of *bbs8* morpholino (4 ng and 6 ng) and fixed at eight somites. *In situ* hybridisation was carried out using markers *myoD* and *krox20*, which show the shape of the somites and the position and shape of rhombomeres 3 and 5, respectively. Both morpholino concentrations gave similar results. Expression of both markers in tri sib embryos was not affected by injection of *bbs8* morpholino at 4 or 6 ng, at this stage. However, homozygous *tri* mutants injected with *bbs8* morpholino had more severely compressed somites, a wider presumptive neural tube, and a shorter relative distance between rhombomere 5 and the first somite compared with uninjected homozygous *tri* mutants (Fig 10.11), indicating that the body axis compression results from an enhancement of abnormal convergent extension movements during gastrulation.

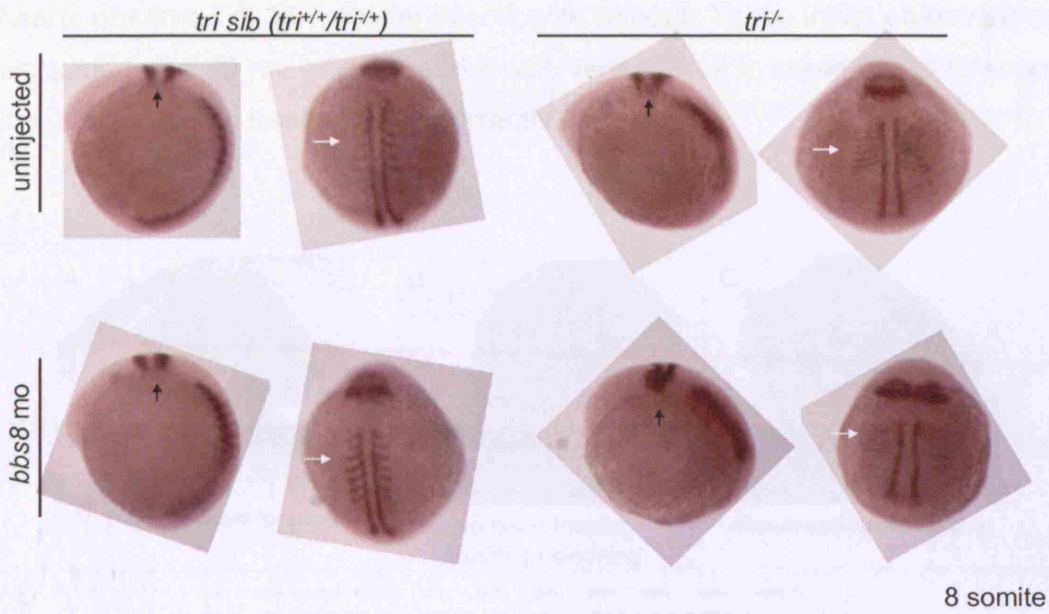

Figure 10.11: Expression of *myoD* and *krox20* in zebrafish with *bbs8* morpholino injection. Lateral views (left) and dorsal views (right) of eight-somite embryos. Injected wild-type embryos were no different from uninjected. Homozygous tri embryos injected with *bbs8* morpholino had more severe convergent extension defects than uninjected embryos. As evidenced by compressed somites and a wider presumptive neural tube (white arrows) and a shorter distance between rhombomere 5 and the first somite (black arrows).

10.3.3.4 Laterality defects in *bbs8* morphant *tri* zebrafish

Abnormal heart looping at 30 hpf was observed in the *tri* zebrafish when injected with *bbs8* morpholino. In some cases the heart tube was straight (no looping) and in others we observed reversed heart looping (Fig 10.12). 98.6% (77/78) of uninjected *tri* sib embryos were normal, however after injection of 6 ng *bbs8* morpholino only 86% (60/70) were normal, after injection of 4 ng *bbs8* morpholino only 75% (12/16) were normal.

The effect on *tri* homozygous embryos was more striking. 84% (16/19) of uninjected animals were normal, but only 38% (8/21) after injection of 6 ng *bbs8* morpholino and 50% (3/6) after injection of 4 ng *bbs8* morpholino were normal. There did not appear to be a dosage correlation between number of effected embryos and *bbs8* morpholino concentration. The graph shown in figure 10.12 D is a quantitative representation of the percentage of abnormal

hearts observed at 30 hpf after injection or without. These initial observations were made on 30 hpf animals and it was very difficult in some cases to score the position of the beating heart correctly.

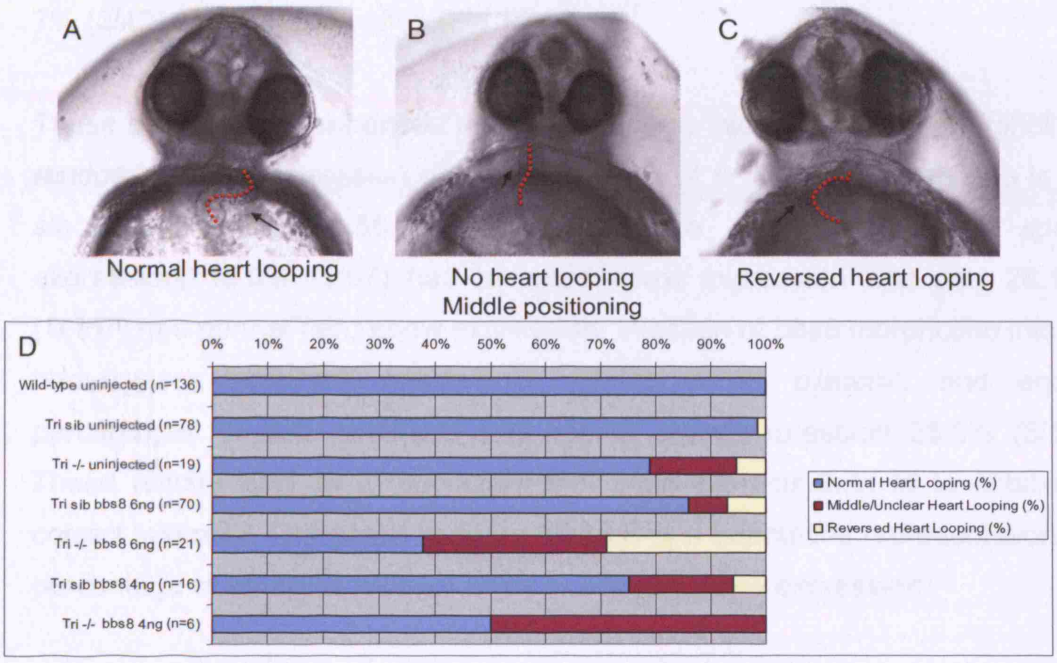

E

Condition	n	Heart looping (%) Normal	Heart looping (%) Middle/Unclear	Heart looping (%) Reversed
Wild-type (uninjected)	136	100	0	0
Tri sib (uninjected)	78	98.6	0	1.4
Tri -/- (uninjected)	19	78.9	15.8	5.3
Tri sib (bbs8 6 ng)	70	86	7	7
Tri -/- (bbs8 6 ng)	21	38	33	29
Tri sib (bbs8 4 ng)	16	75	19	6
Tri -/- (bbs8 4 ng)	6	50	50	0

Figure 10.12: Heart looping in 30hpf embryos. A,B,C) Normal heart looping is seen on the left hand side of an embryo (ventral view) (arrow). In some cases no looping was observed, just the aortic tube down the centre of the embryo (arrow B). Some embryos exhibited reversed positioning of the heart looping, with the aortic tubing curved to the right (arrow C). D) Quantative representation of percentage abnormal hearts observed at 30 hpf. The fractions of embryos of each category are noted in percent along the x-axis. E) Table of data represented in D.

For a more definitive measure of laterality *in situ* hybridisation using a probe against *southpaw* (*spaw*) was carried out on 15-16 somite stage embryos. *Spaw* is a *nodal*-related gene expressed in the left lateral mesoderm. We observed laterality defects in *bbs8* injected zebrafish as injection caused bilateral *spaw* expression in 46.5% (20/43) or reversed *spaw* expression in 7% (3/43) wild-type zebrafish (Fig 10.13).

These defects were enhanced in *tri* zebrafish, as injection of *bbs8* morpholino randomised the expression of *spaw*. Injection of 6 ng *bbs8* morpholino in *tri* sib embryos led to 56.1% (32/57) embryos displaying bilateral *spaw* expression, 15.8% (9/57) had reversed *spaw* expression and only 28.1% (16/57) had normal (left) spaw expression. Injection of *bbs8* morpholino into *tri* homozygous embryos resulted in 47.4% (9/19) bilateral, and equal percentages of both reversed and normal spaw expression 26.3% (5/19) These results lead us to speculate that *bbs8* interacts with *tri* to establish correct laterality. The graph in figure 10.13 D is a quantative representation of percentage of embryos with left, right or bilateral *spaw* expression.

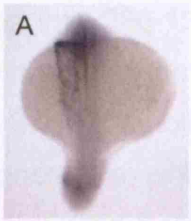

Left *spaw* expression

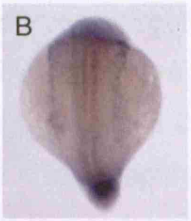

Bilateral *spaw* expression

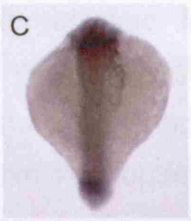

Right *spaw* expression

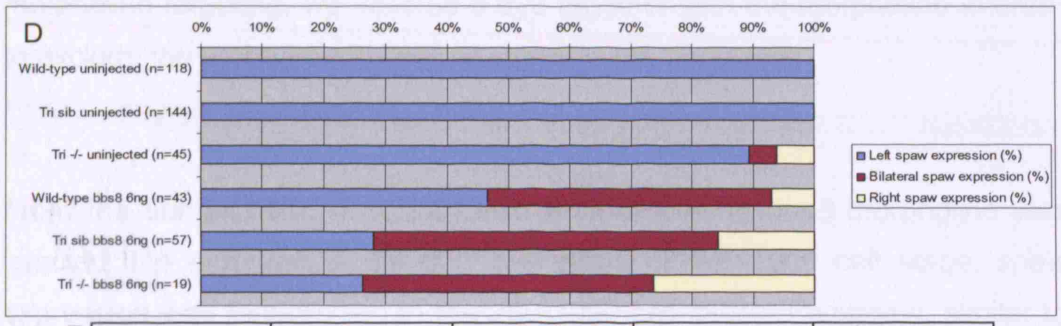

E

Condition	n	*spaw* expression (%) Left/Normal	*spaw* expression (%) Bilateral	*spaw* expression (%) Right/Inverted
Wild-type (uninjected)	118	100	0	0
Tri sib (uninjected)	144	100	0	0
Tri -/- (uninjected)	45	89.1	4.4	6.2
Wild-type (*bbs8* 6 ng)	43	46.5	46.5	7
Tri sib (*bbs8* 6 ng)	57	28.1	56.1	15.8
Tri -/- (*bbs8* 6 ng)	19	26.3	47.4	26.3

Figure 10.13: *spaw* expression in 15-16 somite embryos. *bbs8* morpholino causes randomised expression of *spaw* in *tri* embryos. A,B,C) Normal *spaw* expression is observed on the left hand side of an embryo (dorsal view). In *bbs8* injected embryos we observe bilateral (B) and inverted (C) *spaw* expression. D) A schematic representation of percentage of embryos with left, right or bilateral *spaw* expression. Injection of *bbs8* morpholino caused bilateral *spaw* expression in wild type embryos. *spaw* expression was randomised following injections on the *tri* mutant background. E) Table of data represented in D.

10.3.2.6 Laterality is caused by Kupffer's vesicle defects

The Kupffer's vesicle in zebrafish is a ciliated organ responsible for the establishment of left-right asymmetry in the early embryo. It is the equivalent of the embryonic node found in mammals. The cilia found within the Kupffer's vesicle are responsible for generating a fluid flow across this organ and play a similar role in establishing the left-right axis of a developing embryo, as do the node monocilia in mice. To evaluate whether our observed laterality defects

were caused by disruption to the Kupffer's vesicle, *bbs8* morpholino was injected into 250-1000 cell embryos, directly into the yolk sac. Morpholino injection at this stage specifically targets the Kupffer's vesicle (Bisgrove *et al.*, 2005). The morpholino diffuses throughout the yolk and is taken up by dorsal forerunner cells, which form the ciliated epithelium within the Kupffer's vesicle, but is excluded from the rest of the embryo. In order to confirm specificity of morpholino targeting, we injected a dye together with the morpholino in order to exclude the embryos with leaked signal in the body axis.

From the same batch of *tri* zebrafish embryos, 4 ng *bbs8* morpholino was injected into embryos at either 1 cell stage or 250-1000 cell stage. *spaw* expression was randomised in the 250-1000 cell injected embryos, similar to the 1 cell injected embryos (Fig 10.14). This suggested that laterality defects were in part due to disruption at the Kupffer's Vesicle.

A

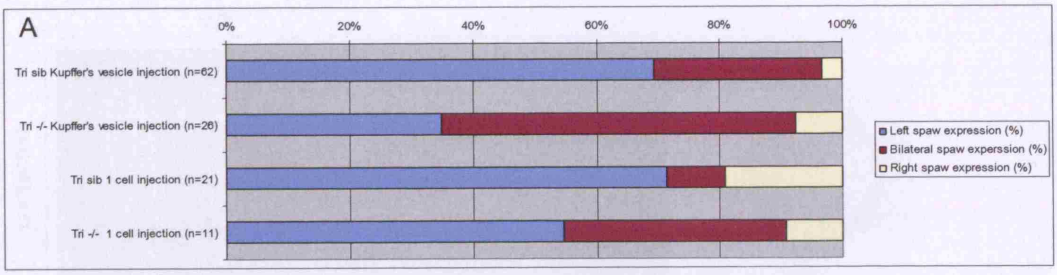

B

Condition	n	*spaw* expression (%) Left/Normal	*spaw* expression (%) Bilateral	*spaw* expression (%) Right/Inverted
Tri sib KV injection	62	69.4	27.4	3.2
Tri -/- KV injection	26	34.8	57.6	7.6
Tri sib 1 cell injection	21	71.4	9.5	19.0
Tri -/- 1 cell injection	11	54.6	36.3	9.1

Figure 10.14: Kupffer's vesicle injection vs 1 cell injection. A) Quantative representation of spaw expression after tri embryos injected at 1 cell stage vs 1000 cell stage (targeting the Kupffer's vesicle). Expression was randomised under both conditions. B) Table of data represented in A.

To further evaluate the effect of the *bbs8* morpholino at the Kupffer's vesicle, immunohistochemistry with an antibody against α-acetylated tubulin was carried out on 16 somite stage embryos to visualise the cilia. At this stage the Kupffer's vesicle appears as a hollow sphere lined with long cilia. Results are

shown in figure 10.15. We observed that injection of *bbs8* morpholino decreased the length of individual cilia, whilst the *trilobite* mutant background reduced the total number of cilia. This was qualitatively observed in n=21 embryos, but not quantified.

In very preliminary experiments, n=1 of each class of embryo, cilia length and number were precisely quantified. These measurements are ongoing to supply statistically significant data. However, based on these very early measurements, it appears that injection of *bbs8* morpholino decreased the length of individual cilia from an average of 18 µm in the uninjected wild-type to 9.7 µm in the injected wildtype embryo. The *trilobite* mutant background reduced the total number of cilia observed at the Kupffer's vesicle from 71 in the uninjected wild-type compared to 45 in the uninjected homozygous *trilobite* embryo. Combination of the two (injection of *bbs8* morpholino on the *tri* mutant background) resulted in a severe reduction in number and cilia length (23 cilia average lenths 4.3 µm).

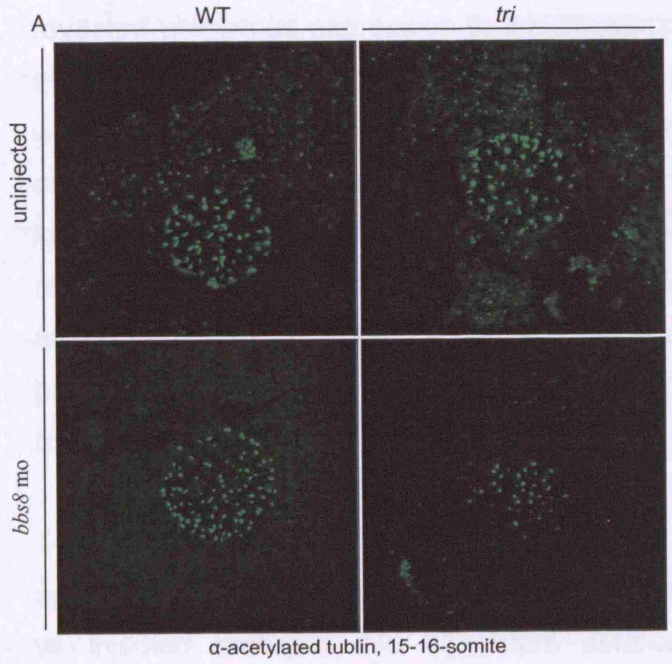

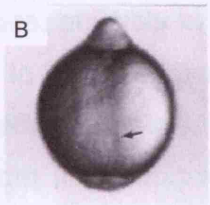

C	Number of cilia	Average cilia length (µm)
WT uninjected	71	18
WT bbs8 6 ng	69	9.7
tri -/- uninjected	45	8
tri -/- bbs8 6 ng	23	4.3

Figure 10.15: Visualisation of Kupffer's vesicle cilia in 16 somite embryos. A) Immunohistochemistry using an antibody against α-acteylated tubulin. B) Localisation of the Kupffer's vesicle organ in embryos at this developmental stage. C) Table with average number of cilia and cilia length.

10.4 Discussion

The use of targeted gene knockdown by morpholino injection in zebrafish, shed more light on the role of *bbs8* in this vertebrate model system. Injection of *bbs8* morpholino into one cell-stage wild-type zebrafish embryos produces a pronounced phenotype. We observe severe disruption to body axis and abnormal cranial and facial reduction. Injected embryos also develop cardiac oedema, which appears to worsen over time. Additionally these embryos all display a lack of pigmentation. Injection of equal concentrations of scrambled/mismatched morpholino was carried out by other members of the lab (J. Tobin, M.Kai) and resulted in no detectable phenotype. Importantly, work also done by other members in the lab have shown that co-injection with *bbs8* mRNA reversed these phenotypes, confirming specificity of the morpholino.

Initial *in situ* hybridization using a probe against *bbs8 on* wild-type embryos revealed ubiquitous expression in the developing embryo, becoming stronger over time and localizing to the head and tail regions, possibly in concordance with the craniofacial and body axis abnormalities. In hindsight, we would have expected to see expression of *bbs8* at the Kupffer's Vesicle, due to *bbs8* knock down affecting the cilia in this organ. From these experiments such staining was not observed however at the time no detailed analysis in this region of the embryo was carried out. As such, further analysis is required potentially dissecting the embryo before hybridization, so enabling the probe to penetrate deeper into the specimen.

To analyse the nature of disruption in *bbs8* morpholino injected zebrafish, specific brain markers were used for *in situ* hybridization analysis of wild-type vs injected embryos. No significant differences where observed in the expression pattern of *eng2a* and *shh*. Expression of *emx1* in injected embryos does appear more concentrated and much closer to the yolk sac of the embryo, however this can be explained by the craniofacial anomalies, disrupting the structure of embryo. The additional expression, that could potentially be hypothalamic, needs further investigation and could be

intriguing. Whilst control *in situs* were performed on uninjected controls, a more robust control would have been to use embryos injected with equal volumes of scrambled morpholino.

The craniofacial pattern in the *bbs8* knockdown zebrafish was reminiscent of Shh mutants (Wada *et al.*, 2005). Shh signaling depends on two transmembrane proteins; Ptc1, the receptor, which binds Shh, and Smoothened (Smo), responsible for transducing the signal intracellularly (Marigo *et al.*, 1996; Zhang *et al.*, 2001). Downstream of Smo the signal culminates in the regulation of the transcription factor Gli3 (Riobo and Manning, 2007).

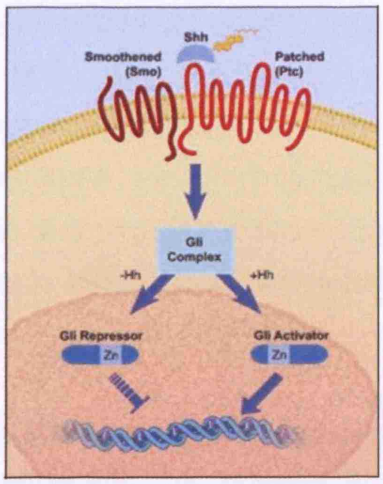

Figure 10.16: The Shh signaling pathway involves two transmembrane proteins, Patched (Ptc) and Smoothened (Smo). Ptc binds Shh, whereas Smo acts as a signal transducer. In the absence of ligand, Ptc interacts with and inhibits Smo. This inhibition activates a transcriptional repressor (e.g. Gli in vertebrates). In the presence of ligand, the interaction of Ptc and Smo is altered and Smo is no longer inhibited. Gli protein may then enter the nucleus and function as a transcriptional activator. Adapted from McMahon, 2000.

The cilium and IFT (Intraflagellar transport) machinery has been shown to play an essential role in Shh signal transduction (Huangfu *et al.*, 2003). Mammalian Smoothened (Smo) is expressed on the primary cilium. This ciliary expression is regulated by Shh pathway activity; Shh or activating mutations in Smo promote ciliary localization, whereas the Smo antagonist cyclopamine inhibits ciliary localization (Corbit *et al.*, 2005). Additionally in the

mouse, IFT proteins have been shown to be crucial in the control of both the positive and negative transcriptional activities of Gli proteins, and essential for Hh ligand-induced signaling cascade (Liu *et al.*, 2005).

The phenotypic overlap of *bbs8* morphant fish, coupled with the recent findings implicating cilia and IFT in Shh signaling, led us to investigate a possible interaction between *bbs8* and the Shh pathway. As *smo* mutant zebrafish were available to us, we investigated whether disruption of *bbs8* further affected these embryos.

After injection of *bbs8* morpholino into the *smo* mutant zebrafish they were phenotypically scored at 30 hpf, although there was no observed enhancement of the *smo*/*bbs8* phenotype it is possible that more detailed analysis and at later time points might have revealed an interaction between these two genes. Experimental design could be improved. A more sensitive approach may be to titrate the *bbs8* morpholino down to the point that injection into wild-type does not give a phenotype. If this dose is then injected into $smo^{-/+}$ embryos, any dysregulation or deviation from normal development could be assumed to be due to a genetic interaction between *bbs8* and *smo*.

Lack of a synergistic phenotype suggested no genetic interaction between Shh signaling and *bbs8* at this level, however subsequent work carried out by other members in our lab has implicated *bbs8* in the Shh pathway further downstream in the signaling process.

The following work was carried out using the same *bbs8* morpholino as in this study. In accordance with this study at earlier time points, *bbs8* morpholino injected fish at five dpf maintained severe defects: depigmentation, partial cyclopia, severe cranial and facial reduction in which the anterior neurocranial cartilage (ANC), mandible and pharyngeal skeleton disruption. Co-injections of human *bbs8* mRNA rescued these defects. Flat mount preparations of alcian blue stained *bbs8* morphants at five dpf revealed shortening and midline fusion of the trabeculae and complete absence of the anterior ethnoid plate. These two main cartilages of the ANC arise from distinct precursors and

depend on Shh signaling for their development (Wada *et al.*, 2005). In 24 hpf *bbs8* morphant embryos, overall expression of ptc1 was reduced. The transcription factor pax6, normally repressed by Shh signaling, was upregulated and ectopically expressed throughout the neural tube, signifying misregulation of Shh signaling.

Further analyses have shown that *bbs8* potentially acts downstream of Ptc1, regulating Gli3. Implicating normal production of Shh but perturbed down stream interpretation of the signal, similar to IFT mutants. Another aspect of development dependent on Shh signaling, neural crest cell migration is also abnormal in *bbs8* morphants.

Several aspects of BBS are consistent with a Shh phenotype, such as polydactyly, dental development and Hirschsprungs disease (Beales *et al.*, 1999). Additionally abnormal craniofacial development, seen here in zebrafish, but also observed in BBS knockout mice and human patients (unpublished data) could provide a further link between the BBS proteins and sonic signaling. Whilst this line of research is still in its infancy, evidence is mounting for the involvement of BBS proteins in the Shh pathway.

As with *bbs4* and *bbs6,* suppression of *bbs8* phenocopies somitic and notochordal defects of PCP mutants (Badano *et al.*, 2006). Similarly, we see suppression of *bbs8* also enhances convergent extension defects of the zebrafish mutation *trilobite* (orthologous to *Vangl2*)*(Ross et al., 2005)*. We see a more severe compression of body axis and longer somites, as judged by staining with *myoD* and *krox20.* In addition we also observed a cardiac looping abnormality in *bbs8* injected trilobite fish suggesting a possible laterality defect.

Initially the cardiac abnormality was observed as abnormal heart looping seen whilst scoring the embryos for a PCP phenotype. The beating hearts were often very difficult to score due to the decreased beating strength of the injected and mutant animals. Expression analysis of a laterality marker *spaw*

confirmed our initial observations. Laterality was randomized in *bbs8* morpholino injected mutants. This phenotype was enhanced in *trilobite* embryos. Cloning of the *BBS8* gene in humans was aided by the identification of an affected family in which a homozygous null *BBS8* mutation leads to BBS with randomization of left-right body axis symmetry (situs inversus), a known defect of the nodal cilium (Ansley *et al.*, 2003). Situs inversus is recognized as one of the rarer secondary features associated with the disease (P. Beales, personal communication).

An explanation for the mechanism behind this altered laterality during development could be a result of cilial defects at the Kupffer's vesicle (KV). This organ is a transient structure containing monocilia, and is proposed to have a similar function to the node of chick and mouse in gastrulation and establishment of Left-Right (LR) symmetry during development (Essner *et al.*, 2002) (Bisgrove *et al.*, 2005).

The KV, a transient embryonic 'organ of asymmetry' is known to regulate the earliest step in LR axis specification in zebrafish (Amack and Yost, 2004). This structure was first described in 1868 by Kupffer, and is conserved among teleost fishes. Electron microscopy has shown that a single cilium protrudes into the lumen from each cell lining the KV (Brummett and Dumont, 1978). These cilia inside the KV are motile and generate a consistent counterclockwise fluid flow that triggers asymmetric gene expression, very similar to cilia function in the mouse node. It has been proposed that asymmetric fluid flow functions to activate non-motile mechanosensory cilia which initiate an asymmetric calcium influx, triggering signaling pathways resulting in the asymmetric expression of genes necessary for proper LR development (Nonaka *et al.*, 2002; McGarth *et al.*, 2003). In the zebrafish, ciliated KV cells are required during early somitogenesis for subsequent correct LR patterning in the brain, heart and gut (Essner *et al.*, 2005).

The KV originates from dorsal forerunner cells during gastrulation, expands as a spherical vesicle during the somite stages and is readily observable in the tail bud region (Melby *et al.*, 1996). Morpholino injection into the yolk sac at

the 250-1000 cell stage targets the morpholino directly to the KV (Bisgrove *et al.*, 2005). *bbs8* morpholino injection at this stage produced a similar laterality defect to that seen with injection at the one cell stage. From these data we deduced that the laterality defects observed by suppression of *bbs8* were due to disruption at the KV. To investigate this further, immunohistochemistry against α-acetylated tubulin in *bbs8* morpholino injected *trilobite* mutants visualized the KV cilia, allowing analysis of length and number.

In very preliminary work and on very small numbers of embryos, we observed KV cilia length was reduced in *bbs8* morpholino injected animals, whilst the presence of the *tri* mutation reduced the overall number of cilia in the KV. Whilst a reduction in cilia length due to *bbs8* supression caused randomization of spaw expression, this was enhanced when combined with the reduction in number of cilia. Further implicating an interaction between *bbs8* and the PCP pathway. These experiments need repeating. Ideally higher power images, possible using an electron microscope, could be used to visualize the cilia within this structure.

As the KV cilia have been shown to be responsible for producing a fluid flow across this organ, it would be of interest to see how this is potentially disrupted. Future work in the fish could allow analysis of cilial movement in real time by injecting fluorescent beads into live embryos. Investigation of the LR pattering of the brain and gut in *bbs8* morphants (alone or on the *tri* mutant back ground) may also be rewarding, as normal KV function is known to be required for normal LR patterning in these tissue (Essner *et al.*, 2005).

Our preliminary work on the KV has been confirmed in a similar study focusing primarily on *bbs7* but also encompassing *bbs2,4,5,6* and *8* morphant zebrafish using morpholino to suppress gene expression. Yen *et al* see a reduction in size of the KV amongst all injected embryos to varying degrees. *bbs7* morphants had shorter and dispersed cilia, whilst *bbs2*, *bbs4* and *bbs6* morphants revealed few or no cilia at the KV. These defects were also associated with laterality defects. Abnormal heart looping was also observed in *bbs4, bbs5, bbs6, bbs7* and *bbs8* morphants with a range of penetrance.

Additionally this study noted specific defects altering retrograde melanosome transport. All *bbs* genes knocked down in this study resulted in epinephrine-induced melanosome retraction delay suggesting that BBS proteins play a role in intracellular transport. *bbs7* morphants were also shown to have disrupted ocular morphology and ultrastructure a phenotype which mimics retinitis pigmentosa a cardinal feature of the human BBS patients (Yen *et al.*, 2006).

Whilst work using the *bbs8* morpholino appears to give promising results, there is a great need for more work to be carried out in particular with respect to more robust controls. As mentioned before, injection of equal concentrations of scrambled/mismatched morpholino was carried out by other members of the lab (J. Tobin, M.Kai) and resulted in no detectable phenotype. Co-injection with *bbs8* mRNA reversed these phenotypes, confirming specificity of the morpholino. However these scrambled/mismatched morpholino and rescue with mRNA experiments must be extended to the remainder of the experiments in particular with regard to their affect on the mutant fish. Additionally, to confirm the affect of the *bbs8* knockdown in the mutant animals, co-injection with various mRNAs for the various mutants could be carried out and should revert the resulting animals back to their wildtype condition. Finally using additional morpholinos designed against *bbs8*, such as splice morpholinos, would be recommendable. In this study, translational morpholinos against the start ATG were employed. Translation initiation is blocked in the cytosol by targeting the 5' UTR through the first 25 bases of coding sequence however, more recently morpholinos have been designed to block miRNA activity, inhibiting maturation and activity of microRNAs.

Analysis of *BBS* gene function using zebrafish as a model vertebrate system is still in its infancy, and much more work is required to fully establish the role *bbs* genes play in development. However it has been shown that such experiments are a good accompaniment to, and further validation of, previously established theoretical models. As such these can be used in conjunction with other *in vitro* or even *in vivo* studies to dissect the BBS

pathway(s). Additionally rescue experiments may further enable elucidation of genetic pathways involved. Whilst much more work can be done by targeting total *bbs* gene suppression, more specific morpholinos could be used to target known BBS mutations. Of note is the ability to co-inject morpholinos, mimicking gene suppression of more than one gene product. In light of the trialleic nature of BBS (requiring mutations in two BBS genes for disease manifestation) the ability to co-inject different morpholinos together is a valuable feature, enabling further research into the involvement of multiple gene loci in disease.

10.5 Summary

Targeted gene knockdown by morpholino injection in zebrafish was used to suppress *bbs8* expression. Loss of *bbs8* expression resulted in a severe phenotype which was shown to overlap with those of Shh and PCP mutants. As with *bbs4* and *bbs6,* suppression of *bbs8* resulted in enhancement of convergent extension defects in PCP mutant *trilobite* zebrafish. Observed randomization of LR asymmetry in *bbs8* injected zebrafish embryos, thought to result from defective cilia at the Kupffer's vesicle, was enhanced on the PCP mutant background. These data suggest an interaction between *bbs8* and the PCP pathway.

Chapter 11: Conclusion

Over 140 years ago, on the 10th February 1865, a seven year old 'short, flat-featured, heavy-looking' girl with a history of visual impairment and obesity became the first reported case of Bardet-Biedl syndrome (Laurence and Moon, 1866). Since then there have been numerous clinical reports but until 2003 the pathogenesis of the condition remained elusive. However, upon identification of *BBS8* (Ansley *et al.*, 2003), an association with basal bodies and primary cilia was established. This is now a well established connection and BBS is classified as one of the emerging ciliopathies (Mykytyn and Sheffield, 2004; Badano *et al.*, 2006b). More recently the involvement of BBS proteins in cell signalling pathways is further expanding our understanding of this subset of proteins and implicating cilia in a wider variety of processes (Gerdes and Katsanis, 2005; Ross *et al.*, 2005; Eggenschwiler and Anderson, 2007). This thesis has contributed to the wider understanding of this field of research and has also opened new avenues of research which require further investigation.

Resulting from this thesis has been the identification of further possible BBS loci, *BAIAP1* and *TUBB4Q* (chapter three); the identification of pathogenic sequence mutations, confirming the validity of candidate genes for *BBS3* and *BBS5* (chapter four). Furthermore, pedigree analysis of sequence variations, at a novel locus, *MGC1203*, were shown to contribute epistatically to the BBS phenotype (chapter four). A yeast two-hybrid screen isolated protein interactors with the Bbs6 protein, these included BBS2 and other microtubule associated proteins (MACF1 and CCT6A) (chapter five). Phenotypic analysis of the $Bbs6^{-/-}$ mouse showed that this model recapitulates the human phenotype (with exception of polydactyly), displaying age related retinal degeneration, obesity, renal and olfactory defects (chapter six). It was the observation of rotated stereociliary bundles in the organ of Corti of $Bbs6^{-/-}$ mice which suggested an association between BBS and planar cell polarity (PCP).

The emergence of an auditory phenotype amongst the *Bbs6*$^{-/-}$ mice raised awareness of an auditory component of the disease and so expression of BBS proteins in the developing cochlea was examined (chapter seven, eight, nine). Bbs6 was shown to localise to all basal bodies, Bbs2 was restricted to apical microtubules in supporting cells, potentially capturing nucleated microtubules and Bbs4 associated with microtubules and basal bodies, and was shown to play a role in protein trafficking as PCM1 was mislocalised in Bbs4$^{-/-}$ mice. These results suggested that BBS proteins play distinct roles in the processes of microtubule organisation and growth, and are not just restricted to the function of the cilium or basal body. Finally, the role of *bbs8* in zebrafish development was examined (chapter 10). Loss of *bbs8* expression resulted in a severe phenotype which was shown to overlap with those of Shh and PCP mutants. Suppression of *bbs8* resulted in enhancement of convergent extension defects in PCP mutant *trilobite* zebrafish. Observed randomization of LR asymmetry in *bbs8* injected zebrafish embryos, thought to result from defective cilia at the Kupffer's vesicle, was enhanced on the PCP mutant background.

11.1 Further BBS loci

The emphasis of the first two chapters of this thesis was the identification of novel BBS loci. Whilst the use of traditional linkage analysis was used to identify the first BBS genes, since then, limited availability of large consanguineous pedigrees has exhausted such studies. For this reason novel methods of gene identification were required.

For example, comparative genomic approaches including the creation of a ciliary proteome and the identification of an imperfect X-box promoter 5' of all orthologous *C.elegans* bbs genes, were employed for the identification of candidate *BBS3* and *BBS5* genes. In this study identification of pathogenic sequence mutations in candidate genes for *BBS3* and *BBS5*, in which the corresponding proteins were contained in the FABB (flagellar apparatus and

basal body) proteome and contained an X-box sequence, confirmed them as novel BBS genes (Fan *et al.*, 2004; Li *et al.*, 2004).

Also, in this study fluorescent *in situ* hybridisation was used to map the breakpoints of a balanced reciprocal translocation in an Iranian BBS patient to the region for *BBS3* on chromosome 3. Unfortunately the breakpoint in this region mapped to an as yet incomplete region of the genome sequence meaning it could not be defined and could still harbor further possible BBS genes. In a parallel study, the gene for BBS3 was cloned outside the region of the breakpoint. The breakpoint on the reciprocal chromosome was mapped to a region containing two genes *TUBB4Q* and *ZMYND11*. These remain to be validated as BBS causing genes. TUBB4Q is contained in the ciliary proteome and is comprised of only four exons, making it an attractive candidate to sequence in a subset of BBS patients, preferentially of Middle Eastern origin, that still remain unlinked for any of the known BBS genes.

An additional layer of genetic complexity associated with disease manifestation was revealed by the identification of the first genetic modifier allele. Sequence variations identified during this study, at a novel locus, *MGC1203*, were shown to contribute epistatically to the BBS phenotype (Badano *et al.*, 2006a). Identification of further such loci may enable further understanding behind the current discrepancy of any genotype/phenotype relationships.

The identification of a modifying locus affecting the penetrance of BBS is important in light of the observed triallelic mode of inheritance amongst BBS patients. Oligogenic inheritance has been reported for *BBS1*, *BBS2*, *BBS3*, *BBS4*, *BBS6*, *BBS7* and *BBS10* (Katsanis *et al.*, 2002; Badano *et al.*, 2003; Beales *et al.*, 2003; Fan *et al.*, 2004; Stoetzel *et al.*, 2006). Triallelic mutations are not always necessary for manifestation of the disease, but might potentiate a phenotype that is caused by two recessive mutations at an independent locus (Badano *et al.*, 2003). Distinguishing between 'oligogenic' vs 'modifier' roles of future BBS loci will be important to fully understand the

patterns of inheritance, but also to aid the elucidation of the disease mechanisms involved.

Similar oligogenic inheritance patterns have now been reported in other related disorders, Senior Löken syndrome (SLS) and Nephronophthisis (Mollet *et al.*, 2002; Olbrich *et al.*, 2003; Otto *et al.*, 2003) (Hoskins B, Thesis). Furthermore in addition to contributing to non-Mendelian inheritance in BBS patients, *BBS4* and *BBS6* have also be found to be associated with complex inheritance in these two disorders (Hoskins B, Thesis). These findings reveal a degree of genetic and mechanistic overlap amongst ciliopathies and as such warrants further investigation.

11.2 BBS protein interactors

A yeast two-hybrid screen outlined in chapter five, using full length Bbs6 as bait, identified a number of interesting interactors. In total 44 potential interacting proteins were identified. Of these six where chosen for further analysis and confirmed to be real interactors. These are given in the table below.

Identified Interactor	Predicted Cellular Function
Bardet-Biedl syndrome 2 (BBS2)	Basal body & cilium function
Chaperonin containing TCP1, subunit 6A (zeta 1)(CCT6A)	Chaperone (actin & tubulin)
DNA (cytosine-5-)-methyltransferase 1 (DNMT1)	DNA methylation
EH-domain containing 2 (EHD2)	GLUT4/actin interactor
Microtubule-actin crosslinking factor 1 (MACF1)	Cytoskeletal linker protein
Translocase of outer mitochondrial membrane (TOMM70A)	Mitchondrial chaperone

Table 11.1: Summary of confirmed Bbs6 interactors and their predicted cellular functions.

Significantly, the association of BBS6 with another BBS protein, BBS2 suggested a functional interaction between these BBS proteins. Since this finding, further data from our lab examining pair-wise combinations of all BBS proteins (BBS1-12) in yeast has shown further interactions between pairs of BBS proteins. These experiments revealed that BBS2 interacts with BBS6 and BBS9, BBS9 with BBS5 and BBS8, BBS5 with BBS6 and BBS9, and

BBS6 and BBS11 self-associate (A.Ross, unpublished data). These findings provide evidence for a functional interactome and a mechanistic explanation for the oligogenic mode of allele transmission in BBS. Some BBS patients have been shown to harbor three mutated alleles in two BBS genes and it has been proposed that the third allele could modify the penetrance or severity of the clinical phenotype (Katsanis, 2004). This could be explained by the instability of a multiply 'crippled' BBS complex.

Further evidence that several of the BBS proteins work in conjunction with one another has recently been shown using a proteomics approach by Nachury *et al.*(Nachury *et al.*, 2007). They identified a complex consisting of seven highly conserved BBS proteins (BBS1, BBS2, BBS4, BBS5, BBS7, BBS8 and BBS9) that binds PCM1 and α/β tubulin. This complex has been termed the BBSome and has been shown to localise to nonmembranous centriolar satellites in the cytoplasm and also to the ciliary membrane. The BBSome has been shown to be required for ciliogenesis but is dispensible for centriolar satellite function (Nachury *et al.*, 2007). Association of the BBSome with the GDP/GTP exchange factor Rab8, at the basal body, mediates its ciliogenic function. $Rab8^{GTP}$ enters the primary cilium promoting extension of the ciliary membrane. Conversely disruption of $Rab8^{GTP}$ disrupts ciliation in cells and yields characteristic BBS phenotypes in zebrafish (Nachury *et al.*, 2007). From these data it would seem that a possible role for the BBSome could be the correct targeting of vesicle transport to the ciliary membrane.

Whilst not all BBS proteins are present in these complexes, it is highly likely that they are involved in the same cellular processes and might be interacting via other intermediate proteins.

11.3 Microtubule function of BBS proteins

The identification of MACF1 and CCT6a as interactors of Bbs6, supports a possible microtubule based aspect of BBS protein function. Potentially involving intracellular trafficking, beyond that of solely cilial and basal body

function. MACF1 is a cytoskeletal linker protein that associates with both actin filaments and microtubules. CCT6a is a subunit of the type II chaperonin that assists the folding of actins and tubulins.

The exact role of BBS proteins in the transport process is currently unknown, but possibilities include maintenance of microtubule architecture, molecular motor function and efficiency of cargo loading. Previous work has shown that knockdown of *bbs* function in zebrafish causes significant delay in retrograde melanosome transport mediated by the molecular motor protein dynein (Yen *et al.*, 2006). But this work does not explain the role of BBS4 in intraflagellar transport (e.g. PCM1 to centrosome), nor the dependence of melanosomes on BBS via IFT. Additionally its been shown that suppression of *BBS4* mRNA causes marked disorganisation of centrosomal microtubules *in vitro* (Kim *et al.*, 2004) and *Bbs1*$^{-/-}$, *Bbs4*$^{-/-}$ and *Bbs6*$^{-/-}$ mice have unstable microtubules in their olfactory cilia, and distorted microtubular organisation of dendrites (Kulaga *et al.*, 2004) (Ross *et al.*, 2005). More specifically, BBS4 has been proposed to behave as an adaptor between PCM-1 and dynein molecular motors, implicating the BBS family in the retrograde translocation of subcellular cargo along microtubules (Kim *et al.*, 2004).

Further to the identification of an association of Bbs6 with microtubule/cytoskeletal associated proteins, this study showed direct labeling of microtubule structures with antibodies against BBS2 and BBS4 in the developing cochlea. Moreover PCM-1 was seen to be mislocalised in *Bbs4*$^{-/-}$ animal.

These results support the notion that BBS proteins play distinct roles in microtubule based processes. For this reason the observed association of BBS6 with MACF1 is of particular interest and requires further in depth analysis. Experiments should include expression analysis in BBS mutant animals (for example in zebrafish and mouse models), identification of the specific regions of interaction and closer inspection as to the nature of the interaction.

11.4 Animal models of BBS

The use of animal models has been invaluable for furthering our understanding of disease pathogenesis. In this study phenotypic analysis of the *Bbs6* mutant mouse showed that as with the other mouse mutants, *Bbs1*, *Bbs2* and *Bbs4*, these animals recapitulate the human phenotype of the disease (Kulaga *et al.*, 2004; Mykytyn *et al.*, 2004; Nishimura *et al.*, 2004; Ross *et al.*, 2005).

Significantly, it was the observation of rotated stereociliary bundles in the organ of Corti of *Bbs6*$^{-/-}$ mice which suggested an association between BBS and planar cell polarity (PCP). This initial observation led to further identification of phenotypic overlap between BBS and PCP mutants. This included open eyelids during gestation and anterior neural tube defects in addition to disrupted cochlear stereociliary bundles (Ross *et al.*, 2005).

In support of this theory, genetic interactions between BBS genes and a core PCP gene *Vangl2* were identified. Significant embryonic lethality was observed in mouse embryos doubly heterozygous for *Vangl2* and *Bbs6* and *Bbs1* respectively (*Vangl2*$^{+/-}$/*Bbs6*$^{+/-}$ and *Vangl2*$^{+/-}$/*Bbs1*$^{+/-}$) in contrast with 100% survival of all single heterozygotes or wild-type litter mates. Further to this, bundle stereociliary bundle defects were only observed in double not single heterozygous mice. These interactions were confirmed in another vertebrate system. The zebrafish PCP mutant *trilobite*, having a mutation in *vangl2* results in defective convergent extension during gastrulation. This results in a shortened and widened body axis because of disruption to polarity. Disruption of orthologous *bbs4* and *bbs6* genes in *trilobite* zebrafish embryos enhanced the PCP phenotype affecting convergent extension movements (Ross *et al.*, 2005). This thesis adds to the previous work, showing that disruption of *bbs8* in *trilobite* zebrafish leads to a similar phenotype.

A functional mechanism behind these interactions could be explained by the localization of the VANGL2 protein to the cilium. Labeling of mouse IMCD3

kidney epithelial cells and human respiratory epithelial cells with an antibody against Vangl2 showed strong expression around the base of the cilium and perinuclear region as well as punctate staining along the length of the ciliary axoneme (Ross *et al.*, 2005). Further relationships between this PCP protein and cilia structure and/or function, have been implied in the last chapter of this thesis. Observed randomisation of left-right asymmetry in *bbs8* disrupted zebrafish embryos, thought to result from defective cilia at the Kupffer's vesicle, was enhanced on the *trilobite* mutant background. Closer analysis of the Kupffer's vesicle of a very small number of embryos, suggested cilia length was reduced by *bbs8* disruption, whilst the presence of the *trilobite* mutation reduced the overall number of cilia.

During the phenotypic analysis of the *Bbs6*$^{-/-}$ mice an auditory component of the disease was highlighted. This raised awareness of such aspects of the phenotype in humans and a detailed survey of hearing in BBS patients is currently underway. Further investigation of the hearing defect in mice located one of the origins of the defect to the organ of Corti. Misshapen stereociliary bundles were observed on the cochlea hair cells. Expression analysis in this organ during development suggested that BBS proteins play distinct roles in the processes of microtubule organisation and growth, and are not just restricted to the function of the cilium or basal body. Bbs6 localised to all basal bodies, Bbs2 was restricted to apical microtubules in supporting cells, potentially capturing nucleated microtubules and Bbs4 associated with microtubules and basal bodies, and was shown to be involved in protein trafficking.

11.5 Cilia and signalling pathways

Evidence is mounting that cilia are involved in developmental signalling pathways. In addition to the data mentioned above, further studies have begun to implicate this cellular organelle in both Wnt and Shh signalling. These connections were first noted when both mutants with defective cilia function and Wnt/Shh mutants were shown to have overlapping phenotypes.

More recently the molecular mechanisms behind this involvement have started to be unravelled. The function of cilia in the Shh pathway is discussed in chapter 10, but in short, Shh ligand binding localises Smoothened to the ciliary membrane (mediated via Patched1), from where it activates Gli transcription factors, activating transcription of Shh target genes.

Wnt signalling propagates a variety of cellular responses that influence the fate and function of embryonic and adult tissues. Wnt proteins bind to Frizzled (Fz) family receptors and the signal is then transmitted primarily via the cytoplasmic Disheveled (Dvl) protein. Differential cellular expression of Dvl determines which Wnt signaling pathway will be activated: canonical (β-catenin-dependent) or noncanonical (PCP)(Veeman *et al.*, 2003). The canonical β-catenin Wnt signalling pathway is involved in body axis specification, morphogenic signalling and cancers (Yan *et al.*, 2001; Jho *et al.*, 2002). The noncanonical Wnt signalling pathway is synonomous with the PCP pathway, regulating the polarisation of cells in a plane of epithelium (Keller, 2002; Torban *et al.*, 2004).

Initial findings implicating the role of cilia in Wnt signaling were based on inversin, mutations in which cause polycystic kidney disease. This protein is a component of the cilia-basal body centrosome complex and has been shown to be involved in regulating the Wnt signalling pathway through its interaction with dishevelled which is positioned at a critical branch point of the canonical (β-catenin-dependent) and non canonical (PCP) Wnt pathways (Simons *et al.*, 2005) (Fig 11.1).

The cilium could potentially act as a switch between the two pathways which both require Wnt ligands, frizzled (Fz) receptors and dishevelled (Dvl1), downstream of which they diverge. In the canonical pathway, Wnt binding to Fz leads to the activation of Dvl1 and the stablisation of cytoplasmic β-catenin, through inhibiton of the degradation complex. β-catenin translocates to the nucleus where it activates gene transcription. Significantly, MACF1 has been shown to associate with the Apc2/axin/Gsk3β complex and as such is involved in its regulatory function (Chen *et al.*, 2006).

In response to an environmental stimulus a (potentially) ciliary signal mediates a switch from canonical to noncanonical Wnt signaling. Dvl1 and possibly inversin localise to the plasma membrane, where they interact with PCP proteins. β-catenin is degraded by the Apc2/axin/Gsk3β degradation complex and PCP signalling influences gene transcription and regulates cytoskeletal rearrangements.

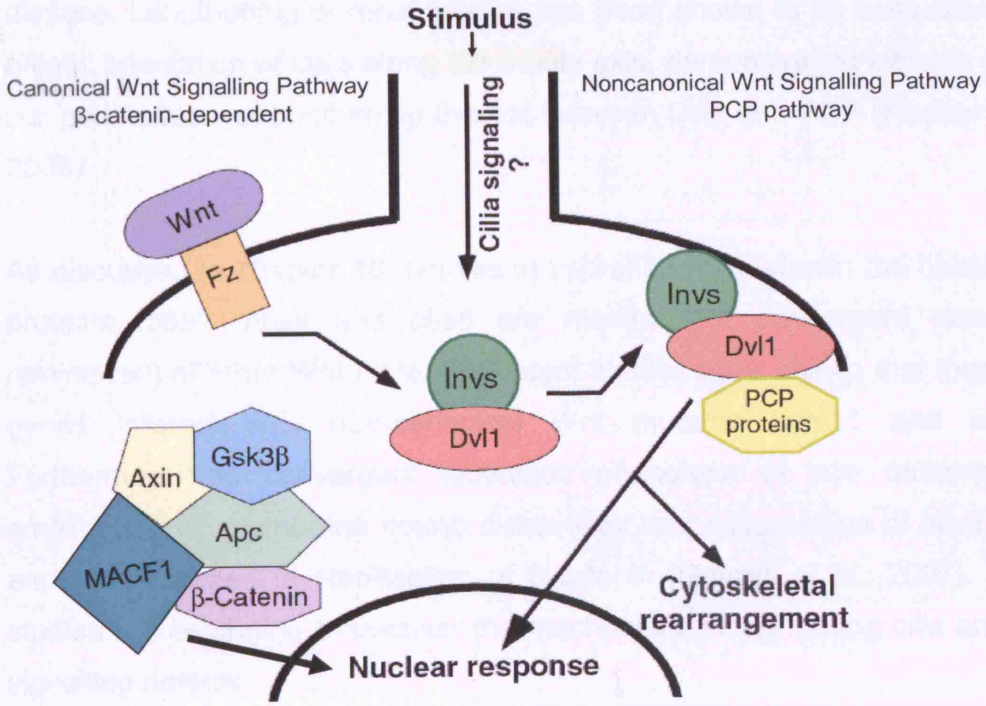

Figure 11.1: Ciliary involvement in Wnt signalling. Cilia may be involved in regulating the switch between canonical to noncanonical Wnt signaling. Cilia could be acting as sensors, receiving an external signal (chemical or mechanical) and transducing intracellular signalling. Cell polarity is defined as asymmetry in cell shape, protein distributions and cell functions. Generation of such polarity involves formation of large protein scaffolds required for the stabilisation of specific membrane domains and local activation of signalling events. (Nelson, 2003). Figure taken from (Bisgrove and Yost, 2006).

PCP signalling is generally implicated in governing the actin cytoskeleton. Actin filaments are required for proper positioning of ciliary basal bodies and in cells where the actin cytoskeleton has been disrupted, 'intercellular cilia' are formed (Boisvieux-Ulrich *et al.*, 1990; Hagiwara *et al.*, 2004). Furthermore, in ciliated cells lacking 'PCP' effectors Inturned and Fuzzy, actin failed to accumulate apically and masses of elongated microtubules amassed in these cells (Park *et al.*, 2006). These results suggest that PCP signals are required to govern the actin network that positions ciliary basal bodies. Furthermore, defective planar cell polarity has recently been implicated in polycystic kidney disease. Lengthening of renal tubules has been shown to be associated with mitotic orientation of cells along the tubule axis, demonstrating intrinsic planar cell polarisation, strengthening the link between Cilia and PCP (Fischer *et al.*, 2006).

As discussed in chapter 10, studies in zebrafish have shown the basal body proteins, *bbs1*, *bbs4* and *bbs6* are required for convergent extension, reminiscent of other Wnt mutants. Recent studies have shown that these *bbs* genes interact with non-canonical Wnt mutants (wnt11 and wnt5b). Furthermore the convergent extension phenotype of *bbs* mutants was ameliorated by membrane bound dishevelled and suppression of *bbs1*, *bbs4* and *bbs6* resulted in stabilisation of β-catenin (Gerdes *et al.*, 2007). These studies are beginning to uncover the mechanistic model linking cilia and Wnt signalling defects.

The identification of MACF1 through the Bbs6 yeast two-hybrid screen is of particular interest, as this protein has also been shown to play a role in the Wnt signalling pathway. *MACF1*$^{-/-}$ embryos are phenotypically similar to *Wnt3*$^{-/-}$ embryos. In the absence of Wnt, MACF1 was seen to associate with a complex containing Axin, β-catenin, Gsk3β and APC. Upon Wnt stimulation, MACF1 appeared to be involved in translocation and binding of the Axin complex to the cell membrane. Reduction of MACF1 decreased the amount of β-catenin in the nucleus, inhibiting Wnt-induced transcriptional activation (Chen *et al.*, 2006) (Fig 11.2). These findings further support the association

of MACF1 with basalbody/ciliary function, possibly via the Bbs6 protein an exciting prospect for further investigation.

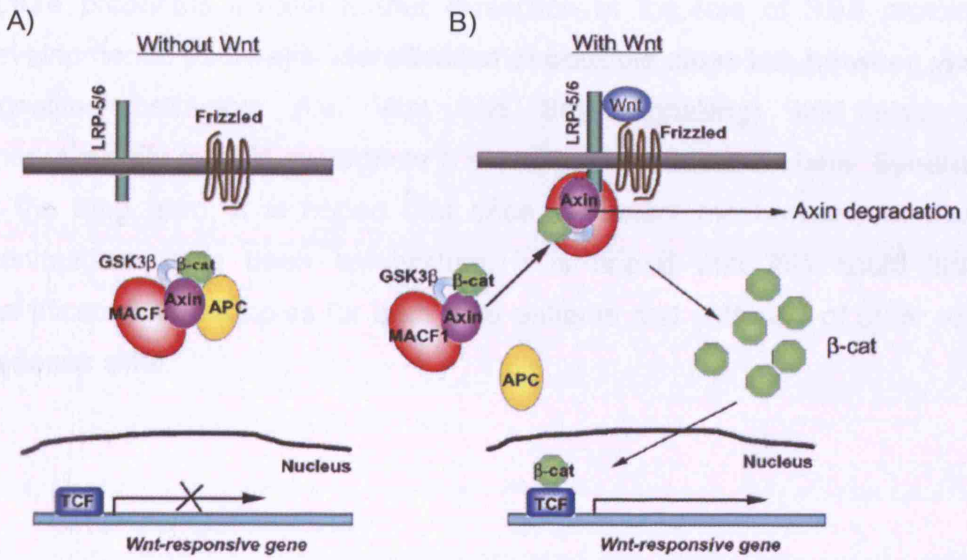

Figure 11.2: Involvement of MACF1 in the Wnt/β-catenin signaling pathway. A) Without Wnt, MACF1 binds to a protein complex containing Axin, APC, β-catenin and GSK3β. There is no expression of TCF controlled genes due to the degradation of β-catenin after phosphorylation by GSK3β. B) Wnt activates its receptor frizzled and its coreceptor LRP-5/6. MACF1 is involved in the translocation of the complex containing Axin, β-catenin, and GSK3β but not APC from the cytosol to the cell membrane, where Axin and MACF1 bind to LRP-5/6. Subsequently, GSK3β is inactivated by phosphorylation, Axin is degraded, and β-catenin is released and enters the nucleus, where it can activate the Wnt-responsive genes. Taken from Chen, 2006.

The majority of mammalian cells have a cilium, an organelle long ignored by developmental biologists. Whilst the function of cilia in some organs is now understood, the roles of cilia in many cell types and organs remains to be elucidated. What is evident is that cilia have many stage, cell and tissue specific functions, the failure of which results in a group of phenotypically overlapping yet genetically distinct diseases known as the ciliopathies. The study of BBS, which has become the archetypal ciliopathy is enabling us to uncover the molecular mechanisms behind these many and varied roles of

cilia. Hopefully this thesis has added to that pool of knowledge, and has created new leads for further exploration of this fascinating organelle.

Future prospects involve further dissection of the role of BBS proteins in developmental pathways, identification of possible cross talk between various signalling pathways (i.e. Wnt and Shh signalling) and also other phenotypically related syndromes (i.e. Nephronophthisis or Usher Syndrome). In the long term, it is hoped that once the exact mechanisms of disease manifestation has been established, it is hoped that this could lead to identification of therapies for both BBS patients and sufferers of other related diseases alike.

References

Ahmad, J., Khan, S.N., Khan, S.Y., Ramzan, K., Riazuddin, S., Ahmed, Z.M., Wilcox, E.R., Friedman, T.B., and Riazuddin, S. **2005**. DFNB48, a new nonsyndromic recessive deafness locus, maps to chromosome 15q23-q25.1. *Hum Genet* 116(5): 407-412.

Ahmed, Z.M., Goodyear, R., Riazuddin, S., Lagziel, A., Legan, P.K., Behra, M., Burgess, S.M., Lilley, K.S., Wilcox, E.R., Riazuddin, S., Griffith, A.J., Frolenkov, G.I., Belyantseva, I.A., Richardson, G.P., and Friedman, T.B. **2006**. The tip-link antigen, a protein associated with the transduction complex of sensory hair cells, is protocadherin-15. *J Neurosci* 26(26): 7022-7034.

Al-Awadi, S.A., Moussa, M.A., Naguib, K.K., Farag, T.I., Teebi, A.S., M, e.K., and el Dossary, L. **1985**. Consanguinity among the Kuwaiti population. *Clinical Genetics* 27: 483-486.

Alagramam, K.N., Murcia, C.L., Kwon, H.Y., Pawlowski, K.S., Wright, C.G., and Woychik, R.P. **2001**. The mouse Ames waltzer hearing-loss mutant is caused by mutation of Pcdh15, a novel protocadherin gene. *Nat Genet* 27(1): 99-102.

Allen, C. and Borisy, G.G. **1974**. Structural polarity and directional growth of microtubules of *Chlamydomonas* flagella. *J Mol Biol* 90: 381-402.

Amack, J.D. and Yost, H.J. **2004**. The T box transcription factor no tail in ciliated cells controls zebrafish left-right asymmetry. *Curr Biol* 14(8): 685-690.

Ammann, F. **1970**. Investigations clinique et genetique sur le syndrome de Bardet-Biedl en Suisse. *J Genet Hum* suppl 18: 1-310.

Andersen, J.S., Wilkinson, C.J., Mayor, T., Mortensen, P., Nigg, E.A., and Mann, M. **2003**. Proteomic characterization of the human centrosome by protein correlation profiling. *Nature* 426(6966): 570-574.

Ansley, S.J., Badano, J.L., Blacque, O.E., Hill, J., Hoskins, B.E., Leitch, C.C., Kim, J.C., Ross, A.J., Eichers, E.R., Teslovich, T.M., Mah, A.K., Johnsen, R.C., Cavender, J.C., Lewis, R.A., Leroux, M.R., Beales, P.L., and Katsanis, N. **2003**. Basal body dysfunction is a likely cause of pleiotropic Bardet-Biedl syndrome. *Nature* 425(6958): 628-633.

Antonarakis, S.E.a.B., J.S. **2006**. Mendelian disorders deserve more attention. *Nature reviews* 7(4): 277-282.

Badano, J.L., Ansley, S.J., Leitch, C.C., Lewis, R.A., Lupski, J.R., and Katsanis, N. **2003a**. Identification of a novel Bardet-Biedl syndrome

protein, BBS7, that shares structural features with BBS1 and BBS2. *Am J Hum Genet* 72(3): 650-658.

Badano, J.L., Kim, J.C., Hoskins, B.E., Lewis, R.A., Ansley, S.J., Cutler, D.J., Castellan, C., Beales, P.L., Leroux, M.R., and Katsanis, N. **2003b**. Heterozygous mutations in BBS1, BBS2 and BBS6 have a potential epistatic effect on Bardet-Biedl patients with two mutations at a second BBS locus. *Hum Mol Genet* 12(14): 1651-1659.

Badano, J.L., Leitch, C.C., Ansley, S.J., May-Simera, H., Lawson, S., Lewis, R.A., Beales, P.L., Dietz, H.C., Fisher, S., and Katsanis, N. **2006a**. Dissection of epistasis in oligogenic Bardet-Biedl syndrome. *Nature* 439(7074): 326-330.

Badano, J.L., Mitsuma, N., Beales, P.L., and Katsanis, N. **2006b**. The Ciliopathies: An Emerging Class of Human Genetic Disorders. *Annu Rev Genomics Hum Genet* 7: 125-148.

Balczon, R., Bao, L., and Zimmer, W.E. **1994**. PCM-1, A 228-kD centrosome autoantigen with a distinct cell cycle distribution. *J Cell Biol* 124(5): 783-793.

Bardet, G. 1920. Sur un syndrome d'obesite congenitale avec polydactylie et retinie pigmentaire (contribution a l'etude des formes clinique de l'obesite hypophysaire). In. Sorbonne, Paris.

Beales, P.L. **2005**. Lifting the lid on Pandora's box: the Bardet-Biedl syndrome. *Curr Opin Genet Dev* 15(3): 315-323.

Beales, P.L., Badano, J.L., Ross, A.J., Ansley, S.J., Hoskins, B.E., Kirsten, B., Mein, C.A., Froguel, P., Scambler, P.J., Lewis, R.A., Lupski, J.R., and Katsanis, N. **2003**. Genetic interaction of BBS1 mutations with alleles at other BBS loci can result in non-Mendelian Bardet-Biedl syndrome. *Am J Hum Genet* 72(5): 1187-1199.

Beales, P.L., Bland, E., Tobin, J.L., Bacchelli, C., Tuysuz, B., Hill, J., Rix, S., Pearson, C.G., Kai, M., Hartley, J., Johnson, C., Irving, M., Elcioglu, N., Winey, M., Tada, M., and Scambler, P.J. **2007**. IFT80, which encodes a conserved intraflagellar transport protein, is mutated in Jeune asphyxiating thoracic dystrophy. *Nat Genet* 39(6): 727-729.

Beales, P.L., Elcioglu, N., Woolf, A.S., Parker, D., and Flinter, F.A. **1999**. New criteria for improved diagnosis of Bardet-Biedl syndrome: Results of a population survey. *Journal of Medical Genetics* 36(6): 437-446.

Beales, P.L., Warner, A.M., Hitman, G.A., Thakker, R., and Flinter, F.A. **1997**. Bardet-Biedl syndrome: A molecular and phenotypic study of 18 families. *Journal of Medical Genetics* 34(2): 92-98.

Beisson, J. and Wright, M. **2003**. Basal body/centriole assembly and continuity. *Current opinion in cell biology* 15(1): 96-104.

Biedl, A. **1922**. Ein Geschwisterpaar mit adiposo-genitaler Dystrophie. *Dtsch med Wschr* 48: 1630.

Bisgrove, B.W., Snarr, B.S., Emrazian, A., and Yost, H.J. **2005**. Polaris and Polycystin-2 in dorsal forerunner cells and Kupffer's vesicle are required for specification of the zebrafish left-right axis. *Developmental biology* 287(2): 274-288.

Bisgrove, B.W. and Yost, H.J. **2006**. The roles of cilia in developmental disorders and disease. *Development* 133(21): 4131-4143.

Blacque, O.E. and Leroux, M.R. **2006**. Bardet-Biedl syndrome: an emerging pathomechanism of intracellular transport. *Cell Mol Life Sci* 63(18): 2145-2161.

Blacque, O.E., Reardon, M.J., Li, C., McCarthy, J., Mahjoub, M.R., Ansley, S.J., Badano, J.L., Mah, A.K., Beales, P.L., Davidson, W.S., Johnsen, R.C., Audeh, M., Plasterk, R.H., Baillie, D.L., Katsanis, N., Quarmby, L.M., Wicks, S.R., and Leroux, M.R. **2004**. Loss of C. elegans BBS-7 and BBS-8 protein function results in cilia defects and compromised intraflagellar transport. *Genes Dev* 18(13): 1630-1642.

Blake, K.D. and Prasad, C. **2006**. CHARGE syndrome. *Orphanet journal of rare diseases* 1(1): 34.

Bobinnec, Y., Khodjakov, A., Mir, L.M., Rieder, C.L., Edde, B., and Bornens, M. **1998**. Centriole disassembly in vivo and its effect on centrosome structure and function in vertebrate cells. *J Cell Biol* 143(6): 1575-1589.

Boisvieux-Ulrich, E., Laine, M.C., and Sandoz, D. **1990**. Cytochalasin D inhibits basal body migration and ciliary elongation in quail oviduct epithelium. *Cell Tissue Res* 259(3): 443-454.

Brailov, I., Bancila, M., Brisorgueil, M.J., Miquel, M.C., Hamon, M., and Verge, D. **2000**. Localization of 5-HT(6) receptors at the plasma membrane of neuronal cilia in the rat brain. *Brain Res* 872(1-2): 271-275.

Brone, B. and Eggermont, J. **2005**. PDZ proteins retain and regulate membrane transporters in polarized epithelial cell membranes. *Am J Physiol Cell Physiol* 288(1): C20-29.

Brown, D.A. and London, E. **1998**. Functions of lipid rafts in biological membranes. *Ann Rev Cell Dev Biol* 14: 111-136.

Brummett, A.R. and Dumont, J.N. **1978**. Kupffer's vesicle in Fundulus heteroclitus: a scanning and transmission electron microscope study. *Tissue & cell* 10(1): 11-22.

Burn, R. **1950**. Deafness and the Laurence-Moon-Biedl syndrome. *Brit J Ophthal* 34: 65-88.

Carmi, R., Elbedour, K., Stone, E.M., and Sheffield, V.C. **1995a**. Phenotypic differences among patients with Bardet-Biedl syndrome linked to three different chromosome loci. *Am J Med Genet* 59(2): 199-203.

Carmi, R., Rokhlina, T., Kwitek-Black, A.E., Elbedour, K., Nishimura, D., Stone, E.M., and Sheffield, V.C. **1995b**. Use of a DNA pooling strategy to identify a human obesity syndrome locus on chromosome 15. *Human Molecular Genetics* 4(1): 9-13.

Chaudhuri, I., Soding, J., and Lupas, A.N. **2007**. Evolution of the beta-propeller fold. *Proteins*.

Chen, H.-J., Lin, C.-M., Lin, C.-S., Perez-Olle, R., Leung, C.L., and Liem, R. **2006**. The role of microtubule actin cross-linking factor 1 (MACF1) in the Wnt signalling pathway. *Genes and Developement* 20: 1933-1945.

Chiang, A.P., Beck, J.S., Yen, H.J., Tayeh, M.K., Scheetz, T.E., Swiderski, R.E., Nishimura, D.Y., Braun, T.A., Kim, K.Y., Huang, J., Elbedour, K., Carmi, R., Slusarski, D.C., Casavant, T.L., Stone, E.M., and Sheffield, V.C. **2006**. Homozygosity mapping with SNP arrays identifies TRIM32, an E3 ubiquitin ligase, as a Bardet-Biedl syndrome gene (BBS11). *Proc Natl Acad Sci U S A* 103(16): 6287-6292.

Chiang, A.P., Nishimura, D., Searby, C., Elbedour, K., Carmi, R., Ferguson, A.L., Secrist, J., Braun, T., Casavant, T., Stone, E.M., and Sheffield, V.C. **2004**. Comparative genomic analysis identifies an ADP-ribosylation factor-like gene as the cause of Bardet-Biedl syndrome (BBS3). *Am J Hum Genet* 75(3): 475-484.

Chien, C.T., Bartel, P.L., Sternglanz, R., and Fields, S. **1991**. The two-hybrid system: a method to identify and clone genes for proteins that interact with a protein of interest. *Proc Natl Acad Sci U S A* 88(21): 9578-9582.

Cohen, M., Bitner-Glindzicz, M., and Luxon, L. **2007**. The changing face of Usher syndrome: clinical implications. *International journal of audiology* 46(2): 82-93.

Cole, D.G. **2003**. The intraflagellar transport machinery of Chlamydomonas reinhardtii. *Traffic*(4): 435-442.

Cole, D.G., Deiner, D.R., Himelblau, A.L., Beech, P.L., Fuster, J.C., and Rosenbaum, J.L. **1998**. *Chlamydononas* kinesin-II-dependent intraflagellar transport (IFT): IFT particles contain proteins required for cilliary assembly in *Caenorhabditis elegans* sensory neurons. *J Cell Biol* 141: 993-1008.

Corbit, K.C., Aanstad, P., Singla, V., Norman, A.R., Stainier, D.Y., and Reiter, J.F. **2005**. Vertebrate Smoothened functions at the primary cilium. *Nature* 437(7061): 1018-1021.

Corey, D.P. **2006**. What is the hair cell transduction channel? *The Journal of physiology* 576(Pt 1): 23-28.

Cramer, B., Green, J., Harnett, J., Johnson, G.J., McManamon, P., Farid, N., Pryse-Phillips, W., and Parfrey, P.S. **1988**. Sonographic and urographic correlation in Bardet-Biedl syndrome (formerly Laurence-Moon-Biedl syndrome). *Urologic Radiology* 10(4): 176-180.

Croft, J.B., Morrell, D., Chase, C.L., and Swift, M. **1995**. Obesity in heterozygous carriers of the gene for the Bardet-Biedl syndrome. *American Journal of Medical Genetics* 55(1): 12-15.

Croft, J.B. and Swift, M. **1990**. Obesity, hypertension, and renal disease in relatives of Bardet-Biedl syndrome sibs. *American Journal of Medical Genetics* 36(1): 37-42.

Cuvillier, A., Redon, F., Antoine, J.C., Chardin, P., DeVos, T., and Merlin, G. **2000**. LdARL-3A, a Leishmania promastigote-specific ADP-ribosylation factor-like protein, is essential for flagellum integrity. *J Cell Sci* 113 (Pt 11): 2065-2074.

Dabdoub, A., Donohue, M.J., Brennan, A., Wolf, V., Montcouquiol, M., Sassoon, D.A., Hseih, J.C., Rubin, J.S., Salinas, P.C., and Kelley, M.W. **2003**. Wnt signaling mediates reorientation of outer hair cell stereociliary bundles in the mammalian cochlea. *Development* 130(11): 2375-2384.

Dammermann, A. and Merdes, A. **2002a**. Assembly of centrosomal proteins and microtubule organization depends on PCM-1. *J Cell Biol* 159(2): 255-266.

-. **2002b**. Assembly of centrosomal proteins and microtubule organization depends on PCM-1. *J Cell Biol* 159: 255-266.

Dascher, C. and Balch, W.E. **1994**. Dominant inhibitory mutants of ARF1 block endoplasmic reticulum to Golgi transport and trigger disassembly of the Golgi apparatus. *J Biol Chem* 269(2): 1437-1448.

David, A., Bitoun, P., Lacombe, D., Lambert, J.C., Nivelon, A., Vigneron, J., and Verloes, A. **1999**. Hydrometrocolpos and polydactyly: a common neonatal presentation of Bardet-Biedl and McKusick-Kaufman syndromes. *J Med Genet* 36(8): 599-603.

De Robertis, E. **1958**. Morphogenesis of retinal rods: an electron microscope study. *J Biophys Biochem Cytol* 2: 209-216.

Deane, J.A., Cole, D.G., Seeley, E.S., Diener, D.R., and Rosenbaum, J.L. **2001**. Localization of intraflagellar transport protein IFT52 identifies basal body transitional fibers as the docking site for IFT particles. *Curr Biol* 11(20): 1586-1590.

Denman-Johnson, K. and Forge, A. **1999**. Establishment of hair bundle polarity and orientation in the deveoping vestibular system of the mouse. *J Neurocytol*(28): 821-835.

Di Palma, F., Holme, R.H., Bryda, E.C., Belyantseva, I.A., Pellegrino, R., Kachar, B., Steel, K.P., and Noben-Trauth, K. **2001**. Mutations in Cdh23, encoding a new type of cadherin, cause stereocilia disorganization in waltzer, the mouse model for Usher syndrome type 1D. *Nat Genet* 27(1): 103-107.

Dooley, K. and Zon, L.I. **2000**. Zebrafish: a model system for the study of human disease. *Curr Opin Genet Dev* 10(3): 252-256.

Driever, W., Solnica-Krezel, L., Schier, A.F., Neuhauss, S.C., Malicki, J., Stemple, D.L., Stainier, D.Y., Zwartkruis, F., Abdelilah, S., Rangini, Z., Belak, J., and Boggs, C. **1996**. A genetic screen for mutations affecting embryogenesis in zebrafish. *Development* 123: 37-46.

Edmonson, A.M., Mayfield, D.K., Vervoort, V., DuPont, B.R., and Argyropoulos, G. **2002**. Characterization of a human import component of the mitichondrial outer membrane, TOMM70A. *Cell Commun Adhes* 9(1): 15-27

Eggenschwiler, J.T. and Anderson, K.V. **2007**. Cilia and developmental signaling. *Annual review of cell and developmental biology* 23: 345-373.

Eichers, E.R., Abd-El-Barr, M.M., Paylor, R., Lewis, R.A., Bi, W., Lin, X., Meehan, T.P., Stockton, D.W., Wu, S.M., Lindsay, E., Justice, M.J., Beales, P.L., Katsanis, N., and Lupski, J.R. **2006**. Phenotypic characterization of Bbs4 null mice reveals age-dependent penetrance and variable expressivity. *Hum Genet* 120(2): 211-226.

Engel, T., Lueken, A., Bode, G., Hobohm, U., Lorkowski, S., Schlueter, B., Rust, S., Cullen, P., Pech, M., Assmann, G., and Seedorf, U. **2004**. ADP-ribosylation factor (ARF)-like 7 (ARL7) is induced by cholesterol loading and participates in apolipoprotein AI-dependent cholesterol export. *FEBS Lett* 566(1-3): 241-246.

Essner, J.J., Amack, J.D., Nyholm, M.K., Harris, E.B., and Yost, H.J. **2005**. Kupffer's vesicle is a ciliated organ of asymmetry in the zebrafish embryo that initiates left-right development of the brain, heart and gut. *Development* 132(6): 1247-1260.

Essner, J.J., Vogan, K.J., Wagner, M.K., Tabin, C.J., Yost, H.J., and Brueckner, M. **2002**. Conserved function for embryonic nodal cilia. *Nature* 418(6893): 37-38.

Fan, Y., Esmail, M.A., Ansley, S.J., Blacque, O.E., Boroevich, K., Ross, A.J., Moore, S.J., Badano, J.L., May-Simera, H., Compton, D.S., Green, J.S., Lewis, R.A., van Haelst, M.M., Parfrey, P.S., Baillie, D.L., Beales, P.L., Katsanis, N., Davidson, W.S., and Leroux, M.R. **2004a**. Mutations in a member of the Ras superfamily of small GTP-binding proteins causes Bardet-Biedl syndrome. *Nat Genet* 36(9): 989-993

Fan, Y., Rahman, P., Peddle, L., Hefferton, D., Gladney, N., Moore, S.J., Green, J.S., Parfrey, P.S., and Davidson, W.S. **2004b**. Bardet-Biedl syndrome 1 genotype and obesity in the Newfoundland population. *Int J Obes Relat Metab Disord* 28(5): 680-684.

Farag, T.I. and Teebi, A.S. **1989**. High incidence of Bardet Biedl syndrome among the Bedouin. *Clin Genet* 36(6): 463-464.

Fath, M.A., Mullins, R.F., Searby, C., Nishimura, D.Y., Wei, J., Rahmouni, K., Davis, R.E., Tayeh, M.K., Andrews, M., Yang, B., Sigmund, C.D., Stone, E.M., and Sheffield, V.C. **2005**. Mkks-null mice have a phenotype resembling Bardet-Biedl Syndrome. *Hum Mol Genet.*

Fauser, S., Munz, M., and Besch, D. **2003**. Further support for digenic inheritance in Bardet-Biedl syndrome. *J Med Genet* 40(8): e104.

Fettiplace, R. **2006**. Active hair bundle movements in auditory hair cells. *The Journal of physiology* 576(Pt 1): 29-36.

Fields, S. and Song, O. **1989**. A novel genetic system to detect protein-protein interactions. *Nature* 340(6230): 245-246.

Fischer, E., Legue, E., Doyen, A., Nato, F., Nicolas, J.F., Torres, V., Yaniv, M., and Pontoglio, M. **2006**. Defective planar cell polarity in polycystic kidney disease. *Nat Genet* 38(1): 21-23.

Flanagan, J.F., Blus, B.J., Kim, D., Clines, K.L., Rastinejad, F., and Khorasanizadeh, S. **2007**. Molecular Implications of Evolutionary Differences in CHD Double Chromodomains. *Journal of molecular biology* 369(2): 334-342.

Flaus, A., Martin, D.M., Barton, G.J., and Owen-Hughes, T. **2006**. Identification of multiple distinct Snf2 subfamilies with conserved structural motifs. *Nucleic Acids Res* 34(10): 2887-2905.

Frolenkov, G.I., Belyantseva, I.A., Friedman, T.B., and Griffith, A.J. **2004**. Genetic insights into the morphogenesis of inner ear hair cells. *Nature Reviews Genetics*(5): 489-498.

Fuchs, J.L. and Schwark, H.D. **2003**. Neuronal primary cilia: a review. *Cell Biology International*(28): 111-118.

Furness, D.N., Katori, Y., Mahendrasingam, S., and Hackney, C.M. **2005**. Differential distribution of beta- and gamma-actin in guinea-pig cochlear sensory and supporting cells. *Hear Res* 207(1-2): 22-34.

Gale, J.E., Marcotti, W., Kennedy, H.J., Kros, C.J., and Richardson, G.P. **2001**. FM1-43 dye behaves as a permeant blocker of the hair-cell mechanotransducer channel. *J Neurosci* 21(18): 7013-7025.

Gerdes, J.M. and Katsanis, N. **2005**. Microtubule transport defects in neurological and ciliary disease. *Cell Mol Life Sci* 62(14): 1556-1570.

Gerdes, J.M., Liu, Y., Zaghloul, N.A., Leitch, C.C., Lawson, S.S., Kato, M., Beachy, P.A., Beales, P.L., Demartino, G.N., Fisher, S., Badano, J.L., and Katsanis, N. **2007**. Disruption of the basal body compromises proteasomal function and perturbs intracellular Wnt response. *Nat Genet* 39(11): 1350-1360.

Ghadami, M., Tomita, H.A., Najafi, M.T., Damavandi, E., Farahvash, M.S., Yamada, K., Majidzadeh, A.K., and Niikawa, N. **2000a**. Bardet-Biedl syndrome type 3 in an Iranian family: clinical study and confirmation of disease localization. *Am J Med Genet* 94(5): 433-437.

-. **2000b**. Bardet-Biedl Syndrome Type 3 in an Iranian Family: Clinical Study and Confirmation of Disease Localization. *Am J Hum Genet*(94): 433-437.

Giusto, T.J. and Sciubba, J.J. **2004**. Kartagener's syndrome: a review of the literature and case report of oral findings in two siblings. *J N J Dent Assoc* 75(1): 30-32.

Grantham, J., Llorca, O., Valpuesta, J.M., and Willison, K.R. **2000**. Partial occlusion of both cavities of the eukaryotic chaperonin with antibody has no effect upon the rates of beta-actin or alpha-tubulin folding. *J Biol Chem* 275(7): 4587-4591.

Grantham, J.J., Nair, V., and Winklhofer, F. **1996**. Cystic diseases of the kidney. in Brenner & Rector's The Kidney (ed. Brenner, B.M.). *(WB Saunders, Philadelphia)*: 1699-1730.

Green, J.S., Parfrey, P.S., Harnett, J.D., Farid, N.R., Cramer, B.C., Johnson, G., Heath, O., McManamon, P.J., E, O.L., and Pryse-Phillips, W. **1989**. The cardinal manifestations of Bardet-Biedl syndrome, a form of Laurence-Moon-Biedl syndrome. *New England Journal of Medicine* 321(15): 1002-1009.

Gribble, S.M., Prigmore, E., Burford, D.C., Porter, K.M., Ng, B.L., Douglas, E.J., Fiegler, H., Carr, P., Kalaitzopoulos, D., Clegg, S., Sandstorm, R., I.K., T., Youings, S.A., Thomas, N.S., Denis, N.R., Jacobs, P.A., Crolla, J.A., and Carter, N.P. **2005**. The complex nature of constitutional de novo apparently balanced translocations in patients presenting with abnormal phenotypes. *JMed Genet* 42: 8-16.

Gruenbaum, Y., Cedar, H., and Razin, A. **1982**. Substrate and sequence specificity of a eukaryotic DNA methylase. *Nature* 295(5850): 620-622.

Haffter, P., Granato, M., Brand, M., Mullins, M.C., Hammerschmidt, M., Kane, D.A., Odenthal, J., van Eeden, F.J., Jiang, Y.J., Heisenberg, C.P., Kelsh, R.N., Furutani-Seiki, M., Vogelsang, E., Beuchle, D., Schach, U., Fabian, C., and Nusslein-Volhard, C. **1996**. The identification of genes with unique and essential functions in the development of the zebrafish, Danio rerio. *Development* 123: 1-36.

Hagiwara, H., Ohwada, N., and Takata, K. **2004**. Cell biology of normal and abnormal ciliogenesis in the ciliated epithelium. *International review of cytology* 234: 101-141.

Hearn, T., Renforth, G.L., Spalluto, C., Hanley, N.A., Piper, K., Brickwood, S., White, C., Comnnolly, V., Taylor, J.F.N., Russell-Eggitt, I., Bonneau, D., Walker, M., and Wilson, D.I. **2002**. Mutation of *ALMS1*, a large gene with a tandem repeat encoding 47 amino acids, causes Alstrom sndrome. *Nature Genetics* 31: 79-83.

Henderson, C.G., Tucker, J.B., Mogensen, M.M., Mackie, J.B., Chaplin, M.A., Slepecky, N.B., and Leckie, L.M. **1995**. Three microtubule-organizing centres collaborate in a mouse cochlear epithelial cell during supracellularly coordinated control of microtubule positioning. *J Cell Sci* 108 (Pt 1): 37-50.

Heon, E., Westall, C., Carmi, R., Elbedour, K., Panton, C., Mackeen, L., Stone, E.M., and Sheffield, V.C. **2005**. Ocular phenotypes of three genetic variants of Bardet-Biedl syndrome. *Am J Med Genet A* 132(3): 283-287.

Hermann, A., Gowher, H., and Jeltsch, A. **2004**. Biochemistry and biology of mammalian DNA methyltransferases. *Cell Mol Life Sci* 61(19-20): 2571-2587.

Hichri, H., Stoetzel, C., Laurier, V., Caron, S., Sigaudy, S., Sarda, P., Hamel, C., Martin-Coignard, D., Gilles, M., Leheup, B., Holder, M., Kaplan, J., Bitoun, P., Lacombe, D., Verloes, A., Bonneau, D., Perrin-Schmitt, F., Brandt, C., Besancon, A.F., Mandel, J.L., Cossee, M., and Dollfus, H. **2005**. Testing for triallelism: analysis of six BBS genes in a Bardet-Biedl syndrome family cohort. *Eur J Hum Genet* 13(5): 607-616.

Hidaka, S., Konecke, V., Osten, L., and Witzgall, R. **2004**. PIGEA-14, a novel coiled-coil protein affecting the intracellular distribution of polycystin-2. *J Biol Chem* 279(33): 35009-35016.

Huangfu, D., Liu, A., Rakeman, A.S., Murcia, N.S., Niswander, L., and Anderson, K.V. **2003**. Hedgehog signalling in the mouse requires intraflagellar transport proteins. *Nature* 426(6962): 83-87.

Ikeda, A., Zheng, Q.Y., Zuberi, A.R., Johnson, K.R., Naggert, J.K., and Nishina, P.M. **2002**. Microtubule-associated protein 1A is a modifier of tubby hearing (moth1). *Nature Genetics* 30: 401-405.

Ikegami, K., Heier, R.L., Taruishi, M., Takagi, H., Mukai, M., Shimma, S., Taira, S., Hatanaka, K., Morone, N., Yao, I., Campbell, P.K., Yuasa, S., Janke, C., Macgregor, G.R., and Setou, M. **2007**. Loss of alpha-tubulin polyglutamylation in ROSA22 mice is associated with abnormal targeting of KIF1A and modulated synaptic function. *Proc Natl Acad Sci U S A* 104(9): 3213-3218.

Ingley, E., Williams, J.H., Walker, C.E., Tsai, S., Colley, S., Sayer, M.S., Tilbrook, P.A., Sarna, M., Beaumont, J.G., and Klinken, S.P. **1999**. A novel ADP-ribosylation like factor (ARL-6), interacts with the protein-conducting channel SEC61beta subunit. *FEBS Lett* 459(1): 69-74.

Jaeger, R.G., Fex, J., and Kachar, B. **1994**. Structural basis for mechanical transduction in the frog vestibular sensory apparatus: II. The role of microtubules in the organization of the cuticular plate. *Hear Res* 77(1-2): 207-215.

Jawad, Z. and Paoli, M. **2002**. Novel sequences propel familiar folds. *Structure* 10: 447-454.

Jessen, J.R., Topczewski, J., Bingham, S., Sepich, D.S., Marlow, F., Chandrasekhar, A., and Solnica-Krezel, L. **2002**. Zebrafish trilobite identifies new roles for Strabismus in gastrulation and neuronal movements. *Nat Cell Biol* 4(8): 610-615.

Jho, E.H., Zhang, T., Domon, C., Joo, C.K., Freund, J.N., and Costantini, F. **2002**. Wnt/beta-catenin/Tcf signaling induces the transcription of Axin2, a negative regulator of the signaling pathway. *Molecular and cellular biology* 22(4): 1172-1183.

Johnson, K.R., Gagnon, L.H., Webb, L.S., Peters, L.L., Hawes, N.L., Chang, B., and Zheng, Q.Y. **2003**. Mouse models of USH1C and DFNB18: phenotypic and molecular analyses of two new spontaneous mutations of the Ush1c gene. *Hum Mol Genet* 12(23): 3075-3086.

Kahn, R.A., Cherfils, J., Elias, M., Lovering, R.C., Munro, S., and Schurmann, A. **2006**. Nomenclature for the human Arf family of GTP-binding proteins: ARF, ARL, and SAR proteins. *J Cell Biol* 172(5): 645-650.

Karmous-Benailly, H., Martinovic, J., Gubler, M.C., Sirot, Y., Clech, L., Ozilou, C., Auge, J., Brahimi, N., Etchevers, H., Detrait, E., Esculpavit, C., Audollent, S., Goudefroye, G., Gonzales, M., Tantau, J., Loget, P., Joubert, M., Gaillard, D., Jeanne-Pasquier, C., Delezoide, A.L., Peter, M.O., Plessis, G., Simon-Bouy, B., Dollfus, H., Le Merrer, M., Munnich, A., Encha-Razavi, F., Vekemans, M., and Attie-Bitach, T. **2005**. Antenatal presentation of Bardet-Biedl syndrome may mimic Meckel syndrome. *Am J Hum Genet* 76(3): 493-504.

Katsanis, N. **2004**. The oligogenic properties of Bardet-Biedl syndrome. *Hum Mol Genet* 13 Spec No 1: R65-71.

Katsanis, N., Ansley, S.J., Badano, J.L., Eichers, E.R., Lewis, R.A., Hoskins, B.E., Scambler, P.J., Davidson, W.S., Beales, P.L., and Lupski, J.R. **2001**. Triallelic inheritance in Bardet-Biedl syndrome, a Mendelian recessive disorder. *Science* 293(5538): 2256-2259.

Katsanis, N., Beales, P.L., Woods, M.O., Lewis, R.A., Green, J.S., Parfrey, P.S., Ansley, S.J., Davidson, W.S., and Lupski, J.R. **2000**. Mutations in MKKS cause obesity, retinal dystrophy and renal malformations associated with bardet-biedl syndrome. *Nat Genet* 26(1): 67-70.

Katsanis, N., Eichers, E.R., Ansley, S.J., Lewis, R.A., Kayserili, H., Hoskins, B.E., Scambler, P.J., Beales, P.L., and Lupski, J.R. **2002**. BBS4 is a minor contributor to Bardet-Biedl syndrome and may also participate in triallelic inheritance. *Am J Hum Genet* 71(1): 22-29.

Kazmierczak, P., Sakaguchi, H., Tokita, J., Wilson-Kubalek, E.M., Milligan, R.A., Muller, U., and Kachar, B. **2007**. Cadherin 23 and protocadherin 15 interact to form tip-link filaments in sensory hair cells. *Nature* 449(7158): 87-91.

Keller, R. **2002**. Shaping the vertebrate body plan by polarized embryonic cell movements. *Science* 298(5600): 1950-1954.

Kelly, M. and Chen, P. **2007**. Shaping the mammalian auditory sensory organ by the planar cell polarity pathway. *Int J Dev Biol* 51(6-7): 535-547.

Kemp, D.T., Ryan, S., and Bray, P. **1990**. A guide to the effective use of otoacoustic emissions. *Ear Hear* 11: 93-105.

Kibar, Z., Vogan, K.J., Groulx, N., Justice, M.J., Underhill, D.A., and Gros, P. **2001**. Ltap, a mammalian homolog of Drosophila Strabismus/Van Gogh, is altered in the mouse neural tube mutant Loop-tail. *Nat Genet* 28(3): 251-255.

Kim, J.C., Badano, J.L., Sibold, S., Esmail, M.A., Hill, J., Hoskins, B.E., Leitch, C.C., Venner, K., Ansley, S.J., Ross, A.J., Leroux, M.R., Katsanis, N., and Beales, P.L. **2004**. The Bardet-Biedl protein BBS4 targets cargo to the pericentriolar region and is required for microtubule anchoring and cell cycle progression. *Nat Genet* 36(5): 462-470.

Kim, J.C., Ou, Y.Y., Badano, J.L., Esmail, M.A., Leitch, C.C., Fiedrich, E., Beales, P., Archibald, J.M., Katsanis, N., Rattner, J.B., and Leroux, M.R. **2005**. MKKS/BBS6, a divergent chaperonin-like protein linked to the obesity disorder Bardet-Biedl syndrome, is a novel centrosomal component required for cytokinesis. *Journal of Cell Science* 118: 1007-1020.

Klein, D. and Ammann, F. **1969**. The syndrome of Laurence-Moon-Bardet-Biedl and allied diseases in Switzerland. Clinical, genetic and epidemiological studies. *Journal of the Neurological Sciences* 9(3): 479-513.

Klein, T.J. and Mlodzik, M. **2005**. Planar cell polarization: an emerging model points in the right direction. *Annual review of cell and developmental biology* 21: 155-176

Kodama, A., Karakesisoglou, I., Wong, E., Vaezi, A., and Fuchs, E. **2003**. ACF7: an essential integrator of microtubule dynamics. *Cell* 115: 343-354.

Kozminski, K.G., Johnson, K.A., Forscher, P., and Rosenbaum, J.L. **1993**. A motility in the eukaryotic flagellum unrelated to flagellar beating. *Proc Natl Acad Sci USA* 90: 5519-5523.

Kremer, H., van Wijk, E., Marker, T., Wolfrum, U., and Roepman, R. **2006**. Usher syndrome: molecular links of pathogenesis, proteins and pathways. *Hum Mol Genet* 15 Spec No 2: R262-270.

Kubo, A., Saski, H., Yuba-Kubo, A., Tsukita, S., and Shiina, N. **1999**. Centriolar satelites: Molecular characterization, ATP-dependent movement toward centrioles and possible involvement in ciliogenesis. *J Cell Biol* 147: 969-979.

Kubo, A. and Tsukita, S. **2003**. Non-membranous granular organelle consisting of PCM-1: subcellular distribution and cell-cycle-dependent assembly/disassembly. *J Cell Sci* 116(Pt 5): 919-928.

Kulaga, H.M., Leitch, C.C., Eichers, E.R., Badano, J.L., Lesemann, A., Hoskins, B.E., Lupski, J.R., Beales, P.L., Reed, R.R., and Katsanis, N. **2004**. Loss of BBS proteins causes anosmia in humans and defects in olfactory cilia structure and function in the mouse. *Nat Genet* 36(9): 994-998.

Kumandas, S., Akcakus, M., Coskun, A., and Gumus, H. **2004**. Joubert syndrome: review and report of seven new cases. *Eur J Neurol* 11(8): 505-510.

Kwitek-Black, A.E., Carmi, R., Duyk, G.M., Buetow, K.H., Elbedour, K., Parvari, R., Yandava, C.N., Stone, E.M., and Sheffield, V.C. **1993**. Linkage of Bardet-Biedl syndrome to chromosome 16q and evidence for non-allelic genetic heterogeneity. *Nature Genetics* 5(4): 392-396.

Kyttala, M., Tallila, J., Salonen, R., Kopra, O., Kohlschmidt, N., Paavola-Sakki, P., Peltonen, L., and Kestila, M. **2006**. MKS1, encoding a component of the flagellar apparatus basal body proteome, is mutated in Meckel syndrome. *Nat Genet* 38(2): 155-157.

Lagziel, A., Ahmed, Z.M., Schultz, J.M., Morell, R.J., Belyantseva, I.A., and Friedman, T.B. **2005**. Spatiotemporal pattern and isoforms of cadherin 23 in wild type and waltzer mice during inner ear hair cell development. *Developmental biology* 280(2): 295-306.

Laurence, J.Z. and Moon, R.C. **1866**. Four cases of "retinitis pigmentosa" occurring in the same family, and accompanied by general imperfections of development. *Ophthalmol Rev* 2: 32-41.

Lawrence, P.A., Struhl, G., and Casal, J. **2007**. Planar cell polarity: one or two pathways? *Nature Reviews* 8(7): 555-563.

Leppert, M., Baird, L., Anderson, K.L., Otterud, B., Lupski, J.R., and Lewis, R.A. **1994**. Bardet-Biedl syndrome is linked to DNA markers on chromosome 11q and is genetically heterogeneous. *Nature Genetics* 7(1): 108-112.

Lettice, L.A., Heaney, S.J.H., Purdie, L.A., Li, L., de Beer, P., Oostra, B.A., Goode, D., Elgar, G., Hill, R.E., and de Graff, E. **2003**. A long-range *Shh* enhancer regulates expression in the developing limb and fin and is associated with preaxial polydactyly. *Hum Mol Genet* 12(14): 1725-1735.

Li, E., Bestor, T.H., and Jaenisch, R. **1992**. Targeted mutation of the DNA methyltransferase gene results in embryonic lethality. *Cell* 69(6): 915-926.

Li, J.B., Gerdes, J.M., Haycraft, C.J., Fan, Y., Teslovich, T.M., May-Simera, H., Li, H., Blacque, O.E., Li, L., Leitch, C.C., Lewis, R.A., Green, J.S., Parfrey, P.S., Leroux, M.R., Davidson, W.S., Beales, P.L., Guay-Woodford, L.M., Yoder, B.K., Stormo, G.D., Katsanis, N., and Dutcher, S.K. **2004**. Comparative genomics identifies a flagellar and basal body proteome that includes the BBS5 human disease gene. *Cell* 117(4): 541-552.

Lin, C.-M., Chen, H.-J., Leung, C.L., Parry, D., and Liem, R. **2005**. Microtubule actin crosslinking factor 1b: a novel plakin that localizes to the Golgi complex. *Journal of Cell Science* 118: 3727-3738.

Liu, A., Wang, B., and Niswander, L.A. **2005**. Mouse intraflagellar transport proteins regulate both the activator and repressor functions of Gli transcription factors. *Development* 132(13): 3103-3111.

Lorda-Sanchez, I., Ayuso, C., Sanz, R., and Ibanez, A. **2001**. Does Bardet-Biedl syndrome have a characteristic face? *J Med Genet* 38(5): E14.

Lu, L., Horstmann, H., Ng, C., and Hong, W. **2001**. Regulation of Golgi structure and function by ARF-like protein 1 (Arl1). *J Cell Sci* 114(Pt 24): 4543-4555.

Lu, X., Borchers, A.G., Jolicoeur, C., Rayburn, H., Baker, J.C., and Tessier-Lavigne, M. **2004**. PTK7/CCK-4 is a novel regulator of planar cell polarity in vertebrates. *Nature* 430(6995): 93-98.

Luczak, M.W. and Jagodzinski, P.P. **2006**. The role of DNA methylation in cancer development. *Folia histochemica et cytobiologica / Polish Academy of Sciences, Polish Histochemical and Cytochemical Society* 44(3): 143-154.

Marigo, V., Scott, M.P., Johnson, R.L., Goodrich, L.V., and Tabin, C.J. **1996**. Conservation in hedgehog signaling: induction of a chicken patched homolog by Sonic hedgehog in the developing limb. *Development* 122(4): 1225-1233.

Marshall, J.D., Beck, S., Maffei, P., and Naggert, J.K. **2007**. Alstrom syndrome. *Eur J Hum Genet* 15(12): 1193-1202.

Maurer, L. and Orndorff, P.E. **1987**. Identification and characterization of genes determining receptor binding and pilus length of *Escherichia coli* type 1 pili. *J Bacteriol* 169: 640-645.

McGarth, J., Somlo, S., Makova, S., Tian, X., and Brueckner, M. **2003**. Two populations of Node Monocilia Initiate Left-Right Asymmetry in the Mouse. *Cell* 114: 61-73.

McMahon, A.P. **2000**. More surprises in the Hedgehog signaling pathway. *Cell* 100(2): 185-188.

Melby, A.E., Warga, R.M., and Kimmel, C.B. **1996**. Specification of cell fates at the dorsal margin of the zebrafish gastrula. *Development* 122(7): 2225-2237.

Menco, P. **1994**. Ultrastructural aspects of olfactory transduction and perireceptor events. *Semin Cell Biol* 5: 11-24.

Merz, A.J., So, M., and Sheetz, M.P. **2000**. Pilus retraction powers bacterial twitching motility. *Nature* 407: 98-102.

Mogensen, M.M., Henderson, C.G., Mackie, J.B., Lane, E.B., Garrod, D.R., and Tucker, J.B. **1998**. Keratin filament deployment and cytoskeletal networking in a sensory epithelium that vibrates during hearing. *Cell Motil Cytoskeleton* 41(2): 138-153.

Mogensen, M.M., Mackie, J.B., Doxsey, S.J., Stearns, T., and Tucker, J.B. **1997**. Centrosomal deployment of gamma-tubulin and pericentrin: evidence for a microtubule-nucleating domain and a minus-end docking domain in certain mouse epithelial cells. *Cell Motil Cytoskeleton* 36(3): 276-290.

Mogensen, M.M., Malik, A., Piel, M., Bouckson-Castaing, V., and Bornens, M. **2000**. Microtubule minus-end anchorage at centrosomal and non-centrosomal sites: the role of ninein. *J Cell Sci* 113 (Pt 17): 3013-3023.

Mogensen, M.M., Tucker, J.B., Mackie, J.B., Prescott, A.R., and Nathke, I.S. **2002**. The adenomatous polyposis coli protein unambiguously localizes to microtubule plus ends and is involved in establishing parallel arrays of microtubule bundles in highly polarized epithelial cells. *J Cell Biol* 157(6): 1041-1048.

Mollet, G., Salomon, R., Gribouval, O., Silbermann, F., Bacq, D., Landthaler, G., Milford, D., Nayir, A., Rizzoni, G., Antignac, C., and Saunier, S. **2002**. The gene mutated in juvenile nephronophthisis type 4 encodes a novel protein that interacts with nephrocystin. *Nat Genet* 32(2): 300-305.

Montcouquiol, M., Rachel, R.A., Lanford, P.J., Copeland, N.G., Jenkins, N.A., and Kelley, M.W. **2003**. Identification of Vangl2 and Scrb1 as planar polarity genes in mammals. *Nature* 423(6936): 173-177.

Moore, S.J., Green, J.S., Fan, Y., Bhogal, A., Dicks, E., B.A., F., Stefanelli, M., Murphy, C., Cramer, B.C., Dean, J.C.S., Beales, P., Katsanis, N., Bassett, A.S., Davidson, W.S., and Parfrey, P.S. **2005**. Clinical and Genetic Epidemiology of Bardet-Biedl Syndrome in Newfoundland: A22-Year Prospective, Population-Based, Cohort Study. *Am J Hum Genet* 132A: 352-360.

Murcia, N.S., Richards, W.G., Yoder, B.K., Mucenski, M.L., Dunlap, J.R., and Woychik, R.P. **2000**. The Oak Ridge Polycystic Kidney (orpk) disease gene is required for left-right axis determination. *Development* 127(11): 2347-2355.

Mykytyn, K., Braun, T., Carmi, R., Haider, N.B., Searby, C.C., Shastri, M., Beck, G., Wright, A.F., Iannaccone, A., Elbedour, K., Riise, R., Baldi, A., Raas-Rothschild, A., Gorman, S.W., Duhl, D.M., Jacobson, S.G., Casavant, T., Stone, E.M., and Sheffield, V.C. **2001**. Identification of the gene that, when mutated, causes the human obesity syndrome BBS4. *Nat Genet* 28(2): 188-191.

Mykytyn, K., Mullins, R.F., Andrews, M., Chiang, A.P., Swiderski, R.E., Yang, B., Braun, T., Casavant, T., Stone, E.M., and Sheffield, V.C. **2004**. Bardet-Biedl syndrome type 4 (BBS4)-null mice implicate Bbs4 in flagella formation but not global cilia assembly. *Proc Natl Acad Sci U S A* 101(23): 8664-8669.

Mykytyn, K., Nishimura, D.Y., Searby, C.C., Beck, G., Bugge, K., Haines, H.L., Cornier, A.S., Cox, G.F., Fulton, A.B., Carmi, R., Iannaccone, A., Jacobson, S.G., Weleber, R.G., Wright, A.F., Riise, R., Hennekam, R.C., Luleci, G., Berker-Karauzum, S., Biesecker, L.G., Stone, E.M., and Sheffield, V.C. **2003**. Evaluation of complex inheritance involving

the most common Bardet-Biedl syndrome locus (BBS1). *Am J Hum Genet* 72(2): 429-437.

Mykytyn, K., Nishimura, D.Y., Searby, C.C., Shastri, M., Yen, H.J., Beck, J.S., Braun, T., Streb, L.M., Cornier, A.S., Cox, G.F., Fulton, A.B., Carmi, R., Luleci, G., Chandrasekharappa, S.C., Collins, F.S., Jacobson, S.G., Heckenlively, J.R., Weleber, R.G., Stone, E.M., and Sheffield, V.C. **2002**. Identification of the gene (BBS1) most commonly involved in Bardet-Biedl syndrome, a complex human obesity syndrome. *Nat Genet* 15: 15.

Mykytyn, K. and Sheffield, V.C. **2004**. Establishing a connection between cilia and Bardet-Biedl Syndrome. *Trends Mol Med* 10(3): 106-109.

Nachury, M.V., Loktev, A.V., Zhang, Q., Westlake, C.J., Peranen, J., Merdes, A., Slusarski, D.C., Scheller, R.H., Bazan, J.F., Sheffield, V.C., and Jackson, P.K. **2007**. A core complex of BBS proteins cooperates with the GTPase Rab8 to promote ciliary membrane biogenesis. *Cell* 129(6): 1201-1213.

Nakamura, T. **2000**. Cellular and molecular constituents of olfactory sensation in vertebrates. *Comp Biochem Physiol A Mol Integr Physiol* 126(17-32).

Nasevicius, A. and Ekker, S.C. **2000**. Effective targeted gene 'knockdown' in zebrafish. *Nat Genet* 26(2): 216-220.

Naslavsky, N. and Caplan, S. **2005**. C-terminal EH-domain-containing proteins: consensus for a role in endocytic trafficking, EH? *J Cell Sci* 118(Pt 18): 4093-4101.

Nayak, G.D., Ratnayaka, H.S., Goodyear, R.J., and Richardson, G.P. **2007**. Development of the hair bundle and mechanotransduction. *Int J Dev Biol* 51(6-7): 597-608.

Nelson, W.J. **2003**. Adaptation of core mechanisms to generate cell polarity. *Nature* 422(6933): 766-774.

Nishimura, D.Y., Fath, M., Mullins, R.F., Searby, C., Andrews, M., Davis, R., Andorf, J.L., Mykytyn, K., Swiderski, R.E., Yang, B., Carmi, R., Stone, E.M., and Sheffield, V.C. **2004**. Bbs2-null mice have neurosensory deficits, a defect in social dominance, and retinopathy associated with mislocalization of rhodopsin. *Proc Natl Acad Sci U S A* 101(47): 16588-16593.

Nishimura, D.Y., Searby, C.C., Carmi, R., Elbedour, K., Van Maldergem, L., Fulton, A.B., Lam, B.L., Powell, B.R., Swiderski, R.E., Bugge, K.E., Haider, N.B., Kwitek-Black, A.E., Ying, L., Duhl, D.M., Gorman, S.W., Heon, E., Iannaccone, A., Bonneau, D., Biesecker, L.G., Jacobson, S.G., Stone, E.M., and Sheffield, V.C. **2001**. Positional cloning of a

novel gene on chromosome 16q causing Bardet-Biedl syndrome (BBS2). *Hum Mol Genet* 10(8): 865-874.

Nishimura, D.Y., Swiderski, R.E., Searby, C.C., Berg, E.M., Ferguson, A.L., Hennekam, R., Merin, S., Weleber, R.G., Biesecker, L.G., Stone, E.M., and Sheffield, V.C. **2005**. Comparative genomics and gene expression analysis identifies BBS9, a new Bardet-Biedl syndrome gene. *Am J Hum Genet* 77(6): 1021-1033.

Nonaka, S., Shiratori, H., Saijoh, Y., and Hamada, H. **2002**. Determination of left-right patterning of the mouse embryo by artificial nodal flow. *Nature* 418(6893): 96-99.

Nonaka, S.*e.a.* **1998**. Randomization of left-right symmetry due to loss of nodal cilia generating leftward flow of extraembryonic fluid in mice lacking KIF3B motor proteins. *Cell* 95: 829-837.

O'Dea, D., Parfrey, P.S., Harnett, J.D., Hefferton, D., Cramer, B.C., and Green, J. **1996**. The importance of renal impairment in the natural history of Bardet-Biedl syndrome. *American Journal of Kidney Diseases* 27(6): 776-783.

Okada, Y., Yamazaki, H., Sekine-Aizawa, Y., and Hirokawa, N. **1995**. The neuron-specific kinesin superfamily protein KIF1A is a unique monomeric motor for anterograde axonal transport of synaptic vesicle precursors. *Cell* 81(5): 769-780.

Olbrich, H., Fliegauf, M., Hoefele, J., Kispert, A., Otto, E., Volz, A., Wolf, M.T., Sasmaz, G., Trauer, U., Reinhardt, R., Sudbrak, R., Antignac, C., Gretz, N., Walz, G., Schermer, B., Benzing, T., Hildebrandt, F., and Omran, H. **2003**. Mutations in a novel gene, NPHP3, cause adolescent nephronophthisis, tapeto-retinal degeneration and hepatic fibrosis. *Nat Genet* 34(4): 455-459.

Omran, H., Sasmaz, G., Haffner, K., Volz, A., Olbrich, H., Melkaoui, R., Otto, E., Wienker, T.F., Korinthenberg, R., Brandis, M., Antignac, C., and Hildebrandt, F. **2002**. Identification of a gene locus for Senior-Loken syndrome in the region of the nephronophthisis type 3 gene. *J Am Soc Nephrol* 13(1): 75-79.

Otto, E.A., Schermer, B., Obara, T., O'Toole, J.F., Hiller, K.S., Mueller, A.M., Ruf, R.G., Hoefele, J., Beekmann, F., Landau, D., Foreman, J.W., Goodship, J.A., Strachan, T., Kispert, A., Wolf, M.T., Gagnadoux, M.F., Nivet, H., Antignac, C., Walz, G., Drummond, I.A., Benzing, T., and Hildebrandt, F. **2003**. Mutations in INVS encoding inversin cause nephronophthisis type 2, linking renal cystic disease to the function of primary cilia and left-right axis determination. *Nat Genet* 34(4): 413-420.

Ou, G., Blacque, O.E., Snow, J.J., Leroux, M.R., and Scholey, J.M. **2005**. Functional coordination of intraflagellar transport motors. *Nature* 436(7050): 583-587.

Parfrey, P.S., Davidson, W.S., and Green, J.S. **2002**. Clinical and genetic epidemiology of inherited renal disease in Newfoundland. *Kidney Int* 61(6): 1925-1934.

Park, S.Y., Ha, B.G., Choi, G.H., Ryu, J., Kim, B., Jung, C.Y., and Lee, W. **2004**. EHD2 interacts with the insulin-responsive glucose transporter (GLUT4) in rat adipocytes and may participate in insulin-induced GLUT4 recruitment. *Biochemistry* 43(23): 7552-7562.

Park, T.J., Haigo, S.L., and Wallingford, J.B. **2006**. Ciliogenesis defects in embryos lacking inturned or fuzzy function are associated with failure of planar cell polarity and Hedgehog signaling. *Nat Genet* 38(3): 303-311.

Pasqualato, S., Renault, L., and Cherfils, J. **2002**. Arf, Arl, Arp and Sar proteins: a family of GTP-binding proteins with a structural device for 'front-back' communication. *EMBO Rep* 3(11): 1035-1041.

Pazour, G.J., Baker, S.A., Deane, J.A., Cole, D.G., Dickert, B.L., Rosenbaum, J.L., Witman, G.B., and Besharse, J.C. **2002a**. The intraflagellar transport protein, IFT88, is essential for vertebrate photoreceptor assembly and maintenance. *J Cell Biol* 157(1): 103-113.

Pazour, G.J., Dickert, B.L., Vucica, Y., Seeley, E.S., Rosenbaum, J.L., Witman, G.B., and Cole, D.G. **2000**. Chlamydomonas IFT88 and its mouse homologue, polycystic kidney disease gene tg737, are required for assembly of cilia and flagella. *J Cell Biol* 151(3): 709-718.

Pazour, G.J., Dickert, B.L., and Witman, G.B. **1999**. The DHC1b (DHC2) isoformof cytoplasmic dynein is required for flagellar assembly. *J Cell Biol* 144: 473-481.

Pazour, G.J., San Agustin, J.T., Follit, J.A., Rosenbaum, J.L., and Witman, G.B. **2002b**. Polycystin-2 is localized to kidney cilia and its ciliary level is elevated in orpk mice with polycystic kidney disease. *Curr Biol* 12: R378-R380.

Pazour, G.J., Wilkerson, C.G., and Witman, G.B. **1998**. A dynein light chain is essential for retrograde particle movement in intraflagellar transport (IFT). *J Cell Biol* 141: 979-992.

Perkins, L.A., Hedgecock, E.M., Thomson, J.N., and Culotti, J.G. **1986**. Mutant sensory cilia in the nematode *Caenorhabditis elegans*. *Dev Biol* 117: 456-487.

Pickett-Heaps. **1971**. The autonomy of the centriole: fact or fallacy? *Cytobios*(3): 205-214.

Piperno, G., Siuda, E., Henderson, S., Segil, M., Vaananen, H., and Sassaroli, M. **1998**. Distinct mutants of retrograde intraflagellar transport (IFT) share similar morphological and molecular defects. *J Cell Biol* 143: 1591-1601.

Praetorius, H.A., Praetorius, J., Nielsen, S., Frokiaer, J., and Spring, K.R. **2004**. Beta1-integrins in the primary cilium of MDCK cells potentiate fibronectin-induced Ca2+ signaling. *American journal of physiology* 287(5): F969-978.

Praetorius, H.A. and Spring, K.R. **2001**. Bending the MDCK cell primary cilium increases intracellular calcium. *J Membr Biol* 184: 71-79.

Raphael, Y. and Altschuler, R.A. **2003**. Structure and innervation of the cochlea. *Brain research bulletin* 60(5-6): 397-422.

Raphael, Y., Lenoir, M., Wroblewski, R., and Pujol, R. **1991**. The sensory epithelium and its innervation in the mole rat cochlea. *The Journal of comparative neurology* 314(2): 367-382.

Riobo, N.A. and Manning, D.R. **2007**. Pathways of signal transduction employed by vertebrate Hedgehogs. *The Biochemical journal* 403(3): 369-379.

Rosenbaum, J.L. and Witman, G.B. **2002**. Intraflagellar Transport. *Nature Reviews Cell Biology* 3: 813-825.

Ross, A.J., May-Simera, H., Eichers, E.R., Kai, M., Hill, J., Jagger, D.J., Leitch, C.C., Chapple, J.P., Munro, P.M., Fisher, S., Tan, P.L., Phillips, H.M., Leroux, M.R., Henderson, D.J., Murdoch, J.N., Copp, A.J., Eliot, M.M., Lupski, J.R., Kemp, D.T., Dollfus, H., Tada, M., Katsanis, N., Forge, A., and Beales, P.L. **2005**. Disruption of Bardet-Biedl syndrome ciliary proteins perturbs planar cell polarity in vertebrates. *Nat Genet* 37(10): 1135-1140.

Saccone, V., Palmieri, M., Passamano, L., Piluso, G., Meroni, G., Politano, L., and Nigro, V. **2007**. Mutations that impair interaction properties of TRIM32 associated with limb-girdle muscular dystrophy 2H. *Hum Mutat*.

Sakamoto, I., Kishida, S., Fukui, A., Kishida, M., Yamamoto, H., Hino, S., Michiue, T., Takada, S., Asashima, M., and Kikuchi, A. **2000**. A novel beta-catenin-binding protein inhibits beta-catenin-dependent Tcf activation and axis formation. *J Biol Chem* 275(42): 32871-32878.

Sanlaville, D. and Verloes, A. **2007**. CHARGE syndrome: an update. *Eur J Hum Genet* 15(4): 389-399.

Schaap, C., ten Tusscher, M.P., Schrander, J.J., Kuijten, R.H., and Schrander-Stumpel, C.T. **1998**. Phenotypic overlap between McKusick-Kaufman and Bardet-Biedl syndromes: are they related? [letter; comment]. *Eur J Pediatr* 157(2): 170-171.

Schachat, A.P. and Maumenee, I.H. **1982**. Bardet-Biedl syndrome and related disorders. *Archives of Ophthalmology* 100(2): 285-288.

Schoehn, G., Hayes, M., Cliff, M., Clarke, A.R., and Saibil, H.R. **2000**. Domain rotations between open, closed and bullet-shaped forms of the thermosome, an archaeal chaperonin. *Journal of molecular biology* 301(2): 323-332.

Schultz, J., Copley, R.R., Doerks, T., Ponting, C.P., and Bork, P. **2000**. SMART: a web-based tool for the study of genetically mobile domains. *Nucleic Acids Res* 28: 231-234.

Schwartz, E.A., Leonard, M.L., Bizios, R., and Bowser, S.S. **1997**. Analysis and modeling of the primary cilium bending response to fluid shear. *Am J Physiol* 272: F132-F138.

Self, T., Mahony, M., Fleming, J., Walsh, J., Brown, S.D., and Steel, K.P. **1998**. Shaker-1 mutations reveal roles for myosin VIIA in both development and function of cochlear hair cells. *Development* 125(4): 557-566.

Sheffield, V.C., Carmi, R., Kwitek-Black, A., Rokhlina, T., Nishimura, D., Duyk, G.M., Elbedour, K., Sunden, S.L., and Stone, E.M. **1994**. Identification of a Bardet-Biedl syndrome locus on chromosome 3 and evaluation of an efficient approach to homozygosity mapping. *Human Molecular Genetics* 3(8): 1331-1335.

Simons, M., Gloy, J., Ganner, A., Bullerkotte, A., Bashkurov, M., Kronig, C., Schermer, B., Benzing, T., Cabello, O.A., Jenny, A., Mlodzik, M., Polok, B., Driever, W., Obara, T., and Walz, G. **2005**. Inversin, the gene product mutated in nephronophthisis type II, functions as a molecular switch between Wnt signaling pathways. *Nat Genet* 37(5): 537-543.

Singla, V. and Reiter, J.F. **2006**. The primary cilium as the cell's antenna: signaling at a sensory organelle. *Science* 313(5787): 629-633.

Slavotinek, A.M., Stone, E.M., Mykytyn, K., Heckenlively, J.R., Green, J.S., Heon, E., Musarella, M.A., Parfrey, P.S., Sheffield, V.C., and Biesecker, L.G. **2000**. Mutations in MKKS cause bardet-biedl syndrome. *Nat Genet* 26(1): 15-16.

Slepecky, N.B., Henderson, C.G., and Saha, S. **1995**. Post-translational modifications of tubulin suggest that dynamic microtubules are present in sensory cells and stable microtubules are present in supporting cells of the mammalian cochlea. *Hear Res* 91(1-2): 136-147.

Sloboda, R.D. **2002**. A Healthy Understanding of Intraflagellar Transport. *Cell Motility and the cytoskeleton* 52: 1-8.

Smith, U.M., Consugar, M., Tee, L.J., McKee, B.M., Maina, E.N., Whelan, S., Morgan, N.V., Goranson, E., Gissen, P., Lilliquist, S., Aligianis, I.A., Ward, C.J., Pasha, S., Punyashthiti, R., Malik Sharif, S., Batman, P.A., Bennett, C.P., Woods, C.G., McKeown, C., Bucourt, M., Miller, C.A., Cox, P., Algazali, L., Trembath, R.C., Torres, V.E., Attie-Bitach, T., Kelly, D.A., Maher, E.R., Gattone, V.H., 2nd, Harris, P.C., and Johnson, C.A. **2006**. The transmembrane protein meckelin (MKS3) is mutated in Meckel-Gruber syndrome and the wpk rat. *Nat Genet* 38(2): 191-196.

Snell, W.J., Pan, J., and Wang, Q. **2004**. Cilia and flagella revealed: from flagellar assembly in Chlamydomonas to human obesity disorders. *Cell* 117(6): 693-697.

Solis-Cohen, S. and Weiss, E. **1925**. Dystrophia adiposogenitalis, with atypical retinits pigmentosa and mental deficiency. The Laurence-Biedl syndrome: a report of four cases in one family. *American Journal of Medical Science* 169: 489-505.

Stoetzel, C., Laurier, V., Davis, E.E., Muller, J., Rix, S., Badano, J.L., Leitch, C.C., Salem, N., Chouery, E., Corbani, S., Jalk, N., Vicaire, S., Sarda, P., Hamel, C., Lacombe, D., Holder, M., Odent, S., Holder, S., Brooks, A.S., Elcioglu, N.H., Silva, E.D., Rossillion, B., Sigaudy, S., de Ravel, T.J., Lewis, R.A., Leheup, B., Verloes, A., Amati-Bonneau, P., Megarbane, A., Poch, O., Bonneau, D., Beales, P.L., Mandel, J.L., Katsanis, N., and Dollfus, H. **2006**. BBS10 encodes a vertebrate-specific chaperonin-like protein and is a major BBS locus. *Nat Genet* 38(5): 521-524.

Stoetzel, C., Muller, J., Laurier, V., Davis, E.E., Zaghloul, N.A., Vicaire, S., Jacquelin, C., Plewniak, F., Leitch, C.C., Sarda, P., Hamel, C., de Ravel, T.J., Lewis, R.A., Friederich, E., Thibault, C., Danse, J.M., Verloes, A., Bonneau, D., Katsanis, N., Poch, O., Mandel, J.L., and Dollfus, H. **2007**. Identification of a novel BBS gene (BBS12) highlights the major role of a vertebrate-specific branch of chaperonin-related proteins in Bardet-Biedl syndrome. *Am J Hum Genet* 80(1): 1-11.

Stone, D.L., Slavotinek, A., Bouffard, G.G., Banerjee-Basu, S., Baxevanis, A.D., Barr, M., and Biesecker, L.G. **2000**. Mutation of a gene encoding a putative chaperonin causes McKusick-Kaufman syndrome. *Nat Gen* 25(1): 79-82.

Summerton, J. and Weller, D. **1997**. Morpholino antisense oligomers: design, preparation, and properties. *Antisense & nucleic acid drug development* 7(3): 187-195.

Surapureddi, S., Yu, S., Bu, H., Hashimoto, T., Yeldandi, A.V., Kashireddy, P., Cherkaoui-Malki, M., Qi, C., Zhu, Y.J., Rao, M.S., and Reddy, J.K. **2002**. Identification of a transcriptionally active peroxisome proliferator-activated receptor alpha -interacting cofactor complex in rat liver and characterization of PRIC285 as a coactivator. *Proc Natl Acad Sci U S A* 99(18): 11836-11841.

Swoboda, P., Adler, H.T., and Thomas, J.H. **2000**. The RFX-type transcription factor DAF-19 regulates sensory neuron cilium formation in *C. elegans*. *Mol Cell* 5: 411-421.

Takai, Y., Sasaki, T., and Matozaki, T. **2001**. Small GTP-binding proteins. *Physiol Rev* 81: 153-208.

Thulasiraman, V., Yang, C.F., and Frydman, J. **1999**. In vivo newly translated polypeptides are sequestered in a protected folding environment. *The EMBO journal* 18(1): 85-95.

Toby, G.G. and Golemis, E.A. **2001**. Using the yeast interaction trap and other two-hybrid-based approaches to study protein-protein interactions. *Methods (San Diego, Calif* 24(3): 201-217.

Torban, E., Kor, C., and Gros, P. **2004**. Van Gogh-like2 (Strabismus) and its role in planar cell polarity and convergent extension in vertebrates. *Trends Genet* 20(11): 570-577.

Tsiokas, L., Kim, S., and Ong, E.C. **2007**. Cell biology of polycystin-2. *Cellular signalling* 19(3): 444-453.

Tsujikawa, M. and Malicki, J. **2004**. Intraflagellar Transport Genes Are Essential for Differentation and Survival of Vertebrate Sensory Neurons. *Neuron* 42: 703-716.

Tucker, J.B., Mogensen, M.M., Paton, C.C., Mackie, J.B., Henderson, C.G., and Leckie, L.M. **1995**. Formation of two microtubule-nucleating sites which perform differently during centrosomal reorganization in a mouse cochlear epithelial cell. *J Cell Sci* 108 (Pt 4): 1333-1345.

Tucker, J.B., Paton, C.C., Henderson, C.G., and Mogensen, M.M. **1993**. Microtubule rearrangement and bending during assembly of large curved microtubule bundles in mouse cochlear epithelial cells. *Cell Motil Cytoskeleton* 25(1): 49-58.

Tucker, J.B., Paton, C.C., Richardson, G.P., Mogensen, M.M., and Russell, I.J. **1992**. A cell surface-associated centrosomal layer of microtubule-organizing material in the inner pillar cell of the mouse cochlea. *J Cell Sci* 102 (Pt 2): 215-226.

Vale, R.D. **2003**. The molecular motor toolbox for intracellular transport. *Cell* 112(4): 467-480.

Valpuesta, J.M., Martin-Benito, J., Gomez-Puertas, P., Carrascosa, J.L., and Willison, K.R. **2002**. Structure and function of a protein folding machine: the eukaryotic cytosolic chaperonin CCT. *FEBS Lett* 529(1): 11-16.

Vaughan, K.T. and Vallee, R.B. **1995**. Cytoplasmic dynein binds dynactin through a direct interaction between the intermediate chains and p150Glued. *J Cell Biol* 131(6 Pt 1): 1507-1516.

Veeman, M.T., Axelrod, J.D., and Moon, R.T. **2003**. A second canon. Functions and mechanisms of beta-catenin-independent Wnt signaling. *Developmental cell* 5(3): 367-377.

Vissers, L.E.L.M., van Ravenswaaij, C.M.A., Admiraal, R., Hurst, J.A., de Vries, B.B.A., Janssen, I.M., van der Vilet, W.A., Huys, E., de Jong, P.J., Hamel, B., Schoenmakers, E., Brunner, H.G., Veltman, J.A., and van Kassel, A.G. **2004**. Mutations in a new member of the chromodomain gene family cause CHARGE syndrome. *Nature Genetics* 36: 955-958.

Wada, N., Javidan, Y., Nelson, S., Carney, T.J., Kelsh, R.N., and Schilling, T.F. **2005**. Hedgehog signaling is required for cranial neural crest morphogenesis and chondrogenesis at the midline in the zebrafish skull. *Development* 132(17): 3977-3988.

Wang, J., Mark, S., Zhang, X., Qian, D., Yoo, S.J., Radde-Gallwitz, K., Zhang, Y., Lin, X., Collazo, A., Wynshaw-Boris, A., and Chen, P. **2005**. Regulation of polarized extension and planar cell polarity in the cochlea by the vertebrate PCP pathway. *Nat Genet* 37(9): 980-985.

Wang, Y. and Nathans, J. **2007**. Tissue/planar cell polarity in vertebrates: new insights and new questions. *Development* 134(4): 647-658.

Wiederhold, M.L. **1976**. Mechanosensory transduction in "sensory" and "motile" cilia. *Annual review of biophysics and bioengineering* 5: 39-62.

Woods, M.O., Young, T.L., Parfrey, P.S., Hefferton, D., Green, J.S., and Davidson, W.S. **1999**. Genetic heterogeneity of Bardet-Biedl syndrome in a distinct Canadian population: evidence for a fifth locus. *Genomics* 55(1): 2-9.

Yan, D., Wiesmann, M., Rohan, M., Chan, V., Jefferson, A.B., Guo, L., Sakamoto, D., Caothien, R.H., Fuller, J.H., Reinhard, C., Garcia, P.D., Randazzo, F.M., Escobedo, J., Fantl, W.J., and Williams, L.T. **2001**. Elevated expression of axin2 and hnkd mRNA provides evidence that Wnt/beta -catenin signaling is activated in human colon tumors. *Proc Natl Acad Sci U S A* 98(26): 14973-14978.

Yen, H.J., Tayeh, M.K., Mullins, R.F., Stone, E.M., Sheffield, V.C., and Slusarski, D.C. **2006**. Bardet-Biedl syndrome genes are important in

retrograde intracellular trafficking and Kupffer's vesicle cilia function. *Hum Mol Genet* 15(5): 667-677.

Yoder, B.K., Hou, X., and Guay-Woodford, L.M. **2002**. The polycystic kidney disease proteins:polycystin-1, polycystin-2, polaris, and cystin, are co-localized in renal cilia. *J Am Soc Nephrol* 13: 2508-2516.

Yonekawa, Y., Harada, A., Okada, Y., Funakoshi, T., Kanai, Y., Takei, Y., Terada, S., Noda, T., and Hirokawa, N. **1998**. Defect in synaptic vesicle precursor transport and neuronal cell death in KIF1A motor protein-deficient mice. *J Cell Biol* 141(2): 431-441.

Young, A., Dichtenberg, J.B., Purohit, A., Tuft, R., and Doxsey, S.J. **2000**. Cytoplasmic dynein-mediated assembly of pericentrin and gamma tubulin onto centrosomes. *Mol Biol Cell* 11: 2047-2056.

Young, J.C., Hoogenraad, N.J., and Hartl, F.U. **2003**. Molecular chaperones Hsp90 and Hsp70 deliver preproteins to the mitochondrial import receptor Tom70. *Cell* 112(1): 41-50.

Young, R.W. **1976**. Visual cells and the concept of renewal. *Invest Ophthalmol Vis Sci* 15: 700-725.

Young, T.L., Penney, L., Woods, M.O., Parfrey, P.S., Green, J.S., Hefferton, D., and Davidson, W.S. **1999**. A fifth locus for Bardet-Biedl syndrome maps to chromosome 2q31. *Am J Hum Genet* 64(3): 900-904.

Young, T.L., Woods, M.O., Parfrey, P.S., Green, J.S., E, O.L., Hefferton, D., and Davidson, W.S. **1998**. Canadian Bardet-Biedl syndrome family reduces the critical region of BBS3 (3p) and presents with a variable phenotype. *American Journal of Medical Genetics* 78(5): 461-467.

Zallen, J.A. **2007**. Planar polarity and tissue morphogenesis. *Cell* 129(6): 1051-1063.

Zhang, X.M., Ramalho-Santos, M., and McMahon, A.P. **2001**. Smoothened mutants reveal redundant roles for Shh and Ihh signaling including regulation of L/R symmetry by the mouse node. *Cell* 106(2): 781-792.

Zimmerman, W., Sparks, C.A., and Doxsey, S.J. **1999**. Amorphous no longer: the centrosome comes into focus. *Current opinion in cell biology* 11(1): 122-128.

Zon, L.I. **1999**. Zebrafish: a new model for human disease. *Genome research* 9(2): 99-100.

Appendices

Appendix A: Primer Lists

BBS1

Primer	Sequence	Size	PCR
x1F	TGTAAAACGACGGCCAGTATTCCTCAACCCAGGAAGGT	401	TD55
x1R	CAGGAAACAGCTATGACCGCGACCTCCAGACACACATA		
x2+3F	TGTAAAACGACGGCCAGTCCTGGACTTGTACCCAGACG	460	TD55
x2+3R	CAGGAAACAGCTATGACCTTTCAGCCGTCAGGAAATCT		
x4F	TGTAAAACGACGGCCAGTTTGGTGCAGGAATGAATGAA	523	TD55
x4R	CAGGAAACAGCTATGACCATAGCTGACCTCCTGCCACC		
x5+6F	TGTAAAACGACGGCCAGTGGAGGCAGAGACCAAGAGGT	417	TD55
x5+6R	CAGGAAACAGCTATGACCTCCATCATTCTGGCACATTC		
x7F	TGTAAAACGACGGCCAGCCATCCAGTCACTCAGGTAAG	381	TD55
x7R	CAGGAAACAGCTATGACCTGGCTGGAAGGGATATAGCA		
x8F	TGTAAAACGACGGCCAGTTCTTCTGTCACATCTCTGATATTTCC	396	TD55
x8R	CAGGAAACAGCTATGACCACAAGGAACATATATATTACCCAGAAC		
x9F	TGTAAAACGACGGCCAGTGCTTTTGCTAAATGTTGCCC	417	TD55
x9R	CAGGAAACAGCTATGACCAAATTCCAGCCTTAAAGCCC		
x10F	TGTAAAACGACGGCCAGTGTTTTCCAAGGCCACACATT	432	TD55
x10R	CAGGAAACAGCTATGACCGAAAGAACGGTTTCTGGGGT		
x11F(Barts)	TGTAAAACGACGGCCAGTGAGAGAGTCCTCTGGCTTCCC	323	PCR71
x11R(Barts)	CAGGAAACAGCTATGACCAAGGAGGAGTGAGTGGCAGA		
x12F	TGTAAAACGACGGCCAGTTATTAGGAGGTTGACCCCA	458	TD55
x12R	CAGGAAACAGCTATGACCAGGCCTTACTTTCCACACCC		
x13F	TGTAAAACGACGGCCAGTCTCGTCTGGAAGACGGATGT	460	TD55/PCR65
x13R	CAGGAAACAGCTATGACCTGGATTTGCAGAGGTGAGTG		
x14F	TGTAAAACGACGGCCAGTGCAGACTCCTCCTGCAGCAC	408	TD55/PCR65
x14R	CAGGAAACAGCTATGACCCTGAGTTGGCTTGGAATTGG		
x15F	TGTAAAACGACGGCCAGTTTGAGTAGGAGGAGGGGACA	431	TD55
x15R	CAGGAAACAGCTATGACCCTGGTCTGTGGTGGGAGAGT		
x16F	TGTAAAACGACGGCCAGTTGGGAGTCCAGAGGTCTAGG	457	TD55
x16R	CAGGAAACAGCTATGACCCTCCACTGTGCAGATACCC		
x17F	TGTAAAACGACGGCCAGTGACATCATCAAGGTAGGCCC	472	TD55
x17R	CAGGAAACAGCTATGACCGGGTGCTTAAGAGAGGGGAG		

Appendix 1: *BBS1* primer sequences including amplicon size and PCR conditions. M13 tags (Forward - TGTAAAACGACGGCCAGT, Reverse – CAGGAAACAGCTATGACC) were added to all primer pairs to improve stability.

BBS2

Primer	Sequence	Size	PCR
x1F	GCGTGAGGCCAGCTCCGCTGC	254	Failsafe H
x1R	GCGCGGCCGGCGGAGATCCTG		
x2F	TTTTAAGGGAATGTAATTAGT	325	TD55
x2R	TGGACATTAATGAGTAATGAC		
x3F	CTGTTTTACTCAAAATCTGCTCAG	409	PCR61/PCR65
x3R	TTAGCTACATGAAGGAGAGGATTAC		
x4F	AATCCTCTCCTTCATGTAGCT	239	TD55
x4R	GGAGAAGCTTACACTTCTGTC		
x5F	AGAAGCAGCATGCAAAGTACT	240	TD55
x5R	TCATCTGACAGTACTGATCTA		
x6F	TATAAAGCCGTACTTGACAGT	222	TD55
x6R	CAATAACTATCAAGCGCCTGA		
x7F	TATTGTGAGACTTCTGTGCTA	213	TD55
x7R	TGTTACTGTTCTAAGTCCTAC		
x8F	AGAATACTCTTGAAAACTGCT	349	TD55
x8R	ATCTCGGTACAAATACTTCAG		
x9F	TAAGAGCAGGTAATTGATGAC	308	TD55
x9R	CCCTGGCAATGACACTCTCAT		
x10F	GGCTCTGTCTTTTGAAGCTGA	338	TD55
x10R	CCAAGACAGAGGAAGACTCTG		
x11F	ACCTCCTGACCTCGTGATCTG	344	TD55
x11R	CCCCAAGAATCCACTGGGCAT		
x12F	CCTTAAATATCAATTGATGAC	344	TD55
x12R	ACTGCTACCAATATAACACAT		
x13F	GAATGTTACTTAAGAGCATAG	481	TD55
x13R	CTGAATGGTAAACACCACATG		
x14F	GCTAAGTTTGTCTAACATCTG	281	PCR55
x14R	ACATAAGTACATTTGTAGTAC		
x15F	TTAATTGGTATAAGCGAACAG	330	TD55
x15R	TTATACTTCTATTGGTAACAT		
x16F	TAAGCTTGCCATATCAACATG	291	TD55
x16R	ATATGAATTATTGGATGCTAC		
x17F	TTGTTTTAAAACTGACGTCTA	389	TD55
x17R	ATTCAGCAACAGTACTACTAC		

Appendix 2: *BBS2* primer sequences including amplicon size and PCR conditions.

BBS3

Primer	Sequence	PCR
x1F	GCAGGAAATAGGCAGCTCAC	TD52
x1R	TACACGCGTGGAGTGAAAAA	
x2aF	GTGTCTCTCGCTGCACACTT	TD52
x2aR	TTTTAAAAACGACAACTTCTCACA	
X2bF	GGCACAAATGGAAGTACCTGA	TD52
X2bR	TCATCTCCATCTAAGGTTGCAT	
X3F	CTGCAAATCTGCGTGTCAGT	TD52
X3R	CTGCAAATTATGGCTGAGGA	
X4F	CACACAGAGTGATCCTATTGAAAAA	TD52
X4R	AAACCAGCCATAGTGGTTAGAAA	
X5F	ATTGGCACATGTTGAATATTGC	TD52
X5R	CTGAAGTGAAGTAGGATAGAATGGG	
X6F	ATAATACTTAGGTTAGGAAATGCCC	TD52
X6R	GTTAGACACCCCAAAAACAATG	
X7F	CTGCTCAAATACATGCCTAACA	TD52
X7R	GCTTATATGCCACCATGTTTGA	
X8F	TGTTCCTGAGCACTCAGACTTTT	TD52
X8R	GGAACAAGGTATTGGATACTTACTGT	
X9F	GACCACTTGCACCCAGAAGT	TD50
X9R	GGATGAGATGGCTTATAACTGACTTT	
x10F	CCCTATTCAGCCTGTGCTTT	TD52
x10R	TCGCAGACGTACACAAACCT	

Appendix 3: *BBS3* primer sequences and PCR conditions.

BBS4

Primer	Sequence	Size	PCR
x1F	GAGCAGACCCTAATCCTCCC	343	TD55
x1R	CAGTTCCCGGGACAGTAAAA		
x2F	TTGCATAATTGGTGAGCTACTGA	300	TD55
x2R	AGGTGGCAGTGAGCCAAGAT		
x3F	TGTGATATTGCAGTATGTTTATGGT	343	TD55
x3R	TCACTACCATAGCAAAAGATAACCAG		
x4F	CATAATCTGCCTGCCTTGGT	371	TD55
x4R	TCACACAATGACAAAATTGCC		
x5F	TGTCAGCAGTTTTGGTTGTTG	417	PCR63
x5R	ACCATTCCCCCACTTGTGTA		
x6F	GCAGCTTCACTGACCAAACC	413	PCR63
x6R	CAGCAATGCCTGCAAAGTTA		
x7F	AAAAAGCTGACTGTAATGCATAGTTT	376	PCR63
x7R	CAAGCAGAAAACAACAGATGAA		
x8F	GGCTGTTTGCTGAAATGTGA	417	PCR63
x8R	TCTACCTTATTGAAGCTACTGGGA		
x9F	CACCAGGGTTGAGATGACCT	418	PCR63
x9R	GCTTCCAATTTAAATGCAGAAAA		
x10F	ATGTTGGTCAGGCTGGTCTC	389	TD55
x10R	TTTCAAATAAGAAGAGCCACCTTT		
x11F	CTGATGGGCCTGCTGAGTAT	434	PCR63
x11R	TGCATGGTCAAATGGACAAG		
x12F	TGGAATGTGTTTCTTTGGCA	420	PCR63
x12R	CAGGATCTCTAAGGGAATGGC		
x13F	GGATGCATAGAACCTGGCAACTG	318	PCR71
x13R	CACCTCATGGCTTTGGAGAGTCC		
x14F	TTAACCAGTTTTGTTTTGTTTTTGTG	321	TD55
x14R	TGGATTTGGATGATCTGGGCTTG		
x15F	TTTGATAAGTACTTCCTGCCTCAA	473	TD55
x15R	TCCCCTTGTGGCCAATACTA		
x16F	GGCAAACTTGACTGTTGCTTT	429	TD55
x16R	CTTAGGCTCAACTGCTGGCT		

Appendix 4: *BBS4* primer sequences including amplicon size and PCR conditions.

BBS5

Primer	Sequence	Size	PCR
x1F	CGTAGACGTCGTGACAGAGG		1mM $MgCl_2$ TD55
x1R	GAACCAGCCTGAGGTCTCTC		
x2F	CCACTGATCTTCAGGTTC		TD55
x2R	CACTGGAAAATGATGCTGTTTC		
x3F	TGGGCCAGAAGTTCCATATC		TD55
x3R	TATCAAAGGCACCATGCAAA		
x4F	AAGGAGACAGAATTGACCCTCT		PCR60
x4R	GCTTCAGTTTGGCCTCGTAA		
x5F	TGCTCTTTACATTCTTTGCTTTTG		PCR60
x5R	TGGAAAAACTGTCTTCCATGA		
x6F	AAACATAACCCAAGAAAATCACA		TD55
x6R	GAAAAGTAATACGCTTTCCTATAATGC		
x7F	AAGTCCAGGCTGTCACTCGT		TD55
x7R	GGAGAAAGAACTCATCTAAAAGTCCA		
x8F	GGAAGGAGGGAGAATTCTGTT		TD55
x8R	CCTCTGGGGACAATTTCTG		
x9F	TGTTCTTCAGACTTGTTGGGTTT		TD55
x9R	ATGCCCACTTGAGCAGAATC		
x10F	TTTGCAGTTCTCATGGTACATT		TD55
x10R	TTCAAACTCAGGTTTAAGACACCA		
x11+12F	CCTTAGCCCACTGATCTATTCG		TD55
x11+12R	CGGTTACTAGGCCATGTGTC		

Appendix 5: *BBS5* primer sequences including amplicon size and PCR conditions.

BBS6

Primer	Sequence	Size	PCR
x3aF	GATTTTATAGCCACAATGCT	492	TD55
x3aR	ATGACAGTGGTGGGTGTCAA		
x3bF	TCTGGTGAGCATACAGGCAG	498	TD55
x3bR	CGTTTGGAAGCTAAGAAGCC		
x3cF	GATCCTCCTTTGTTTGGTGC	392	TD55
x3cR	GGTTAAGCAGCTGGTCCAAG		
x3dF	AATCAACTGCCCTCAAGGTG	421	TD55
x3dR	CCTTTGCTGCCAGAAATGAT		
x4F	ATGCTTGTGGGGCTTTTATG	475	TD55
x4R	AATGGCAACACATGCCAAAT		
x5F	GCACCACACAAGTTTTGTTC	378	TD55
x5R	CCTATACATGCACCCCTGAA		
x6aF	GTGCCAGACCCCAAATTAAA	391	TD55
x6aR	CCAGTTGAGTTCTTCCTGGC		
x6bF	GGCAGATTCTCCCTGTGTTG	447	TD55
x6bR	GCATTTCCATTCACGAATCA		

Appendix 6: *BBS6* primer sequences including amplicon size and PCR conditions.

BBS7

Primer	Sequence	PCR
x1F	TGTAAAACGACGGCCAGTGCCCTATCCCTTGGGTTT	TD55
x1R	CAGGAAACAGCTATGACCGTCTGGGGTCTCTGTGGA	
x2F	TGTAAAACGACGGCCAGTAAGCATCTTGCCAGTCAT	TD55
x2R	CAGGAAACAGCTATGACCTGTCCCTTGGTATTCCAG	
x3F	TGTAAAACGACGGCCAGTTTACTTTTGTGCTACCCG	TD55
x3R	CAGGAAACAGCTATGACCGGAACAAAATCTATGGCC	
x4F	TGTAAAACGACGGCCAGTTTCCAGAAAGCCTATTAA	TD55
x4R	CAGGAAACAGCTATGACCAAAAACCTGAAGACCTGC	
x5F	TGTAAAACGACGGCCAGTTTCAGCTTTCAAAATCAA	TD55
x5R	CAGGAAACAGCTATGACCATAACAGCAACCTGTAA	
x6F	TGTAAAACGACGGCCAGTCGTGCTGTTAGTTACTGG	TD55
x6R	CAGGAAACAGCTATGACCTGCAAAATTGCTAACAAA	
x7F*	TGTAAAACGACGGCCAGTAGATAAATCAAGGTGTGA	TD55
x7R	CAGGAAACAGCTATGACCAATGGGGAAATGTCTTAT	
x8F	TGTAAAACGACGGCCAGTTCCTGCTTAAAGGCAAGA	TD55
x8R	CAGGAAACAGCTATGACCTTGCTCACCATTCTGAGT	
x9F	TGTAAAACGACGGCCAGTTGAGGTTTGAGGCTTCCA	TD55
x9R	CAGGAAACAGCTATGACCTTCCTGCCATTTGTTCAA	
x10F	TGTAAAACGACGGCCAGTCAGCACTTACGCTAATTT	TD55
x10R	CAGGAAACAGCTATGACCGATATTGGTGGACAAAGG	
x11F	TGTAAAACGACGGCCAGTGCACTCCAGTCTAGGTGA	TD55
x11R	CAGGAAACAGCTATGACCTCAACCAATAAAAACCCA	
x12F	TGTAAAACGACGGCCAGTCCGACACAGATTTTGAAG	TD55
x12R	CAGGAAACAGCTATGACCTAAGGGGGTGGTGAGAGA	
x13F	TGTAAAACGACGGCCAGTGAGATTGTGGTGTGGGCT	TD55
x13R	CAGGAAACAGCTATGACCCATGTTTGAAAAGCGCTG	
x14F	TGTAAAACGACGGCCAGTTCCAACTCAAACCAGCCT	TD55
x14R	CAGGAAACAGCTATGACCGGAACAGAGTGGGACAGG	
x15F	TGTAAAACGACGGCCAGTTCAATCAGATTACTCACA	TD55
x15R	CAGGAAACAGCTATGACCAGCACAGGTGCAGGTATA	
x16F	TGTAAAACGACGGCCAGTGTCCACGACGACACATGT	TD55
x16R	CAGGAAACAGCTATGACCCAATTTCCTTCTACAGCT	
x17F	TGTAAAACGACGGCCAGTTTTCAAGATGTGCAGGTT	TD55
x17R	CAGGAAACAGCTATGACCGCTACAAAAAGGAAAATT	
x18F	TGTAAAACGACGGCCAGTTTGTCAACTGATTCATGA	TD55
x18R	CAGGAAACAGCTATGACCAAGTACATGTGTCGTCGT	

Appendix 7: *BBS7* primer sequences and PCR conditions. M13 tags (Forward - TGTAAAACGACGGCCAGT, Reverse – CAGGAAACAGCTATGACC) were added to all primer pairs to improve stability. *The *BBS7* x7 amplicon resultes in a 468bp fragment.

MGC1203

Primer	Sequence	Size	PCR
X1F	ACAGGGTCCCCTAGGTTCAG		PCR60
X1R	GCGACCGGGGATCTATTT		
X2F	AGACACTGGCATCTGGCTCT		PCR65
X2R	TAGGGACTGGGTCTGAGTGA		
x3F	CCCAAGGGGAACCATAAAGT		PCR65
x3R	CTGTCTGAACCCTGGGAAAG		
X4F	AGGCCTTCGGTGAGTCCTG		PCR68
X4R	CTCTGGGGGCTATCTTCTGG		
X5F	TACTCCCAAGCCATTCCTG		PCR68
X5R	ACTGAGGACCAGGTGAGGTG		

Appendix 8: *MGC1203* primer sequences including amplicon size and PCR conditions.

TUBB4Q

Primer	Sequences	Sizes	PCR
x1F	AGGTGGGTGCACCTGTGTGGAAGTA	~300	2mM $MgCl_2$ PCR 55
x1R	CAAGAGACGGGAGGAGACAGACA		
x2+3F	GTGGCCGGGGAAGGTGTTGGCAGTGGC	~300	Failsafe D
x2+3R	CCCAGAGGATGACCTTAGCA		
x4aF	TTCATCTGCTCCACCTGCAGGGCGAAC	~300	PCR 68
x4aR	GGGCACGTGGTGACCCCACTCAT		
x4bF	GGAGGAGTACCCAGACAGGA	~300	PCR 68
x4bR	CACAGACGGCTGTTTTTACG		
x4cF	ACATGATGGCTGCCTGTGA	~300	PCR 68
x4cR	GTCAGAACACAGTAAAGAATCCACA		

Appendix 9: *TUBB4Q* primer sequences including amplicon size and PCR conditions.

BAIAP1

Primer	Sequence	Size	PCR
x1F	TGTTTCTCCCATGAACAAGC	499	TD55 2 mol Betaine
x1R	GAGGAGGGAAGCAGGAAATC		
x2F	TGTGGCTTTCTTGCAATCAG	281	TD58
x2R	TCCTTTCTCCCCTGGACTTT		
x3F	TTGGTAGGGTAGGAGTCATGC	401	TD58
x3R	GAGTCACCAAGAGGGGGA		
x4F	CGTTTGGTAAATCACCTCACA	342	TD58
x4R	CAAGGGACCCAGGAGACA		
x5F	TGGTGGTATTCCTGCCAA	310	TD58
x5R	AGGGCTTCTGCACACCTC		
x6F	GGGATGAATAAAGCTGCCA	397	TD58
x6R	CCCTTTGCTATATTCCCACG		
x7F	TTCTGCACGTGAGGTCTGA	347	TD55
x7R	CACAGTAGCAACCAGCCG		
x8F	CGAGGACACGATGACGAA	389	TD55
x8R	CAGGTGCTGTCTCCTCCC		
x9F	TTGATTCCAGGGACTTGGTC	297	TD58
x9R	GACCACACGAGGGTGTCAG		
x10F	CCCAATGAGAAACCCACAC	346	TD55
x10R	TCCATCTGATCAAGCACCA		
x11F	AGCACTTCCCTTCATGCC	335	
x11R	CAGCCATGACCTTTATTGTGA		
x12F	TTCAGCTTTATGTTAGTGGGAGA	806	TD55
x12R	TTTAAAAAGCCCCCAGTGGT		
x13F	CTGTCTCCCCCATCCACT	183	TD58
x13R	TCCCCTCCTTGTTGCATT		
x14F		415	TD55
x14R			
x15F	CGTTGCTTGGTCTTGCTC	396	TD58
x15R	GGCTCTAGGGCATAAGCG		
x16F	TTGGGAGTTACGAGATTCCA	293	TD55
x16R	TGCCCTTGGTTTATTGCC		
x17F	GACCACACGAGGGTGTCA	265	PCR68
x17R	TGCTGGTGGGATGAACTG		
x18F	TAGCAGGAGTTGCTGGAAGG	478	TD55 2 mol Betaine
x18R	TTCTGCACGTGAGGTCTGAG		
x19F	TTCCCTTTTCAACCCTTTTTC	381	TD55
x19R	CACGAACACTAATCAAAGAGAGAGA		
x20F	CCCGACTGACCTGGCTAC	243	TD55
x20R	TCCGTCATTGGGCTTCTT		
x21F	GCAACTGCTAGACAGAGGGA	360	TD58
x21R	TTCCCGGGTATGGGGTAT		
x22F	GCAAGCACTGTGTGGTCC	379	TD55
x22R	CATGCAAATGTGTCTCTCCA		
x23F	GATGTTCTGCCACGTGCTTA	425	TD55
x23R	ATGCCCCAGTCCACGTAA		
x24aF	TCGAGTGTGGGTGGGAAC	465	TD55 2 mol Betaine
x24aR	CCCTCCTCTCCAAAGTGTTG		
x24bF	CAGCGCCGACAACACTTT	465	TD55 2 mol Betaine
x24bR	AATTTCAGGTTTGTGACTTTCC		
Exonic primer for RT-PCR Between 4-5			
F	GCCAGTCAGTGGGAAAGTGA	400	
R	CCAAGATGTTGTTTTCGTGTT		

Appendix 10: *BAIAP1* primer sequences including amplicon size and PCR conditions.

Apendix B: Additional yeast information

Yeast Strain: PJ69-4A

Genotype: *Mata, trp1-901, leu2-3,-112, ura3-52, his3-200, gal4Δ, gal80Δ, GAL2-ADE2, LYS2::GAL1-HIS3, met2::GAL7-lacZ*

Appendix 1: Genotype of S.cerevisiae yeast used for the yeast two-hybrid screen.

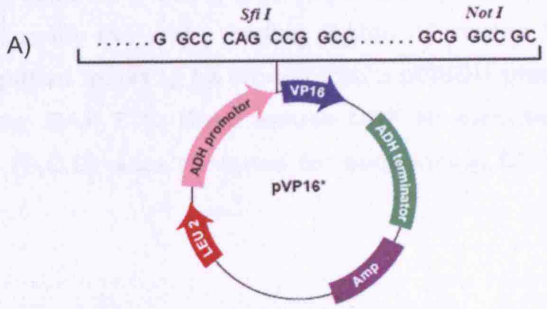

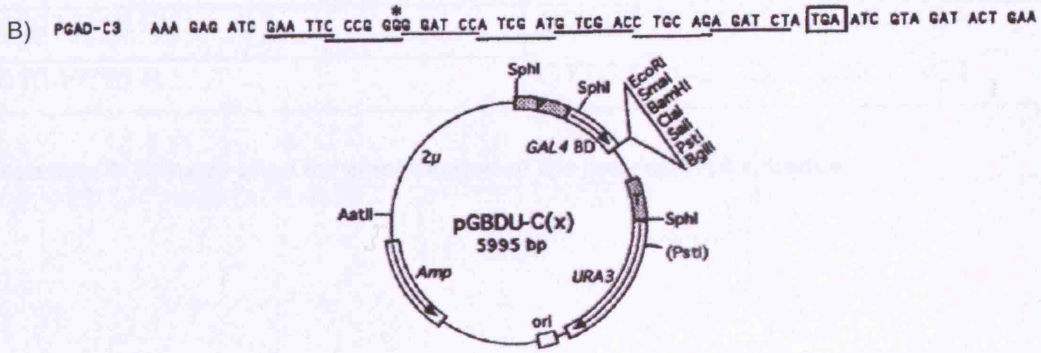

Appendix 2: Vector maps for A) pVP16 and B) pGBDU plasmid used during the yeast two-hybrid screen.

Primer	Sequences
Bbs6 mouse ORF F (A)	CCG GAA TTC ATG TCT CGG TTA GAA GCT AAG
Bbs6 mouse ORF R (E)	CCG GTC GAC TTA GTT TTT ATC TTC AAT GAC ATA TG
Bbs6 mouse ORF (B)	TGACTGCGGCTTATTCACAG
Bbs6 mouse ORF (C)	CAGCCTGTATGCTCACCAGA
Bbs6 mouse ORF (D)	ATCGACAGAGTTGGGGTGAC

Apendix 3: Primers used for Cloning and Yeast two-hybrid analysis of Bbs6. Primers were designed to amplify the entire coding region of murine BBS6. Restriction sites were to enable amplified insert to be cloned into a pGBDU plasmid. Bbs6 mouse ORF includes EcoR1 site: GAA TTC. Bbs6 mouse ORF R: includes Sal1 site: GTC GAC. Additional primers (B,C,D) were designed for sequencing BBS6 insert in the pGBDU plasmid.

Primers	Sequence
509 VP16 F	CGACTTCGAGTTTGAGCAGA
510 VP16 R	GTTGTAAAACGACGGCCAGT

Apendix 4: Primers used for amplification of the prey cDNA sequence

Apendix C: Additional mouse information

Primer	Sequences	PCR
A	TACAGAGGCACCTGGCTACC	PCR65
B	TCCTGTGGCATTATGGGTCT	
LTR	AAATGGCGTTACTTAAGCTAGCTTGC	
Exonic primer for RT-PCR Between 4-5		
x4	GTGTGCTCTGCAAGATTTGG	TD55
x5	AAGACGTGCATTGCTGTTTG	

Appendix 1: Primer sequences including PCR condition for genotyping of the *Bbs6*$^{-/-}$ mouse.

Primer	Sequences	PCR
Forward	GTAACTGGCTTTTTGCATCACTCA	TD55
Reverse	TCAGTTGGGGATACACAAATAAAC	
LTR	AAATGGCGTTACTTAAGCTAGCTTGC	

Appendix 2: Primer sequences including PCR condition for genotyping of the *Bbs4*$^{-/-}$ mouse.

Day 1		Day 2		Day 3	
Wild Type	*Bbs -/-*	Wild Type	*Bbs -/-*	Wild Type	*Bbs -/-*
3	71	30	190	88	105
9	62	22	144	33	109
28	37	31	33	155	119
10	30	37	300	108	210
12	35	9	23	32	59
8	27	20	24	71	200
30	43		50		219
	44				

Appendix 3: Raw data from the olfactory behavioural tests. Numbers are seconds taken for an individual mouse to retrieve the buried food treat.

male		14	21	28	35	42	49	56	63	70	77	84	91	98	105	112	119	126	133	140	147	154	161	168	175	182
Bbs6+/+	2.1.7	*8*	*10*	*16*	*22*	*24*	*26*	*28*	*29*	*30*	*30*	*31*	*32*	*33*	*33*	*34*	*35*	*35*	*35*	*35*	*35*	*36*	*36*	*37*	*38*	*38*
Bbs6+/+	3.1.7	*8*	*11*	*17*	*24*	*25*	*27*	*29*	*29*	*30*	*31*	*31*	*32*	*33*	*34*	*35*	*35*	*36*	*37*	*38*	*38*	*38*	*38*	*38*	*38*	*39*
Bbs6+/+	4.1.5	*7*	*9*	*14*	*18*	*22*	*23*	*25*	*26*	*26*	*28*	*28*	*28*	*28*	*28*	*28*	*28*	*28*	*28*	*28*	*29*	*29*	*29*	*30*	*30*	*30*
Bbs6+/+	11.1.3	*8*	*10*	*15*	*21*	*24*	*27*	*28*	*29*	*30*	*31*	*31*	*32*	*32*	*33*	*33*	*34*	*34*	*35*	*35*	*35*	*35*	*36*	*36*	*37*	*37*
Bbs6-/-	2.1.8	*5*	*7*	*11*	*17*	*22*	*23*	*25*	*26*	*28*	*28*	*28*	*29*	*30*	*30*	*32*	*32*	*32*	*32*	*32*	*33*	*33*	*33*	*34*	*35*	*34*
Bbs6-/-	9.1.2	*5*	*6*	*8*	*12*	*17*	*18*	*20*	*23*	*24*	*25*	*24*	*26*	*26*	*25*	*26*	*27*	*27*	*25*	*25*	*26*	*26*	*26*	*26*	*26*	*26*
Bbs6-/-	11.1.1	*7*	*8*	*13*	*19*	*22*	*26*	*27*	*27*	*28*	*29*	*29*	*30*	*29*	*30*	*30*	*30*	*30*	*31*	*31*	*31*	*32*	*32*	*33*	*33*	*33*
Bbs6-/-	11.1.5	*7*	*9*	*12*	*18*	*20*	*23*	*23*	*23*	*26*	*27*	*29*	*30*	*31*	*32*	*33*	*33*	*34*	*34*	*35*	*35*	*36*	*35*	*36*	*36*	*36*
female																										
Bbs6+/-	2.1.3	*6*	*8*	*12*	*16*	*19*	*19*	*21*	*22*	*22*	*23*	*23*	*24*	*24*	*24*	*23*	*23*	*24*	*24*	*24*	*25*	*24*	*24*	*died*		
Bbs6+/+	2.1.5	*7*	*9*	*13*	*18*	*20*	*21*	*22*	*22*	*23*	*25*	*25*	*25*	*26*	*27*	*26*	*26*	*27*	*28*	*29*	*30*	*30*	*30*	*31*	*31*	*29*
Bbs6+/-	4.1.9	*8*	*11*	*15*	*19*	*20*	*21*	*22*	*24*	*24*	*24*	*25*	*25*	*26*	*26*	*26*	*26*	*26*	*27*	*27*	*27*	*27*	*27*	*27*	*27*	*28*
Bbs6+/-	9.1.3	*8*	*9*	*11*	*15*	*19*	*21*	*22*	*23*	*23*	*24*	*25*	*26*	*26*	*26*	*26*	*26*	*27*	*28*	*27*	*28*	*29*	*28*	*31*	*30*	*30*
Bbs6-/-	2.1.6	*6*	*7*	*11*	*16*	*18*	*19*	*21*	*21*	*22*	*24*	*25*	*26*	*28*	*27*	*27*	*28*	*29*	*30*	*31*	*32*	*32*	*32*	*32*	*32*	*32*
Bbs6-/-	3.1.5	*7*	*8*	*10*	*14*	*16*	*18*	*19*	*19*	*19*	*20*	*20*	*21*	*21*	*21*	*22*	*22*	*22*	*22*	*23*	*23*	*23*	*24*	*24*	*24*	*24*
Bbs6-/-	4.1.1	*5*	*6*	*8*	*10*	*13*	*15*	*16*	*16*	*17*	*17*	*18*	*18*	*19*	*19*	*19*	*19*	*20*	*20*	*20*	*20*	*20*	*20*	*21*	*22*	*22*
Bbs6-/-	11.1.2	*8*	*11*	*13*	*17*	*20*	*20*	*20*	*21*	*22*	*22*	*22*	*23*	*22*	*23*	*24*	*25*	*26*	*25*	*25*	*24*	*25*	*25*	*25*	*27*	*27*

Appendix 4: Mouse weights over a period of six months. Age along the top (bold) given in days, weights (italics) are in grams.

Apendix D: Antibody Information

Primary Antibodies	Animal Raised In	Supplier	Concentration
BBS6	Rabbit	M. Leroux, Simon Fraser University, Canada	1 in 50 - 1 in 200
BBS4	Rabbit	N. Katsanis, Johns Hopkins, Baltimore	1 in 100
BBS2	Rabbit	M. Leroux, Simon Fraser University, Canada	1 in 100
Acetylated α tubulin (611B1)	Mouse	Sigma	1 in 800
γ tubulin (RγT)	Rabbit	Sigma	1 in 50
γ tubulin (GTU88)	Mouse	Sigma	1 in 50
MACF1	Mouse (polyclonal)	Abnova	1 in 500
CCT6A	Rabbit	Dr K. Willison, CRUK	1 in 100
KIF1A	Rabbit	N.Hirokawa, University of Tokyo	1 in 1000
PCM1	Rabbit	Dr A. Merdes, University of Edinburgh	1 in 400
$P150^{glued}$	Goat	BD Transduction Laboratories	1 in 100
Neuro Filament 200	Mouse	Sigma	1in 400

Appendix 1: Primary antibodies used.

Secondary Antibodies	Supplier	Concentration
Alexa Fluor anti rabbit/mouse 488	Molecular Probes	1 in 1000
Alexa Fluor anti rabbit/mouse 594	Molecular Probes	1 in 1000
FITC-tagged Phalloidin	Sigma	1 in 1000

Appendix 2: Secondary antibodies used.